Multi-glider Cooperation for Underwater Oil Spill Delineation

by

©Wang Yaomei

A thesis submitted to the School of Graduate Studies

in partial fulfillment of the requirements for the degree of

Doctor of Philosophy

Faculty of Engineering and Applied Science

Memorial University of Newfoundland

February 2022

St. John's Newfoundland and Labrador Canada

Abstract

Underwater oil spill reconnaissance and delineation is challenging as the spilled oil can cover a large area and may form plumes beneath the water surface. Autonomous underwater vehicles (AUVs), with improved intelligence, are used more widely for oil spill tracking nowadays. Underwater gliders, a type of AUVs, are favorable for underwater oil spill mapping as they can work for longer durations with less energy storage required. This thesis investigates the capabilities of gliders, especially multiple gliders, as platforms for mapping subsurface oil plumes.

Considering the limited payload capability and energy availability of a glider, a lightweight Cyclops submersible fluorometer and a Ping360 sonar were used on gliders to detect oil in the water in this thesis. The sensors were tested in a tank experiment with oil and the cross-validation from fluorescence measurements and sonar images was expected to improve the reliability in detecting oil. Furthermore, a Slocum glider was developed as a platform for the sensors before it was tested in the ocean with air bubbles which were used as proxies for oil droplets to avoid discharging oil into the environment. This glider was also developed with a backseat driver controller to provide it with an intelligence to adaptively map underwater oil plumes. In addition, a cooperation strategy was proposed for multiple gliders to delineate underwater oil patches simultaneously to overcome the challenges in oil spill mapping such as spatiotemporal aliasing and to improve data redundancy. In this cooperation strategy, a scout glider was commanded to follow a lawn-mower path to cover the area and find potential patches with rich information for follower gliders. A data compression method was designed for the scout glider to reduce the amount of information to be transmitted to the follower gliders. An adaptive path planning strategy was proposed for the follower gliders to

ensure they spent most of their mission time inside patches. The proposed cooperation strategy was compared with other strategies without cooperation and/or without adaptive control and the influence of having adaptive control and multiple gliders on a strategy was investigated through simulations. This developed Slocum glider was used as a follower glider to test the adaptive control in my cooperation strategy through a field experiment.

The tank experiment with oil and the field experiment with air bubbles conducted in this thesis proved the feasibility and necessity of having two or more sensors to cross-validate their measurements as a single sensor was not reliable in proving the existence of a particular substance, such as oil droplets, in the water. The developed backseat driver was able to provide the glider with an ability of adaptive control. However, having adaptive control or multiple gliders cannot guarantee a good score of performance when delineating underwater oil patches. The proposed cooperation strategy with multiple gliders was found to have the best score of performance, especially for long-endurance missions. The performance of the cooperation strategy could be further improved by having a thruster for the follower gliders to overcome the influence of the ocean environment, such as strong currents, when mapping moving underwater patches.

Co-authorship Statement

I (Yaomei Wang) hold the principal author status for all the manuscript chapters and the co-authorship from Chapter 3 to 7 in this thesis is presented as follows:

- Chapter 3 is co-authored by Yaomei Wang, Worakanok Thanyamanta, Craig Bulger, Neil Bose, and Robert Brown.
- Chapter 4 is co-authored by Yaomei Wang, Craig Bulger, Worakanok Thanyamanta, and Neil Bose.
- Chapter 5 is co-authored by Yaomei Wang, Worakanok Thanyamanta, Craig Bulger, Neil Bose, and Jimin Hwang.
- Chapter 6 is co-authored by Yaomei Wang, Worakanok Thanyamanta, and Neil Bose.
- Chapter 7 is co-authored by Yaomei Wang, Neil Bose, Worakanok Thanyamanta, Craig Bulger, and Sarik Shaikh-Upadhye.

Acknowledgements

This research is funded by Fisheries and Oceans Canada through the Multi-partner Oil Spill Research Initiative (MPRI) 1.03: Oil Spill Reconnaissance and Delineation through Robotic Autonomous Underwater Vehicle Technology in Open and Iced Waters and the School of Graduate Studies at Memorial University of Newfoundland.

I would like to thank my supervisor, Dr. Neil Bose, who provided me with excellent opportunities to do research on autonomous underwater robotics, an area which I had no experience with before my PhD study. I am grateful for his unconditional support and outstanding mentorship through my program study. I also appreciate his respect and kindness at any moment.

I would like to thank Craig Bulger, who joined all the experiments I had during my PhD program. Craig is a generalist who knows both software and hardware on marine research. Craig never refused my requests for help and provided me with plenty of helpful suggestions. He is the person I want to work with most. I also would like to thank Worakanok Thanyamanta, who was like a babysitter arranging almost everything during my program. I would like to express my gratitude to her valuable suggestions on my academic writing.

I am grateful for the help from Nicolai von Oppeln-Bronikowski and Mark Downey for their training on the deployment and testing of the Slocum glider. Without their help, I cannot be a glider operator. I also do appreciate Sarik Shaikh-Upadhye who helped me test the glider in the last few months of my experiments. I extremely enjoyed the time that we did experiments together, and I was really confident to deploy the glider when he was by my side.

I would like to thank Federico Luchino for his suggestions on electronics, Robert Brown for his arrangement on a tank experiment, Mae Seto and Len Zedel for their courses, people from technical service for their help in realizing lots of hardware. I really thank the company of my friends in St. John's, Xi, Huan, Yuhui, Zhibin, Ginelle.

Last but not least, I would like to express my sincere gratitude and deepest appreciation to my family for their support to accomplish this work.

Table of Contents

List of Tables

List of Figures

List of Abbreviations and Symbols

ADCP	Acoustic Doppler current profiler
AUVs	Autonomous underwater vehicles
CDOM	Coloured dissolved organic matter
CTD	Conductivity, temperature, and depth
DBSCAN	Density-Based Spatial Clustering of Applications with Noise
DVL	Doppler Velocity Log
G1	Generation 1
KTM	Karyu Turbo Mixer
LISST	Laser In-Situ Scattering and Transmissometry
MBARI	Monterey Bay Aquarium Research Institute
MOOS	Mission Oriented Operating Suite
MOOS-IvP	Mission Oriented Operating Suite-Interval Programming
OERC	Ocean Engineering Research Centre
One_Gld	One glider without adaptivity
One_Gld_Adp	One glider with adaptivity
Multi_Glds	Multiple gliders without adaptivity and cooperation
Multi_Glds_Adp	Multiple with adaptivity but without cooperation
Multi_Glds_Adp_Coop	Multiple gliders with adaptivity and cooperation
RMSE	Root mean square error
ROS	Robot Operating System
SoP	score of performance

SVM	Support Vector Machine
SVM_DBSCAN	Support Vector Machine with Density-Based Spatial Clustering of Applications with Noise algorithm
SVM_MeanShift	Support Vector Machine with the mean-shift clustering algorithm
SVM_Only	With the use of only Support Vector Machine (SVM_Only)
UMS	Underwater mass spectrometers
USBL	Ultra-Short Baseline
UMS	Underwater mass spectrometers
WHOI	Woods Hole Oceanographic Institution

1. Chapter 1

Introduction

1.1 Background and Motivation

The increasing prevalence of offshore oil spills caused by human activities attracts much research on oils in water as oils are complex substances and many of their constituents are toxic to the marine ecosystem (Transportation Research Board and National Research Council, 2003). The environmental impact of oil spills includes oil-coated shorelines, seabirds, and marine mammals. For example, the oil can destroy the waterproof properties of the plumage on seabirds and as it sticks to their feathers, it leads to a loss of buoyancy and power of flight. Therefore, it is essential to characterize the oil in the water and forecast the movement of oil before utilizing intervening or mitigating measures.

The density of most oil is less than water, and the source of oil spills is often from or near the surface, leading to many previous oil spill investigations to have been concentrated on methods relevant to the water surface. However, the increase in subsea exploration contributes to a higher number of subsurface oil spill events and related research. The Deepwater Horizon blowout on April 20, 2010 spilled millions of barrels of oil into the Gulf of Mexico and was recorded as the largest accidental marine oil spill in U.S. history (Deepwater Horizon Study Group, 2011). From May 17 to June 4 of 2010, the Dorado autonomous underwater vehicle was deployed by the Monterey Bay Aquarium Research Institute (MBARI) to survey this disaster (Zhang et al., 2011). It was found that a horizontally oriented subsurface hydrocarbon plume formed at a depth between

1,150 m and 1,200 m, southwest of the Deepwater Horizon wellhead. On November 15, 2018, an underwater pipe was disconnected when the SeaRose platform prepared to restart the production of oil during a fierce storm, leading to an oil spill of 250,000 litres in Newfoundland, Canada (Lord, 2018).

A variety of systems have been employed in oil spill research, such as moorings, satellite systems, surface vessels. However, moorings are limited to a small coverage area while oil could spread thousands of meters away from a source. Satellite systems require a clear sky, although they can cover a large area. Surface vessels have a high daily cost and can only survey a small range. Before the Deepwater Horizon oil spill, it was rarely believed that oil would stay under the water. After the investigation of the Deepwater Horizon oil spill, scientists found that oil was trapped and suspended at a depth of over 1,000 m for several months. Unlike oil on the surface, a subsurface release is impractical to be monitored by traditional methods such as remote sensing. To deal with this problem, autonomous underwater vehicles (AUVs) are increasingly employed to detect spilled oil underwater. AUVs, which belong to the class of unmanned underwater vehicles, can travel underwater autonomously without input from operators once they are programmed above the water prior to a mission (Wynn et al., 2014). Besides, multiple sensors have been used in propeller-driven vehicles to improve the reliability of measurements for underwater oil spill detection (Abt Associates et al., 2020). Oil spill reconnaissance and delineation cover a large area of research. It is complicated by the characteristics of oil, sensors and AUVs. Some studies focus primarily on theoretical research, some on models and algorithms, and some on experiments. It is notable that the progress in underwater oil spill research with the use of AUVs is built on successful field trials (Brito et al., 2012).

This research explores the potential of using Slocum gliders, a type of AUVs, as platforms for delineating underwater oil plumes. Slocum gliders have a reputation for their long endurance, low energy consumption, and ability to survey from the surface to a depth of 1,000 m at relatively low cost. The features of a Slocum glider meet the requirements of underwater oil spill mapping as oil can disperse over long distances. Despite the limited payload capability of Slocum gliders, there is advantage in using multiple sensors as the detection from different sensors can be cross-validated to improve the reliability of measurements. Thus, a lightweight fluorometer and a compact sonar were selected as the payload for the gliders in this work. In addition, multiple cooperative gliders with adaptive control were considered in this research as a team of gliders can overcome challenges existing with using only one glider when delineating oil spills in the water column, such as the spatiotemporal aliasing problem. The adaptive ability is expected to drive gliders to interesting regions to increase the quality of information acquired during a mission. The use of multiple gliders is expected to decrease the duration of a mission and bring data redundancy to improve the reliability of a mission.

1.2 Research Questions

This research will explore the following questions:

- Q1: Is it possible to improve the reliability of measurements by using a fluorometer and a sonar in a Slocum glider? Considering the limited payload capability and energy availability of a Slocum glider, oil sensors for underwater gliders are limited compared to other active-propelled underwater vehicles. However, oil is a complex substance and the reliability in detecting oil relies on the sensors used.

- Q2: Is it possible to equip a Slocum glider with the ability of adaptive control? With adaptive control, a glider can change its states such as heading and depth based on the measurements obtained from its sensors. Theoretically, this intelligent work will increase the real working time of the glider and decrease the time spent on searching for oil plumes.
- Q3: Is there an advantage in using a multi-glider strategy for oil spill detection? Multiple cooperative gliders have been used in other research areas and the performance of this cooperation system in oil mapping has not been tested.
- Q4: What are the benefits of using multiple cooperative gliders with adaptive control in mapping oils underwater? Uncertainties from the sensors, the vehicle, and the surrounding environment may challenge the advantage of using multiple cooperative gliders. The superiority of multiple gliders with adaptive control needs to be explored.

1.3 Research Objectives

The main objectives of this research are to **investigate the capabilities of gliders to delineate subsurface oil plumes**. This main objective consists of several sub-objectives as follows:

- O1: To investigate the performance of a Slocum glider with cooperation between more than one sensor to delineate underwater oil;
- O2: To develop a Slocum glider with adaptive control to investigate oil spills in the ocean intelligently;
- Q3: To improve the performance of multiple cooperative gliders to delineate subsurface oil;
- O4: To investigate the performance of a multi-glider cooperation strategy with adaptive control in delineating underwater oil plumes.

1.4 Research Contributions

The contributions of this research include five points.

(1) Cooperation of sensors

This research proposed to improve the reliability to detect oils in water by using a combination of a fluorometer and a sonar in Slocum gliders. The working principles of these two sensors are different: the fluorometer detects the fluorescent substances in oil while the sonar captures the acoustic scattering from oil droplets (Maksym et al., 2014). It is not certain that the acoustic information from sonar images will be able to discern oil from other substances with similar acoustic scattering properties (Fingas, 2017); however, the fluorometer can complement the sonar result from another point of view – fluorescence. In a report on oil spill detection and mapping with AUVs, the results from the sensor evaluation suggested a combination of multiple types of sensors for better oil detection (Maksym et al., 2014). The report concluded that "*Techniques for fusion of data from multiple sensors for the most reliable detection of oil should be developed*". In another work on using an acoustic method to detect oil, the author emphasized that non-acoustic methods should be used to verify the presence of oil along with acoustic methods to detect oil in the water column (Eriksen, 2013).

The data collocated by a sonar and a fluorometer was cross-validated. Different from other sampling methods that used sonar as a remote sensor (Eriksen, 2013), this work set the sonar to a short work range and only considered the measurements within that short range to minimize the time lag between the detection by the sonar and the fluorometer.

(2) Integration of adaptive control in gliders

This work proposed to equip Slocum gliders with adaptive control to delineate underwater oil spills. Due to the dynamics of underwater oil plumes and the patchy characteristics of oils, gliders may miss plumes or spend lots of time outside of oil plums. Adaptive control can solve this problem as it can replan the mission for a glider based on the measurements from its sensors and the states from the main vehicle control system of the glider. In this thesis, adaptive control was realized in a Slocum glider by installing a backseat driver hardware to the glider. A series of simulations were tested in the lab by using the glider's electronics and control system as a hardware-in-the-loop simulator and to check the adaptive heading behaviour, adaptive waypoint behavior, adaptive depth behaviour, and activation and deactivation of behaviours. As uncertainties of the ocean environment and vehicles cannot be comprehensively considered in these simulations, the backseat driver hardware was also tested through field experiments.

(3) Cooperative measurement with underwater gliders

Although there are some studies on collaboration amongst underwater gliders, work on cooperation of gliders for delineating oil spill is scarce. A multiple-glider cooperation strategy was proposed to delineate oil patches underwater and the performance of this strategy was investigated by comparing it to other non-cooperation strategies and strategies without adaptive control. The advantage of using multiple gliders includes the ability to continuously search large areas and precisely detect oil underwater. A team of long-range vehicles is beneficial as oil spills can cover a large area. For example, researchers from Woods Hole Oceanographic Institution manifested the existence of a hydrocarbon plume at a depth of 1,100 m which covered an area of over 35 km in length and 200 m in height (Camilli et al., 2010). The range of a Slocum glider can reach 350-

1,200 km, 700-3,000 km, and 3,000-13,000 km when using alkaline, rechargeable, and lithium batteries, respectively (Teledyne Webb Research, 2013). However, one glider cannot be equipped with many sensors. When each glider in a multiple glider system is outfitted with different sensors, the gliders can share information between each other.

(4) Underwater acoustic communication with compressed data

In the proposed cooperation strategy, a scout glider had to share the information about oils patches with other gliders. To realize the real-time underwater acoustic communication, the support vector machine was proposed in this thesis to classify the boundaries of patches and compress the amount of information shared between gliders. However, the performance of the support vector machine was affected by the choice of kernel functions and parameters and might not provide the correct boundaries of patches due to the complexity of data sets. A clustering method was proposed in this thesis to simplify the characteristics of data sets before the application of the support vector machine. The performance of the proposed method by including a clustering method was tested in simulations which was proven to be a potential tool to classify the boundaries of oil patches before sending this compressed information to other gliders.

(5) Field experiments with novelty methods

Field experiments were desired to investigate the performance of a Slocum glider with the cooperation of sensors to delineate underwater oil. Considering the environmental issues induced by releasing oil in the water and the cost of transporting a glider to an oil spill area to test a newly developed glider, environmentally friendly air bubbles were proposed in this thesis to be used as proxies for oil droplets in the field experiments involving gliders. Air bubbles are buoyant and can represent oil droplets better than water-soluble dye tracers. This is expected to allow a glider with some onboard oil detection sensors to be tested in realistic oil spill conditions.

1.5 Notes on the Research Scope

This study was conducted under the following conditions:

(1) This research proposed to use gliders to detect oil of known composition. Knowing the composition of the oil is vitally important for selecting suitable fluorometers for detecting the oil. For example, a MiniFluo sensor detects specific PAHs in oil (the MiniFluo-1 detects Naphthalene-like and Phenanthrene-like PAHs while the MiniFluo-2 detects Pyrene-like and Fluorene-like PAHs) (Cyr et al., 2019). The percentage of Naphs (the sum of Naphthalene and alkylated compounds) measured in the Saumaty harbour accounts for 81.8% of total PAHs measured, while only 3% of Naphs are Naphthalene. This is similar to the samples collected in the North Sea, where Naphthalene makes up 3% of Naphs, although Naphs constitute 85.3% of PAHs detected (Cyr et al., 2019). Without knowing the composition of oil to be detected, challenges will be raised when associating measurements from a fluorometer with the concentration of oil. Otherwise, reliable detection should be realized by using an array of fluorometers in order to cover multiple detection ranges, which is not practical considering the payload capacity and energy availability of a glider. Therefore, in this research, only one fluorometer was installed in the glider and the type of oil to be detected was pre-determined.

(2) As a fluorometer cannot detect air bubbles in a field experiment which uses air bubbles as proxies for oil droplets, a turbidity sensor with the same size and weight as the fluorometer was installed in the glider to detect air bubbles in combination with sonar.

(3) As only one glider was fully available for this research, an acoustic modem was used to represent a glider when testing the cooperation of gliders with underwater acoustic communication.

(4) As it was not easy to test gliders in a true oil spill considering the environmental and cost issues, a series of experiments were conducted to realize the objectives of this study. The cooperation of a sonar and a fluorometer was tested in a tank with oil in water without the presence of gliders, as it was impossible to deploy a glider in this tank. The performance of the developed glider was tested with a simulated oil plume.

1.6 Thesis Outline

The thesis consists of 9 chapters. This thesis aims to answer the research questions in Section 1.2 and realize the research sub-objectives in Section 1.3 at the same time.

Chapter 1 introduces the background, motivation, objectives, contribution, scope, and outline of this thesis. **Chapter 2** reviews the sensors and AUVs that have been used for underwater oil spill detection, which are references for developing underwater gliders for oil delineation. The cooperation of multiple underwater gliders is also reviewed, which is a foundation for proposing a multiple-glider cooperation strategy for oil spill research.

Chapter 3 presents the testing of the cooperation of a sonar and a fluorometer through an experiment in an outdoor tank with a true oil release before installing the sensors on a Slocum glider in order to answer the first research question in Section 1.2 (**Q1**: Is it possible to improve the reliability of measurements by using a fluorometer and a sonar in a Slocum glider?). **Chapter 3** aims to reach the first sub-objective in Section 1.3 (**O1**: To investigate the performance of a Slocum glider with cooperation between more than one sensor to delineate underwater oil).

Chapter 4 introduces the proposal and testing of microbubble generators to generate gas bubbles as proxies for oil droplets to test developed gliders with oil sensors as it is impractical to spill oils into the ocean or wait for an actual oil spill to become available. This chapter is a preparation for reaching the first sub-objective in Section 1.3 (**O1**: To investigate the performance of a Slocum glider with cooperation between more than one sensor to delineate underwater oil).

Chapter 5 develops a backseat driver system in a Slocum glider to equip it with an ability to perform an adaptive sampling task underwater to answer the second research question in section 1.2. (**Q2**: Is it possible to equip a Slocum glider with the ability of adaptive control?). **Chapter 5** reaches the second sub-objective in Section 1.3 (**O2**: To develop a Slocum glider with adaptive control to investigate oil spills in the ocean intelligently).

Chapter 6 proposes a cooperation strategy with a data compression method for multiple gliders to map oil spills in the ocean to answer the third research question in this thesis (**Q3**: Is there an advantage in using a multi-glider strategy for oil spill detection?) and reach the third sub-objective (**O3:** To improve the performance of multiple cooperative gliders to delineate subsurface oil).

Chapter 7 compares the performance of the strategy with multiple cooperative and adaptive gliders with other strategies without cooperation and/or without adaptive control in underwater oil spill detection missions in order to answer the fourth research question (**Q4**: What are the benefits of using multiple cooperative gliders with adaptive control in mapping oils underwater?). **Chapter 7** reaches the fourth sub-objective (**O4**: To investigate the performance of a multi-glider cooperation strategy with adaptive control in delineating underwater oil plumes) through simulation experiments.

Chapter 8 presents field experiments in testing the developed glider. **Chapter 8** aims to address the first sub-objective (**O1**: To investigate the performance of a Slocum glider with cooperation between more than one sensor to delineate underwater oil) and address the fourth sub-objective in

Section 1.3 (**O4**: To investigate the performance of a multi-glider cooperation strategy with adaptive control in delineating underwater oil plumes).

Chapter 9 is a summary of this research with the main objective of investigating the capabilities of gliders to map subsurface oil plumes. Future work that can be conducted to improve the performance of underwater gliders in underwater oil delineation is also presented in this chapter.

2. Chapter 2

Literature Review

As the thesis consists of a series of articles and each article has its own literature review, this chapter briefly reviews sensors and AUVs that have been used in oil spill detection for references in developing underwater gliders for oil spill research. Also, the cooperation of multiple underwater gliders is also reviewed, which is a foundation for the proposed multiple-glider cooperation strategy for oil spill investigation in this thesis.

2.1 Sensors for oil detection

Petroleum hydrocarbons can be measured by fluorometers, sonar, underwater mass spectrometers (UMS), particle size sensors, dissolved oxygen meters and conductivity, temperature and depth (CTD) sensors, cameras (Battelle Memorial Institute, 2014), etc. A fluorometer measures the fluorescence or light emitted by the material when a certain wavelength of light excites the electrons in it (Kalaji et al., 2012). It is a point-based detection tool that can only detect a limited discrete volume of the water column at a time (Fitzpatrick et al., 2014). Moreover, the fluorescence substances in natural seawater can reduce the efficiency of a fluorometer in detecting oil (Baszanowska and Otremba, 2016). Sonar can complement fluorometers in oil detection as sonar detects backscattered sound from oil droplets, a different working principle from fluorometers (Wilkinson et al., 2013). The strength of the backscattering is determined by the acoustic impedance contrast between ambient water and oil droplets (Loranger, 2019). In a test with the use of a 400 kHz Wide Band Multi-Beam sonar, freshwater could be detected by this sonar when being injected into saltwater (Fitzpatrick and Tebeau, 2013). As the difference in reflectivity between freshwater and saltwater was small, this test showed the viability of sonars in distinguishing two fluids with low impedance contrast, such as crude oil and seawater (Loranger, 2019). In a test performed in the Oil and Hazardous Materials Simulated Environmental Test Tank, New Jersey of the U.S., a well-dispersed plume with small concentrations was captured by sonars with a nominal operating frequency of 400 kHz (Eriksen, 2013). However, the detection of oil by sonar can be confused by other substances in the water that possess a similar acoustic property to the oil droplets (Fitzpatrick and Tebeau, 2013).

The UMS is based on the method of membrane inlet mass spectrometry, which samples continuously with a high resolution (Chua et al., 2016). During the Deepwater Horizon oil spill investigation, the TETHYS mass spectrometer was carried by both a rosette frame and the Sentry AUV for a survey and collection of samples (Camilli et al., 2010). The TETHYS is the fourth generation of a UMS which can be used at a depth of 5,000 m and detect a minimum concentration of 500 ppb (Camilli and Duryea, 2007). Although the use of UMS has increased, the application of UMS is limited by its operability as a trained user is required. In addition, a portion of UMS systems are customized to detect specific substances, leading to the systems being inaccessible to other users interested in other substances (Chua et al., 2016).

The size of oil droplets is critical to the transport of oil. Small oil droplets are easily biodegraded by microbes, while chemical dispersants can promote the breakup of oil into smaller droplets (Driskell and Payne, 2018). Laser In-Situ Scattering and Transmissometry (LISST) system, an instrument which can provide size distribution of particles underwater, was used in the Deepwater Horizon oil spill investigation to support the environmental impact assessment (Li et al., 2011).

Underwater cameras can offer a visual scene of an underwater leakage and the origin of oil seeps in comparison with other sensors (Marques et al., 2011). However, this method tends to be affected by environmental factors such as light, weather and sea conditions. Nevertheless, this is the most straightforward method and is used to detect oil spills both on the surface and underwater. A Holographic camera and a GoPro camera have been used in the field tests at the Santa Barbara natural seeps to record gas bubbles and oil droplets, which further supported the presence of oil in the water (Abt Associates et al., 2020).

Environmental information, particularly currents, is also important when detecting underwater oil spills. For the oil on the surface of the water, dispersion of oil is driven by waves, wind and currents. When it comes to the subsurface, dispersion of oil is mainly influenced by currents. The acoustic Doppler current profiler (ADCP) measures velocities of water currents by using the Doppler effect. The 600 kHz Teledyne RDI Explorer Doppler Velocity Log is upgradable to include ADCP capability which can be integrated to a Slocum G2 glider. During the Deepwater Horizon oil spill investigation, the strongest hydrocarbon signal was found in the south-west of the source, which coincided with the direction of the current at the relevant depth measured by the Doppler Velocity Log (DVL) (Camilli et al., 2010). The water current also affects the localization of vehicles underwater, which in turn affects the geolocation of the oil. In the work of Medagoda et al. (2016), the current information obtained from an ADCP along with data from other sensors were used to bound the error of localization in the mid-water column.

While fluorometers and UMS have irreplaceable strengths in tracking oil, these instruments are not always reliable due to inevitable measurement noise and other operational limitations, which can then affect both real-time and post-mission analysis of measurements. Integration of various sensors is capable of providing more reliable measurements, compared to a single sensor configuration (Pärt et al., 2017).

2.2 AUVs in oil spill detection

AUVs, as unmanned underwater vehicles, are able to travel underwater autonomously. They can be propelled by thrusters, known as active-propelled vehicles, or driven by changing buoyancy or weight. The latter group are autonomous underwater gliders. A comprehensive introduction to AUVs can be seen in the report from the Battelle Memorial Institute (2014). A portion of them have been employed in oil spill reconnaissance (Table 2-1).

SOTAB-I, which was a 2.5-m long AUV (Kato et al., 2017), could be actuated by both a buoyancy control device and thrusters. The buoyancy control system consumed less energy, brought less disturbance to the surrounding water, and increased the reliability of data collected by the sensors when compared with the use of a thruster. This AUV was equipped with a UMS to delineate dissolved gas and oil, and with a camera to capture gas plume blowouts from the seabed (Kato et al., 2017). The data collected by SOTAB-I could be transmitted in real-time to a land station for improving the simulation of the movement of spilled oil. This oil was ultimately recovered by pre-deployed devices based on the predictions from simulations.

Scientists from MBARI and the National Oceanic and Atmospheric Administration employed both a ship and an AUV to investigate and confirm the existence of underwater oil after the Deepwater Horizon blowout. After a maximum deep plume signal was captured by a ship's hydrocast-rosette system over a comparatively large area, the AUV Dorado (Thompson et al., 2013) was released and did a high-resolution survey and sampling focusing on the high-signal area. Dorado, initially designed for coastal marine research, was equipped with a propulsion system, sensor suite and sample acquisition system for the Deepwater Horizon blowout investigation.

Unlike the Dorado AUV, which is torpedo-shaped, the AUV Sentry looks like a flying bar of soap, more like a clownfish to some extent (Kaiser et al., 2016). It can dive to a depth of 6,000 m and operate for more than one day. The Sentry AUV was also employed by the scientists from WHOI in the Deepwater Horizon oil spill detection.

Developed by MBARI, the long-range AUV Tethys is a kind of propeller-driven vehicle which can operate for more than 1,800 km at a speed of 1 m/s (Hobson et al., 2012; Kukulya et al., 2016). In recent years, a collaboration was developed between MBARI and WHOI to make practical use of the Tethys in detecting and tracking oil spills, with the aim of making it feasible for under-ice missions. During an experiment in 2018 in Monterey Bay (Fulton-Bennett, 2018), a non-toxic, biodegradable dye was poured into the water to simulate an oil spill, and the Tethys was used to detect the plume and its concentration. The experiment verified that the long-range AUV was able to perform tasks required for oil tracking.

The speed of a glider is lower than that of a propeller-actuated AUV. A glider changes its buoyancy or weight, and transforms the vertical motion into horizontal motion with wings, driving the glider in a saw-tooth motion. Shortly after the oil spill in the Gulf of Mexico, scientists from WHOI deployed a Spray glider to obtain water current information, which helped in evaluating the diffusion rate of oil and managing the risk of oil to the environment (Lippsett, 2011). Panetta et al. (2017) demonstrated the ability of a Slocum glider to measure the thickness of oil slicks with the use of acoustic sensors under both wave and no wave conditions. Russell-Cargill et al. (2018) integrated a Slocum Glider with the Franatech laser methane sensor to sense the methane released from the active thermogenic seep field in the Yampi Shelf in Australia. Due to the extra weight of the sensor and its bracket, a bay section was added to provide additional buoyancy. The glider was deployed for a 17-day work in the eastern active seeps, validating the effectiveness of gliders in detecting the existence of methane in geochemical exploration.

Table 2-1. AUVs that has been used in oil spill research.

Name	Length/ Diameter (m)	Weight (kg)	Depth (m)	Speed (m/s)	Communication	Navigation	Endurance
SOTAB-I	L: 2.5	312	2000		WLAN, Iridium, acoustic modem	GPS, USBL	
REMUS 100	L: >=1.70 D: 0.19	>=36	100 (120*)	Max: 2.6**	Iridium, Wi-Fi, Acoustic Communications	LBL, INS, Doppler-assisted dead reckoning, GPS	>10 hours at 2.3m/s with standard sensor setup
REMUS 100s	L: >=1.84 D:0.19	>=45	100	Nominal: 1.54 Max:2.6 **			10 hours at 3.0 kts depending on sensors
REMUS 600	L: 2.7-5.5 D: 0.324	220-385	600 (1500*)	Max: 2.3 **	Acoustic modem, Iridium modem, 100 Base-T Ethernet (standard), 1000 Base-T Ethernet (optional), Wi-Fi	Inertial, LBL, GPS, USBL	Typical mission endurance is up to 24 hours in standard configuration
REMUS 600s	L: > 4.27 D:0.324	>326	600 (1500*)	Nominal: 1.5 Max: 2.6			
REMUS 6000	L: 3.96 D: 0.71	862	6000	Max: 2.3**	Acoustic modem, Iridium, modem, Wi-Fi	LBL, Dead Reckon with ADCP INS	22 hours
Dorado	L: 4.2 D: 0.53	680.0	6000	Nominal: 1.54 Max:2.06 **	Freewave, Iridium, Radio Direction finder beacon	INS and DVL	17.5 hours with 55-85 km range
Sentry	L: 2.9 Height: 1.8 Width: 2.2	1250	4500	Nominal: 1.0 Max:1.2**	Acoustic modem. Iridium, RF, and strobe	DVL, INS, USBL or LBL	24 hours
LAUV	L: >=1.1 D:0.15	>=18	100	Max: 2.57	GSM/HSDPA, Iridium, Wi-Fi, acoustic modem	INS	Lupis: 6 hours Xplore-1:24 hours
IVER2-Ecomapper	L: >=1.10 D: 0.15	>=18	100	Nominal: 1.29 Max:2.06**	GSM/HSDPA, Wi-Fi, Acoustic Modem	GPS, DVL	6 hours
Tethys	L: 2.3 D: 0.31	110	300	0.5-1.0	Acoustic modem, Iridium	DVL-aided dead reckoning, GPS, USBL/LBL	740 hours/1000 km
Bluefin 21	L: 4.93 D: 0.53	750 (dry)	4500	Gimbaled, ducted thruster 2.3	Iridium and acoustic; Ethernet via shore power cable, RF	INS, DVL, SVS, GPS, USBL	25 hours when 1.54m/s with standard payload
Slocum glider G2	L: 1.5 D: 0.22	54	4 -200 / 40-1000	Average Horizontal: 0.35	RF Modem, Iridium (RUDICS), ARGOS, Acoustic Modem	GPS Waypoints, Pressure Sensor, Altimeter	15-50 days (Alkaline batteries) / 4 - 12 months (Lithium batteries)
Spray glider	L: 2.0 Wingspan: 1.2	51	1500	0.23m/s or 20km/day	Iridium, acoustic modem	GPS	4320 hours

* can be configure to this value

**With the use of propeller

2.3 Cooperation of gliders

It was in the late 1980s that Henry Stommel proposed to use a fleet of underwater Slocum gliders for monitoring the global ocean (Stommel, 1989). A fleet of gliders can perform this mission better than a single glider. For example, in the project Autonomous Ocean Sampling Network II, a fleet of gliders was used to find the local minima and maxima of the environmental field while minimizing the error in estimating the gradient in the measured field (Leonard et al., 2003). Using a single glider, the glider has to make a significant effort to change direction to collect enough data to calculate the gradient (Ögren et al., 2004).

The cooperation of gliders includes two aspects: team formation and team steering (Chen and Pompili, 2012). Team formation is to drive each vehicle to its position when given the number of vehicles and the formation geometry. After the shape of the team is formed, this formation is forced to move along the desired path and keep the configuration, which is called team steering.

In the work of Edwards et al. (2004), each vehicle followed a given path and was controlled by a trajectory control algorithm. The leader then broadcasted its position to its followers and the distance of each follower to the leader was controlled by a formation control algorithm. Although the leader-follower algorithm in this work was not specific to gliders, it offered a reference to the control of gliders in the horizontal plane. This paper also showed how to form a team before the mission where the vehicles formed themselves into a circle until all of the vehicles were in position. However, seldom have studies explicitly explained the process of calling all the gliders together. Although the team steering step can realize the function of team formation to some extent, arranging each glider to a specific position and decreasing the formation error before the mission starts are beneficial for the whole mission.

Various algorithms have been proposed for the formation of gliders but most of these algorithms have only been tested through simulations. For example, in the work of Chen and Pompili (2012), a hybrid team formation scheme was proposed for different numbers of gliders. A team steering strategy which incorporated absolute formation adjustment (AFA) and relative formation adjustment (RFA) was applied to reduce the overhead of sharing position information. The AFA was used when the absolute positions of gliders were available while the RFA was used when relative inter-glider velocity information was available. In the work of Fonti et al. (2011), each glider v^i followed one leader v^j, $i \neq j$; v^1 followed the virtual leader v^0; the trajectory of the virtual leader was generated by the unicycle model. This decentralized coordination strategy was proven to be able to help avoid collisions between vehicles and be generalized to formation of heterogeneous autonomous agents. Alvarez and Mourre (2014) compared the efficiency of a coordinated and a cooperative-unaware glider network in sampling the ocean variability. The difference between the cooperative-unaware and the coordinated glider network was whether the behaviour of the gliders affected one another while reaching the global goal. A glider in the cooperative-unaware glider network was not affected by the rest of gliders, while a glider in the coordinated network was influenced by other gliders' behaviours. In the coordinated network, a leader-follow formation method was used, with three gliders keeping a triangle formation. The glider fleet in the coordinated network moved between waypoints and rotated as a whole when a waypoint was reached. Simulation experiments showed that the coordinated network performed better than the cooperative-unaware network in sampling eddy structures of ocean process. The above algorithms have only been realized in simulations and have not been verified in field experiments. In field experiments, uncertainties induced by the ocean environment and the sensors used could bring various challenges to the algorithms such as stability of the algorithms. These uncertainties are difficult to be predicted or to be simulated through a computer.

In general, existing cooperation strategies were designed for 3 and more gliders. Most of the presented formation algorithms were verified through simulations. In the simulation, communications between vehicles were assumed to be ideal. However, the cooperation of gliders is inevitably affected by uncertainties from the environment, vehicles, sensor measurements and communications in field trials. For example, the uncertainty of ocean currents would result in the deviation from the desired path and a loss of communication among vehicles. Xue et al. (2015). analyzed the uncertainties of the formation control of a fleet of gliders with a statistical method. In their work, the interaction between vehicles was controlled by the artificial potential field approach. Results from the simulation showed that uncertainty analysis should be conducted in the design of a glider formation.

3. Chapter 3

An experimental study of the cooperation between sonar and a fluorometer for detecting underwater oil using autonomous underwater vehicles

Yaomei Wang[1], Worakanok Thanyamanta[1], Craig Bulger[2], Neil Bose1, Robert Brown[3]

[1] Department of Ocean and Naval Architectural Engineering, Memorial University of Newfoundland, St. John's, Canada

[2] Centre for Applied Ocean Technology, Fisheries and Marine Institute of Memorial University of Newfoundland, St. John's, Canada

[3] Offshore Safety and Survival Centre, Fisheries and Marine Institute of Memorial University of Newfoundland, St. John's, Canada

This chapter is a conference paper which has been accepted by conference of Oceans 2022 Chennai (Article No.1 (Oceans Chennai 2022)).

Table 3-1. Individual Author Contribution – Article No.1 (Oceans Chennai 2022)

Author	**Contribution**
Yaomei Wang	Conceptualization, Methodology, Software, Validation, Formal analysis, Investigation, Resources, Data curation, Writing—original draft preparation, Writing—review and editing, Visualization
Worakanok Thanyamanta	Formal analysis, Resources, Writing—original draft preparation, Writing—review and editing, Supervision, Project administration
Craig Bulger	Conceptualization, Methodology, Software, Validation, Formal analysis, Investigation, Resources
Neil Bose	Formal analysis, Resources, Writing—original draft preparation, Writing—review and editing, Supervision, Project administration, Funding acquisition
Robert Brown	Methodology, Resources, Writing—original draft preparation, Writing—review and editing

Abstract

In oil spill events, using a combination of multiple types of sensors is favorable to improve the performance of oil detection and the reliability of data collected. An experiment was conducted to investigate the feasibility of using a fluorometer and a sonar to detect and cross-validate the presence of spilled oil before being installed and used on a Slocum glider. Considering the limited payload capability and energy availability of a Slocum glider, a lightweight Cyclops submersible fluorometer and a Ping360 sonar were used to cross-validate fluorescence measurements and sonar images. The results from the experiment conducted in a tank with oil release confirmed the feasibility of using both fluorometers and sonar to verify the existence of spilled oil.

Keywords: Fluorometer; Sonar; Cross validation; Underwater oil

3.1 Introduction

Subsurface oil spill events can occur from potential oil spill events from offshore oil operations (e.g., Deep Water Horizon), ships in distress, natural deep water oil seeps or other subsurface exploration operations. Autonomous underwater vehicles (AUVs) have shown advantages in mobility, autonomy, and robustness in delineating oil underwater compared to methods such as moorings, satellite systems, and surface vessels. Reliable detection of submerged oil by using AUVs is critical to evaluate environmental concerns.

Petroleum hydrocarbons can be directly detected by sensors or indirectly detected by measuring the changes of marine properties. Direct measurements include the use of sensors such as fluorometers, underwater mass spectrometers, cameras, etc. Indirect measurement tools include turbidity meters, dissolved oxygen meters, and conductivity, temperature, and depth (CTD) sensors. In a report on oil spill detection and mapping with AUVs, results from a sensor evaluation study suggested that a combination of multiple types of sensors could provide better oil detection than single sensors (Maksym et al., 2014). In another work on using an acoustic method to detect oil, the author emphasized the benefits of using non-acoustic methods to verify the presence of oil when an acoustic method was used to detect oil in the water column (Eriksen, 2013). In previous studies on cooperation of multiple sensors, sonar was used as a remote sensor. For example, in an oil mapping project using AUVs, a sonar was used to identify the location of oil droplets and/or gas bubbles in the water (Abt Associates et al., 2020). The use of sonar as a prescreen tool to detect the presence of oil over a large area enabled the AUV to target its detailed data collection mission over a smaller area.

In our research, we aimed to develop a Slocum glider to delineate subsurface oil. Despite the limited payload capability of a Slocum glider, there is an advantage in using multiple sensors and thus a compact fluorometer and a sonar were selected as a payload for the glider. This chapter presents the results from our experiments conducted to test the cooperation of these two sensors in a tank in the presence of oil prior to using them on our developed underwater glider.

3.2 Background

3.2.1 Previous work

Underwater gliders have been used for oil spill detection. However, only one sensor or one type of sensor was used to directly detect the existence of oil. In the work of Cyr et al. (2019), a SeaExplorer glider was installed with a MiniFluo sensor for detecting specific PAHs in oil in the natural marine environment (the MiniFluo-1 detects Naphthalene-like and Phenanthrene-like PAHs while the MiniFluo-2 detects Pyrene-like and Fluorene-like PAHs). This glider could be fitted with two MiniFluo sensors to detect four kinds of fluorescent PAHs. In research done by Pärt et al. (2017), a Uvilux sensor was towed to emulate a glider trajectory in experiments in Tallin Bay because the Slocum glider used was not compatible with the Uvilux UV fluorometer.

Multiple direct sensors have been used in propeller-driven vehicles for oil spill detection. Vasilijevic et al. (2015) presented the application of a fluorometer and an underwater camera on an autonomous underwater vehicle to detect a submersible Rhodamine plume, a simulated oil spill plume. In the experiment, the distribution of the Rhodamine plume and the entrance of the AUV into the plume were captured through a camera on the AUV, which showed the potential use of the proposed system in underwater oil spill detection. For underwater vehicles, the use of a camera onboard the vehicle is a good option for checking the performance of a sensor system by providing underwater visualization. However, it is not a preferred option for field experiments for gliders due to their large area of coverage and limited energy storage.

In a project involving AUVs to characterize oil spills off the coast of Santa Barbara, California, multiple sensors were proposed to be used on AUVs to increase the reliability of oil detection (Abt Associates et al., 2020). A CTD sensor, a water gulper, a holographic camera, and a SeaOWL UV-A fluorometer, were installed on a REMUS-600 AUV and used to sample the survey area simultaneously. The CTD sensor could establish the background value of fluorescent dissolved organic matter (FDOM) as the value of FDOM changed with the salinity and/or depth. The salinity detected from the CTD sensor also helped to detect the malfunction of the water gulper, as the sampling bottles in the water gulper were pre-filled with clean, hydrocarbon-free water and would be replaced with sample water when the gulper worked properly. A holographic camera was used to estimate concentrations and size distribution of oil droplets in the water column. However, a water sampler is too large for an underwater glider liker a Slocum glider and the sampling process of a water sampler can pose a challenge to the dynamics of a glider which is propelled by changing its weight or buoyancy. A camera is considered power-intensive relative to a glider's power storage. The SeaOWL UV-A sensor used could measure FDOM, chlorophyll, and light backscattering simultaneously. However, the sensitivity and the accuracy of backscattering relied on the tuning and calibration of the sensor before the experiment. In addition, the in-situ light scattering from the SeaOWL UV-A could only provide measurements at limited points.

Sonar has a better ability to detect oil droplets over the point-based sensors such as the SealOWL UV-A fluorometer as it can detect the distribution of oil within an adjustable range, however, it cannot determine the exact nature of the disturbance in the water column that it senses. Sonar can be used as a remote sensor to check the distribution of oil from a distance. The intensity of the backscatter sound increases with the number of reflecting particles within the measurement volume and scattering cross-section (Chmiel et al., 2018). Weber et al. (2012) used an acoustic method to quantify the amount of surfacing oil with ship-mounted acoustic Simrad ES60 echo sounders. These echo sounders were operated at the frequencies of 12, 38, and 200 kHz. The high return detected by the 200-kHz echo sounder above the depth of 200 m was in accordance with the visual observation of oil from the surface.

The size of an oil droplet is an important parameter critical to the transport of oil in water. Oil droplets with higher rise velocity and larger diameters are more likely to rise to the water surface, smaller droplets can remain in the water column (Zhao et al., 2016). In addition, the droplet size affects the biodegradation process (Vilcáez et al., 2013). Laser In-Situ Scattering and Transmissometry (LISST), an optical instrument, can obtain particle sizes and their distribution underwater. This device was used in the Deepwater Horizon oil spill investigation, which supported the environmental impact assessments and the modeling of oil plumes in the water (Li et al., 2011). However, the measurement from a LISST sensor is limited to a certain range of particle size (0-500 microns). A sonar with an operating frequency of 5 MHz, which was much higher than the resonant frequency for the size measured, was applied to the measurement of oil droplets in a mixture of oil-water-dispersant (Panetta et al., 2012). A LISST sensor was used to benchmark the detection from the sonar (Panetta et al., 2013). The comparison with the measurements from the LISST sensor showed a good performance of the sonar used.

3.2.2 Concept in this work

Accurate measurement of oil spills is essential for characterizing the oil in the water and forecasting the movement of oil before utilizing intervening measures. Acknowledging the limitations of using a single sensor found in previous research with gilders and the benefit of using multiple sensors on other larger AUVs, in this study, we propose to improve the accuracy in detecting underwater oil spills through the concept of cooperation of multiple sensors. The concept was tested and planned to be used in underwater glider missions.

In this chapter, we cross-validated data collected by a sonar and a fluorometer when the sensors were close to or inside an oil plume. This method is different from other sampling methods that use a sonar as a remote sensor. As sonar is typically used to provide acoustical images of objects within a specified range ahead, when used together with an in-situ sensor like a fluorometer, the sonar is expected to detect the objects first (Figure 3-1). In order to cross-validate data, we have to ensure that the two sensors measure the same object or take measurements at the same time and location in the water column. Therefore, we set the sonar to work at a short range (5 m) and only considered measurements within a short range to minimize the time lag between the detection by the sonar and the fluorometer.

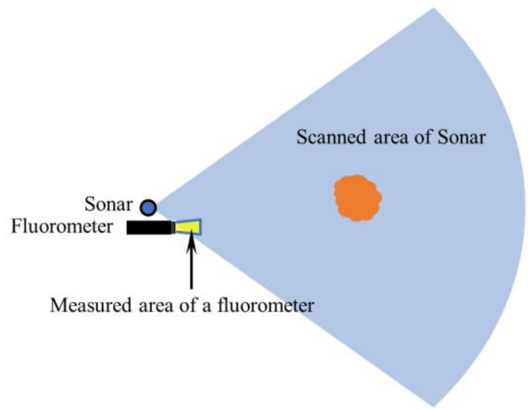

Figure 3-1. Detection range of the fluorometer and sonar.

3.3 Experimental testing

3.3.1 Experimental setup

This experiment was conducted in an outdoor reinforced concrete tank (Figure 3-2) at the Offshore Safety and Survival Center of the Marine Institute, Memorial University, NL, Canada. The dimensions of the tank are 20 m x 10 m x 2 m (LWD). Freshwater was pumped into the tank before the experiment from a nearby pond. The depth of water in the tank was approximately 1.5 m. Sonar can detect the backscattered sound from oil droplets in the water with the strength of the backscattering determined by the acoustic impedance contrast between ambient water and the oil droplets. For these tests, it was not feasible to fill the tank with seawater. As the density difference between oil and saltwater is larger than the density difference between oil and freshwater, the acoustic impedance contrast is higher for oil in seawater. As such, if the sonar can detect oil in the tank filled with freshwater, it should be able to effectively detect oil when it is spilled in the ocean.

Figure 3-2. Outdoor tank at the Offshore Safety and Survival Center of Memorial University's Marine Institute.

As we could not test a Slocum glider in the tank, a Ping360 sonar and a Cyclops 7 fluorometer were positioned on a small ROV according to their relative location on the Slocum glider (Figure 3-3). This sonar is a single-beam mechanical scanning sonar with a frequency of 750 kHz. Its scanning speed changes depending on the working range. In this experiment, the working range of the sonar was set to be 5 m and the scanning angle was set to be 60° to prevent the sonar from missing the oil plume. As the main objective of this experiment was to test the cooperation between the fluorometer and the sonar, only a noticeable change in the response of the fluorometer that indicated the existence of oil was required when the sonar captured the oil plume. Used engine oil was chosen for this experiment as it was dark in color making it more visible in the water. An initial test was conducted in the laboratory prior to the tank experiments by introducing the used engine oil into freshwater. The change in measurements from the Cyclops was observed and it was found that the Cyclops could clearly detect this oil sample. In the experiment in the outdoor tank, the oil was pumped into the tank from an oil release nozzle (Figure 3-4), thus creating an oil plume in the tank (Figure 3-5).

Figure 3-3. Setup of sensors on a ROV.

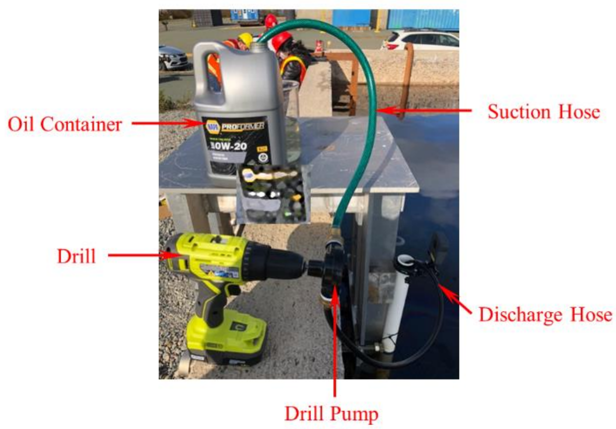

Figure 3-4. Setup of the oil pump in the tank.

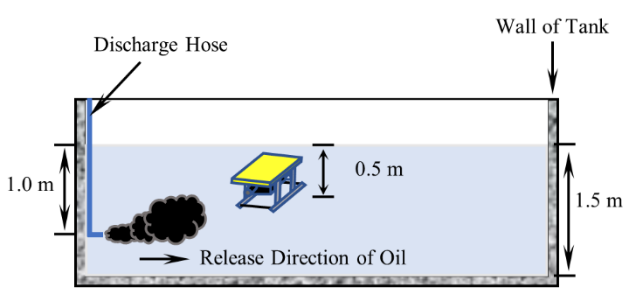

Figure 3-5. Experiment Facility setup.

3.3.2 Experimental results

Before the oil release, there was no oil plume detected in the sonar image (image 1 in Figure 3-6) which corresponded to the relatively low response values from the Cyclops 7 fluorometer. This represented background data for this experiment. In the second sonar image (image 2 in Figure 3-6), an oil plume is visible between the wall of the tank and the sonar, corresponding to the increase in the fluorometer readings from the background level. In the third sonar image, the oil dispersed over a larger space, corresponding to the decrease in the fluorescence readings.

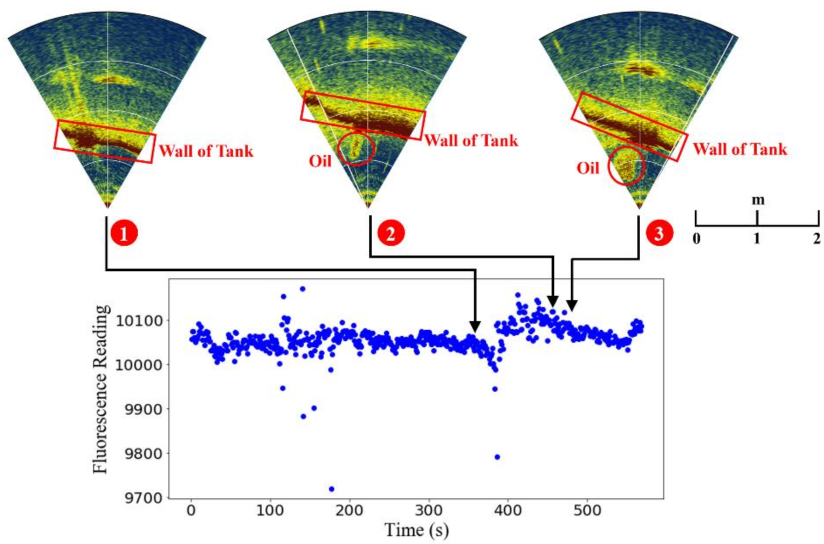

Figure 3-6. Detection of oil by the Cyclops fluorometer (blue dots) and the Ping360 sonar.

In this test, the oil was detected by both the fluorometer and the sonar when the sonar was set at a range of 5 m. The time lag between when the oil was first captured by the sonar and when the oil was detected by the fluorometer was mainly related to the dynamics of the oil as the sensors were static in their position. The dynamics of the oil included the rate of the oil injected into the tank and the dispersion of the oil. The scanning speed of the sonar also contributed to the time lag.

When the sensors are used on a glider, the forward speed of the glider will reduce the time lag between the two sensors.

3.4 Discussion

The variation of the fluorescence readings showed a strong correlation with the sonar image in terms of both time and location of the oil plume. The largest reading was found when the plume reached the sensors and the plume was concentrated as visually seen in the sonar image. The reading from the Cyclops 7 fluorometer started to decrease as the plume dispersed and a lower intensity of acoustic scattering was observed in the sonar image.

The Ping360 sonar used in this experiment with a frequency of 750 kHz was proven to have the ability to detect the oil. In this research, the ROV was steered to a nearly fixed position. In a field experiment with the use of underwater vehicles, the working range and scanning angle should be set based on the working speed of the underwater vehicles and the anticipated motion of the underwater target if a single beam scanning sonar is used.

The fluorometer could detect the used engine oil, however, the sensor used was not sufficiently sensitive when being used in the outdoor tank with water from a pond. Only small changes in the fluorometer readings were observed after the oil was released, which may be due to the sensitivity of the sensor to detect the oil sample or the level of the existing background fluorescence. However, the sensor was found to be sensitive to the oil sample when tested in the lab with clean water. It is possible that the measurements taken with the Cyclops fluorometer in the outdoor tank were affected by background fluorescence. Selecting sensors by using sampled water from the target environment, in this case from the outdoor tank, is important for obtaining sensitive measurements.

In the experiment, the fluorometer was found to be easily coated with oil leading to a constant reading being recorded once oil was encountered. This confirms the benefits of using a sonar to cross validate data from a fluorometer. On the other hand, interpretation of sonar images can be complicated by other naturally occurring particles in the ocean, using a fluorometer can help differentiate oil droplets in an oil detection mission using gliders.

3.5 Conclusion

The experiment verified that it is feasible to measure the presence of oil by using both fluorometers and sonar together to improve the reliability of data collected. The results showed that the proposed cross-validation concept worked well and the time lag could be minimized by setting a short range for the sonar. The benefits of cross-validating data from both sensors were also confirmed from the reduced ability of the fluorometer used in the experiment to provide distinct signal changes when oil was detected. In glider field missions, a sonar can be used to help confirm the presence of oil when a fluorometer is contaminated or affected by surrounding noise, and vice versa.

The experiment in this chapter answered the first research question in Section 1.2 (Q1: Is it possible to improve the reliability of measurements by using a fluorometer and a sonar in a Slocum glider?) and reached the first sub-objective in Section 1.3 (O1: To investigate the performance of a Slocum glider with cooperation between more than one sensor to delineate underwater oil).

Acknowledgement

Funding was received from Fisheries and Oceans Canada through the Multi-partner Oil Spill Research Initiative (MPRI) 1.03: Oil Spill Reconnaissance and Delineation through Robotic

Autonomous Underwater Vehicle Technology in Open and Iced Waters and the School of Graduate Studies at Memorial University of Newfoundland.

References

Abt Associates, Woods Hole Oceanographic Institution, National Oceanic and Atmospheric Administration, U.S. Environmental Protection Agency, Water Mapping, L., 2020. Report to BSEE: Three-Dimensional Mapping of Dissolved Hydrocarbons and Oil Droplets Using a REMUS-600 Autonomous Underwater Vehicle.

Chmiel, O., Baselt, I., Malcherek, A., 2018. Applicability of Acoustic Concentration Measurements in Suspensions of Artificial and Natural Sediments Using an Acoustic Doppler Velocimeter. Acoustics 1, 59–77. https://doi.org/10.3390/acoustics1010006

Cyr, F., Tedetti, M., Besson, F., Bhairy, N., Goutx, M., 2019. A glider-compatible optical sensor for the detection of polycyclic aromatic hydrocarbons in the marine environment. Front. Mar. Sci. 6. https://doi.org/10.3389/fmars.2019.00110

Eriksen, P.K., 2013. Leakage and oil spill detection utilizing active acoustic systems, in: 2013 IEEE International Underwater Technology Symposium, UT 2013. Tokyo, Japan, pp. 1–8. https://doi.org/10.1109/UT.2013.6519891

Li, Z., Lee, K., Kepkey, P.E., Mikkelsen, O., Pottsmith, C., 2011. Monitoring Dispersed Oil Droplet Size Distribution at the Gulf of Mexico Deepwater Horizon Spill Site, in: International Oil Spill Conference Proceedings. International Oil Spill Conference, pp. 1–15. https://doi.org/10.7901/2169-3358-2011-1-377

Maksym, T., Singh, H., Bassett, C., Lavery, A., Freitag, L., Sonnichsen, F., Wilkinson, J., 2014. Oil spill detection and mapping under Arctic sea ice using autonomous underwater vehicles.

Panetta, P.D., Bland, L.G., Cartwright, G., Friedrichs, C.T., 2012. Acoustic scattering to measure dispersed oil droplet size and sediment particle size, in: OCEANS 2012 MTS/IEEE: Harnessing the Power of the Ocean. pp. 1–9. https://doi.org/10.1109/OCEANS.2012.6405103

Panetta, P.D., Bland, L.G., Winfield, K., McElhone, D., Cartwright, G.G., Friedrichs, C.T., 2013. Assessment of Dispersant Effectiveness Using Ultrasound to Measure Oil Droplet Particle Size Distributions.

Pärt, S., Tarmo, K., Kaimo, V., 2017. Oil detection using oil sensors on Autonomous Underwater Vehicles.

Vasilijevic, A., Stilinovic, N., Nad, D., Mandic, F., Miskovic, N., Vukic, Z., 2015. AUV based mobile fluorometers: System for underwater oil-spill detection and quantification, in: SAS 2015 - 2015 IEEE Sensors Applications Symposium, Proceedings. Institute of Electrical and Electronics Engineers Inc., Zadar, Croatia, pp. 1–6. https://doi.org/10.1109/SAS.2015.7133650

Vilcáez, J., Li, L., Hubbard, S.S., 2013. A new model for the biodegradation kinetics of oil droplets: Application to the Deepwater Horizon oil spill in the Gulf of Mexico. Geochem. Trans. 14, 1–14. https://doi.org/10.1186/1467-4866-14-4

Weber, T.C., De Robertis, A., Greenaway, S.F., Smith, S., Mayer, L., Rice, G., 2012. Estimating oil concentration and flow rate with calibrated vessel-mounted acoustic echo sounders. Proc. Natl. Acad. Sci. U. S. A. 109, 20240–20245. https://doi.org/10.1073/pnas.1108771108

Zhao, L., Shaffer, F., Robinson, B., King, T., D’Ambrose, C., Pan, Z., Gao, F., Miller, R.S., Conmy, R.N., Boufadel, M.C., 2016. Underwater oil jet: Hydrodynamics and droplet size distribution. Chem. Eng. J. 299, 292–303. https://doi.org/10.1016/j.cej.2016.04.061

4. Chapter 4

Microbubbles as Proxies for Oil Spill Delineation in Field Tests

Yaomei Wang[1], Craig Bulger[2], Worakanok Thanyamanta[1], Neil Bose[1], Jimin Hwang[3]

1 Department of Ocean and Naval Architectural Engineering, Memorial University of Newfoundland, St. John's, NL A1B 3X7, Canada

2 Centre for Applied Ocean Technology, Fisheries and Marine Institute of Memorial University of Newfoundland, St. John's, NL A1C 5R3, Canada

3 Australian Maritime College, University of Tasmania, Launceston, TAS 7250, Australia

This chapter is a journal paper which has been published in Journal of Marine Science and Engineering (2021), 9(2), 126; https://doi.org/10.3390/jmse9020126 (Article No. 2 (JMSE1)).

Table 4-1. Individual Author Contribution – Article No.2 (JMSE1)

Author	**Contribution**
Yaomei Wang	Conceptualization, Methodology, Software, Validation, Formal analysis, Investigation, Resources, Writing—original draft preparation, Writing—review and editing, Visualization
Worakanok Thanyamanta	Conceptualization, Methodology, Validation, Formal analysis, Investigation, Resources, Writing—original draft preparation, Writing—review and editing, Visualization, Supervision
Craig Bulger	Validation, Investigation, Resources, Writing—review and editing
Neil Bose	Conceptualization, Resources, Writing—original draft preparation, Writing—review and editing, Supervision, Project administration, Funding acquisition
Jimin Hwang	Conceptualization, Validation, Investigation, Resources, Writing—original draft preparation, Writing—review and editing

Abstract

To overcome the environmental impacts of releasing oil into the ocean for testing acoustic methods in field experiments using autonomous underwater vehicles (AUVs), environmentally friendly gas bubble plumes with low rise velocities are proposed in this research to be used as proxies for oil. An experiment was conducted to test the performance of a centrifugal-type microbubble generator in generating microbubble plumes and their practicability to be used in field experiments. Sizes of bubbles were measured with a Laser In-Situ Scattering and Transmissometry sensor. Residence time of bubble plumes was estimated by using a Ping360 sonar. Results from the experiment showed that a larger number of small bubbles were found in deeper water as larger bubbles rose quickly to the surface without staying in the water column. The residence time of the generated bubble plumes at the depth of 0.5 m was estimated to be over 5 minutes. The microbubble generator is planned to be applied in future field experiments, as it is effective in producing relatively long-endurance plumes that can be used as potential proxies for oil plumes in field trials of AUVs for delineating oil spills.

Keywords: Microbubbles; proxy; Oil spill; sonar; Size of bubbles; Residence time

4.1 Introduction

An accidental oil spill can be a major threat to public health resulting in a variety of environmental impacts as well as fatal consequences to the marine ecosystem (Saadoun, 2015). Rapid response and the use of appropriate detection methods and sensors are key to mitigate the undesirable consequences of a spill accident. When released, oil is broken up by turbulence into droplets of various sizes where large droplets tend to rise rapidly to the surface while small droplets tend to be transported horizontally by ocean currents (Socolofsky et al., 2011). Small oil droplets released in the subsurface, particularly those treated with chemical dispersant can stay in the water column for hundreds of hours and form subsurface plumes (Chan et al., 2015; North et al., 2015). Detecting these subsurface plumes attracts our interest as it is an ideal task for AUVs that collect and communicate high resolution information of the plumes in near real-time from the subsurface, a task unachievable by many traditional methods including remote sensing.

The clustering of oil plumes in general ocean conditions is a distinct characteristic that poses challenges in detecting oil plumes with submersible sensors that have been commonly used in the field including fluorometers, particle size analyzers and other chemical sensors (Conmy et al., 2014). By using these sensors and conventional point-based in-situ measurements onboard an autonomous underwater vehicle (AUV), gradient methods have been widely employed to track an oil plume (Pang and Farrell, 2006). However, recent experiments done by our research team have revealed severe limitations of in-situ sensors as a primary sensor to conduct an adaptive mission (Hwang et al., 2020b, 2019), which allows the path of the AUV to be updated and optimized based on real-time sensor data. The clustering characteristics of oil in water can inherently generate consecutive noise-like positive and negative peaks from a fluorometer that might confuse an autonomous signal processor algorithm. The system would have to determine whether these peaks are true positive signals or noise from other possible unknown sources. Hence, gradient approaches using single point sensors are likely to cause confusion to maneuver an AUV in real-time (Hwang et al., 2019). In addition, a point-based sensor can only take measurements where the vehicle is located. As a result, the vehicle must be constantly moving in order to carry out continuous measurements and cannot pre-detect the target oil without entering inside of the body of a plume. It also implies that the survey design requires a relatively high resolution, hence an exhaustive search by the vehicle, to acquire reasonably comprehensive information of the plume such as oil concentrations and its approximate extent. This is neither efficient nor suitable to conduct an adaptive mission. Another common sensor used to detect oil droplets in water is an optical laser diffraction instrument which measures the sizes of particles suspended in water based on scattering technology. The data provided by this sensor may lead to ambiguity especially in the non-confined real ocean that may contain a great number of natural particles. Without measuring additional morphological information of the detected particles in real-time, it is not feasible to differentiate the regular shapes that oil droplets would have from those of other substances in nature.

To overcome these challenges, acoustic backscattering has been used as an alternative means to detect oil plume (Eriksen, 2013). Acoustic devices such as sonars utilize remote detection approach to capture and visually display acoustic backscatters of dynamically dispersing oceanographic targets including oil droplets and methane bubbles in the water column. As such, using this method allows for the use of buoyant acoustic backscattering materials as tracers in field studies.

Another challenge in oil spill research is the ability to perform field experiments in oil spill conditions, as it is inappropriate to release oil into the ocean. Dye tracers, such as Rhodamine WT, are typically used to study oceanographic processes including dispersion of spilled oil as they can be detected effectively at low concentrations (López-Castejón and (Eds), 2019). However, as these tracers are water-soluble, they do not behave like oil which can be distributed in the water column as dispersed, dissolved, and gas phases (Battelle, 2014; Siim Pärt and Kõuts, 2016).

Gas bubbles have a potential of being used as proxies for oil as they are expected to reasonably represent the patchy characteristics oil plumes once released into the ocean. Gas bubbles are environmentally friendly and can be detected well by sonar sensors. Similar to oil droplets, they are buoyant and do not dissolve readily in the water column and thus they are expected to show similar clustering characteristics of oil in water. In addition to their similar transport behaviors in ocean waves and currents, oil droplets and gas bubbles are both acoustic scatters and can be detected by sonars. When released continually, they can form bubble clouds or plumes similar to plumes of oil spills, which can be used during AUV field trials. As gas bubbles rise more quickly than oil droplets, bubbles of micron size, also known as microbubbles, are proposed here for being used as the oil proxy. Definition of microbubbles in the field of fluid physics are bubbles of diameters less than 100 μm (Tsuge, 2014). Different from typical bubbles which rise to the surface and burst, microbubbles rise up and shrink before disappearing in the liquid (Tamura and Adachi, 2014). These tiny bubbles have low buoyancy and slow rise velocities allowing them to stay in the water column for some period until they are detected by sonars equipped on AUVs. Microbubbles have been widely studied and used in various fields including water treatment, water purification, mineral processing, natural ecology restoration, cleaning and medicine (Khuntia et al., 2012;

Tsuge, 2014). Different types of microbubble generators have been developed for large scale applications and many are commercially available.

In this chapter, we propose the use of gas bubble as a proxy for oil in AUV field missions. This chapter presents an initial investigation on the suitability of using air bubbles as proxies for oil droplets. We did not aim to replicate oil droplets but to find some kind of tracer that generates plumes that could be detected by acoustic devices in AUVs. For this purpose, our main interest was the residence time and distribution of gas bubble plumes in the water column to demonstrate that bubble plumes could represent the buoyant characteristics of oil plumes and could stay in the water for a period of time before being detected by acoustic devices. As acoustic backscatters of oil and gas are different, it is not necessary for the bubble plume to have the same quantities of bubbles as oil droplets in order to be effectively detected by acoustic sensors. To prove this concept, we evaluated plumes of air bubbles generated by a commercial microbubble generator and used a sonar sensor to detect the generated plumes. Results from the experiment and the suitability of using microbubbles for oil spill detection studies are presented and discussed.

4.2 Sonar Applications for Oil and Gas Detection

4.2.1 Previous Work

Sonar systems have been used to measure the sizes of oil droplets (Panetta et al., 2012), to detect the oil under surface ice, encapsulated in ice, and sunken on the seafloor (Maksym et al., 2014; Parthiot et al., 2004; Wen and Sinding-Larsen, 1996; Wendelboe et al., 2009), to measure concentrations of oil and gas in the water column (Bello et al., 2017; Clarke, 2011), and to measure the flow rates of oil released during a spill event (Camilli et al., 2012).

Sonars have an advantage over point-based in-situ sensors when used to detect subsurface oil as they can cover a large continuous area as opposed to sampling a discrete volume of the water column (Fitzpatrick et al., 2014). Fluorometers, the most commonly used point-based in-situ oil sensors, are also susceptible to false positives due to disturbance from natural sources of fluorescence present in seawater (Baszanowska and Otremba, 2016). In order to attain effective detection of oil in the water column, a combination of multiple methods employing different working principles are typically required. The use of sonars in conjunction with fluorometers can increase reliability of the detection and help confirm the existence of the oil (Bello et al., 2016). Sonars detect oil by recording the backscattered sound from oil droplets (Wilkinson et al., 2013). The strength of the backscattering is determined by the acoustic impedance contrast between the oil and ambient water (Loranger, 2019). The advantages of sonar systems include the capability of seeing a long distance, seeing at low visibility, and provide quantitative information from acoustic backscatter when the frequency of the system is sufficiently high (Maksym et al., 2014). Besides, sonar systems are less affected by the biofouling compared to the Laser In-Situ Scattering and Transmissometer (LISST) when measuring the size of oil droplets (Panetta et al., 2012).

Sonars are capable of distinguishing two fluids with low impedance contrast, such as crude oil and seawater, and detecting oil at low concentrations (Loranger, 2019). This was proven in a study where a 400 kHz Wide Band Multi-Beam sonar was used to effectively detect freshwater injected into the saltwater, two fluids with small difference in reflectivity (Fitzpatrick and Tebeau, 2013). Another test performed at the Navy facility Oil and Hazardous Materials Simulated Environmental Test Tank, New Jersey of the U.S. showed that sonars with a nominal operating frequency of 400 kHz were able to capture a well-dispersed plume with low oil-in-water concentrations (Eriksen, 2013). The result exceeded the expectation of a high-frequency sonar to detect oil at low concentration. For detection of gas bubbles, such as greenhouse gas methane, sonar is the most commonly used sensor as gas bubbles have strong acoustic scattering (Leifer et al., 2017; Scandella et al., 2013; Veloso et al., 2015). In the work of Uchimoto et al. (2018), the experiment found that a 600 kHz side-scan sonar could detect underwater CO2 bubbles of 1 – 2 mm and 1 cm in diameter, the sizes of natural seep bubbles (von Deimling et al., 2010). Moreover, sonars are superior to underwater video cameras in surveying well-dispersed gas bubbles as videos are restricted to smaller areas (Klaucke et al., 2005; Leifer et al., 2017).

As there were no industry-accepted means to measure the flow rate of the hydrocarbon fluid, an acoustic imaging sonar (1.8 MHz) and an acoustic Doppler sonar (1.3 MHz) were used to measure the flow rates of the hydrocarbon released from the Deepwater Horizon Macondo well on 31 May 2010 (Camilli et al., 2012). The acoustic imaging sonar was used to record horizontal cross-section images of the flowing fluid, while the Doppler sonar provided vertical velocities of the flow. The method used provided consistent result with other studies (Crone and Tolstoy, 2010), which verified usefulness of sonar systems and suitability of sonars for oil detection.

The effectiveness of sonars in detecting oil droplets and gas bubbles is highly dependent on their operating frequencies. Weber et al. (2012) used an acoustic method to quantify the amount of oil surfacing with ship-mounted acoustic Simrad ES60 echo sounders. These echo sounders were operated at the frequencies of 12, 38 and 200 kHz. The anomalously high return detected by the 200-kHz echo sounder above the depth of 200 m was in accordance with the visual observation of the oil from the surface. However, similar anomalous backscattering was not observed by the echo sounders operating at lower frequencies of 12 and 38 kHz. Another study used a sonar with the operating frequency of 5 MHz to measure oil droplets size in an oil-water-dispersant mixture (Panetta et al., 2012). The frequency of the sonar was much higher than the resonant frequency for the size of detected oil droplets. The comparison with measurements from a LISST sensor showed a good performance of the acoustic method. From the above studies, high operating frequencies tend to provide better oil detection. However, the frequency should not be too high as the signal attenuation will increase at a higher frequency leading to a shorter range of the sonar (Panetta et al., 2012). The optimum frequency of a sonar depends on the size of oil droplets, the coverage distance, and the level of ambient noise (Wilkinson et al., 2013). A tank experiment with the use of an Acoustic Zooplankton and Fish Profiler multiple-frequency echo sounder showed that the submerged oil was detectable with the frequencies of 455, 769, 1250 and 2000 kHz (David and Mudge, 2018). Results from the study showed that the size of oil droplets was in the order of 100 µm (David and Mudge, 2018). Moreover, the lower frequency could be also effective in detecting oil droplets if the size of the droplets was larger. Similarly, the size of gas bubbles is essential when selecting the frequency of a sonar. Szczucka (Joanna Szczucka, 1989) noted that "acoustic determination of the concentration of gas bubbles in the sea is based on the phenomenon of resonant backscattering" and "a bubble of a definite size resonates with an incident acoustic wave of a precisely defined frequency, inversely proportional to a bubble radius".

Types of sonars are also important in selecting a sonar system for oil and gas detection. The types of sonars that have been used to detect suspended oil droplets and gas bubbles include echo sounders, sider-scanning sonars, multibeam sonars (Balsley et al., 2013; Blomberg et al., 2017; Johansen et al., 2003; Klaucke et al., 2005). Multibeam echo sounders excelled the single-beam echo sounders in determining the plume's geometric feature (Leifer et al., 2017). An experiment with a focus on detecting sunken oil on the sea bottom compared capabilities of various types of sonars including a side-scan sonar, a multibeam/panoramic sonar, a 3D acoustic camera, and a front-looking sonar, with frequencies ranging from 100 kHz to 600 kHz. The high-frequency sonars (200–500 kHz) were found to have the ability to detect oil patches with low reflectivity. The side-scan sonar can quickly find the position of oil as a wide swath. More precise detection was achieved from the multibeam sonar, the 3D acoustic camera, and the front-looking sonar (Parthiot et al., 2004). These findings related to sunken oil can be used as a reference when considering the application of sonars in detecting oil droplets and gas bubbles in the water column.

To confirm the potential use of sonar for oil detection in future AUV experiments, proof-of-concept experiments were conducted as described below.

4.2.2 Proof-of-Concept Sonar Experiment

Aiming to overcome the challenges in using point-based in-situ sensors in AUV oil spill missions, we investigated the use of sonar in future AUV experiments. Two sonar instruments were tested for proof-of-concept. A set of tests were conducted in the wave tank facility at the Bedford Institute of Oceanography, Dartmouth, Nova Scotia, Canada on 31 July 2019 (Hwang et al., 2020a). The facility is operated by the Centre for Offshore Oil, Gas and Energy Research, Department of Fisheries and Oceans Canada. Alaska North Slope crude oil and two different sonar sensors were selected for the test: the BV5000 3D scanning sonar and the M450 2D sonar of Teledyne Blueview. The frequencies of these sonars were 1.35 MHz and 450 kHz, respectively. The results demonstrated that both sonars were capable of detecting oil in advance of an AUV (by using a forward-looking sonar) and at a distance, unlike other in-situ oil sensors that had been used to date. An oil plume consisting of a number of small droplets as well as a significant amount of noise were detected by the M450 sonar. By comparison, the acoustic pings at higher frequency generated by the BV5000 resulted in clearer sonar images at a distance of 2.5 m from the sonar head. The fan-shaped sonar images also captured the upward moving process of the plume as it rose to the surface. These proof-of-concept-test results indicated that acoustic sensors may have the following potential advantages in detecting oil from an AUV in the ocean:

(1) An oil plume can potentially be pre-detected by an AUV prior to entering the plume.

(2) Sonar fan-shaped image display is more suitable than point-based oil sensors for discontinuous oil patches to make an adaptive decision on the next waypoints or trajectory to delineate the plume.

(3) The two-dimensional survey of the scanning sonar has advantages over a point-based survey to undertake an adaptive mission for a dynamically dispersing target such as an oil plume.

4.3 Experiment Setup

In this study, we propose using gas bubbles as environmentally friendly proxy for oil in AUV field experiments so as to allow AUVs equipped with sonars to be tested in realistic oil spill conditions without releasing oil into the ocean. When bubbles are generated with hydrocarbon gas, such as methane or butane, a sonar can be used with hydrocarbon gas sensor for cross-validation. However, in our experiments, air bubbles were used to minimize health and environmental risks posed by releasing hydrocarbon gases, such as methane which is a known greenhouse gas. The proposed gas bubble plumes were generated using a commercial microbubble generator. Microbubbles have slow rise velocity leading to plumes that remain in the water column for a period of time before being detected by a sonar and/or other sensors. An experiment was conducted to test the microbubble generator in creating bubble plumes and characterize the plumes in terms of bubble size, residence time, and suitability to be used in the ocean. The experiment also aimed to evaluate a sonar sensor on its performance in detecting the bubble plumes.

4.3.1 Bubble Generator

The system that we tested was a microbubble pump, Karyu Turbo Mixer (KTM) pump, developed by Nikuni Co., Ltd in Kawasaki, Kanagawa, Japan, (see Figure 4-1). The centrifugal pump uses a principle similar to the dissolved air flotation method (Zedel and Butt, 2011). However, the air dissolution and mixing occur simultaneously as the air and water are drawn in and pressurized by the mechanics of the uniquely designed turbine impeller. A combination of frictional, axial, and centrifugal forces created by the impeller helps enhance entrainment of air by breaking the air into small bubbles and generating high operating pressure (Etchepare et al., 2017). Atmospheric air is drawn into the low-pressure suction side of the pump eliminating the need of an air compressor. A large mixing tank is also not required leading to a more compact system that is suitable to be used at sea if needed. The average size of the microbubbles produced by this system is 25 μm but a dimeter of less than 10 μm can be obtained by varying operating conditions including air and water flowrates and pressure (Aeration & Mixing Ltd, 2015).

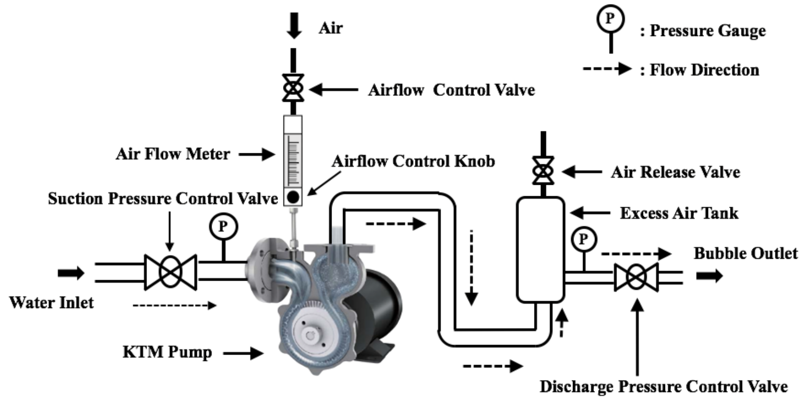

Figure 4-1. A sketch of the microbubble generator with the use of KTM pump.

4.3.2 Sensor Suite

The sonar used in the experiment was a Ping360 sonar from Blue robotics, Torrance, CA, USA (see Figure 4-2). Specifications of the sonar are presented in Table 4-2. The Ping360 is a mechanical scanning imaging sonar that has a 50 m range and can work to a depth of 300 m. It was designed to be used for navigation on ROVs such as BlueROV2 (BlueRobotics, 2020a), but can also be used for obstacle avoidance, inspection, tracking, and so on. In the experiment, we used the Ping360 to detect microbubbles generated by the KTM pump and evaluated the residence time of bubbles. In this chapter, the residence time was the length of time that the bubble plume stayed in the water column at one depth (within the vertical range of the sonar) as captured by the sonar.

The sizes of bubbles generated by the microbubble generator were measured using a Laser in-situ Scattering and Transmissometry (LISST-200X) sensor (see Figure 4-3). LISST-200X, developed by Sequoia Scientific Inc. in Bellevue, WA, USA, was designed for measuring particle sizes and concentrations in water. The LISST-200X is rated to a depth of 600 m and can cover a size range between 1 and 500 microns, which is the range of our interest (Sequoia Scientific, 2018). Other measurements provided by LISST-200X also include temperature and depth.

Figure 4-2. Ping360 mechanical scanning imaging sonar.

Table 4-2. Specifications of Ping360 (BlueRobotics, 2020b).

Parameter	**Value**
Frequency	750 kHz
Supply Voltage	11–25 volts
Beamwidth (Horizontal)	2°
Beamwidth (Vertical)	25°
Working Range	0.75–50 m
Weight in Air	510 g
Scan Speed at 2 m	9 s/360°
Scan Speed at 50 m	35 s/360°
Range Resolution	0.08% of the range

Figure 4-3. LISST-200X.

4.4 Experiment and Results

4.4.1 Experimental Setup

A detailed experiment was conducted in the tow tank of the Ocean Engineering Research Centre (OERC) at the Memorial University of Newfoundland (see Figure 4-4). The tank has a length of 54 m which was beneficial as the dispersion of the microbubbles was not restricted by the tank boundaries. The observation window looking into the side of the tow tank helped to capture the motion of the bubbles. The tank was filled with clean water before the experiment which was favorable for the measurements of the sonar and the LISST-200X. Figure 4-5 shows the setup of the KTM microbubble generator on a bridge in the tow tank.

Figure 4-4. OERC tow tank of Memorial University of Newfoundland.

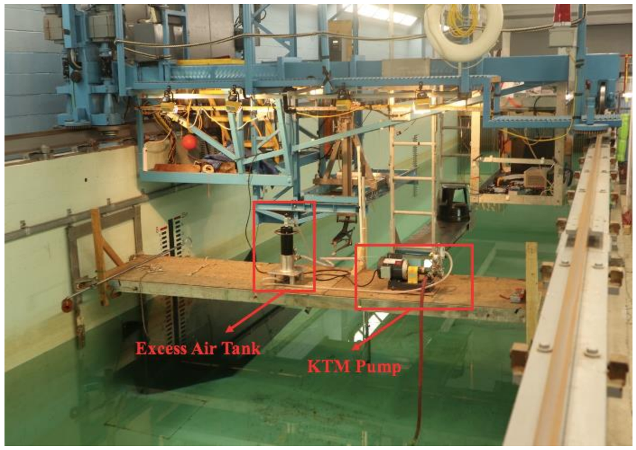

Figure 4-5. The setup of the Nikuni KTM pump in the tow tank.

In the experiment, the LISST-200X sensor was set up in front of the release nozzle; the bubble cloud passed through the sensing range of the LISST-200X (see Figure 4-6). The Ping360 sonar was placed to one side of the release nozzle, with its horizontal scanning direction covering the passing plume. Nine sets of sampling positions were selected to precisely measure the distribution and motion of the bubbles (see Table 4-3 and Figure 4-7). The horizontal and vertical distances between adjacent sampling positions were selected to be 0.5 m to cover the length and height of the plume based on visual observation. In our experiment, the water in the tank remained static except for the disturbance from the water and bubbles coming from the discharge nozzle.

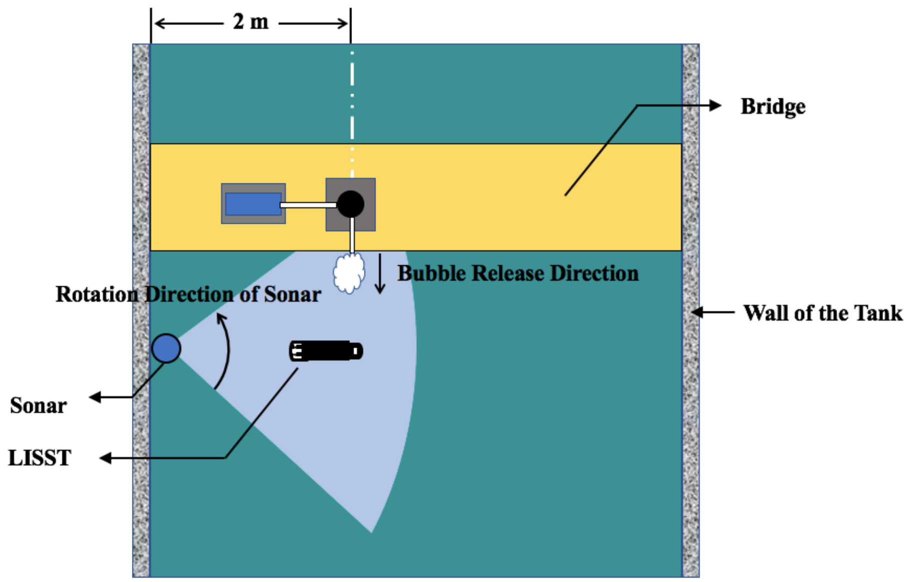

Figure 4-6. Top view of the setup of the sonar and LISST-200X in the tow tank.

Table 4-3. The number of test and corresponding positions of sonar and LISST-200X.

Test No.	Position of Sonar	Position of LISST-200X
1	1	A
2	2	B
3	3	C
4	4	D
5	5	E
6	6	F
7	7	G
8	8	H
9	9	I

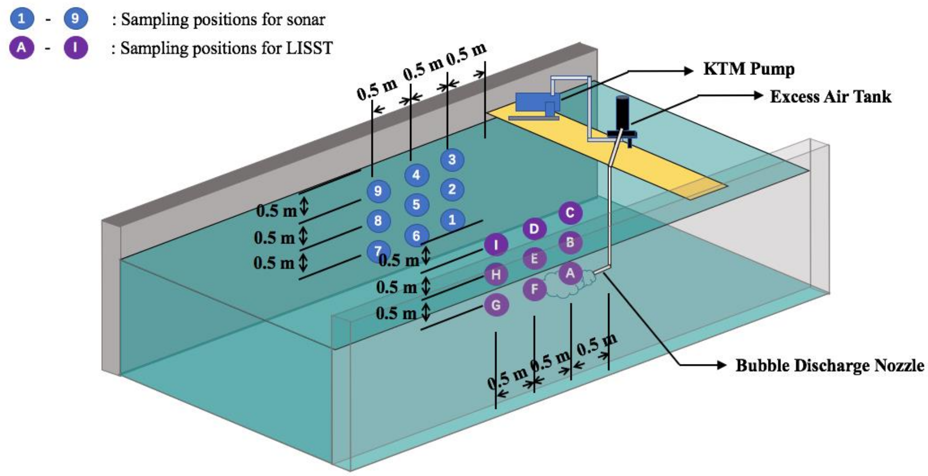

Figure 4-7. Sampling positions for the sonar and LISST-200X in the tow tank.

The sequence of the tests is indicated by the red arrows shown in Figure 4-8. When the sonar and the LISST were set in their positions, these two sensors were started up to collect background information for one minute. This background information was a reference for calculating the residence time of bubbles. Then, the bubble generator was turned on to generate bubbles for more than 3 min in order to get stable a plume. The bubble generator was then stopped and the sonar and the LISST continued their measurements until there was no clear plume visible in the sonar image. The amount of time after pump was shut off until the plume disappeared from the sonar image was approximated as the residence time of the bubbles in the water at the specified depth. The bubble plume generated by the KTM pump can be seen in Figure 4-9.

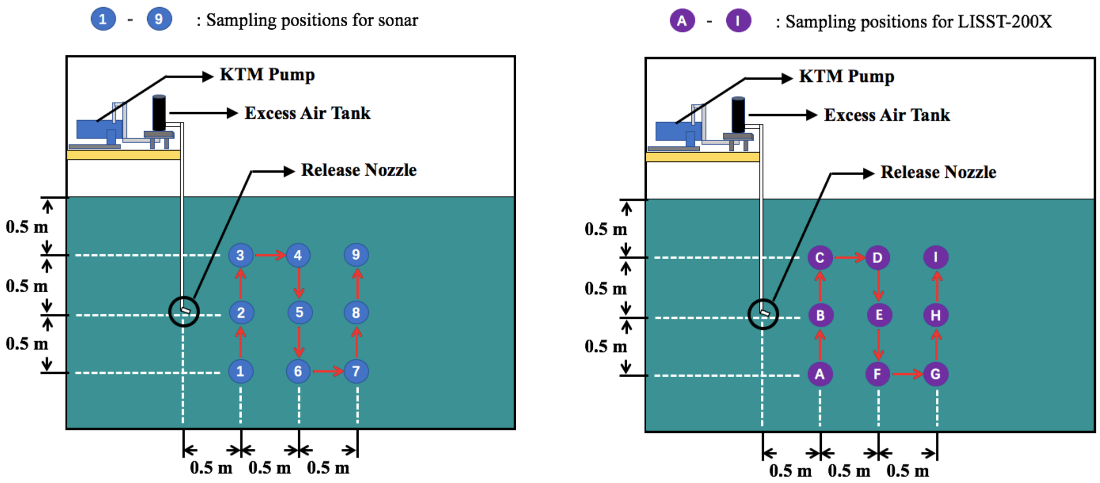

(a) (b)

Figure 4-8. Side view of the sampling positions for (a) sonar and (b) LISST-200X in the tow tank.

Figure 4-9. Bubble plume generated by the KTM pump in the tow tank.

4.4.2 Measurements from the Experiment

4.4.2.1 Bubble Size Distribution

The size distributions of the bubbles collected by the LISST-200X sensor at the 9 sampling positions when the bubble generator was working are shown in Figure 4-10. This can help understand size distribution of the bubbles at different locations within the plume. The sampling position C, D, and I were at a higher altitude than the release nozzle, the sampling position B, E, and H were at the same depth as the release nozzle, and the sampling position A, F, and G were lower than the release nozzle. From the bubble size distribution, it can be observed that:

(1) A higher proportion of smaller bubbles was found at deeper positions. For example, at position F which was at a depth of 1.5 m, more than 90% of the bubbles were smaller than 100 microns, while at position E which was at the depth of 1.0 m, the majority were within the range of 100–150 microns. At a shallower position (position D), more large bubbles between 200 and 250 microns were found. The difference in size distribution at varied depths was owing to the rise velocities of differently sized bubbles. Large bubbles rose quickly toward the water surface while small bubbles rose more slowly leading to a larger proportion of small bubbles staying at depth.

(2) A larger percentage of smaller bubbles were collected at the farthest distance from the release nozzle. For example, at the water depth of 1.5 m, only 80% of bubbles found at position A were smaller than 100 microns while almost all the bubble (99%) found at position G were smaller than 100 microns. For position C, D, and I, a larger proportion of bubbles with sizes smaller than 250 microns were collected at position I, the longest distance from the release nozzle among the 3 positions placed at 0.5 m water depth.

The variation of bubble sizes in the horizontal direction was partly impacted by the different rise velocities of the bubbles where larger bubbles, having higher rise speeds velocities, surfaced quickly without travelling a long distance horizontally. In addition, in the experiment, the release nozzle released the bubbles at an angle of inclination of 20° (see Figure 4-11), which defined the path of the plume and made bubbles, especially smaller bubbles as they tend to travel horizontally rather than upwards, go to deeper water as they moved further away from the nozzle.

There was also some exception to the size distribution in the horizontal direction. For example, at the water depth of 1.0 m, bubbles smaller than 150 microns comprised more than 50% of the bubbles found at position H, and only 41% for position E. However, at position B which was closest to the release nozzle, a higher percentage of more than 70% were observed. At both C and I, 3% of bubbles were between 50–100 microns while there were no bubbles in this size range at position D. 37% of bubbles at position C was in the size range of 100–200 microns, 32% of bubbles at position D were in the size range of 100–200 microns, and 32% of bubbles at the position I were in the size range of 100–200 microns.

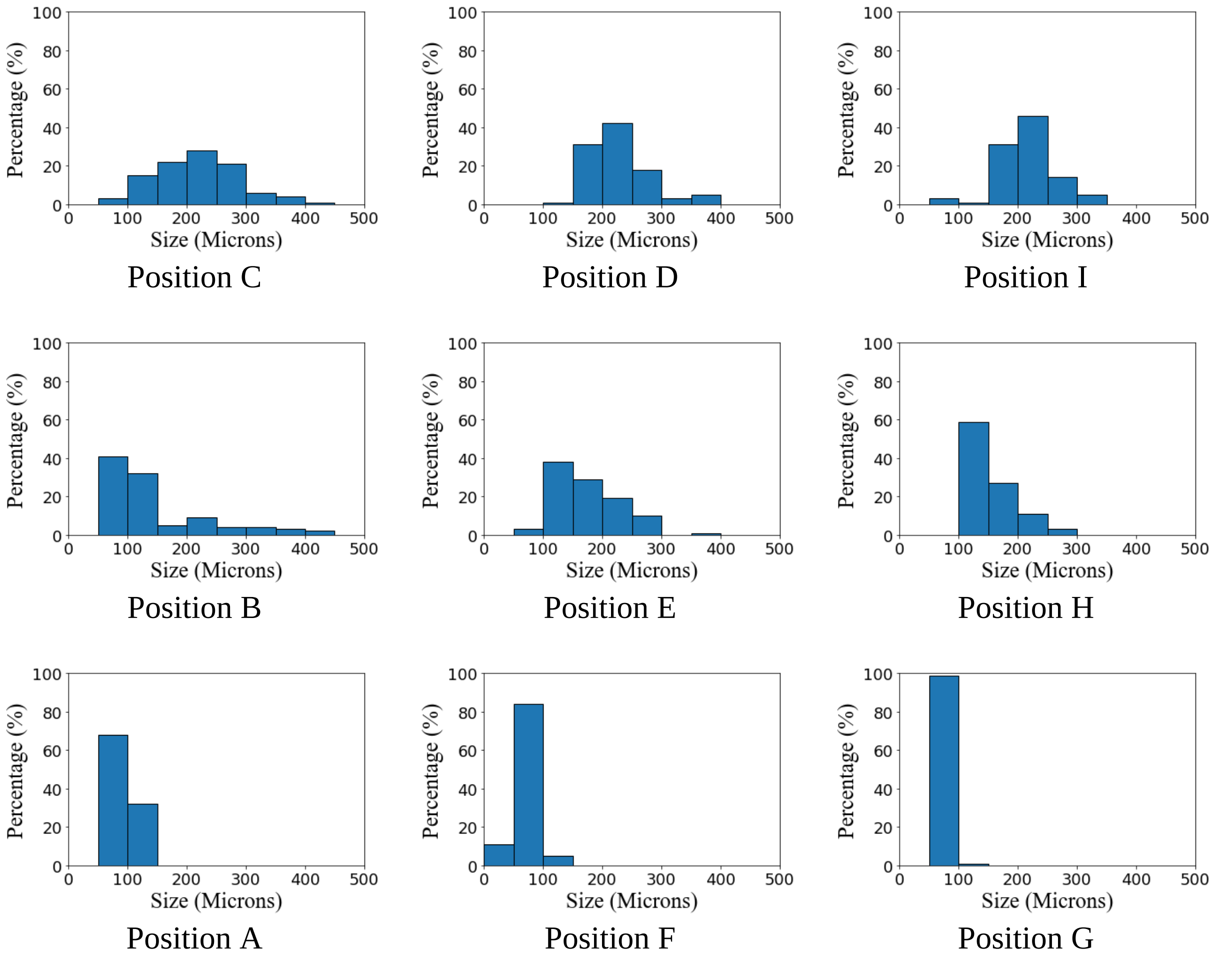

Figure 4-10 Distribution of the bubble size at 9 sampling positions.

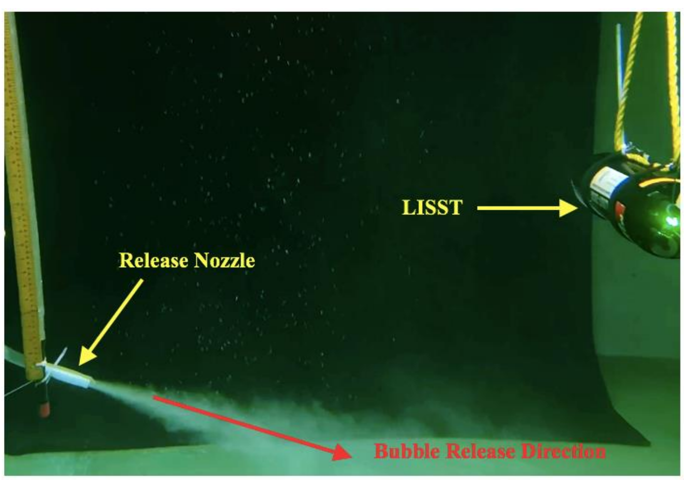

Figure 4-11. Bubbles released from the nozzle.

4.4.2.2 Residence Time of Bubbles

The residence time of bubbles was estimated based on sonar images. The length of time from when the bubble generator was stopped until the time when no clear bubble plume could be observed from the sonar image was assumed to be the residence time of bubbles in the water column. In this experiment, it was assumed that the highest concentration of bubbles was on the vertical plane along the centerline of the plume and parallel to the side wall of the tank (Plane A in Figure 4-12). Therefore, the length of time that bubbles stayed on this plane after the bubble generator was shut off was measured as the residence time. As the sonar used was a mechanical scanning sonar and had a vertical beamwidth of 25°, the residence time of bubbles measured at sampling point 1 represents the residence time of the bubbles within the rectangle area (region 1) in Figure 4-13, which overlaps the sampling region of point 2.

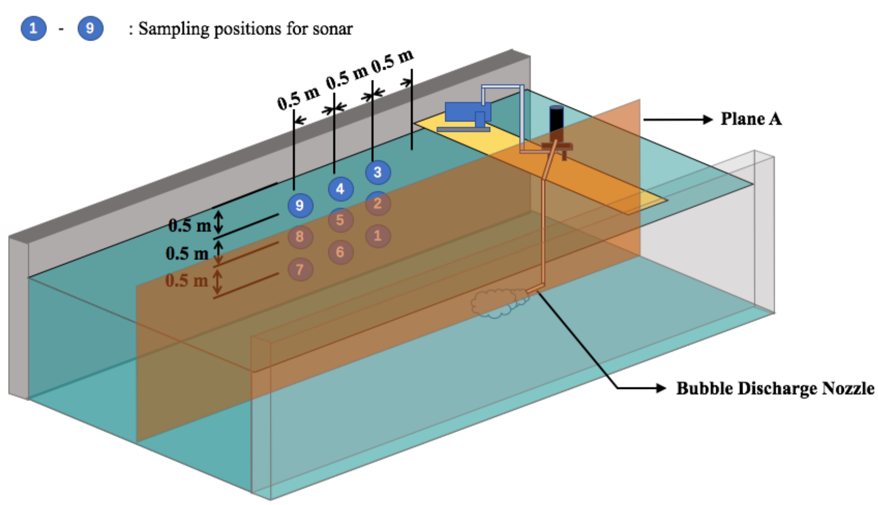

Figure 4-12. Sketch of plane A that intersected the release nozzle and was parallel to the sidewall of the tank which was used for measuring the residence time of bubbles.

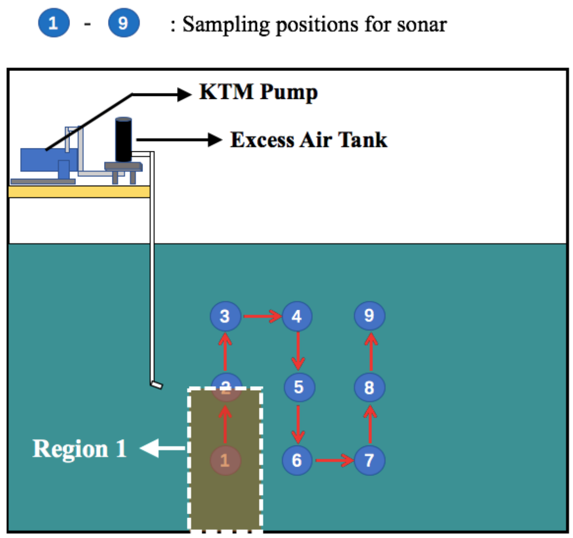

Figure 4-13. Sketch of the area that was used to measure the residence time of bubbles detected by the sonar at sampling point 1.

The sonar images collected from position 3, before the start of the bubble generator, when the bubble generator was working, and when there was no plume on the vertical plane for calculating residence time after the bubble generator was stopped, are presented in Figure 4-14. In Figure 4-14 (c), there were no visible bubbles in the sonar image in region 1 and above, which was regarded as the disappearance of bubbles.

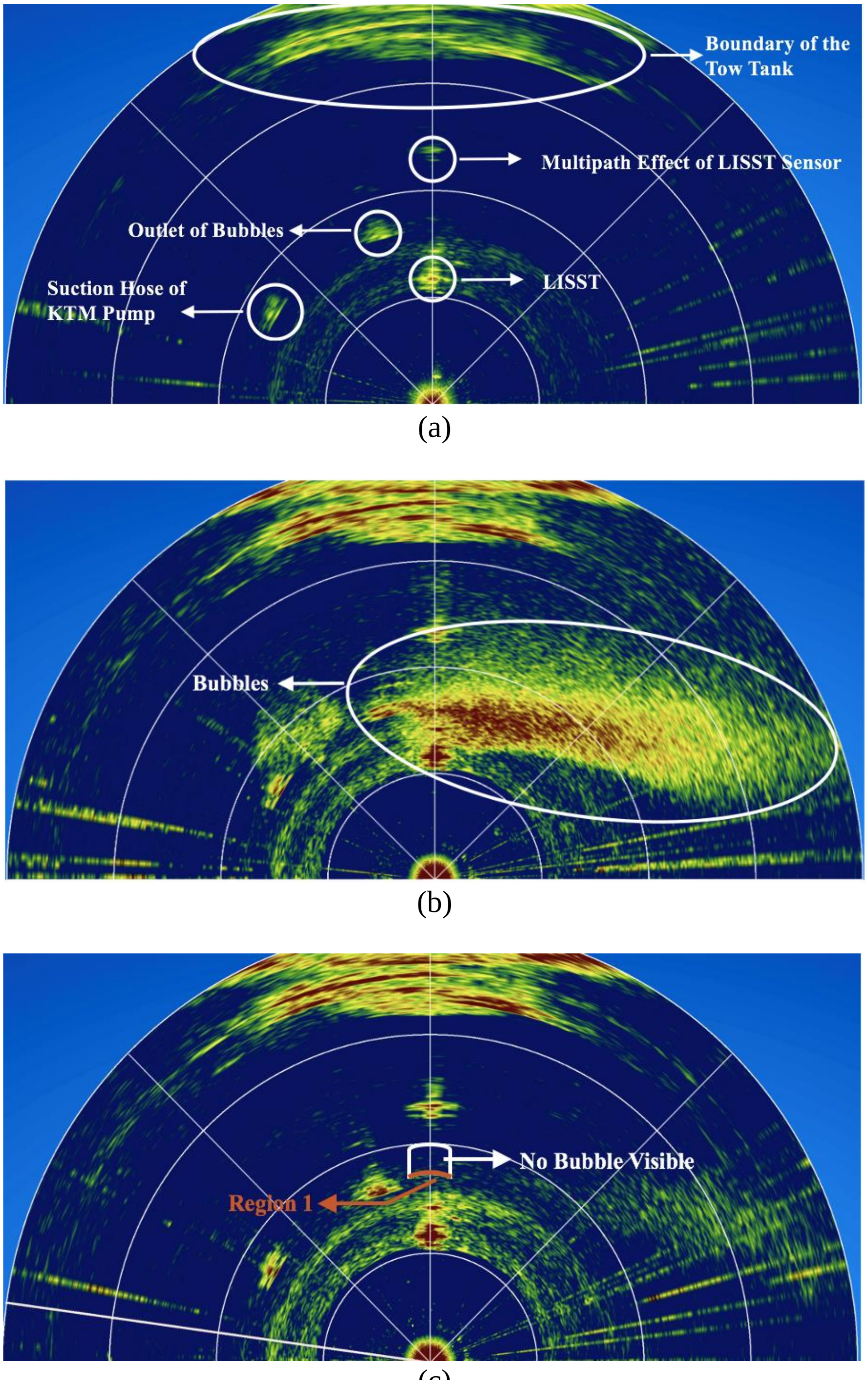

Figure 4-14. Sonar image collecting at sampling position 3: (a) before the start of the bubble generator; (b) with the bubble generator working; (c) and when there was no plume on the vertical plane for calculating residence time.

The residence times of bubbles calculated at the nine sampling positions are presented in Table 4-4:

(1) The residence time decreased with an increase in water depth. One can expect bubbles to rise up from deeper to shallower water. Therefore, the residence time measured at a shallower position, e.g., position 3, can be considered to be the length of time from the first bubbles appeared in this shallow water region when the bubble generator was stopped until the time when the last bubble that rose from the deeper water to this region disappeared.

(2) In most cases, the residence time of bubbles increased with the distance from the release nozzle. This was because the release nozzle had an inclination angle which drove the bubbles deeper away from the nozzle. There was an exception at the depth of 0.5 m where the residence times of bubbles at position 3, 4, and 9 were 304 s, 364 s, and 323 s respectively. For position 9, the residence time of the bubbles was shorter than that collected at position 4. Considering position 9 to be the furthest point from the center of the plume, this phenomenon was possibly caused by bubbles disappearing due to shrinking or dissolution of the gas as they rose through the water column toward the surface. Besides, at a longer distance from the nozzle, the low density of bubbles at shallower depth also affected the images collected by the sonar, which affects the calculation of residence time at the end. Moreover, the residence times obtained at these positions may have been affected by the bubbles that rose up from positions directly underneath them (position A, F, and G, respectively). As position F had a higher percentage of bubbles below the size of 50 microns compared with position A and G, these bubbles may have risen up slowly to the depth of 0.5 m, contributing to longer residence time collected at position 4. This was

also witnessed at position A and G. Position G has a higher percentage of small bubbles within the size range of 50-100 microns than position A, which probably resulted in the residence time collected at position 9 being longer than that at position 3.

Table 4-4. Residence time of bubbles calculated at different sampling positions from sonar.

	Distance *: 0.5 m	**Distance: 1.0 m**	**Distance: 1.5 m**
Depth: 0.5 m	Position 3: 304 s	Position 4: 364 s	Position 9: 323 s
Depth: 1.0 m	Position 2: 106 s	Position 5: 148 s	Position 8: 214 s
Depth: 1.5 m	Position 1: 65 s	Position 6: 77 s	Position 7: 133 s

* Distance means the horizontal distance from sonar to the nozzle which is shown in Figure 4-7.

4.5 Discussion

In the experiment, a LISST-200X was used to evaluate the size that a microbubble generator can generate, and a sonar was used to investigate the residence times of bubble plumes generated by the pump in the water column. By comparing the data from the LISST-200X and Ping360 sonar, at the water depth of 1.5 m, a larger proportion of smaller bubbles was observed at a longer distance from the release nozzle; the residence time was also longer. As smaller bubbles have low rise velocities, they took a longer time to surface. This observation cross validates the data collected from the LISST-200X sensor and the sonar. When the depth was reduced to 1 m, the residence time of bubbles was longer away from the release nozzle, and longer than the residence time at the corresponding position at the depth of 1.5 m. Although the size of bubbles collected at the point closest to the release nozzle at the depth of 1.0 m did show a higher percentage of smaller bubbles than at a further distance, the small bubbles that rose up from the depth of 1.5 m could have contributed to the longer residence time at the points further away from the nozzle. At the water depth of 0.5 m, a larger proportion of bubbles smaller than 200 microns was collected at a distance of 0.5 m, closest to the nozzle; however, the residence time at this location was shorter than the other two positions. This could be due to different bubble concentrations at different positions within the plume. For the depth of 0.5 m, a higher concentration of bubbles was found at the distance of 1 m where the longest residence time was observed.

From the sonar images of the experiment conducted in the tow tank, the generated bubble plumes were invisible at approximately 6 m from the release nozzle. In this experiment, there were no waves or current and thus the influence of waves and currents on the motion of the bubble plumes was not tested. When releasing microbubbles in the ocean, waves and currents may have various effects on the plume; they may help extend the outer boundary of the plume providing the AUVs with larger survey area but may also cause the bubble clouds to disperse so thinly that they are undetectable by sonars.

Our next step will be to test this KTM pump and the sonar in the ocean before being applied in AUV missions. It is expected that the bubbles will stay for a longer time than the residence time observed in the lab experiment by releasing the bubbles from deeper water. Moreover, it is also expected that the disturbance from waves and current could drive the bubbles to a further distance from the release nozzle and break the plume into patches of bubble clouds in the water.

4.6 Conclusions

In this chapter an experiment was conducted in a lab to investigate the possibility of using gas bubbles as proxies for oil in AUV field missions. The main interest of this investigation was the residence time and distribution of gas bubble plumes in the water column. The residence time and distribution of gas bubble plumes can represent the buoyant characteristics of gas bubbles and the length of time of bubbles remain in the water column before being detected by acoustic sensors on an AUV. Results from the experiment showed that:

(1) A Nikuni KTM pump was able to generate bubbles with sizes less than 100 microns.

(2) A Ping360 sonar with a frequency of 750 kHz was found to have the ability to detect microbubble plumes which contain bubbles with sizes less than 100 microns.

(3) Smaller bubbles were found at a higher percentage of the total numbers of bubbles in deeper water, such as at the depth of 1.5 m, as large bubbles having higher rise velocities surfaced quickly without staying in the water column.

(4) The residence time of the bubble plumes at the depth of 0.5 m was estimated to be over 5 min. The bubbles were generated by the Nikuni KTM pump and released in less than 2 m of water at a depth of 1 m and an inclination angle of 20°.

From the experiment results, it is expected that the residence time of the bubbles can be longer if the bubbles are released from deeper water. The bubble generator developed based on the KTM pump is planned to be applied in future field experiments, as it was effective in producing long-endurance plumes that can be used as a potential proxy for oil plumes in field trials of AUVs for delineating oil spills. It is also expected that the disturbance from waves and current could drive the bubbles to a further distance from the release nozzle and break the plume into patches of bubble clouds in the water.

As field experiments were desired to investigate the performance of a Slocum glider with the cooperation of sensors to delineate underwater oil, the experiment done in this chapter was a preparation for testing the developed glider with sensors (shown in Section 8.2) for reaching the first sub-objective in Section 1.3 (O1: To investigate the performance of a Slocum glider with cooperation between more than one sensor to delineate underwater oil). The possibility of using microbubbles as proxies for oil droplets was investigated in this chapter before testing the developed glider in the simulated oil plumes.

Acknowledgement

Funding was received from Fisheries and Oceans Canada through the Multi-partner Oil Spill Research Initiative (MPRI) 1.03: Oil Spill Reconnaissance and Delineation through Robotic Autonomous Underwater Vehicle Technology in Open and Iced Waters and the School of Graduate Studies at Memorial University of Newfoundland.

References

Aeration & Mixing Ltd, 2015. Nikuni KTM gas-mixing fine bubble generating pumps [WWW Document]. URL https://www.aerationmixing.co.uk/products/nikuni-ktm-gas-mixing-fine-bubble-generating-aerator-pumps/ (accessed 10.27.20).

Balsley, A., Hansen, K., Fitzpatrick, M., 2013. Detection of oil within the water column, in: Proceedings of the 36th AMOP Technical Seminar on Environmental Contamination and

Response. pp. 548–564. https://doi.org/10.7901/2169-3358-2014.1.2206

Baszanowska, E., Otremba, Z., 2016. Fluorometry in application to fingerprint of petroleum products present in the natural waters. J. Eur. Opt. Soc. 12, 1–9. https://doi.org/10.1186/s41476-016-0018-4

Battelle, 2014. Capabilities and Uses of Sensor-Equipped Ocean Vehicles for Subsea and Surface Detection and Tracking of Oil Spills, IPIECA/IOGP Oil Spill Response JIP.

Bello, J., Eriksen, P., Pocwiardowski, P., 2017. Oil Leak Detections with a Combined Telescopic Fluorescence Sensor and a Wide Band MultiBeam Sonar, in: International Oil Spill Conference Proceedings. International Oil Spill Conference, pp. 1559–1573. https://doi.org/10.7901/2169-3358-2017.1.1559

Bello, J.M., Eriksen, P., Pocwiardowski, P., 2016. Report to BSEE: Oil Leak Detections with a Combined Fluorescence Polarization Instrument and a Wide Band MultiBeam Sonar Phase II Final Report Work Performed Under Contract E14PC00033 Bureau of Safety and Environmental Enforcement (BSEE) Oil Spill Response Research Branch.

Blomberg, A.E.A., Sæbø, T.O., Hansen, R.E., Pedersen, R.B., Austeng, A., 2017. Automatic Detection of Marine Gas Seeps Using an Interferometric Sidescan Sonar. IEEE J. Ocean. Eng. 42, 590–602. https://doi.org/10.1109/JOE.2016.2592559

BlueRobotics, 2020a. BlueROV2 - Affordable and Capable Underwater ROV [WWW Document]. URL https://bluerobotics.com/store/rov/bluerov2/ (accessed 3.11.20).

BlueRobotics, 2020b. Ping360 Scanning Imaging Sonar for ROVs [WWW Document]. URL https://bluerobotics.com/store/sensors-sonars-cameras/sonar/ping360-sonar-r1-rp/ (accessed 10.27.20).

Camilli, R., Di Iorio, D., Bowen, A., Reddy, C.M., Techet, A.H., Yoerger, D.R., Whitcomb, L.L., Seewald, J.S., Sylva, S.P., Fenwick, J., 2012. Acoustic measurement of the Deepwater Horizon Macondo well flow rate, in: Proceedings of the National Academy of Sciences of the United States of America. National Academy of Sciences, pp. 20235–20239. https://doi.org/10.1073/pnas.1100385108

Chan, G.K.Y., Chow, A.C., Adams, E.E., 2015. Effects of droplet size on intrusion of sub-surface oil spills. Environ. Fluid Mech. 15, 959–973. https://doi.org/10.1007/s10652-014-9389-5

Clarke, J.E.H., 2011. Gas Plumes analysis using Multibeam EM710 Water Column Image in Saint John River Hesham Elhegazy. Fredericton, New Brunswick, Canada.

Conmy, R.N., Coble, P.G., Farr, J., Wood, A.M., Lee, K., Pegau, W.S., Walsh, I.D., Koch, C.R., Abercrombie, M.I., Miles, M.S., Lewis, M.R., Ryan, S.A., Robinson, B.J., King, T.L., Kelble, C.R., Lacoste, J., 2014. Submersible optical sensors exposed to chemically dispersed crude oil: Wave tank simulations for improved oil spill monitoring. Environ. Sci. Technol. 48, 1803–1810. https://doi.org/10.1021/es404206y

Crone, T.J., Tolstoy, M., 2010. Magnitude of the 2010 gulf of Mexico oil leak. Science. 330, 634. https://doi.org/10.1126/science.1195840

David, L., Mudge, T., 2018. Acoustic Detection of Subsurface Oil.

Eriksen, P.K., 2013. Leakage and oil spill detection utilizing active acoustic systems, in: 2013 IEEE International Underwater Technology Symposium. Tokyo, Japan, pp. 1–8. https://doi.org/10.1109/UT.2013.6519891

Etchepare, R., Oliveira, H., Nicknig, M., Azevedo, A., Rubio, J., 2017. Nanobubbles: Generation using a multiphase pump, properties and features in flotation. Miner. Eng. 112, 19–26. https://doi.org/10.1016/j.mineng.2017.06.020

Fitzpatrick, M., Balsley, A., Hansen, K.A., 2014. Detection of Oil in Water Column , Final Report :

Detection Prototype Tests.

Fitzpatrick, M., Tebeau, P.A., 2013. Detection of Oil in Water Column: Sensor Design, US Department of Homeland Security.

Hwang, J., Bose, N., Fan, S., Robinson, B., Tenekedjiev, K., 2019. Complications of robotic delineation of oil spills at sea, in: 20th Commemorative Annual General Assembly, AGA 2019 - Proceedings of the International Association of Maritime Universities Conference, IAMUC 2019. pp. 26–33.

Hwang, J., Bose, N., Nguyen, H.D., Williams, G., 2020a. Acoustic search and detection of oil plumes using an autonomous underwater vehicle. J. Mar. Sci. Eng. 8, 1–11. https://doi.org/10.3390/JMSE8080618

Hwang, J., Bose, N., Robinson, B., Nguyen, H., 2020b. Assessing hydrocarbon presence in the waters of port au port bay, newfoundland and labrador, for auv oil spill delineation tests. J. Ocean Technol. 15, 100–112.

Joanna Szczucka, 1989. Acoustic Detection of Gas Bubbles in the Sea. Oceanologia 28, 103–113.

Johansen, Ø., Rye, H., Cooper, C., 2003. DeepSpill-Field study of a simulated oil and gas blowout in deep water. Spill Sci. Technol. Bull. 8, 433–443. https://doi.org/10.1016/S1353-2561(02)00123-8

Khuntia, S., Majumder, S.K., Ghosh, P., 2012. Microbubble-aided water and wastewater purification: A review. Rev. Chem. Eng. https://doi.org/10.1515/revce-2012-0007

Klaucke, I., Weinrebe, W., Sahling, H., Bohrmann, G., B¨rk, D., 2005. Mapping deep-water gas emissions with sidescan sonar. Eos, Trans. Am. Geophys. Union 86, 341. https://doi.org/10.1029/2005EO380002

Leifer, I., Chernykh, D., Shakhova, N., Semiletov, I., 2017. Sonar gas flux estimation by bubble insonification: Application to methane bubble flux from seep areas in the outer Laptev Sea. Cryosphere 11, 1333–1350. https://doi.org/10.5194/tc-11-1333-2017

López-Castejón, (Eds), F.& J.G., 2019. Underwater Robotics ready for Oil Spill. Tech. Pap. URready4OS Proj.

Loranger, S.C., 2019. Acoustic Detection and Quantification of Crude Oil. University of New Hampshire.

Maksym, T., Singh, H., Bassett, C., Lavery, A., Freitag, L., Sonnichsen, F., Wilkinson, J., 2014. Oil spill detection and mapping under Arctic sea ice using autonomous underwater vehicles.

North, E.W., Adams, E.E., Thessen, A.E., Schlag, Z., He, R., Socolofsky, S.A., Masutani, S.M., Peckham, S.D., 2015. The influence of droplet size and biodegradation on the transport of subsurface oil droplets during the Deepwater Horizon spill: A model sensitivity study. Environ. Res. Lett. 10, 1–12. https://doi.org/10.1088/1748-9326/10/2/024016

Panetta, P.D., Bland, L.G., Cartwright, G., Friedrichs, C.T., 2012. Acoustic scattering to measure dispersed oil droplet size and sediment particle size, in: OCEANS 2012 MTS/IEEE: Harnessing the Power of the Ocean. pp. 1–9. https://doi.org/10.1109/OCEANS.2012.6405103

Pang, S., Farrell, J.A., 2006. Chemical plume source localization. IEEE Trans. Syst. Man, Cybern. Part B Cybern. 36, 1068–1080. https://doi.org/10.1109/TSMCB.2006.874689

Parthiot, F., de Nanteuil, E., Merlin, F., Zerr, B., Guedes, Y., Lurton, X., Augustin, J.-M., Cervenka, P., Marchal, J., Sessarego, J.P., R.K., H., 2004. Sonar detection and monitoring of sunken heavy fuel oil on the seafloor, in: Interspill. Trondheim, pp. 1–13.

Saadoun, I.M.K., 2015. Impact of Oil Spills on Marine Life, in: Emerging Pollutants in the Environment - Current and Further Implications. InTech, pp. 75–104.

https://doi.org/10.5772/60455

Scandella, B., Urban, P., Delwiche, K., Greinert, J., Hemond, H., Ruppel, C.D., Juanes, R., Scandella, B., Urban, P., Delwiche, K., Greinert, J., Hemond, H., Ruppel, C.D., Juanes, R., 2013. Quantifying methane flux from lake sediments using multibeam sonar. Am. Geophys. Union, Fall Meet. 2013, Abstr. id. B53B-0456.

Sequoia Scientific, 2018. LISST-200X Particle Size Analyzer User's Manual.

Siim Pärt, Kõuts, T., 2016. In-situ oil detection sensor – technology overview and experiment design WP1 : Oil spill detection , monitoring , fate and distribution, Grace.

Socolofsky, S.A., Adams, E.E., Sherwood, C.R., 2011. Formation dynamics of subsurface hydrocarbon intrusions following the Deepwater Horizon blowout. Geophys. Res. Lett. 38, 1–6. https://doi.org/10.1029/2011GL047174

Tamura, I., Adachi, K., 2014. Developing a micro-bubble generator and practical system for purifying contaminated water. Stud. Sci. Technol. 3, 87–90. https://doi.org/10.11425/sst.3.87

Tsuge, H., 2014. Micro- and Nanobubbles: Fundamentals and Applications. Jenny Stanford Publishing. https://doi.org/10.4032/9789814463119

Uchimoto, K., Nishimura, M., Xue, Z., Watanabe, Y., 2018. A preliminary experiment on the detection of bubbles in the sea with side-scan sonar, in: 14th Greenhouse Gas Control Technologies Conference. 14th Greenhouse Gas Control Technologies Conference, Melbourne, pp. 1–9. https://doi.org/10.2139/ssrn.3365765

Veloso, M., Greinert, J., Mienert, J., De Batist, M., 2015. A new methodology for quantifying bubble flow rates in deep water using splitbeam echosounders: Examples from the Arctic offshore NW-Svalbard. Limnol. Oceanogr. Methods 13, 267–287. https://doi.org/10.1002/lom3.10024 von Deimling, J.S., Greinert, J., Chapman, N.R., Rabbel, W., Linke, P., 2010. Acoustic imaging of natural gas seepage in the North Sea: Sensing bubbles controlled by variable currents. Limnol. Oceanogr. Methods 8, 155–171. https://doi.org/10.4319/lom.2010.8.155

Weber, T.C., De Robertis, A., Greenaway, S.F., Smith, S., Mayer, L., Rice, G., 2012. Estimating oil concentration and flow rate with calibrated vessel-mounted acoustic echo sounders. Proc. Natl. Acad. Sci. U. S. A. 109, 20240–20245. https://doi.org/10.1073/pnas.1108771108

Wen, R., Sinding-Larsen, R., 1996. Mapping oil seeps on the sea floor by gloria side-scan sonar images - A case study from the Northern Gulf of Mexico. Nat. Resour. Res. 5, 141–154. https://doi.org/10.1007/BF02257658

Wendelboe, G., Fonseca, L., Eriksen, M., Hvidbak, F., Mutschler, M., 2009. Detection of heavy oil on the seabed by application of a 400 kHz multibeam echo sounder, in: Proceedings of the 32nd AMOP Technical Seminar on Environmental Contamination and Response. pp. 791–816.

Wilkinson, J., Maksym, T., Singh, H., 2013. Capabilities for detection of oil spills under sea ice from autonomous underwater vehicles.

Zedel, L., Butt, S., 2011. Using micro-bubbles as acoustic targets for large scale fluid flow experiments, in: 2011 IEEE/OES/CWTM 10th Working Conference on Current, Waves and Turbulence Measurement, CWTM 2011. pp. 224–229. https://doi.org/10.1109/CWTM.2011.5759556

5. Chapter 5

A Backseat Control Architecture for a Slocum Glider

Yaomei Wang[1], Worakanok Thanyamanta[1], Craig Bulger[2], Neil Bose[1]

[1] Department of Ocean and Naval Architectural Engineering, Memorial University of Newfoundland, St. John's, NL A1B 3X7, Canada

[2] Centre for Applied Ocean Technology, Fisheries and Marine Institute of Memorial University of Newfoundland, St. John's, NL A1C 5R3, Canada

This chapter is a journal paper which has been published in Journal of Marine Science and Engineering (2021), 9(5), 532; https://doi.org/10.3390/jmse9050532 (Article No.3 (JMSE2)).

Table 5-1. Individual Author Contribution – Article No.3 (JMSE2)

Author	Contribution
Yaomei Wang	Conceptualization, Methodology, Software, Validation, Formal analysis, Investigation, Resources, Data curation, Writing—original draft preparation, Writing—review and editing, Visualization
Craig Bulger	Conceptualization, Methodology, Software, Validation, Formal analysis, Investigation, Resources
Worakanok Thanyamanta	Formal analysis, Resources, Writing—original draft preparation, Writing—review and editing, Supervision, Project administration
Neil Bose	Conceptualization, Formal analysis, Resources, Writing—original draft preparation, Writing—review and editing, Supervision, Project administration, Funding acquisition

Abstract

Adaptive sampling provides an innovative and favorable method of improving the effectiveness of underwater vehicles in collecting data. Adaptive sampling works by controlling an underwater vehicle by using measurements from sensors and states of the vehicle. A backseat driver system was developed in this work and installed on a Slocum glider to equip it with an ability to perform adaptive sampling tasks underwater. This backseat driver communicated with the main vehicle control system of the glider through a robot operating system (ROS) interface. The external control algorithms were implemented through ROS nodes, which subscribed simulated sensor measurements and states of the glider and published desired states to the glider. The glider was set up in simulation mode to test the performance of the backseat driver as integrated into the control architecture of the glider. Results from the tests revealed that the backseat driver could effectively instruct the depth, heading, and waypoints as well as activate or deactivate behaviors adaptively. The developed backseat driver will be tested in future field experiments with sensors included and safety rules implemented before being applied in adaptive sampling missions such as adaptive oil spill sampling.

Keywords: Slocum glider; Backseat driver; Adaptive behavior

5.1 Introduction

Underwater gliders are characterized by long endurance, low energy consumption, and low noise (Graver et al., 2003). The sawtooth-like motion endows gliders with inherent advantages in sampling data in the water column. Sensors such as current profilers, fluorometers, and sonar have been equipped on gliders for various missions (Cetinić et al., 2009; Todd et al., 2017; Zhou et al., 2019). Underwater gliders have been active components in underwater observation including ecosystem monitoring (Mansour et al., 2014), hurricane prediction (Domingues et al., 2019), climate change investigation (Dent, 2014), hydrography and circulation measurement (Alvarez et al., 2013), oil spill survey (Dhont et al., 2019), and gradient tracking (Fiorelli et al., 2003). A fleet of underwater gliders was proposed in the late 1980s to monitor the global ocean (Stommel, 1989). Target-based control is critical to getting the utmost out of an underwater glider fleet. In addition, the growing needs for more complex missions such as delineating underwater plumes call for underwater gliders with the ability to respond in real time. Adaptive sampling has emerged as a possible solution.

Adaptive missions or adaptive sampling means that the vehicle changes its states such as heading and depth based on sensor measurements obtained in real time (see Figure 5-1) (Ivic et al., 2017; Mavrommati et al., 2017). The adaptive strategy can help drive gliders to regions of higher interest to, for example, increase the quantity of information acquired during a mission (Ferri et al., 2016). Theoretically, this intelligent work increases the real working time of gliders by spending more time in information rich areas. In the work of Fiorelli et al. (2003), an adaptive sampling strategy was proposed for the coordination of gliders. The glider fleet was controlled by a virtual body and artificial potential multi-vehicle control method to maintain the group motion of gliders. The artificial potentials defined the interaction between vehicles and reference points on a virtual body. The direction of the virtual body was adaptively controlled by a gradient estimated from the feature measurement of gliders. This gradient information could drive gliders to the maximum or minimum of a field, or to track the boundary of oceanic features.

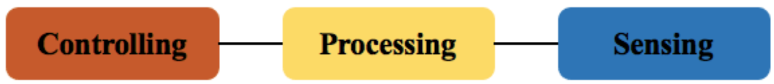

Figure 5-1 Structure of an adaptive sampling system.

Adaptive sampling can be realized in practice by adding a backseat driver to an underwater vehicle. Backseat drivers have been successfully implemented on several vehicles. A backseat controller developed by Naglak et al. (2018) was assembled in a General Dynamics Bluefin SandShark AUV. This backseat controller was supported by a small Raspberry Pi single board computer, running the Robot Operating System (ROS) and OpenCV to provide control algorithms and computer vision libraries. The backseat driver processed sensor data, ran control algorithms, and sent commands to the frontseat driver of the vehicle. The frontseat driver was housed in the commercial-off-the-shelf vehicle. This frontseat-backseat control architecture was tested in an open-water environment and was planned to be applied to an open-source vehicle named ROUGHIE (Page et al., 2017). A ROS-based system was also used on a Hydroid REMUS 100 AUV as a backseat driver (Gallimore et al., 2018). In the control architecture, an application programming interface RECON on the REMUS vehicle computer provided an interface between the vehicle computer and a sensor/autonomy computer. The RECON interface was handled by a library pyREMUS on the sensor/autonomy computer. This pyREMUS library could not only be used to build an interface with ROS packages, but also connect with the Mission Oriented Operating Suite (MOOS) or sensors.

Eickstedt and Sideleau (2010) focused on the implementation of a backseat driver architecture on an Iver2 AUV manufactured by Ocean Server Technology. This backseat driver architecture was built based on the Mission Oriented Operating Suite-Interval Programming (MOOS-IvP), an autonomy software for supporting the operation of autonomous marine vehicles (Benjamin et al., 2012). In their implementation, a MOOS module, iOceanServerCommns, created an interface between a backseat controller and the main vehicle control system. An intelligent control component in the backseat controller received data both through the interface and sensors connected directly to the backseat computer. This autonomy system provided decisions on states of the vehicle such as speed, heading, and depth to the dynamic control of the main vehicle control system. The dynamic control component in the main vehicle control system was responsible for executing the commands from the backseat controller and sending navigation information to the backseat driver. In addition to the Iver2 AUV, there are some other underwater vehicles that have implemented a backseat driver by using MOOS-IvP such as the Bluefin 9 and Bluefin 21 (Bluefin Robotics, 2013), Teledyne Gavia AUV (Keane et al., 2020), and so on (Eickstedt and Sideleau, 2010). To facilitate AUVs with adaptive maneuvering capability for homing to a single beacon, a homing application pHomeToBeacon based on the MOOS-IvP was developed and demonstrated on a Teledyne Gavia AUV (Keane et al., 2020). The application pHomeToBeacon received range reports and AUV positions from the frontseat driver through an interface called iGavia between the frontseat driver and the backseat driver. The application then processed these inputs with a localization algorithm to estimate the beacon position. The beacon position was used to obtain the dynamic homing waypoints that were sent back to the frontseat driver operating system to achieve adaptive maneuvering ability.

The existing control system of Slocum gliders is not favorable for carrying out an adaptive mission such as delineating underwater oil plumes intelligently. A mission with existing gliders is defined by simple methods such as waypoints before the gliders are deployed. Due to ocean dynamics or patchy characteristics of oil plumes, gliders can miss some areas or spend a lot of time outside the plume. An adaptive control system can solve this problem by enabling the glider to change its states based on the sensor measurements. This will increase the quality of information acquired during a mission, particularly in time-sensitive missions like an oil spill response (Fiorelli et al., 2003). To equip Slocum gliders with the ability to do an adaptive mission, a backseat driver was developed for Slocum gliders in this chapter. This backseat driver enabled a glider to use the state information from the main vehicle control system and real-time measurements from sensors to re-evaluate its mission when the glider was underwater. The main focus of this chapter was to interface external codes with a Slocum glider. This chapter also investigated the ability of the backseat control system to control the states such as depth, heading, and waypoints of the Slocum glider. With the possibility of controlling the states of the glider through the backseat control system, additional sensors can be included in the backseat driver to further control the motion of the glider such as improving the path following performance considering water currents (Ivić et al., 2020; Kim et al., 2021; Meurer et al., 2020). The glider used in this chapter and the developed backseat driver are introduced in the next section. In Section 5.3, the tests of the backseat driver through simulations are presented, followed by a discussion. A conclusion is included in the final section.

5.2 System Architecture

This section introduces the Slocum glider used for the development and the developed backseat driver. This chapter mainly focuses on the software part of the backseat driver that has been successfully tested in the Slocum glider.

5.2.1 The Slocum Glider

The glider used in this chapter was a Slocum Generation 1 (G1) glider (see Figure 5-2). Specifications of this glider are shown in Table 5-2. This glider was equipped with a 200-meter depth rated ballast pump and had a rated horizontal speed of 0.4 m/s. The glider changes its weight by pumping water in and out of the glider and converts vertical motion into horizontal motion by using body and wing lift. The 200-meter depth rated ballast pump assembly used can move 504 cm^3 of water into and out of the glider (Teledyne Webb Research, 2010). Given that the buoyancy changes from a density change between freshwater and seawater is in the order of 1.04 L to 1.05 L, the ballast pump cannot compensate for the force induced by such a large change in water density. The structure of the glider system including the main part can be referred to the manual of the glider (Teledyne Webb Research, 2010).

Figure 5-2. Slocum G1 glider.

Table 5-2. Specifications of Slocum G1 glider (Teledyne Webb Research, 2010).

Parameter	**Value**
Weight in air	~52 Kg
Dimension	0.213 m (Diameter) 1.003 m (Width) 1.5 m (Length)
Operation Depth	4–200 m
Speed	0.4m/s horizontal
Energy	Alkaline batteries (primary)
Sensors	GPS, altimeter, acoustic modem, conductivity, temperature, depth sensor

The Slocum glider can be commanded to conduct various behaviors by defining mission files that are sent to the glider before a mission. Behaviors that can be defined in a mission file include, but are not limited to:

(1) Yo (a single up and down pattern through water column) behavior: instruct the glider to dive and climb by setting the depth, altitude, and the number of yos;

(2) Go to a waypoint or waypoint list: instruct the glider to go to a waypoint or waypoint list defined in mission files;

(3) Set a heading: instruct the glider to follow a predefined heading;

(4) Surface: instruct the glider to surface for communication or recovery;

(5) Abend: define conditions when a mission should be aborted.

5.2.2 Backseat Driver

A backseat driver system was developed for the Slocum G1 glider. This backseat driver had some features that enabled the glider to conduct adaptive missions and facilitated the application of gliders in various missions:

(1) Onboard replanning. The backseat driver system could receive state information from the main vehicle control system and measurements from sensors connected with the backseat driver. With this information, the backseat driver could replan the trajectory or mission target and publish the new plan to the main vehicle controller in real-time. Onboard replanning enables the glider to deal with unexpected and unforeseen situations and improve the quality of collected data.

(2) Modular design. The modular design in both software and hardware of the backseat driver system facilitated the reconfiguration of the sensors and control system. A new sensor could be easily added to the backseat driver without changing other modules of the control system. The structure of the backseat driver system is concise and clear.

(3) Energy efficient. The backseat driver computer and the sensors used for backseat control were energy efficient, which used minimum energy from the onboard battery. This feature ensured that the Slocum glider would keep its favorable long endurance with low battery energy consumption.

5.2.2.1 Software for the Backseat Driver

The software for the backseat driver consisted of an interface and external controllers.

(1) Interface for the backseat driver

The communication between the backseat driver and the main vehicle computer was realized through a ROS interface, provided by Teledyne Webb Research. ROS is a collection of libraries, tools, and conventions that simplify the development of robot application (Ros.org, 2021). ROS enables a transfer of codes developed in other domains such as aerial robotics to underwater robotics (Naglak et al., 2018). With the ROS interface, state parameters of the glider such as depth (m_{depth}), heading ($m_{heading}$), and location (latitude and longitude measured from GPS: m_{gps_lat} andm_{gps_lon}, latitude and longitude measured dead reckoning: m_{lat} and m_{lon}) can be sent from the main vehicle control system to the backseat driver. Likewise, commands such as activation or deactivation of behaviors ($u_{mission\_mode}$), desired heading and depth can be sent from the backseat driver to the main vehicle control system. Examples of the parameters that can be exchanged between the main vehicle control system and the backseat driver are shown in Figure 5-3. Before the introduction of the backseat driver, the condition for the activation and deactivation of behaviors were defined in mission files before deployment. This restricted the implementation of combinations of individual behaviors and generation of new behaviors. The backseat controllers enabled the vehicle to activate or deactivate behaviors adaptively, for example, to activate a surface behavior by publishing parameter $u_{mission\_mode}$ when the vehicle is in the water for a period of time and needs to come to the surface. Parameters such as $u_{mission\_param\_a}$ and $u_{mission\_param\_b}$ were used to represent mission parameters such as targeted diving depth and targeted heading.

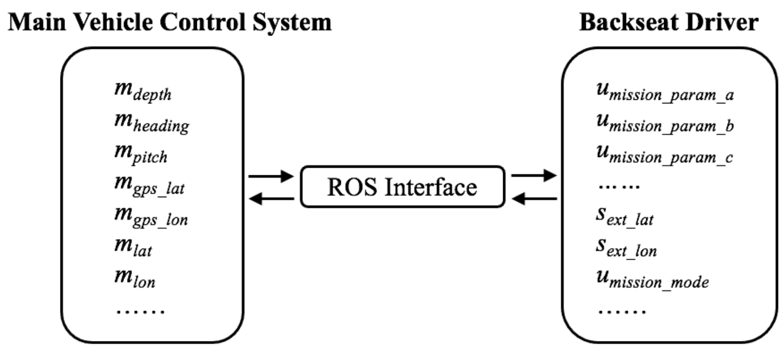

Figure 5-3. Data exchange between the main vehicle control system and backseat driver.

(2) External controllers

The backseat driver adaptively replans a mission by subscribing the state parameters such as location and heading of the vehicle from the main vehicle control system or measurements from sensors. Then, the backseat driver processes the subscribed data and publishes desired state parameter to the glider. This is realized through external controllers in the backseat driver implemented as ROS nodes. These nodes can publish and subscribe information to any nodes in the backseat driver and process the information with control algorithms. For example, a glider might be deployed to adaptively change the target depth of its diving and climbing in the yo behavior based on the fluorescence reading from an onboard fluorometer. In this case, the external controllers consist of two ROS nodes (see Figure 5-4). One is a node called the fluorometer controller, which collects the readings of fluorescence from the fluorometer and publishes the fluorescence data to other nodes. Another is a depth controller node, which sends the target depth to the science processor according to the subscribed fluorescence data.

The introduction of individual, independent nodes in the external controllers is beneficial for module reuse, which helps accelerate the development process of the controllers. Existing modules can be combined or expanded, providing the external controller with more powerful or new functions. For instance, a waypoint controller is added to a backseat driver consisting of a depth controller and a fluorometer controller without changing the configurations of the existing backseat driver (Figure 4). Data from the fluorometer controller can now be supplied to both the depth controller and waypoint controller at the same time. This added waypoint controller subscribes the data related to fluorescence from the fluorometer controller and publishes the processed data to the glider as part of a new adaptive waypoint behavior.

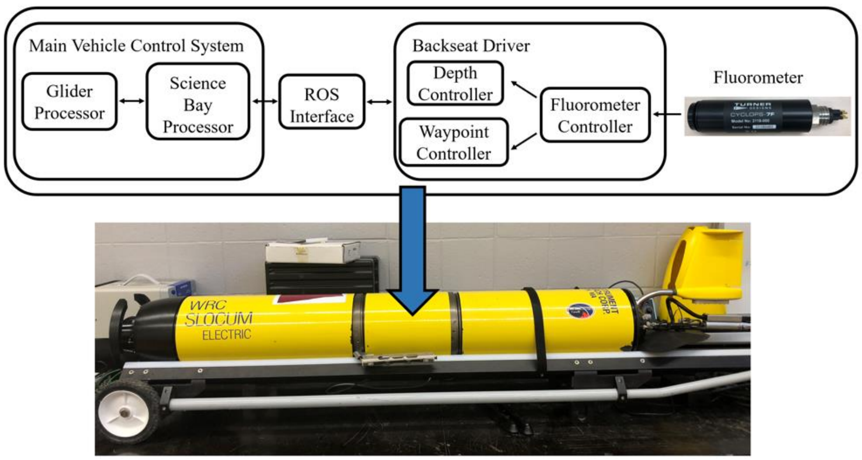

Figure 5-4. Backseat control architecture of Slocum glider with a fluorometer supporting the control of depth and waypoint.

5.2.2.2 Hardware of the Backseat Driver

A Beaglebone Black was used as the platform to support the running of the ROS interface, the backseat driver control algorithms, and the sensor controllers. The BeagleBone Black is a small, low-cost, and community-supported single board computer (BeagleBoard.org, 2019). The computer runs on a 1 GHz processor with a 512 MB RAM, which is sufficient for real-time data processing and backseat control. It requires a maximum of 500mA if the board is powered from the USB port. This computer supports multiple operating systems such as Debian, Ubuntu, and

Android for different users. A BeagleBone Black has two headers, each with 46 pins. These pins provide various functions such as seven analog input pins that can be used for reading sensor data.

5.3 Simulation

A series of simulations were conducted in a lab to test the performance of the backseat driver before being tested in field experiments. The test was done by connecting the BeagleBone Black, serving as the backseat driver computer to the Slocum glider set up in simulation mode (see Figure 5-5). The glider's electronics and vehicle control software were used as a hardware-in-the-loop simulator to test our missions. The mathematical model of the glider in the simulator control software is proprietary to Teledyne Webb, the glider manufacturer. A similar empirical linear model for glider velocity has been published in the work of Zhou (2012; 2017; 2011). The conducted simulations in this chapter used the actual control loops of the glider instead of those developed by the authors, which may introduce simplification and inaccuracy. The backseat driver has the ability to change the depth, heading, waypoint of the glider, and activate or deactivate behaviors during missions. Therefore, the performance of the glider in adaptive depth changing, adaptive heading changing, adaptive waypoint changing, and adaptive activation/deactivation of behaviors were tested through simulations.

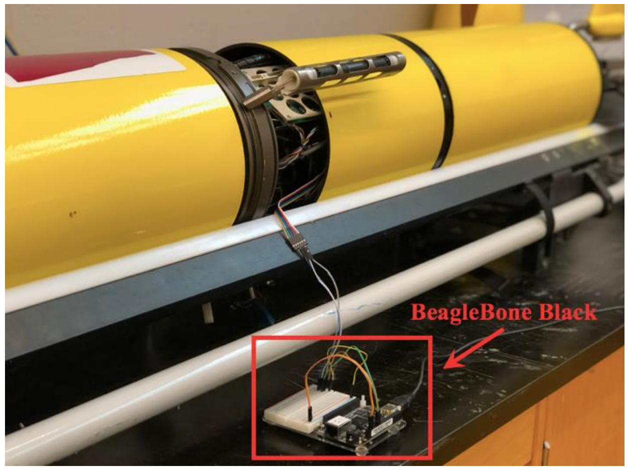

Figure 5-5. Connecting BeagleBone Black to the Slocum G1 glider to test the performance of the backseat driver.

5.3.1 Adaptive Depth Changing

The maximum diving depth and the minimum climb depth of a glider are usually defined before a mission. The ability to adaptively change these depths of a glider is beneficial and can reduce mission time. For example, the glider can change its depth based on sensor readings to spend more time in the depth layer where the target is found. In addition, the ability to change depth can help increase safety by reducing risks associated with the change in water density. By using the backseat driver, the glider can analyze the real-time water density collected by its conductivity, temperature, and depth sensor and respond to any risky water density change. For example, the backseat driver can command the glider to move to a depth where the water density change is within that for which the glider can compensate.

5.3.1.1 Depth Changing When a Waypoint is Reached

In order to test whether the backseat driver can control the glider to change its maximum depth during a mission, the glider was commanded to go to several predefined waypoints in sequence, as shown in Figure 5-6 and Table 5-3. Prior to the mission, the glider's maximum depth was set to 20 m. The backseat driver was programmed to increase the maximum diving depth of the glider by 10 m each time it reached a waypoint (defined as when the glider was within 10 m from the target waypoint). When the first waypoint (Wpt 1) was reached, the glider would change its maximum diving depth from 20 m to 30 m. When the last waypoint (end point) was reached, the glider surfaced and finished its mission.

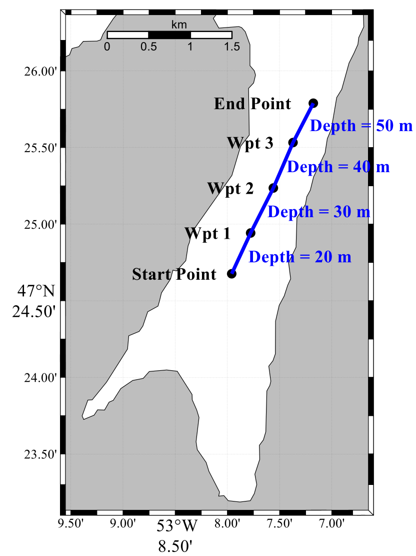

Figure 5-6. Trajectory of the Slocum glider in the mission of changing the maximum diving depth when a waypoint was reached.

Table 5-3. Waypoint list for a mission of the Slocum glider with corresponding maximum diving depth after a waypoint was reached.

Waypoints	Coordinate	Depth
Start Point	47°24.6763'N, 53°07.9585'W	20 m
Wpt 1	47°24.9426'N, 53°07.7769'W	30 m
Wpt 2	47°25.2362'N, 53°07.5591'W	40 m
Wpt 3	47°25.5328'N, 53°07.3706'W	50 m
End Point	47°25.7897'N, 53°07.1758'W	50 m

In this simulation, we used a depth controller in the backseat driver (see Figure 5-7) to control the maximum diving depth of a yo behavior. This depth controller subscribed latitude (m_{lat}) and longitude (m_{lon}) information from the main vehicle control system in real time. Then, the position information was processed by the depth controller to calculate the distance from the predefined waypoints. When a waypoint was reached, the depth controller published a new maximum dive depth ($u_{mission\_param\_a}$) to the main vehicle controller to change the diving depth of the glider. Otherwise, the glider would keep the maximum diving depth of the yo behavior unchanged. The initial value of $u_{mission\_param\_a}$ was set to be 5 m.

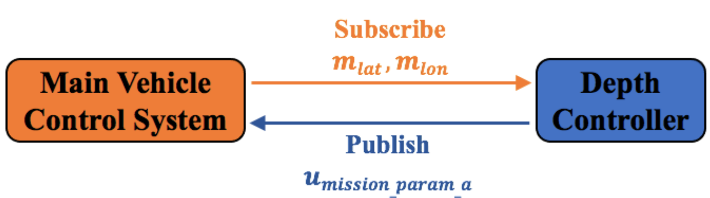

Figure 5-7. Exchange of data between the main vehicle control system and a depth controller when the glider changed its depth when a waypoint was reached.

Results from this simulation are presented in Figure 5-8. The glider went to a depth of around 20 m on its first dive, showing that the $u_{mission\_param\_a}$ was successfully published to the glider main controller as the glider changed its maximum diving depth to the newly received one. When the first waypoint (Wpt 1) was reached, the glider had already finished its diving behavior and had started to climb. In this case, the backseat driver would command the glider to a new maximum depth of 30 m once it started the next diving behavior. Except for the last diving behavior when the glider finished its mission before reaching the target depth, the glider overshot the target depth in all its dives, as it took some finite time for the glider to slow down its dive and start climbing again.

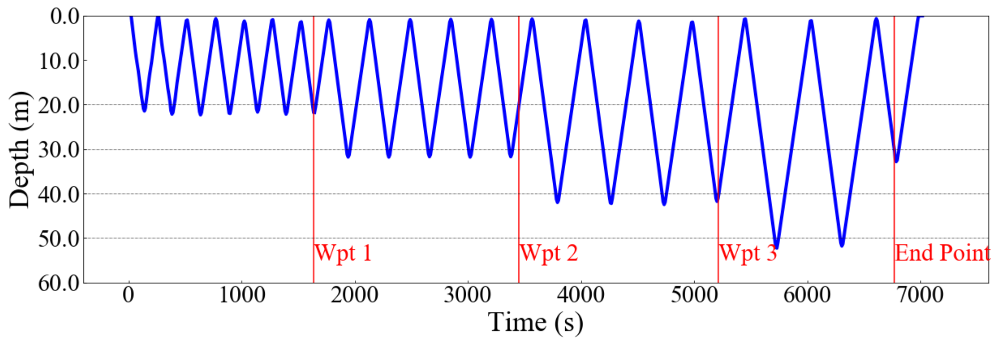

Figure 5-8. The depth of the glider under the control of a depth controller, which changed the maximum dive depth when a waypoint was reached.

5.3.1.2 Depth Changing Based on a Simplified Fluorescence Field

The objective of this simulation was to test the ability to command the glider to change its target depth of diving behavior based on fluorescence readings. A simplified artificial fluorescence field in the vertical plane of the water column was defined by a sinusoid:

$$y = 5\sin\left(\frac{2\pi}{150}x\right) + 30 \tag{5-1}$$

where x is the distance that the glider has moved in the horizontal direction. It was assumed that fluorescence was present in all of the region above the sine curve in the vertical plane and that there was no fluorescence below the sinusoid. In order to get information of the fluorescence field, it is best for the glider to stay in the information-rich area. Therefore, the glider was commanded to change the maximum dive depth of the yo behavior when there was no fluorescence detected. In the simulation, the glider moved from start point [47°24.6763'N, 53°07.9585'W] to the end point [47°25.7897'N, 53°07.1758'W] as shown in Figure 5-9. The mission was ended when the distance to the end point was within 10 m.

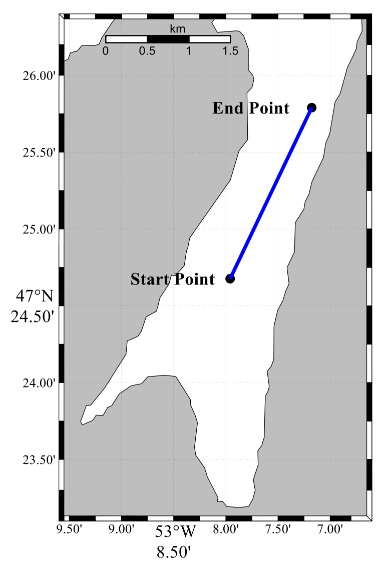

Figure 5-9. Trajectory of the glider in the mission of changing maximum dive depth based on a simplified fluorescence field.

In the control architecture, the main vehicle control system sent current latitude (m_{lat}), longitude (m_{lon}) and depth (m_{depth}) of the glider to a depth controller in the backseat driver (see Figure 5-10). In the depth controller, the backseat control algorithm (see Table 5-4) compared the depth of the glider to the vertical distribution of the fluorescence field. If the glider was within the fluorescence field, a larger maximum diving depth was set $m_{depth} + \delta_{depth}$, where m_{depth} is the measured depth of the glider and δ_{depth} is a parameter with a value larger than 0 m, in order for the glider to dive deeper toward the boundary of the fluorescence field. Otherwise, the desired maximum diving depth was set to m_{depth}, which is the current depth of the glider. The depth controller then sent the desired maximum diving depth ($u_{mission\_param\_a}$ in Figure 5-10) to the main vehicle control system to replan the diving behavior.

Figure 5-10. Exchange of data between the main vehicle control system and a depth controller when the glider changed its depth based on a simplified fluorescence field.

Table 5-4. Control algorithm of a depth controller for backseat control when the glider changes its depth based on a simplified fluorescence field.

Pseudo code for the Depth Controller
 # The location of the glider at the start point is [m_{lat_start}, m_{lon_start}] *Node Depth Controller subscribes latitude (m_{lat}), longitude (m_{lon}), and depth (m_{depth}) of the glider from the main vehicle control system* *# dis is the distance that the glider has moved from the start point* *dis = the distance between [m_{lat}, m_{lon}] and [m_{lat_start}, m_{lon_start}]* *# y is the lower boundary of the simulated plume in the water column* *y = 5*sin(2*pi/150*dis) + 30* *# u_mission_param_a is the desired maximum diving depth* *if $m_{depth} < y$*

$u_{mission\_param\_a} = m_{depth} + \delta_{depth}$

else

$u_{mission\_param\_a} = m_{depth}$

end if

publish $u_{mission\_param\_a}$ *to the Node Main Vehicle Control System*

Depths of the glider in the simulation when δ_{depth} was set to be 5 m is presented in Figure 5-11. The glider reacted to the distribution of the fluorescence field on each dive and changed its maximum dive depth according to the boundary of the fluorescence field. The glider did not reach the boundary of the simplified fluorescence field in the last dive behavior as the end point of the mission was reached.

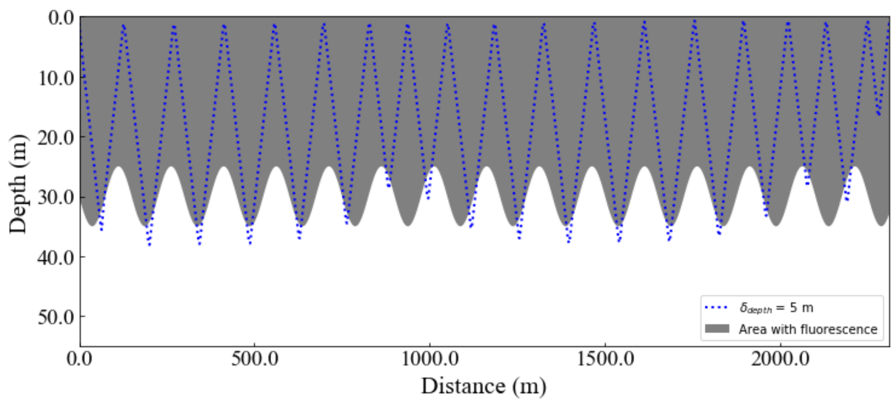

Figure 5-11. The depth of the glider under the control of a depth controller, which changed the maximum dive depth according to a simplified fluorescence field (δ_{depth}= 5 m).

The performance of the depth controller when δ_{depth} was set to be 1 m, 3 m, and 5 m was compared. Figure 5-12 shows the depths of the glider when its distance travelled was between 800 m and 1300 m for better resolution. While the values of δ_{depth} were different, the response of the glider to the boundary of the fluorescence field were similar. For example, at label 1 in Figure 5-12, when the distance travelled of the glider was nearly 900 m, the fluorescence distributed to a deeper depth with the increase in the distance travelled. The overshoot value of the depth of the glider in the diving behavior relative to the boundary of the fluorescence field was almost the same for the three δ_{depth} values at label 1. This also happened at 1000 m (label 2 in Figure 5-12). The similar overshoot values showed that these different δ_{depth} values had little influence on the performance of the glider in reacting to the boundary of the fluorescence field. Even so, the trajectories of the glider in the three simulations were slightly different, as shown in Figure 5-12. This was caused by the iteration error in the main vehicle control system when it calculated the position and heading of the glider underwater. When the value of δ_{depth} was small, which meant the next target depth was close such as 1 m, it would not take a long time before reaching the target depth. As there was little difference in the diving of gliders at different values of δ_{depth}, the depth controller was not sensitive to the value of δ_{depth}. The backseat driver could control well at a depth accuracy of 1 m. This also reviewed that the backseat driver could receive states of the glider from the main vehicle control system and control the depth of the glider in a timely manner.

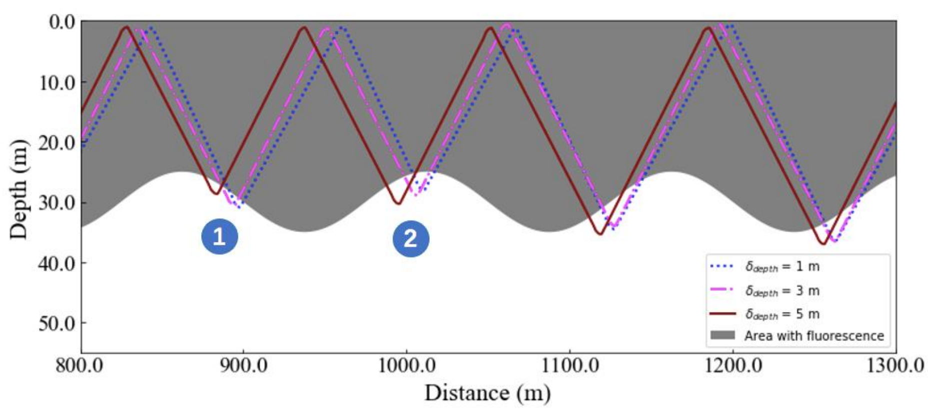

Figure 5-12. The depth of the glider under the control of a depth controller, which changed the maximum dive depth according to a simplified fluorescence field when δdepth was set as 1 m, 3 m, and 5 m, respectively.

5.3.2 Adaptive Heading Changing

Adaptive depth changing enables the glider to change its depth adaptively in the water column, similarly, an adaptive heading change equips the glider with the autonomous capability to change its heading in the horizontal plane. With the ability to change heading adaptively, the glider can be set on a mission to delineate the boundary of ocean features (see Figure 5-13), track the source of plumes, and so on.

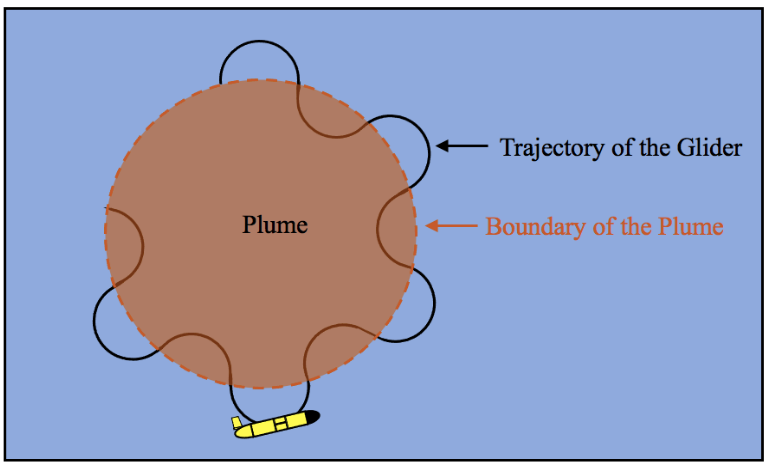

Figure 5-13. Adaptive changing of the heading of a glider to delineate the boundary of a plume based on the detection from sensors.

5.3.2.1 Following a Heading

In this simulation, the glider moved from point [47°24.2509'N, 53°08.1370'W] with an initial heading set to 0° (i.e., heading to the north). A command ($u_{mission\_param\_b}$) was sent from the heading controller in the backseat driver (Figure 5-14) after initiation to the main vehicle controller to steer the glider to a 30° heading, as shown in Figure 5-15.

Figure 5-14. Exchange of data between the main vehicle control system and a heading controller when the glider followed a heading commanded by the backseat driver.

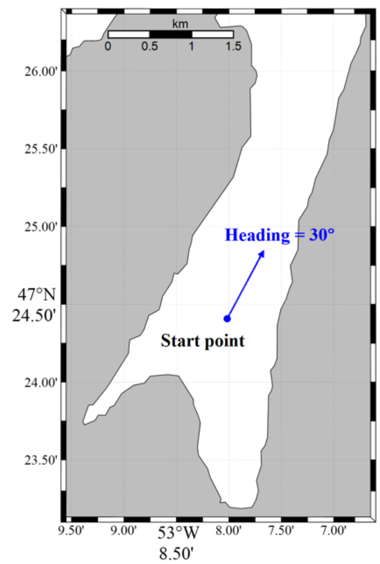

Figure 5-15. Trajectory of the glider during a mission when following a constant heading of 30°.

Results from the simulation, as shown in Figure 5-16, showed that the glider could change its heading from 0° to 30° after receiving the command from the heading controller. There was a discrepancy ranging from −6° to 6° between the commanded heading ($c_{heading}$) from the backseat driver and the measured heading ($m_{heading}$) of the glider. However, the glider kept a constant heading in general. This error could be minimized by changing the deadband for heading error in the mission files. Figure 5-17 shows another simulation when the deadband for heading error was set to 0°. The measured heading coincided with the commanded heading after 200 s when the heading of the glider became stable.

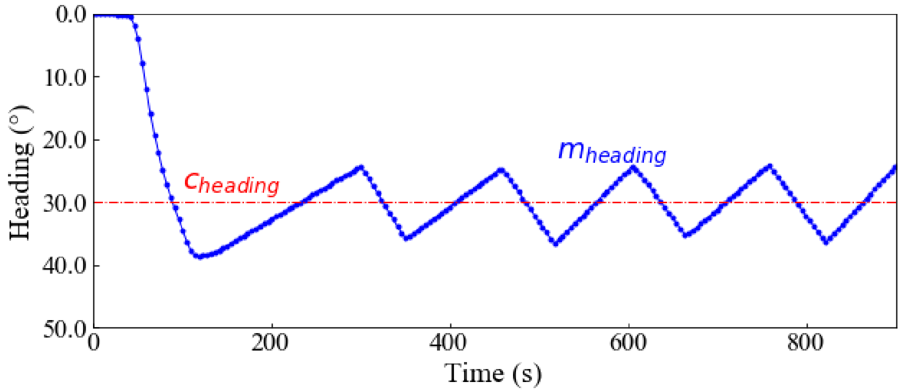

Figure 5-16. The heading of the glider under the control of a heading controller, which maintained the glider to a desired heading with a deadband setting of 5°.

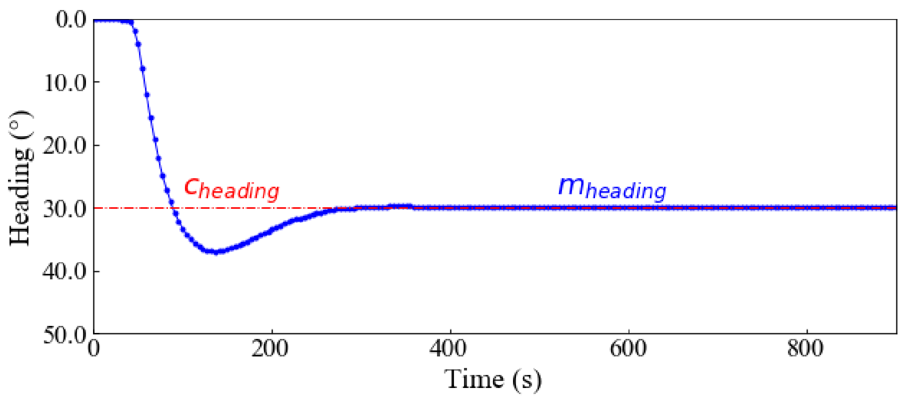

Figure 5-17. The heading of the glider under the control of a heading controller, which maintained the glider to a desired heading with a deadband setting of 0°.

5.3.2.2 Changing Heading Along the Boundary of a Simulated Plume

The glider was operated to follow the boundary of a simulated plume. The heading of the glider was changed from that specified at the start point at [47°23.9304'N, 53°07.8320'W] in this simulation to test the adaptive heading behavior of the glider in boundary tracking. A simulated plume was created to have a circular boundary, with a center at [47°24.0517'N, 53°07.8320'W] and a radius of 100 m. The frontseat driver sent latitude (m_{lat}), longitude (m_{lon}), and heading

($m_{heading}$) information of the glider to a heading controller (see Figure 5-18). This heading controller adopted the location information of the glider and determined whether the glider was within the simulated plume or not. When the glider was inside the plume, the glider was requested to turn to starboard by increasing its heading to go toward the boundary of the plume. Otherwise, the glider turned to port to go into the plume. The pseudo code for control of the heading of the glider in this simulation is presented in Table 5-5.

Figure 5-18. Exchange of data between the main vehicle control system and the heading controller when the glider changed its heading based on detection of a plume from a fluorometer measurement.

The trajectory of the glider in the horizontal plane under the control of the backseat driver for tracking the boundary of a simulated plume is shown in Figure 5-19. The glider could follow the plume boundary, but not precisely. For example, the boundary of the plume within the region labelled by 1 in Figure 5-19 was not tracked. This was caused by the tracking algorithm in the backseat driver. On the other hand, the performance of the glider in an adaptive heading behavior such as the response time and the ability to change heading according to the measurement from sensors was limited by the turning radius of the glider. When the turning radius is larger than the characteristics of an ocean feature such as the size of the plume, the glider will not be able to follow the boundary precisely. The minimum turning radius of this Slocum G1 glider was measured from simulation by publishing desired headings from 0 to 2π to the glider to make it change its heading continuously. These values of desired heading would drive the glider to turn to starboard. The trajectory of the glider in this simulation is shown in Figure 5-20, with a minimum turning radius measured, which was approximately 17 m.

Table 5-5. Control algorithm of the heading controller for backseat control when the glider changed its heading along the boundary of a simulated plume.

Pseudo code for the Heading Controller
 # The location of the center of the simulated plume is [mlat_center, mlon_center]
#Δheading is a desired change of heading which is positive
Node Heading Controller subscribes latitude (mlat), longitude (mlon), and heading (mheading) of the glider from the main vehicle control system
 # dis is the distance that between the location of the glider to the center of the simulated plume
dis = the distance between [mlat, mlon] and [mlat_center, mlon_center]
 # umission_param_b is the desired heading
if dis < radius
umission_param_b=mheading + Δheading
else
umission_param_b=mheading - Δheading
end if
publish umission_param_b to the Node Main Vehicle Control System

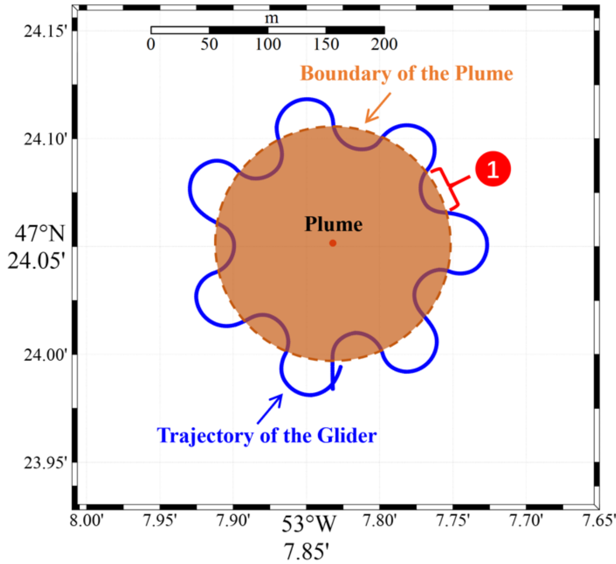

Figure 5-19. Trajectory of the glider in the horizontal plane under the backseat control of a heading controller, which changed the heading along the boundary of a simulated plume. The boundary of the plume within the region labelled by 1 was not tracked by the glider.

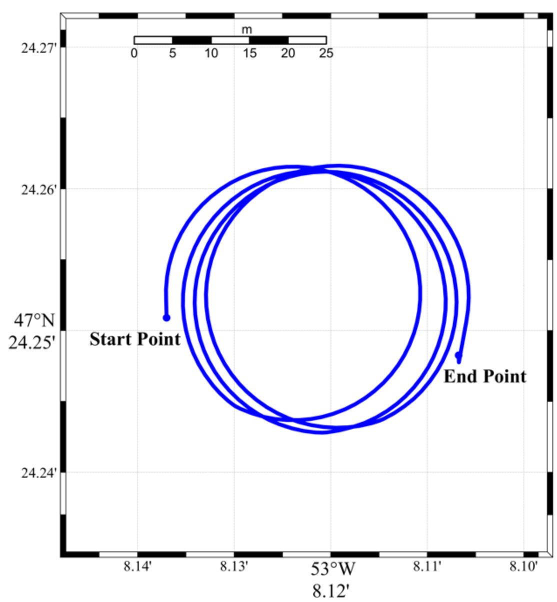

Figure 5-20. The trajectory of the glider when changing its heading from 0 to 2π continuously for estimating the turning radius of the Slocum G1 glider.

5.3.3 Adaptively Going to Waypoints

The glider can go to a waypoint or a list of waypoints by providing the location of the waypoints in the mission files in advance. This limits the trajectory of the glider. With the backseat driver, a new target point can be replanned for the glider when it is conducting a mission. The adaptive behavior to move the glider to a new waypoint is to set a heading for the glider toward the new waypoint and stop the waypoint behavior when the glider is within a specified distance from the target point. This adaptive waypoint behavior is not explicitly defined through the backseat driver and is realized by the behavior of the adaptive heading change, as mentioned in Section 4.3.2.

In the simulation, the glider was commanded to go from the start point to a series of waypoints (Table 5-6) with a maximum diving depth of 30 m. The locations of these target waypoints were not defined in the mission files, but by the backseat driver. The backseat driver translated the locations of the waypoints into the different headings needed to be followed by the glider and instructed the glider to follow the appropriate trajectory. The first heading was sent to the main vehicle controller to drive the glider in the direction of the first waypoint (Wpt 1 in Table 5-6). The backseat driver then kept calculating the distance of the glider from the first waypoint. When the distance was less than 10 m, the glider was instructed to go to the second waypoint by providing it with another desired heading. In addition, when the end point was reached, the glider was commanded to activate the surface behavior to terminate its mission by publishing $u_{mission\_mode}$ to the main vehicle control system (Figure 5-21).

The simulation result of this adaptive waypoint behavior is shown in Figure 5-22, which presents the trajectory of the glider when it was under the multi-waypoint mission control. The deadband for heading error in this simulation was 5°, and the glider could keep a constant heading in general, which instructed the glider to go to the targeted waypoints. Figure 5-23 presents the depth of the glider in this mission, which indicates that the glider surfaced after the end point was reached.

Figure 5-21. Exchange of data between the main vehicle control system and the waypoint controller when the glider changed its target points adaptively.

Table 5-6. Waypoint list for the adaptive waypoint behavior of the glider.

Mission Points	Coordinate
Start Point	[47°24.3704'N, 53°07.9213'W]
Wpt 1	[47°24.4511'N, 53°07.7041'W]
Wpt 2	[47°24.5153'N, 53°07.9173'W]
End Point	[47°24.5844'N, 53°07.7081'W]

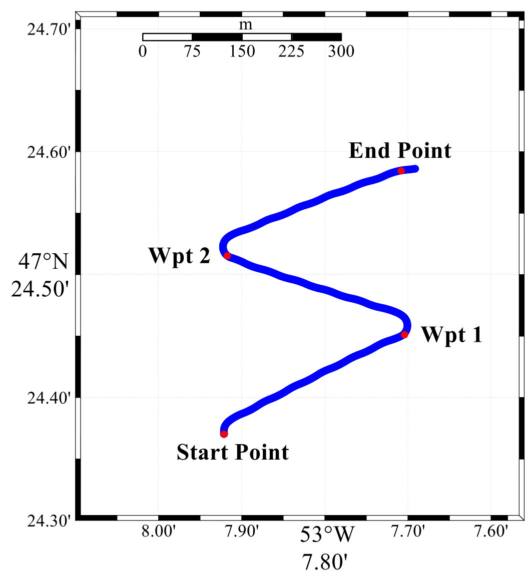

Figure 5-22. Trajectory of the glider in the mission testing the adaptive waypoint behavior.

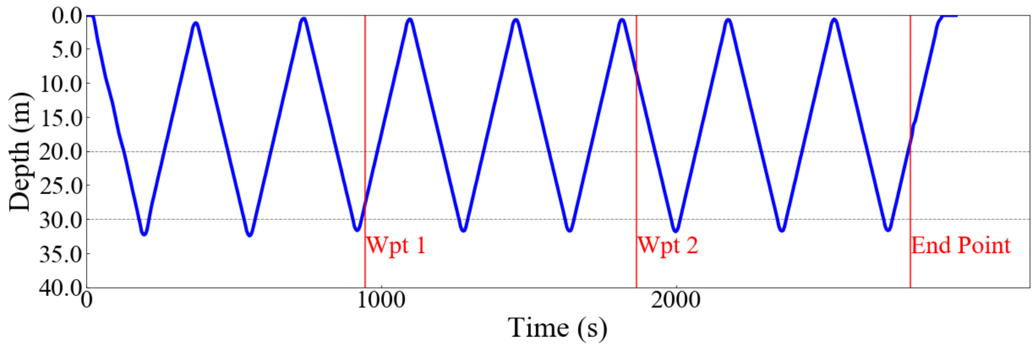

Figure 5-23. The depth of the glider under the control of the waypoint controller, which changed the target point adaptively and activated the surface behavior when the end point was reached.

5.4 Discussion

The existing backseat driver for this Slocum G1 glider was running on ROS, with a ROS node as an interface between the main vehicle control system and the backseat driver and other ROS nodes as parts of the backseat driver for controlling sensors and implementing adaptive control algorithms. However, the glider is not limited in using ROS as the platform for the backseat driver for the adaptive control algorithms and sensor controllers. With the ROS interface, there are various software packages that can be incorporated with our existing system for future development such as MOOS-IvP and LCM, or even ROS that was developed for use in other fields. This chapter was mainly to present the control structure of the backseat driver for the Slocum G1 glider, with some examples showing adaptive behaviors with the backseat controllers. Simulations in this chapter were limited to one ROS node in the backseat driver, which subscribed state information of the glider from the main vehicle control system and published desired states to the glider. Measurements from sensors were simplified and simulated within the ROS node. For field experiments with the backseat driver, the backseat driver can be provided with measurements from real sensors. For instance, for a glider with a fluorometer in field missions, a fluorometer controller can be used by the backseat driver to process measurements from the fluorometer, as shown in Figure 5-24. The processed fluorescence data will be sent to the depth controller to decide the desired depth of a yo behavior, with the desired depth published to the main vehicle control system to realize adaptive depth control. This control structure can also be applied to the adaptive heading control of the glider in field missions, for example, including real-time measurements from an on-board fluorometer (see Figure 5-25).

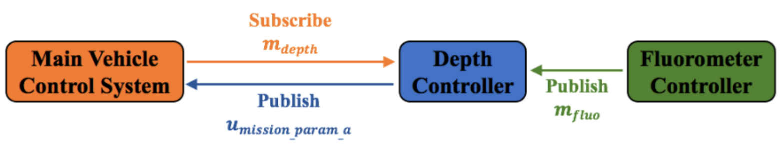

Figure 5-24. The control structure of the glider with a backseat driver, which takes the measurements from a fluorometer for adaptive depth control.

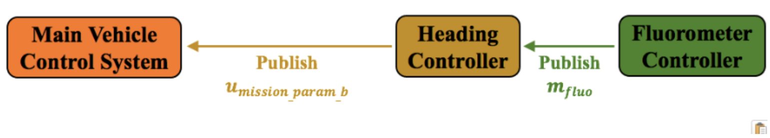

Figure 5-25. The control structure of the glider with a backseat driver, which takes the measurements from a fluorometer for adaptive heading control.

With the incorporation of measurements from sensors in field work, the glider autonomously responds to the environment and the path of the glider is unspecified. Besides, as the operating speed of the Slocum glider is 0.4 m/s, the motion of the glider is subject to environmental disturbances such as currents. If the current speed is high, the glider may drift from its designed path and fail to complete its mission. The safety of the glider is guaranteed by safety rules in the dynamic environment. Safety rules can be implemented through both the mission file and the backseat driver control algorithm.

(1) Implementation through the mission file. For example, a maximum mission time can be defined in the mission file to restrict the duration of a mission. The glider will abort its mission and climb to the surface if it has worked in excess of the maximum mission time. For a yo behavior, a target altitude (from the seabed) can be defined in the mission file. The target altitude will command the glider to abort the diving behavior and climb if the altitude of the glider is smaller than the target altitude, even if the glider has not reached the target diving depth.

(2) Implementation through the backseat driver. A safety zone can be defined in the backseat driver to specify the region of operation for the glider. The backseat driver subscribes the location and depth information of the glider from the main vehicle controller and determines whether the glider is within the safety zone or not. If the glider is outside of this zone, the backseat driver will instruct the glider to either go back to this safety zone or abort its mission.

The developed backseat driver will be tested in field experiments with measurements from sensors included in the control structure of the backseat driver.

5.5 Conclusions

The main focus of this chapter was to interface external codes with a Slocum glider. This backseat driver communicates with the main vehicle control system through an interface developed by using the Robot Operating System. With this backseat driver, state information of the glider and measurements from sensors can be subscribed by backseat control algorithms, with desired state parameters being sent to the main vehicle control system for adaptive control. A series of simulations were conducted with this Slocum G1 glider to test the performance of this backseat driver in adaptively controlling the depth, heading, waypoints, and behavior state of the glider. Performance of the backseat control from these simulations reveals its ability to control the glider adaptively and in real time.

In the adaptive depth changing mission, the depth controller in the backseat driver was insensitive to the value of δ_{depth}, which defines distance from the next target depth, even at a small value of 1 m. This reviewed that the backseat driver could receive states of the glider from the main vehicle control system and control the depth of the glider in a timely manner. In the mission of changing the heading of the glider to track the boundary of a simulated plume in the horizontal plane, the performance of boundary following of the glider was affected by its turning radius. The minimum turning radius of this Slocum G1 glider was approximately 17 m, measured from a simulation in this chapter. When precisely tracking an ocean feature with this glider, the relative size between the ocean feature and the minimum turning radius of the glider should be taken into consideration to plan the path of the glider.

This developed backseat driver will be tested in field experiments in the near future, with sensors and safety rules included in the mission files and control algorithms. The sensors will be used to provide real-time measurements to the backseat driver. With the ability of successful adaptive control, the glider will be able to do intelligent missions and improve its efficiency in sampling interesting targets.

The chapter answered the second research question in section 1.2. (Q2: Is it possible to equip a Slocum glider with the ability of adaptive control?) and reached the second sub-objective in Section 1.3 (O2: To develop a Slocum glider with adaptive control to investigate oil spills in the ocean intelligently). However, the adaptive control was developed by having a backseat driver on the glider and this development was only proved through lab experiments in this chapter. The field test of the development is present in Chapter 8.

Acknowledgement

Funding was received from Fisheries and Oceans Canada through the Multi-partner Oil Spill Research Initiative (MPRI) 1.03: Oil Spill Reconnaissance and Delineation through Robotic Autonomous Underwater Vehicle Technology in Open and Iced Waters and the School of Graduate Studies at Memorial University of Newfoundland.

References

Alvarez, A., Chiggiato, J., Schroeder, K., 2013. Mapping sub-surface geostrophic currents from altimetry and a fleet of gliders. Deep. Res. Part I Oceanogr. Res. Pap. 74, 115–129. https://doi.org/10.1016/j.dsr.2012.10.014

BeagleBoard.org, 2019. BeagleBone Black. [WWW Document]. URL https://beagleboard.org/black (accessed 2.9.21).

Benjamin, M.R., Leonard, J.J., Schmidt, H., Newman, P.M., 2012. Nested Autonomy for Unmanned Marine Vehicles with MOOS-IvP. J. F. Robot. 29, 554–575.

Bluefin Robotics, 2013. Bluefin and MIT Demonstrate AUV Plug-n-Play Payload Autonomy.

[WWW Document]. URL https://defense-unmanned.com/article/1056/bluefin,-mit-demo-auv-payload-autonomy.html (accessed 2.9.21).

Cetinić, I., Toro-Farmer, G., Ragan, M., Oberg, C., Jones, B.H., 2009. Calibration procedure for Slocum glider deployed optical instruments. Opt. Express 17, 15420–15430. https://doi.org/10.1364/oe.17.015420

Dent, S, 2014. Fleet of underwater gliders could improve global weather forecasts. [WWW Document]. URL https://www.engadget.com/2014/03/17/rutgers-challenger-glider-submarine-mission/?ncid=rss_truncated (accessed 9.21.20).

Dhont, D., Jatiault, R., Lattes, P., 2019. Combined Use of SAR and Underwater Gliders for Oil Seeps Detection, in: International Geoscience and Remote Sensing Symposium (IGARSS). Institute of Electrical and Electronics Engineers Inc., Yokohama, Japan, 28 July-2 August, pp. 7865–7868. https://doi.org/10.1109/IGARSS.2019.8898602

Domingues, R., Kuwano-Yoshida, A., Chardon-Maldonado, P., Todd, R.E., Halliwell, G.R., Kim, H.S., Lin, I.I., Sato, K., Narazaki, T., Shay, L.K., Miles, T., Glenn, S., Zhang, J.A., Jayne, S.R., Centurioni, L.R., Le Hénaff, M., Foltz, G., Bringas, F., Ali, M.M., DiMarco, S., Hosoda, S., Fukuoka, T., LaCour, B., Mehra, A., Sanabia, E.R., Gyakum, J.R., Dong, J., Knaff, J., Goni, G.J., 2019. Ocean observations in support of studies and forecasts of tropical and extratropical cyclones. Front. Mar. Sci. 6. https://doi.org/10.3389/fmars.2019.00446

Eickstedt, D.P., Sideleau, S.R., 2010. The backseat control architecture for autonomous robotic vehicles: A case study with the Iver2 AUV. Mar. Technol. Soc. J. 44, 42–54. https://doi.org/10.4031/MTSJ.44.4.1

Ferri, G., Cococcioni, M., Alvarez, A., 2016. Mission planning and decision support for underwater glider networks: A sampling on-demand approach. Sensors (Switzerland) 16, 1–

23. https://doi.org/10.3390/s16010028

Fiorelli, E., Bhatta, P., Leonard, N.E., Shulman, I., 2003. Adaptive sampling using feedback control of an autonomous underwater glider fleet, in: Proc. 13th Int. Symp. on Unmanned Untethered Submersible Technology (UUST). Durham NH, USA, 1-5 August, pp. 1–16.

Gallimore, E., Stokey, R., Terrill, E., 2018. Robot Operating System (ROS) on the REMUS AUV using RECON, in: 2018 IEEE/OES Autonomous Underwater Vehicle Workshop. Porto, Portugal, 6-9 November, pp. 1–6. https://doi.org/10.1109/AUV.2018.8729755

Graver, J.G., Bachmayer, R., Leonard, N.E., Fratantoni, D.M., 2003. Underwater glider model parameter identification, in: Proc. 13th Int. Symp. on Unmanned Untethered Submersible Technology (UUST). Durham NH, USA, 1-5 August, pp. 1–12.

Ivić, S., Crnković, B., Arbabi, H., Loire, S., Clary, P., Mezić, I., 2020. Search strategy in a complex and dynamic environment: the MH370 case. Sci. Rep. 10. https://doi.org/10.1038/s41598-020-76274-0

Ivic, S., Crnkovic, B., Mezic, I., 2017. Ergodicity-Based Cooperative Multiagent Area Coverage via a Potential Field. IEEE Trans. Cybern. 47, 1983–1993. https://doi.org/10.1109/TCYB.2016.2634400

Keane, J.R., Forrest, A.L., Johannsson, H., Battle, D., 2020. Autonomous Underwater Vehicle Homing with a Single Range-Only Beacon. IEEE J. Ocean. Eng. 45, 395–403. https://doi.org/10.1109/JOE.2018.2877535

Kim, E., Fan, S., Bose, N., Nguyen, H., 2021. Current Estimation and Path Following for an Autonomous Underwater Vehicle (AUV) by Using a High-gain Observer Based on an AUV Dynamic Model. Int. J. Control. Autom. Syst. 19, 478–490. https://doi.org/10.1007/s12555-019-0673-5

Mansour, A., Leblond, I., Hamad, D., Artigas, L.F., 2014. Sensor Networks for Underwater Ecosystem Monitoring and Port Surveillance Systems, in: Sensor Networks for Sustainable Development. CRC Press, pp. 431–467. https://doi.org/10.1201/b17124-19

Mavrommati, A., Tzorakoleftherakis, E., Abraham, I., Murphey, T.D., 2017. Real-Time Area Coverage and Target Localization using Receding-Horizon Ergodic Exploration. IEEE Trans. Robot. 34, 62–80.

Meurer, C., Fuentes-Perez, J.F., Schwarzwalder, K., Ludvigsen, M., Sorensen, A.J., Kruusmaa, M., 2020. 2D estimation of velocity relative to water and tidal currents based on differential pressure for autonomous underwater vehicles. IEEE Robot. Autom. Lett. 5, 3444–3451. https://doi.org/10.1109/LRA.2020.2976318

Naglak, J.E., Page, B.R., Mahmoudian, N., 2018. Backseat Control of SandShark AUV using ROS on RaspberryPi ∗, in: OCEANS 2018 MTS/IEEE Charleston, OCEAN 2018. Charleston, SC, USA, 22-25 October, pp. 1–5. https://doi.org/10.1109/OCEANS.2018.8604630

Page, B.R., Ziaeefard, S., Pinar, A.J., Mahmoudian, N., 2017. Highly Maneuverable Low-Cost Underwater Glider: Design and Development. IEEE Robot. Autom. Lett. 2, 344–349. https://doi.org/10.1109/LRA.2016.2617206

Ros.org, 2021. ROS: Powering the world's robots. [WWW Document]. URL https://www.ros.org/ (accessed 2.9.21).

Stommel, H., 1989. The Slocum Mission. Oceanography 2, 22–25. https://doi.org/10.5670/oceanog.1989.26

Teledyne Webb Research, 2010. Slocum G1 Glider Manual. [WWW Document]. URL https://manualzz.com/doc/6922727/slocum-g1-glider-manual (accessed 4.18.20).

Todd, R.E., Rudnick, D.L., Sherman, J.T., Owens, W.B., George, L., 2017. Absolute Velocity

Estimates from Autonomous Underwater Gliders Equipped with Doppler Current Profilers. J. Atmos. Ocean. Technol. 34, 309–333. https://doi.org/10.1175/JTECH-D-16-0156.1

Zhou, M., 2012. The approach of improving the roll control of a slocum autonomous underwater glider. Memorial University of Newfoundland.

Zhou, M., Bachmayer, R., 2011. Working towards single beam acoustic iceberg profiling using active roll control on a Slocum glider, in: 2011 IEEE Symposium on Underwater Technology, UT'11 and Workshop on Scientific Use of Submarine Cables and Related Technologies. Tokyo, Japan, 5-8 April, pp. 1–7. https://doi.org/10.1109/UT.2011.5774106

Zhou, M., Bachmayer, R., Deyoung, B., 2017. Underwater acoustic-based navigation towards multi-vehicle operation and adaptive oceanographic sampling, in: IEEE International Conference on Intelligent Robots and Systems. Vancouver, BC, 24-28 Sept, Canada, pp. 6091–6097. https://doi.org/10.1109/IROS.2017.8206508

Zhou, M., Bachmayer, R., DeYoung, B., 2019. Mapping the underside of an iceberg with a modified underwater glider. J. F. Robot. 36, 1102–1117. https://doi.org/10.1002/rob.21873

6. Chapter 6

Cooperation and compressed data exchange between multiple gliders used to map oil spills in the ocean

Yaomei Wang, Worakanok Thanyamanta, Neil Bose

Department of Ocean and Naval Architectural Engineering, Memorial University of Newfoundland, St. John's, NL A1B 3X7, Canada

This chapter is a journal paper which has been published in Applied Ocean Research (2022), 118, 102999. https://doi.org/10.1016/J.APOR.2021.102999 (Article No.4 (APOR)).

Table 6-1. Individual Author Contribution – Article No.4 (APOR)

Author	Contribution
Yaomei Wang	Conceptualization, Methodology, Software, Validation, Formal analysis, Investigation, Resources, Writing—original draft preparation, Writing—review and editing, Visualization
Worakanok Thanyamanta	Writing—original draft preparation, Writing—review and editing, Supervision
Neil Bose	Writing—original draft preparation, Writing—review and editing, Supervision, Project administration, Funding acquisition

Abstract

This chapter describes a cooperation strategy and method to compress data to be transmitted between multiple underwater gliders used to delineate oil spills in the ocean. In the cooperation strategy, the survey area is discretized into a series of blocks. One glider is used as a scout to map the oil in each block. The scout glider then sends the locations of potential information-rich oil patches to follower gliders to conduct detailed surveys of the oil patch areas. To compress the data to be transmitted between gliders, the Support Vector Machine (SVM) method was used to classify the boundaries of the oil patches. Measurements from the scout glider were mapped onto a grid map to decrease the quantity of data being processed and a clustering method was proposed to be applied prior to the SVM to simplify the characteristics of the data sets. Two clustering methods were compared through simulations, of which a Density-Based Spatial Clustering of Applications with Noise method was found to be more accurate and reliable than a mean-shift method in classifying the correct number of clusters. Based on the classified boundaries of the oil patches, the scout glider could then send compressed data to its followers so that they could further investigate the patches. The proposed method compresses the information communicated between gliders which in turn was found in simulations to improve the efficiency of real-time underwater communication and cooperation between networked gliders.

Keywords: Multiple underwater gliders; Oil patches; Boundary classification; Data compression; Support vector machine; Clustering method

6.1 Introduction

For detecting oil plumes, multiple underwater vehicles can be used as a response tool to perform plume tracking (Melo and Matos, 2019; Schulz et al., 2003) through communication between vehicles. One vehicle can help identify a potential region of interest before calling on more vehicles for a detailed investigation. Multiple cooperative underwater vehicles have adaptability in conducting complex tasks as these tasks can be decomposed into a set of tractable subtasks for each vehicle (Deng et al., 2013). Each vehicle can be fitted with specific sensors and thus the multi-vehicle system can have a wider range of sensor capability than a single vehicle. With the use of more than one vehicle, the performance in terms of fault tolerance can be improved as the malfunction of a single vehicle can be detected and this vehicle can be excluded from the mission work without affecting the work of rest vehicles (Bechlioulis et al., 2019). A variety of applications can benefit from the use of multiple cooperative underwater vehicles. For example, the accuracy in a simultaneous localization and mapping mission is improved when multiple underwater vehicles share information between vehicles, as additional constraints such as observed features from other vehicles can be used to minimize the accumulation of errors (Paull et al., 2015).

In a project involving autonomous underwater vehicles (AUVs) to characterize oil seeps off the coast of Santa Barbara, California, multiple underwater vehicles were used for a mission to investigate underwater oil from the seeps (Abt Associates et al., 2020). A long range AUV equipped with a SeaOWL UV-A fluorometer was used to determine the potential areas where oil was present before missions were planned for other REMUS AUVs to sample the area. This process saved the mission time of the REMUS AUVs in identifying the areas with rich information. Two data collection strategies were applied with the aim to improve the sensitivity and reliability of detecting oil with the REMUS AUVs. The first strategy involved a REMUS-100 with EK80 sonar to survey the ocean first and then the measurements were used to instruct a REMUS-600 AUV to further assess a specific area of interest. This strategy was not fully autonomous as operators were involved in identifying the potential hot spots of oil based on the missions of the REMUS-100 and then instructions were sent to the REMUS-600 vehicle. In the second strategy, a REMUS-600 AUV conducted a pre-defined search pattern first and was triggered to have a detailed search when an anomaly was detected. The detailed survey in the second strategy led to a much longer mission duration when only a single vehicle was used. The duration of the mission could be reduced by using multiple vehicles. Fiorelli et al. (2006) proposed a cooperative control strategy which allowed a fleet of underwater gliders to track features such as plumes. In this strategy, the control of a glider fleet was realized with a virtual body and artificial potential multi-vehicle control method. A set of moving reference points called virtual leaders were introduced to form a virtual body. The virtual leaders controlled the motion of the gliders including the speed and orientation of the group. The fleet of gliders moved with the virtual body by the force derived from artificial potential while maintaining their formation in a desired geometry. Zhang et al. (2007) put forward an approach to control gliders on closed curves for ocean sampling. Each glider was modelled as a Newtonian particle. The velocity of each particle, phase difference and relative velocities between particles, and the guidance of each particle to the desired curve were controlled to achieve an invariant pattern on the closed curves. As the fleet of gliders moved as a group, the flexibility in conducting multiple missions simultaneously, such as exploring and exploiting underwater oil spill, was decreased. Zhang et al. (2020) used measurements from a fleet of gliders to construct a three-dimensional ocean field based on a spatio-temporal Kriging interpolation. However, as the constructed fields were temperature and salinity fields, the location of the fields were known, as opposed to oil plumes which are driven more dynamically by the changing environment. The gliders were therefore not required to explore the locations of temperature and salinity fields before starting the measurements. In the work of Berget et al. (2018), an ocean model SINMOD (Wang et al., 2013) and a Lagrangian particle transport model DREAM (Rye et al., 2014), were used onboard an AUV to create a prior model of the ocean to assist in path planning of the AUV to track dispersed particles. The prior model was updated during missions with measurements from sensors in real time when the vehicle was deployed. Inputs for the model DREAM included hydrodynamic information from the ocean model SINMOD and data of the discharged particles such as discharge amounts. Planning a mission based on simulated environmental models or historical data is challenging as the ocean is dynamic. Applications of environmental model-based methods can be limited when the data of the discharged particles is unavailable.

In our study, we were interested in using an adaptive mapping strategy to sample oil plumes with a cooperative network of gliders. An adaptive mission means that the vehicle can change its states such as heading and depth adaptively in real-time based on measurements from sensors onboard of the vehicles in real time. This strategy is suitable for oil plumes which are typically not continuous but can be patchy in nature, and can disperse quickly in ocean waves and currents. Using a single glider and a pre-defined trajectory can lead to the glider spending a lot of time searching for and hence outside of the plumes. Effective cooperation and communication among gliders are key to successful adaptive missions with multiple gliders. In the adaptive mapping strategy with multiple gliders that we used in our study, a prior survey with the use of one glider, a scout glider, was conducted first to pre-define or explore a portion of the search area for the followers. The scout glider followed a specific path such as a lawn-mower path to do a coarse mapping of the area. The prior survey aimed to overcome the drawback in AUV surveys where a planned path may not cover any interesting oil plume patches (Wang et al., 2021b). The scout glider then sent locations of potential information-rich patches to the followers to conduct detailed surveys of the oil spill patch areas.

The benefits of using multiple cooperating underwater vehicles cannot be separated from issues concerning communication between the vehicles. Underwater vehicles can communicate with each other both on the surface and underwater. Underwater communication is preferred as the vehicles can share information in real-time and update their missions with information in a timely manner. As radio frequency waves and optical waves have very limited range in water, acoustic communication is used more commonly on underwater vehicles (Sahoo et al., 2019). However, acoustic underwater communication is characterized by limited bandwidth (Chen and Pompili, 2014). Due to the limited bandwidth, data exchange between underwater vehicles is challenging as the data transmission rate is limited, leading to a significant time delay proportional to the amount of data being transmitted (Zhang and Ding, 2007).

Data compression is one way to reduce the limitations in communication. An example of this in action is in cooperative path planning with a fleet of gliders where regions with strong currents should be avoided by the gliders. Liu et al. (2014) proposed an approach to compress water current information collected in the vicinity of each glider that could be shared between gliders. The flow information gathered by each vehicle was compressed by a method called Support Vector Data Description (Tax and Duin, 2004). This method found the boundaries of areas with strong currents and simplified the information by using a limited number of points. As only a small number of points were shared between the gliders, the influence from limited communication bandwidth were mitigated even though the exchange of the current information happened frequently. In a second example in mine-countermeasures missions involving the use of multiple AUVs to collaboratively detect underwater mine-like objects, Johnson et al. (2009) proposed to create a multi-layered map with a low-bandwidth acoustic communication to improve the reliability of a mission without losing information if AUVs were lost. This multi-layer map maintained data redundancy with a low-resolution map created using relatively low information and frequent communications and a high-resolution map created using high information, less frequent communications. In creation of the high-resolution map, the locations of mine-like objects were represented in cell coordinates with a cell size of 5 m. This process decreased the amount of data being transmitted. Data compression has also been used in environmental monitoring missions (Rahmati et al., 2019).

In this chapter, we propose a cooperation strategy and method to compress data to be transmitted among gliders in delineating oil patches underwater. We first introduce the proposed cooperation strategy for multiple gliders in Section 6.2.1. The information sent by the scout glider to its followers was compressed by using a boundary classification method which classified boundaries for the information-rich regions resulting in less information needing to be transmitted. For classifying the boundaries between the areas with and without rich information, a machine-learning method, the Support Vector Machine (SVM), is considered and presented in Section 6.2.2. The SVM method is a supervised learning algorithm which can be used for classification and regression problems (Shmilovici, 2005). The limitation of SVM in defining the boundaries of patches is also described, leading to the introduction of clustering methods in Section 6.2.3. The boundary identification strategy used to compress data is proposed in Section 6.3.1, and the compressed mission data are then presented in Section 6.3.2. We assess the boundary classification strategy through simulations in Section 6.4. The performance and future application of the cooperation strategy and the boundary classification method to compress data are discussed in Section 6.5. A conclusion is presented in Section 6.6.

6.2 Research problem statement

In this section, we introduce the cooperation of multiple underwater gliders that our proposed boundary classification strategy is based on and state the limitations of SVM in boundary classification. Clustering methods for remedying the limitations of SVM are also introduced.

6.2.1 Proposed cooperation strategy of multiple underwater gliders

In our simulation, we assumed a team of gliders with sensors were deployed into the ocean for mapping an area with potential oil patches. Each glider was equipped with a backseat driver for adaptive control and this functionality has been realized previously in gliders (Wang et al., 2021a). The mission area was split up into blocks with dimensions specified based on the working range of the acoustic modems installed on the gliders in order to ensure that the gliders can communicate with one another. In the path planning of each glider in this work, only the path in the horizontal plane was planned adaptively and the diving depth was defined beforehand. One glider was assigned as a scout glider and the rest were assigned as followers. The cooperation of the gliders consisted of two stages: overall survey by the scout glider and detailed surveys by follower gliders. Both the scout glider and the followers communicated through acoustic modems. Localization of the gliders was improved through a system mounted under the surface vessel consisting of an Ultra-Short Baseline (USBL) for localization and an acoustic modem for sending location information back to the gliders (Costanzi et al., 2017). This has been found to be practical for an underwater glider in tests by Zhou et al. (2017) on a Slocum glider. In their work, the position of an underwater glider from a surface vehicle SeaDragon was determined by using a USBL/acoustic modem. The position error of the underwater glider was within 15 m when referred to surface buoys attached to the glider, which is considered quite accurate given that the survey area can be of many kilometers.

(1) Overall survey by the scout glider

Within each block, the scout glider was first commanded to follow a search path, such as a lawn-mower path with a starting point at A and an end point at B as shown in Figure 6-1, to cover the area within the block in order to find potential areas with rich information. The path of the scout glider was defined by setting a series of waypoints based on the boundary of the block and the width of the mowed path known prior to the mission. After the scout glider finished delineating the block, it processed its measurements to identify the boundaries of the information-rich patches before sending compressed mission commands to its followers to perform detailed surveys of the identified patches. The method to classify the patch boundaries to compress the data is described in detail in Section 6.3. The size of the data transmitted to the followers depends on the number of patches identified by the scout glider.

The scout glider ended its delineation mission in the first block after sending commands to the followers. Then it crossed over the block boundary (P_3 to P_4 in Figure 6-1 (b)) to start a new mission by conducting another lawn-mower path in a new block (block 2 in Figure 6-1 (b)). The scout glider also had the ability to adaptively reassign its own path to avoid collisions. For example, the scout glider would communicate with followers on the P_3 to P_4 boundary to avoid collisions when crossing the boundary from block 1 to block 2, and it would make sure that all the followers were on the boundaries of block 2 before ending its mission within block 2 and moving on to the next block. This process repeated until all of the blocks in the survey area were mapped, or the maximum mission time was reached.

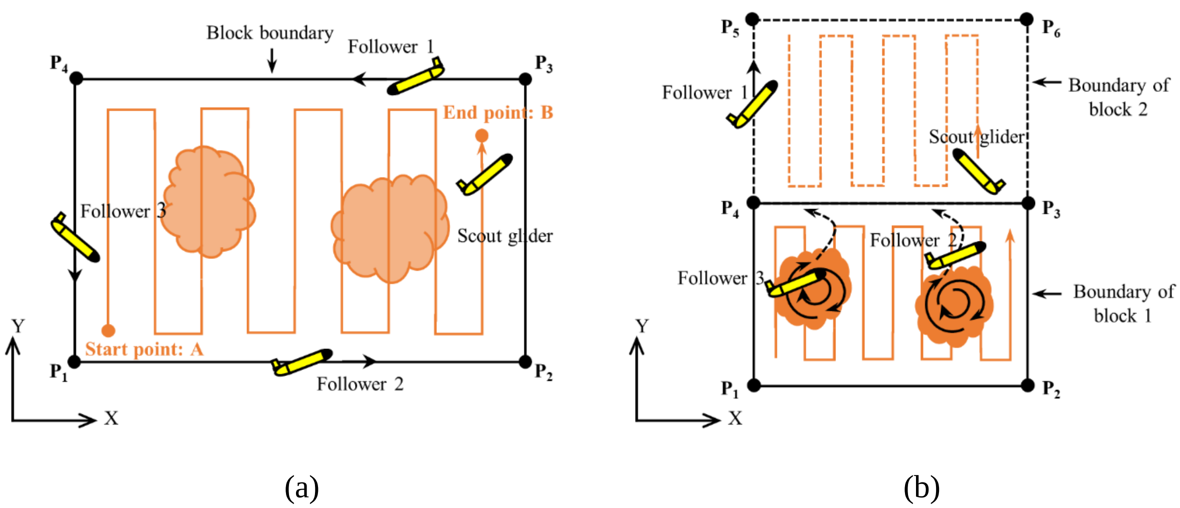

Figure 6-1 Cooperation of gliders: (a) a scout glider delineating the area within a block and followers waiting for commands from the scout glider; (b) a scout glider delineating the area inside a second block and followers mapping the patches with rich information or waiting for commands from the scout glider.

(2) Detailed surveys by the follower gliders

While the scout glider was mapping a block, the other follower gliders waited for the commands from the scout glider by following the path along the boundary of the block using waypoint behaviors with four target waypoints (P_1, P_2, P_3 and P_4 in Figure 6-1 (a)). This was to avoid collisions between the scout glider and the followers as the scout glider only moved inside while the followers moved along the boundary of the block. Each follower communicated with the glider in front of it through acoustic modems to maintain a minimum distance between them. If the distance between the gliders, e.g., Follower 2 and Follower 1 in Figure 6-1 (a), was shorter than a required distance, Follower 2 would calculate the time needed to increase the distance and surfaced for that period of time.

Once the followers received the mission information from the scout glider, they moved inside the block to start their detailed survey missions to search the potential patches by using spiral paths. If the number of missions (equal to the number of patches with rich information) was larger than the number of followers, all of the followers were commanded to delineate the areas within the current block. If the number of missions was less than the number of followers, the followers with no assigned missions would move over to the next block and continued their waypoint behavior along the boundary of a new block (e.g., P_3, P_4, P_5 and P_6 in Figure 6-1 (b)). As usual, the followers communicated with other followers as they moved from block 1 to block 2 to avoid collision. For example, when Follower 2 and Follower 3 finished their missions in block 1 and were trying to enter block 2 through the P_3-P_4 boundary, these two followers would communicate with each other as well as with other followers heading to the waypoint P_4. A follower that was closer to the vertex P_4 was defined as a prior glider to another glider and the minimum distance requirement was applied to all the followers.

6.2.2 Support vector machine (SVM)

6.2.2.1 Principle of SVM

For identifying the boundaries of patches with rich information, the scout glider classifies the data sets with the use of SVM. SVM is a popular classification method (Satapathy et al., 2019) that has been used in ice–water discrimination (Leigh et al., 2014), forest fire detection and urban area extraction from satellite images (Lafarge et al., 2005), area determination of diabetic foot ulcer images (Wang et al., 2017), and face recognition (Qin and He, 2005). For linearly separable data (see Figure 6-2 (a)) with a set of training data x_i $(i = 1, 2, 3, \dots, n)$, data of each class is on the left (y = 1) and on the right (y = -1) of the hyperplane. The aim of SVM is to find a hyperplane with maximum margin between the data in each class by solving (Awad and Khanna, 2015):

$$\min \frac{1}{2} w^T w + C \sum_{i}^{n} \xi_i \, , s.t. \, y_i(w^T x_i + b) \geq 1 - \xi_i, i = 1, 2, 3, \dots, n \tag{6-1}$$

where w is the vector normal to the hyperplane, C is the penalty parameter which controls the training error and classification margin (Tharwat, 2019), ξ_i is an allowed level of error which is to keep the margin as wide as possible so that all data can still be classified correctly, and b is the bias.

For linearly inseparable data (see Figure 6-2 (b)), SVM projects data onto a higher-dimensional space by using kernel functions to find the optimal hyperplane (Gholami and Fakhari, 2017). Support vectors are data points nearest to the hyperplane through which the maximum margin can be decided. They will alter the position of the hyperplane if removed. When solving classification problems with data using SVM, a hyperplane with some sampling points on this plane will be obtained to define the boundary between classes of data. By connecting these sampling points, the shape and size of the areas with rich information can be obtained to plan missions for follower gliders.

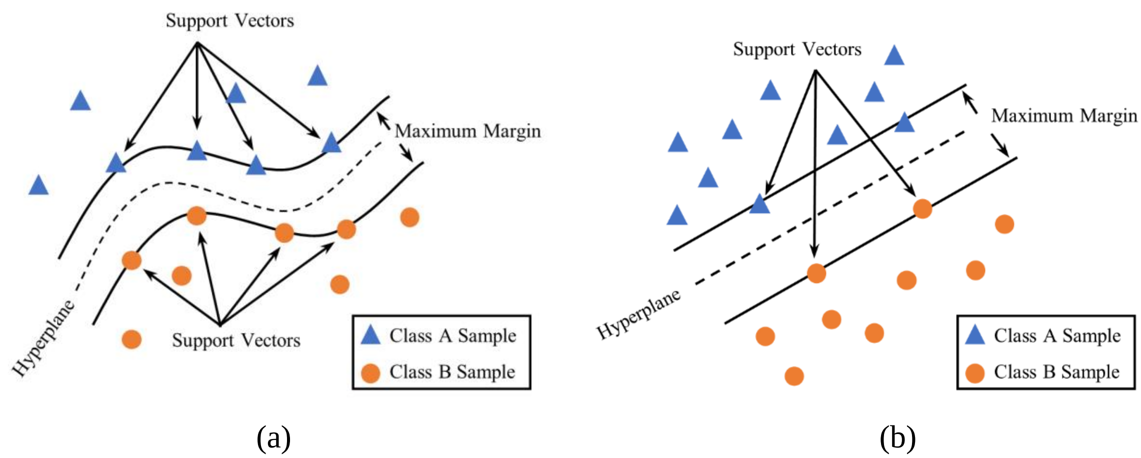

Figure 6-2. Support vector machine for classification: (a) linear separable case; (b) linear inseparable case.

6.2.2.2 Limitations of using SVM in boundary classification

Despite the wide application of SVM, this method has limitations. The performance of SVM is affected by choices of the kernel functions and parameters (Gholami and Fakhari, 2017), such as the penalty parameter C (Tharwat, 2019). One kernel function is not enough if the characteristics of the data sets are complex (Wang and Xu, 2017). In addition, SVM is not suitable for large data sets, as the training time depends on the size of the data sets. Besides, for the problem defined in section 6.2.1 where the scout glider processed measurements to define boundaries of patches, SVM is unable to provide a boundary for each patch.

For example, if there are two patches of areas with rich information (Figure 6-3), two types of boundaries can be obtained through SVM depending on kernel functions and parameters used (Figure 6-4). The boundary shown in Figure 6-4 (a) is preferred to that shown in Figure 6-4 (b) as the area between these two patches is without rich information. It is preferred to classify the data with rich information into two patches. However, unlike for humans, it is difficult for an underwater robot to find the best kernel and parameters that provides optimal boundaries for patches in Figure 6-3. Therefore, clustering methods were considered to help improve accuracy and performance of SVM in identifying boundaries.

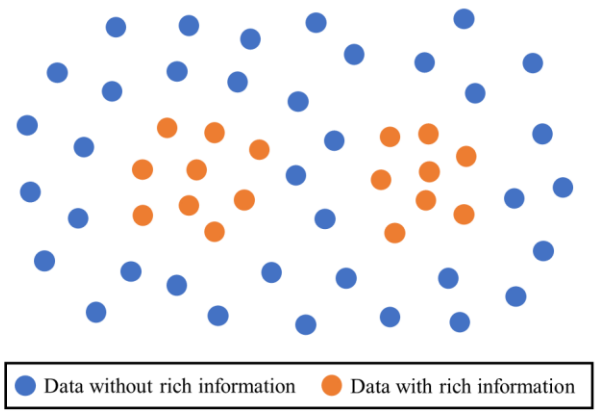

Figure 6-3. Two classes of data with a distribution of two patches of data with rich information.

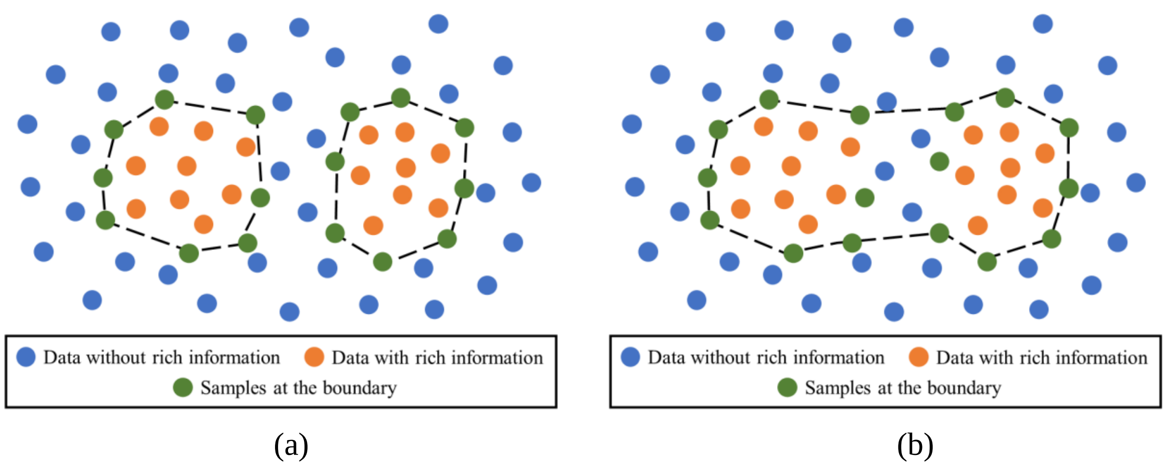

Figure 6-4. Two classes of data with a distribution of two patches of data with rich information: (a) ideal boundary classification result between data with and without rich information; (b) possible boundary classification result between data with and without rich information.

6.2.3 Clustering methods

Clustering methods are used to group a population of data points into clusters based on their similarity. A clustering method can be used to enhance SVM by grouping data according to their position before applying SVM. In Figure 6-5, the set of data with rich information (Figure 6-3) was clustered into two sets of data: data with rich information - 1 and data with rich information - 2. Two boundaries can then be derived surrounding these two clusters. The aim of using a clustering method is to reduce the complexity in the characteristics of data for the classification of SVM, which, ultimately, reduces the sensitivity of SVM to the change in the kernel function and parameters selected.

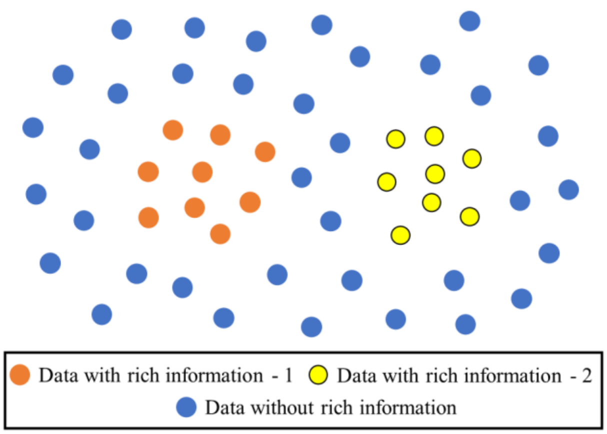

Figure 6-5. Data with rich information are clustered into groups for better classification of the boundaries of rich-information patches.

There are various data-clustering algorithms available. The K-means algorithm is one of the most widely used clustering methods (Sinaga and Yang, 2020). This algorithm requires the number of clusters to be specified beforehand. There are also some other clustering methods such as hierarchical clustering (Guyeux et al., 2019), affinity propagation clustering (Refianti et al., 2016), Gaussian Mixture Models (Zhao et al., 2019). The pros and cons of these clustering algorithms are presented in Table 6-2.

Table 6-2. Pros and cons of several typical Clustering algorithms.

Clustering algorithms	**Pros**	**Cons**
K-Means clustering	· Simple to be implemented.	· Choosing the number of clusters manually. · Initial centroids have influence on the final clustering. · Sensitive to outliers.
Mean-shift clustering	· Number of clusters does not need to be specified beforehand.	· The kernel bandwidth is hard to be defined.
Density-Based Spatial Clustering of Applications with Noise (DBSCAN)	· Number of clusters does not need to be specified beforehand. · Able to find arbitrary shaped clusters. · Able to identity outliers.	· Requires specifying the size of neighborhood (*Eps*) and the minimum density (*MinPts*). DBSCAN is sensitive to the choice of these two parameters. · The clustering result is not ideal in the case of high dimensional data.
Hierarchical Clustering	· Number of clusters does not need to be specified beforehand. · Results are reproducible. · Easy to be implemented.	· Cannot handle big data sets. · Difficult to identify the right number of clusters through dendrogram in some cases.
Affinity propagation	· Number of clusters does not need to be specified beforehand. · Clustering results do not depend on initialization.	· Not effective in processing large-scale data sets.
Gaussian Mixture Models	· A soft clustering method where each point belongs to all clusters, but with different probabilities. · Robust against observation noise.	· Assume that each point is independent of its neighbors.

In the clustering of information-rich data in this chapter, the number of clusters is unknown beforehand. Therefore, the mean-shift clustering algorithm and Density-Based Spatial Clustering of Applications with Noise (DBSCAN) (Ester et al., 1996) clustering algorithm were considered and compared in this chapter based on their application domain and the ability to calculate the number of clusters automatically. They are presented here in detail.

6.2.3.1 DBSCAN clustering algorithm

DBSCAN is a density-based clustering algorithm. The key idea of the DBSCAN algorithm is that for each point in a cluster, the point density in the neighborhood within a given radius has to exceed a threshold (Ester et al., 1996). Two parameters need to be specified in this method: the radius (*Eps*) for defining the size of the neighborhood around a point and the number of points (*MinPts*) for defining the minimum density. In a dataset, a point is defined as a core point if it has a minimum number of neighbors (*MinPts*, including the point itself) in its surrounding. For example, in Figure 6-6, point B is a core point with *MinPts* equal to 4. If a point has a number of neighbors (including the point itself) less than *MinPts* but belongs to the neighborhood of a core point, this point is considered as a border point (point A in Figure 6-6). Points neither belonging to core points nor to border points are defined as noise points or outliers (point D in Figure 6-6). All of the neighbors of a core point are directly reachable from the core point; a point P_1 is density-reachable from P_2 if there are a number of core points leading from P_2 to P_1 (point A is density-reachable from point B in Figure 6-6); a point P_1 is density-connected from P_2 if there is a core point P_3 from which both P_1 and P_2 are density-reachable (point A is density-connected from point C) (Ester et al., 1996). The process of the DBSCAN algorithm is to cluster points which are density-connected.

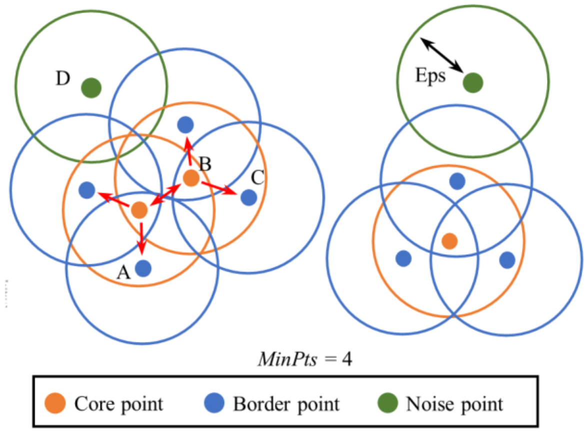

Figure 6-6. Principle of DBSCAN clustering algorithm with *MinPts* = 4 in which the red rows show the direct density reachability.

6.2.3.2 Mean-shift clustering algorithm

The mean-shift method was proposed by Fukunaga and Hostetler in 1975 (Fukunaga and Hostetler, 1975). The mean-shift algorithm is a non-parametric density-based clustering algorithm which does not specify the number of clusters and the shape of each cluster. This algorithm uses a sliding window to find the dense area and clusters a set of points into different classes. To explain how the mean-shift algorithm works, an example with a set of points in two-dimensional space is shown in Figure 6-7. In this example, the sliding window has a radius of R centered at point O. The density inside the sliding window is proportional to the number of points within the sliding window. In each iteration, the position of the center point is updated by the mean of all the points inside the sliding window. The center point is updated until the area with the highest density is found and the center point becomes a cluster center. This process is repeated for multiple sliding windows. When multiple sliding windows overlap, the window containing the most points is preserved; others are deleted. The data points are clustered according to the sliding window in which they lie.

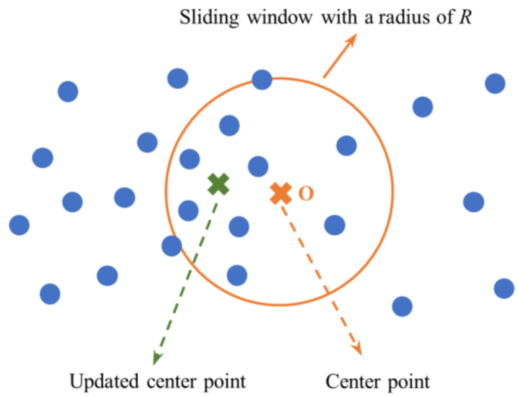

Figure 6-7. Principle of the mean-shift clustering algorithm to update the centroids of clusters.

6.3 Data compression

In this section, the classification strategy for the scout glider to define the boundary between data with and without rich information is illustrated. After identifying the boundaries, the information of patches can be compressed and the compressed data to be sent to the followers are also introduced.

6.3.1 Boundary classification

As mentioned earlier, in the mission planning of each glider in this chapter, only the path in the horizontal plane was planned adaptively. As the gliders moved in three-dimensions, the measurements collected by the scout glider during its mission to delineate a block had to be mapped onto the horizontal plane before it could be processed and generate the data necessary for developing adaptive missions for the followers. As presented in Figure 6-8, each measurement was translated onto the horizontal plane and localized by two coordinates, X and Y.

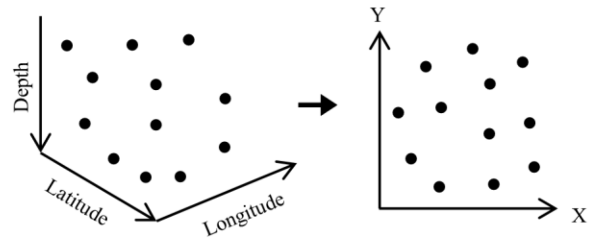

Figure 6-8. Mapping 3D measurements to 2D plane.

These measurements were labeled as being with and without rich information based on a threshold value defined. The steps of identifying the boundaries between data with and without rich information are as follows:

(1) Step 1: Map measurements to a grid map.

(2) Step 2: Cluster the grid data with rich information according to their positions.

(3) Step 3: Define boundaries between grid data with and without rich information with SVM.

The details of each step are explained below.

6.3.1.1 Map measurements to a grid map

The measurements collected by the scout gliders are usually of large quantity. In order to optimize the boundary classification method, a grid map was first applied to reduce the amount of data to be processed at one time.

The area within the block was discretized by a series of grids, with N grids in the X direction and M grids in the Y direction. The grid size was $p \times q$. It is not necessary for the mission area to be a rectangle, but the discretized grids should cover the area of interest. In each grid, there were multiple measurements. If the number of measurements with rich information within a grid was larger than 0, then this grid was defined as a grid with rich information, represented by a center point in this grid, as shown in Figure 6-9 (a). Otherwise, the grid was defined as a grid without rich information (Figure 6-9 (b)). By lumping several measurements into one, the quantity of data was decreased.

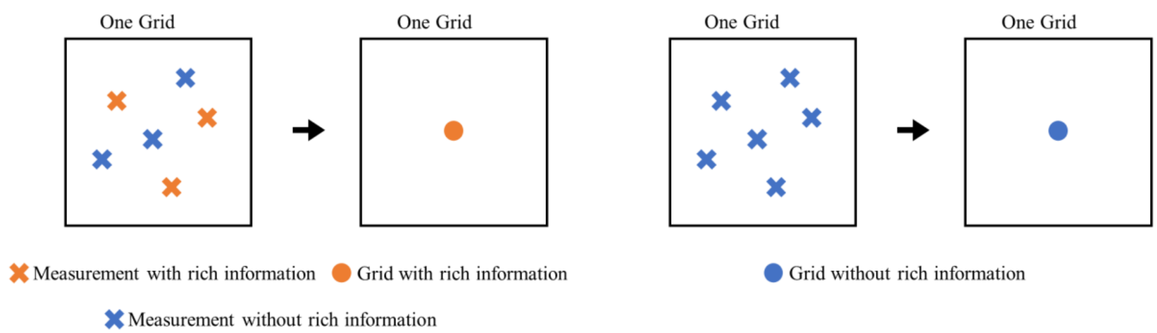

(a) (b)

Figure 6-9. Defining a grid as: (a) with rich information if the number of measurements with rich information within the grid is larger than zero; (b) without rich information if the number of measurements with rich information is zero.

The step of mapping measurements to a grid map has several advantages:

(1) Reduced time delay and increased computational efficiency. A grid map can be created before the mission of the scout glider. The measurements collected by the scout glider can be directly mapped onto the grid map during the mission by updating empty grids when measurements with rich information are detected. As the measurements are mapped onto the grid map and each grid has only one value representing whether the grid is information-rich or not, the number of data to be processed in the following steps is minimized. This

helps improve computational efficiency in processes such as data classification using SVM.

(2) Flexibility in controlling the level of detail in the boundary classification. At the beginning of this step, the area within a block is discretized into a number of grids with grid size of $p \times q$. The size of grids determines the resolution in defining the boundary between areas with and without rich information. One can change the size of a grid to balance between accuracy and computational effort in boundary classification.

6.3.1.2 Cluster the grid data with rich information according to their positions

The aim of clustering in this chapter was to cluster grid data with rich information into groups based on their positions. In this chapter, the mean-shift and the DBSCAN methods were considered. We did a comparison to determine the method that could provide a better accuracy and robustness as presented in Section 6.4.

6.3.1.3 Define boundaries between grid data with and without rich information

After the data with rich information had been clustered into different groups based on their locations, these data were classified with the use of SVM. After classification, a set of points were sampled from the predicted boundaries for later processing, such as calculating the area of each information-rich patch.

6.3.2 Compressed mission data

When the geometric information of each patch was obtained, the scout glider assigned each rich-information patch to a follower associated with survey information including the direction of its long axis and area of the patch, detailed survey mode, starting point(s) for activating the survey mode by sending these compressed data to the follower.

The scout glider commanded each follower to survey the closest patch (Figure 6-10 (a)). When the number of patches was larger than the number of the followers, some of the followers were commanded to survey more than one patch. In this case, if there were several patches with areas of A_1, A_2, and A_3 ($A_1 > A_2 > A_3$) being assigned to a glider, the glider would search for the patch with the maximum area (A_1), then the patch with the next lesser area of A_2, and then with smallest area A_3, respectively (Figure 6-10 (b)).

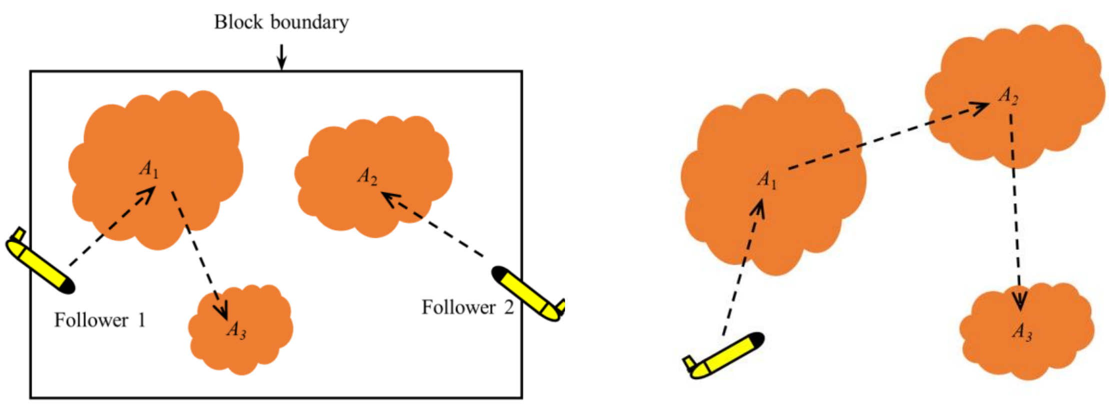

(a) (b)

Figure 6-10. Assign patches to followers: (a) based on distance from the followers; (b) based on area size if the number of patches is larger than the number of followers.

6.3.2.1 Direction of long axis and area of each patch

After defining the boundaries of rich information areas, the number of patches with rich information that required detailed surveys was obtained. The direction of the long axis and the area of each patch were then calculated. The direction of the long axis is found through rotating the local coordinates of a patch around its global coordinates. When the value of the aspect ratio is the largest, the direction of the X´ (Figure 6-11) is the direction of the long axis. Aspect ratio R is defined as

$$R = \frac{L}{W} \tag{6-2}$$

where L is the dimension of a patch in its long axis and W is the dimension of a patch in its short axis in its local coordinate system (Figure 6-11). The direction of long axis is perpendicular to the direction of the short axis.

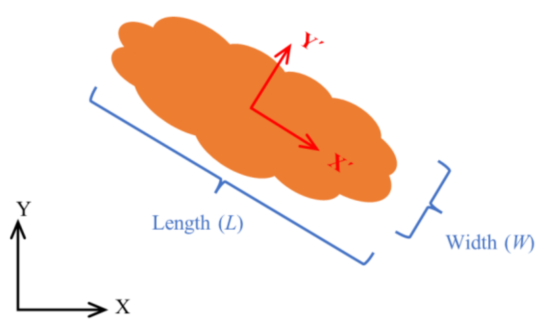

Figure 6-11. A patch with rich information in the global coordinate system (X, Y) and its local coordinate system (X´, Y´).

The area of each patch with rich information was calculated by summing up the area of trapezoids formed by the sampling points along the classified boundary. For example, Figure 6-12 (a) shows the set of points sampled from the classified boundary after using SVM. These points are in a clockwise order and are connected to form an irregular polygon. As the area of the polygon is the approximation of the area of rich information classified using SVM, if the number of sampling points is approaching infinity, we can assume that the area of the polygon is the area of the patch of rich information. For each edge in the polygon, such as an edge from point (x_1, y_1) to (x_2, y_2) in Figure 6-12 (b), the trapezoid is the area encircled by two lines normal to the X-axis through point (x_1, y_1) and (x_2, y_2), X-axis and the edge.

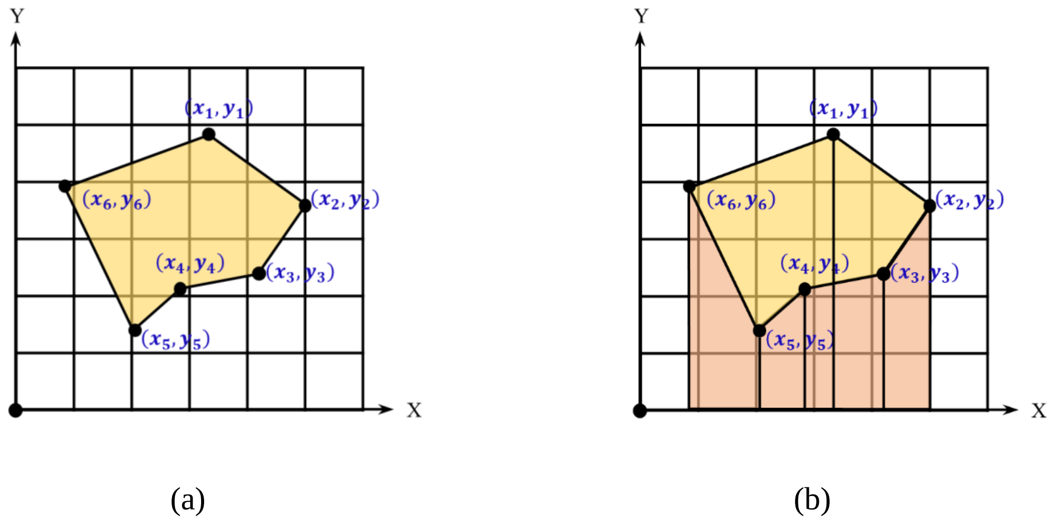

Figure 6-12. Calculate the area of a patch with rich information: (a) a set of points sampled from the predicted boundary to form an irregular polygon; (b) forming a series of trapezoid by using sampled points.

6.3.2.2 Mission mode

For each patch, the patch (mission mode) transmitted and assigned to each of the followers was designed based on the area (A) and aspect ratio (R) of the patch relative to the minimum turning radius, r, of the glider. Three mission modes were defined in this chapter. In mission mode 1, a follower followed a spiral path around the center point of the patch (Figure 6-13 (a)). This mode was activated when the area of the patch was larger than $4\pi r^2$ and the aspect ratio of the patch was lower than 2. If the area of a patch was larger than $4\pi r^2$ but the aspect ratio was not less than 2, the follower was commanded to follow mission mode 2 in which the follower followed a spiral path with a moving center point along the long axis of the patch (Figure 6-13 (b)). In mission mode 3, the follower followed a spiral path crossing the center point and the boundary of a patch (Figure 6-13 (c)) when the area of the patch was smaller than $4\pi r^2$. The smallest size of a patch depended on the grid size, and the scout glider would not be commanded detect a patch that was smaller than the grid size.

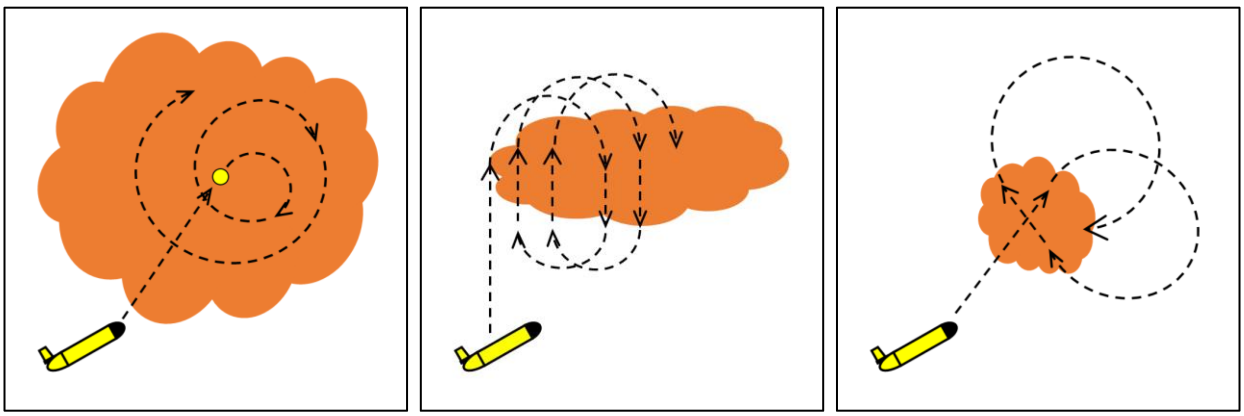

(a) (b) (c)

Figure 6-13. Three mission modes defined based on the area (A) and aspect ratio (R) of a patch relative to the minimum turning radius, r, of the glider: (a) mission mode 1 ($A > 4\pi r^2$, $R < 2$); (b) mission mode 2 ($A > 4\pi r^2$, $R \geq 2$); (c) mission mode 3 ($A < 4\pi r^2$).

6.3.2.3 Start points

Once the followers were assigned patches, start points for activating the missions to delineate these patches were also transmitted to the followers. After receiving mission commands from the scout glider, the followers went to their start points first before activating the commanded missions. For both mission mode 1 and 3, the start point was the center point of the patch. For mission mode 2, two start points were transmitted which were on the long axis of the patch and had a distance of half the length of the patch from the center of the patch (Figure 6-14). One of them was selected by the follower based on its distance from these two start points. In addition, the direction of the long axis of the patch was transmitted in mission mode 2 to instruct the follower to move along this axis while following a spiral path.

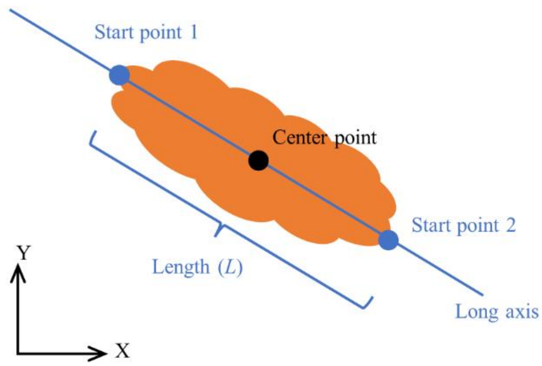

Figure 6-14. Two start points for mission mode 2 which are on the long axis at a distance of half the length of the patch from the center point.

6.4 Simulation research

Simulations were used to evaluate performance of the proposed boundary classification strategy and the benefits of including the mean-shift and DBSCAN clustering methods in SVM for defining boundaries of potential areas with rich information.

6.4.1 Simulation setup

(1) Oil plume dataset

The shape of an oil patch is affected by ocean environmental factors, such as eddies, and even human interventions, such as releasing dispersants (Chen et al., 2018). It may be of a long and thin shape (Kinsey et al., 2011), or a more compact shape (Chen et al., 2018). In our simulation, the concentration of our simulated oil plumes was based on the work of Gonçalves et al. (2016) which simulated the Deepwater Horizon oil spill with the use of a DeepC oil model and a hydrodynamical model. In their work, the oil concentration ranged from 1 ppb to 10,000 ppb in the upper layer of the ocean at a depth of 0 m to 5 m. We assumed that the oil was measured by fluorescence and noise in fluorescence detection was overcome by using multiple sensors on each glider to cross validate the detection. Areas with concentration larger than 10 ppb were considered to be of high fluorescence or have rich information and required a detailed survey by the follower gliders.

(2) Model parameters

The kernel function used in SVM was the radial basis function kernel and the penalty factor C was 10^6 for all the simulations done. In these simulations, the scout glider was commanded to follow a lawn-mower path at a horizontal speed of 0.4 m/s with given waypoints as shown in Figure 6-15. The width of the mowed path was s. In the mowed path, the scout glider collected data at a sampling rate of 2 Hz. The minimum turning radius of our gliders (r) was assumed to be 17 m (Wang et al., 2021a).

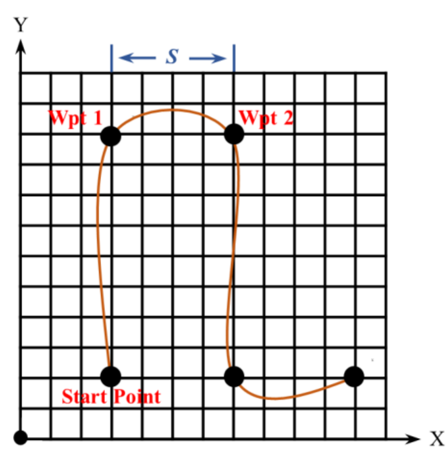

Figure 6-15. Lawn-mower path of the scout glider.

Three classification algorithms, (1) with the use of only SVM (SVM_Only), (2) SVM with the mean-shift clustering algorithm (SVM_MeanShift), and (3) SVM with DBSCAN algorithm (SVM_DBSCAN), were used in our proposed strategy in defining the boundaries of the patches. In the mean-shift clustering method, the parameter needed to be defined was the bandwidth which was automatically estimated through the processed data. In the DBSCAN clustering method, the minimum density (*MinPts*) for a cluster was defined to be 1 for all simulations to group all data into clusters.

6.4.2 Evaluation metrics

Two metrics were introduced to make a quantitative comparison of the classification algorithms: one was the number of patches that was correctly classified, the other was the root mean square error (RMSE) in predicting the boundaries of patches. For the latter metric, we used two calculations,

$$Calculation\ 1: RMSE1 = \sqrt{\frac{1}{n}\sum_{i=1}^{n}\left(1 - \frac{A_{real}^{i} \cap A_{predict}^{i}}{A_{real}^{i}}\right)^{2}} \tag{6-3}$$

$$Calculation\ 2: RMSE2 = \sqrt{\frac{1}{m}\sum_{j=1}^{m}\left(1 - \frac{A_{real}^{j} \cap A_{predict}^{j}}{A_{predict}^{j}}\right)^{2}} \tag{6-4}$$

where *n* is the number of patches in a real distribution and *m* is predicted number of patches after classification, A_{real}^{i} is the area of a patch *i* in a real distribution while $A_{predict}^{i}$ is the predicted area of the real patch i, $A_{real}^{i} \cap A_{predict}^{i}$ is the cross area between the real patch i and its prediction, $A_{predict}^{j}$ is the area of a patch j in the predicted plume which corresponds to a real patch j which has an area of A_{real}^{j}, $A_{real}^{j} \cap A_{predict}^{j}$ is the cross area between the predicted patch j and its corresponding real patch. When the value of each $A_{real}^{i} \cap A_{predict}^{i}$ equals to A_{real}^{i}, the value of *RMSE*1 is 0 which represents there is no error in prediction. This means the predicted patch covers the area of the corresponding real patch, even if the areas of predicted patches are much larger than that of real patches. In this case, we introduced the term *RMSE*2. When the value of *RMSE*2 is small, it means that the value of each $A_{real}^{j} \cap A_{predict}^{j}$ is close to the value of $A_{predict}^{j}$. The value of *RMSE*2 is 0 when the areas of all predicted patches are covered by all patches in the real distribution even if the areas of predicted patches are much smaller than that of the real patches. These two values, *RMSE*1 and *RMSE*2, are interactive, and the performance of a classification algorithm is judged by considering of both values.

6.4.3 Simulation results

6.4.3.1 Simulation 1

In this simulation, the scout glider, with a heading toward the positive X-direction at its start point (0 m, 0 m), was commanded to search an area within a block with a size of 500 m × 500 m. The glider followed a 30 m width lawn-mower path defined by waypoints. The glider was assumed to reach the first waypoint (0 m, 500 m) when the distance to the waypoint was less than 10 m. The distribution of fluorescence plumes in the search area was simulated as presented in Figure 6-16 (a). Each patch with rich information was labeled with a number (Figure 6-16 (b)). The path of the scout glider is shown in Figure 6-16 (c).

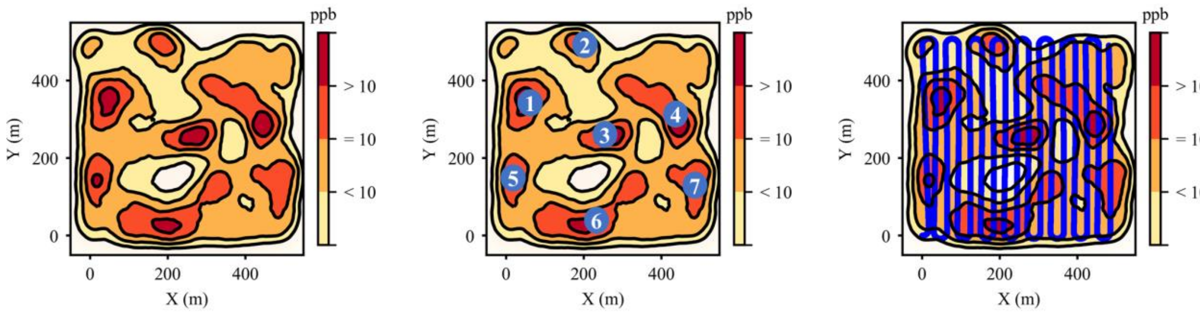

(a) (b) (c)

Figure 6-16. A scout glider was commanded to map simulated plumes: (a) the distribution of plumes; (2) each patch was labelled with a number; (c) the path of the scout glider.

After the scout glider finished mapping the searching area, measurements from the glider were mapped onto a grid map with a grid size of 30 m x 15 m (Figure 6-17). The size of the grid in the X-direction was selected based on the width of the lawn-mover path which determined the distance between measurements in the X-direction and guaranteed the continuity of grid map values in this direction. In the Y-direction, a smaller size of grid was selected as the distance between measurements in this direction was closer than in the X-direction. This selection of grid size helped decrease the quantity of data for processing without losing the continuity of data with high fluorescence. The compressed data in this grid map were then used for defining the boundaries between areas with and without rich information.

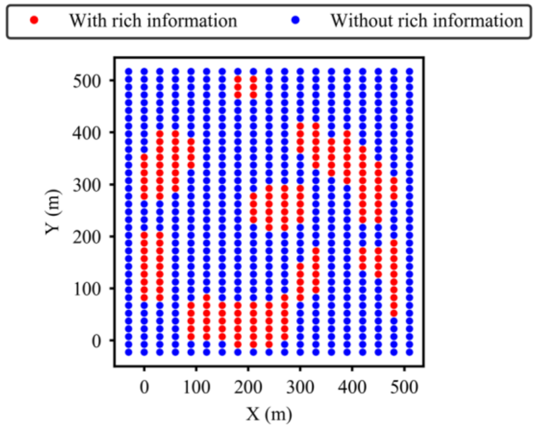

Figure 6-17. Measurements from the scout glider were mapped to a grid map with a grid size of 30 m x 15 m. The red dots show grids with high fluorescence (with rich information) while the blue dots show grids of low fluorescence (without rich information).

From the simulation results in Figure 6-18, when SVM was used with no clustering method, the algorithm classified patch 4 and 7 in Figure 6-16 (b) as only one patch. The *RMSE*2 in the SVM_Only algorithm was the highest among the three algorithms used (Figure 6-19). When the mean-shift clustering method was used, the algorithm classified patch 6 as two patches. The *RMSE*2 in the SVM_MeanShift algorithm decreased compared to the algorithm with the use of SVM only, but its *RMSE*1 was the highest compared to other two algorithms. When DBSCAN was used, the performance in boundary classification was the best amongst the three classification algorithms, with the number of boundaries classified (Figure 6-18) and in the actual plume (Figure 6-16 (a) and Figure 6-17) being the same. With DBSCAN, the errors in predicting the right boundaries were the lowest (Figure 6-19).

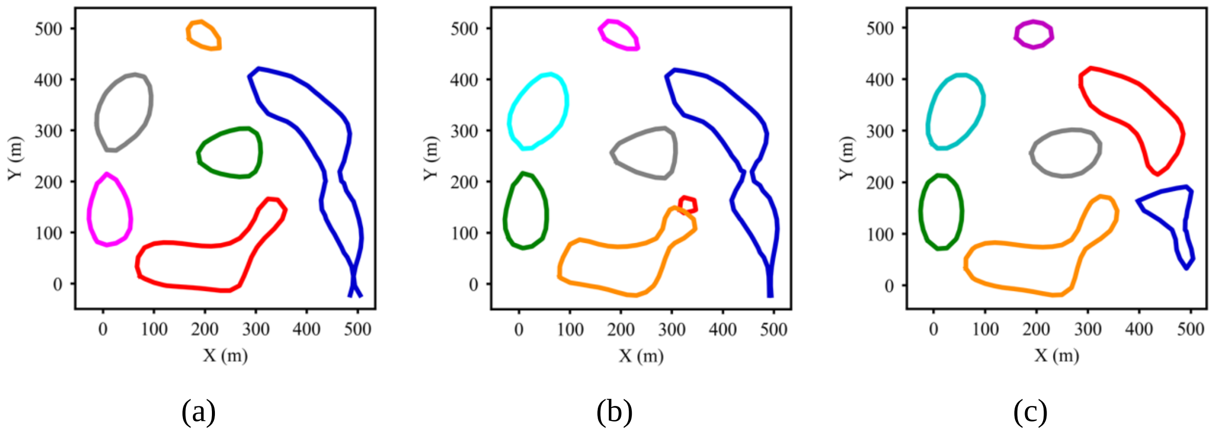

Figure 6-18. Performance of three classification algorithms in simulation 1: (a) with the use of only SVM (SVM_Only); (b) SVM and mean-shift clustering algorithm (SVM_MeanShift); (c) SVM and DBSCAN clustering algorithm (SVM_DBSCAN) in defining the boundaries between areas with and without rich information.

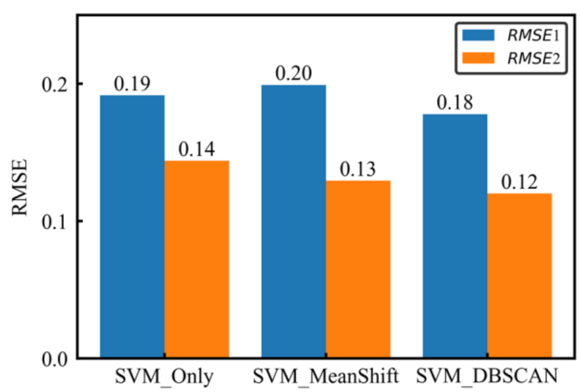

Figure 6-19. Root mean square errors (*RMSE*1 and *RMSE*2) in predicting the boundaries of patches with the use of three classification algorithms: with the use of only SVM (SVM_Only), SVM and mean-shift clustering algorithm (SVM_MeanShift), and SVM and DBSCAN clustering algorithm (SVM_DBSCAN) in simulation 1.

The better performance of the SVM_DBSCAN was a result of the ability of the DBSCAN clustering algorithm to obtain the correct number of clusters. In the SVM_MeanShift simulation, three clusters were obtained as shown in Figure 6-20 (a). Patch 1 and patch 5 which were shown in Figure 6-16 (b), were clustered as one cluster, while patch 6 was split into 3 clusters. This resulted in patch 6 being classified to have two boundaries as shown in Figure 6-18 (b). Patch 2, 3, 4, and 7, shown in Figure 6-16 (b), were clustered into one. After SVM was applied, one boundary was obtained for patch 4 and 7. However, with the use of the DBSCAN clustering algorithm, the number of clusters was the same as the number of actual patches shown in Figure 6-16 (b) and the number of clusters collected by the scout glider shown in Figure 6-17. The application of the DBSCAN clustering method before the application of SVM improved the performance of SVM in defining boundaries for patches with rich information.

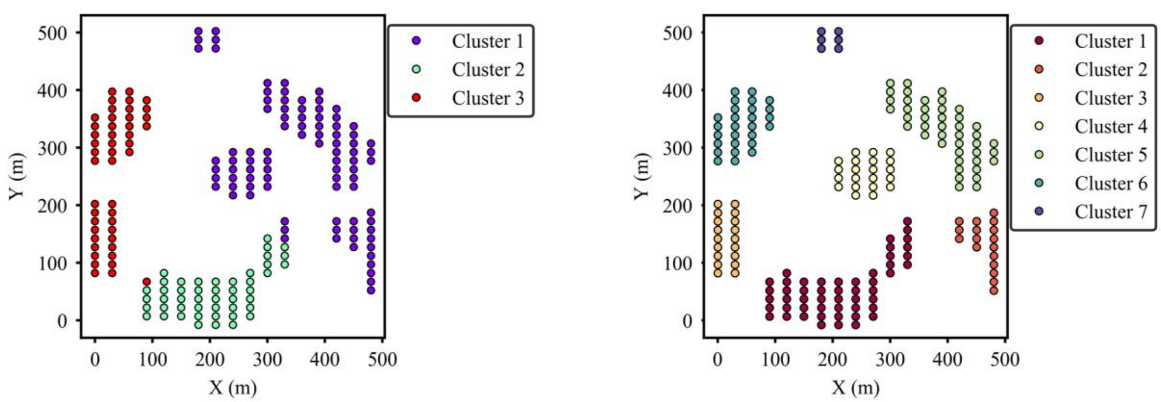

(a) (b)

Figure 6-20. Clustering result for the data with rich information shown in Figure 6-17: (a) with the use of the mean-shift clustering algorithm; (b) with the use of the DBSCAN clustering algorithm.

After the boundary of each patch was classified through SVM_DBSCAN, the area and aspect ratio of each patch were calculated (Table 6-3). Based on the geometric information of each patch, the mission mode, start point(s) for activating the mission mode, and direction of the long axis of the patch (patch direction) were derived by the scout glider and sent along with the area of the patch to a follower for further delineation.

Table 6-3. Mission information (areas, mission modes, start points, and patch directions) sent to followers based on area and aspect ratio of each patch derived from the classification of SVM with DBSCAN clustering algorithm.

Patch number	Area (m^2)	Aspect ratio	Mission mode	Start point(s) (m)	Patch direction (°)
1	11145.52	1.61	1	(40.76, 337.64)	65
2	2592.52	1.39	3	(191.50, 483.17)	15
3	9234.67	1.52	1	(250.74, 256.78)	190
4	18650.22	2.33	2	(315.18, 401.62), (462.39, 254.41)	135
5	9025.06	1.75	1	(14.29, 141.45)	90
6	23351.19	2.04	2	(83.78, 16.39), (351.43, 113.81)	20
7	7163.96	1.67	1	(461.96, 123.13)	125

6.4.3.2 Simulation 2

Another simulation was done to assess the performance of the three algorithms when using a different width of the lawn-mower path. In this simulation, the distribution of fluorescence plumes was the same as in simulation 1. The scout glider, with an initial heading toward the positive X-axis at start point (0 m, 0 m), was also commanded to search an area with a size of 500 m × 500 m. The scout glider went to the first waypoint (0 m, 500 m) and was assumed to reach this waypoint when the distance to this waypoint was within 10 m. Then the glider went to the second waypoint at (60 m, 500 m). The width of the mowed path was 60 m, which was larger than the width in simulation 1 (Figure 6-21). As the size of a grid in the X-direction was based on the width of the lawn-mower path, the size of a grid was defined to be 60 m x 15 m. The size of the grid in the Y direction was the same as in simulation 1 to capture the continuity in measurements without losing too many details. The grid map for this simulation is presented in Figure 6-22.

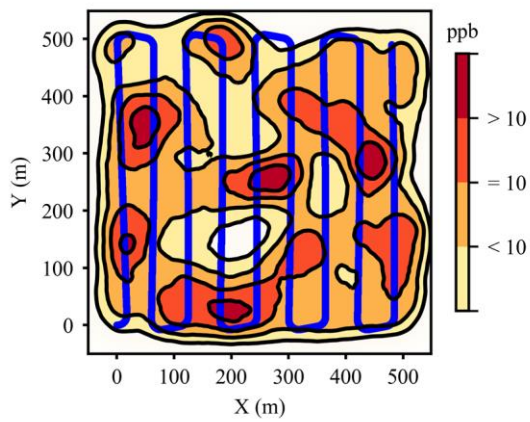

Figure 6-21. The path of the scout glider in simulation 2 with a width of lawn-mower path of 60 m.

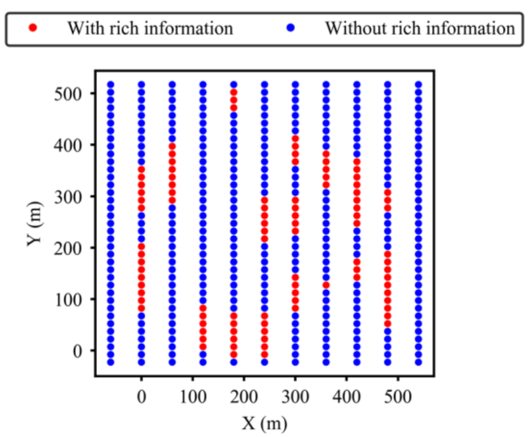

Figure 6-22. Measurements from the scout glider were mapped onto a grid map with a grid size of 60 m x 15 m. The red dots show grids with rich information while the blue dots show grids without rich information.

The results of the three algorithms in detecting the boundaries of high-fluorescence areas are shown in Figure 6-23, with the error in detecting the right boundaries shown in Figure 6-24. Both SVM_Only and SVM-MeanShift detected one boundary for patches 4 and 7 even though these two patches were over 30 m apart. In the SVM_MeanShift algorithm, the mean-shift clustering algorithm had a similar clustering result as it had in simulation 1 (Figure 6-25 (a)). The SVM_DBSCAN detected two boundaries for patch 6 as it clustered this patch as two (Figure 6-25 (b)). However, when examining the shape of patch 6, this patch was a dumbbell shape. This resulted in 2 missions being sent to followers for patch 6 (Table 6-4). The SVM_DBSCAN again gave the most accurate result in predicting the boundaries of the patches (Figure 6-24).

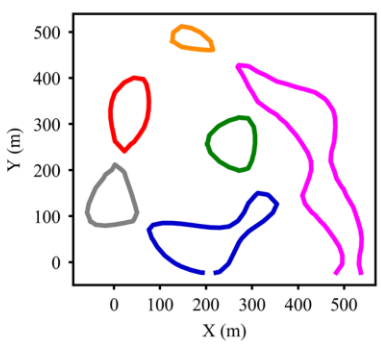

(a)

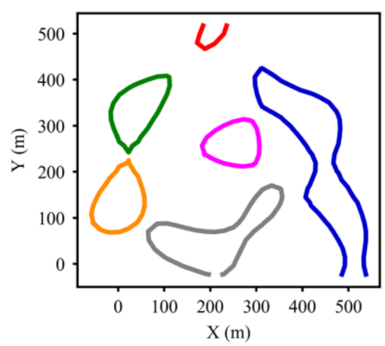

(b)

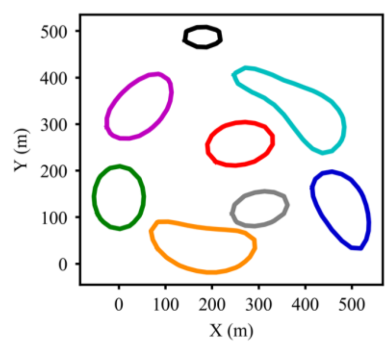

(c)

Figure 6-23. Performance of three classification algorithms in simulation 2: (a) with the use of only SVM (SVM_Only); (b) SVM and mean-shift clustering algorithm (SVM_MeanShift); (c) SVM and DBSCAN clustering algorithm (SVM_DBSCAN) in defining the boundaries between areas with and without rich information.

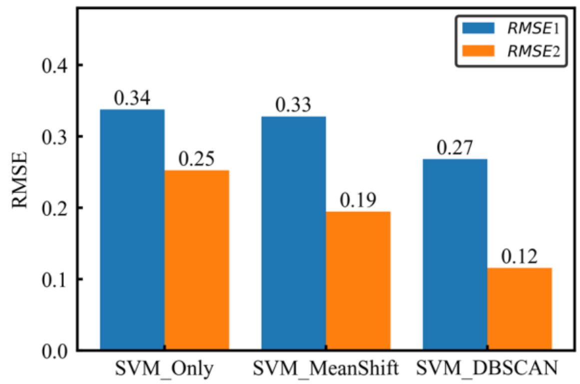

Figure 6-24. Root mean square errors (*RMSE*1 and *RMSE*2) in predicting the boundaries of patches with the use of three classification algorithms: with the use of only SVM (SVM_Only), SVM and mean-shift clustering algorithm (SVM_MeanShift), and SVM and DBSCAN clustering algorithm (SVM_DBSCAN) in simulation 2.

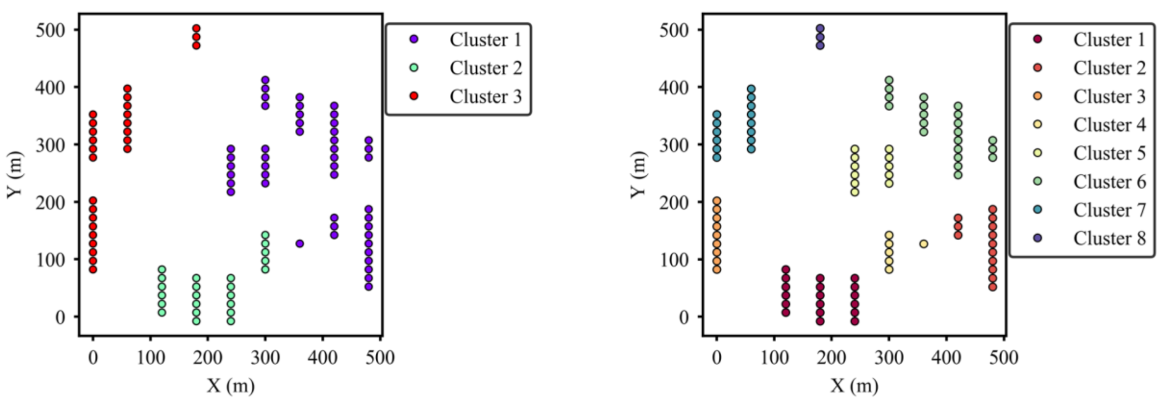

(a) (b)

Figure 6-25. Clustering result for the data with rich information shown in Figure 6-22: (a) with the use of the mean-shift clustering algorithm; (b) with the use of the DBSCAN clustering algorithm.

Table 6-4. Mission information (areas, mission modes, start points, and patch directions) sent to followers based on area and aspect ratio of each patch derived from the classification of SVM with the DBSCAN clustering algorithm.

Patch number	Area (m^2)	Aspect ratio	Mission mode	Start point(s) (m)	Patch direction (°)
1	13127.48	1.71	1	(42.91, 336.86)	45
2	2575.46	1.75	3	(175.72, 487.40)	0
3	10096.01	1.56	1	(257.76, 255.60)	15
4	18615.04	2.59	2	(467.55, 258.49), (279.77, 416.05)	320
5	11161.74	1.26	1	(-0.95, 142.34)	90
6	17386.74	2.26	2	(67.80, 58.335), (289.72,19.20)	170
	6668.23	1.68	1	(298.94, 117.34)	190
7	13459.13	1.85	1	(475.95, 117.08)	300

6.4.3.3 Simulation 3

In this simulation, a different distribution of plume was generated to further assess the performance of the three algorithms (Figure 6-26 (a)). The number of each patch was labelled in Figure 6-26 (b). The width of the mowed path for the scout glider was 60 m, similar to simulation 2, as shown in Figure 6-26 (c). The measurements from the glider were mapped onto a grid map with a grid size of 60 m x 15 m (Figure 6-27).

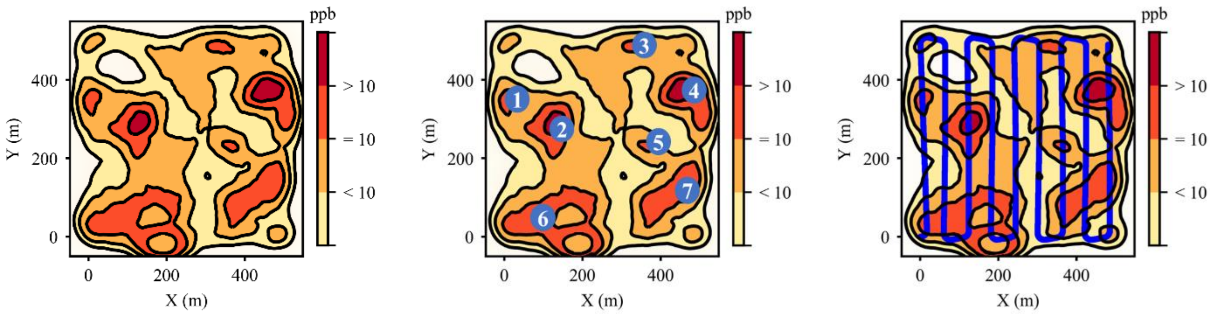

(a) (b) (c)

Figure 6-26. A scout glider was commanded to map simulated plumes: (a) the distribution of plumes; (b) each patch was labelled with a number; (c) the path of the scout glider.

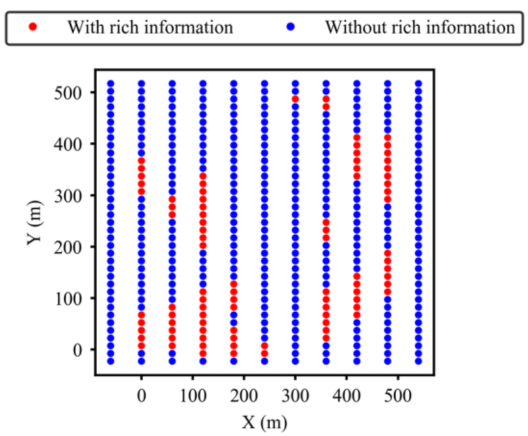

Figure 6-27. Measurements from the scout glider were mapped onto a grid map with a grid size of 60 m x 15 m. The red dots show grids with rich information while the blue dots show grids without rich information.

In the simulation, both SVM_Only and SVM_DBSCAN detected the right number of boundaries (Figure 6-28). When SVM was used with the mean-shift clustering method, two boundaries were provided for patch 7. This is because the mean-shift clustering algorithm classified patch 7 into two clusters (Figure 6-29 (a)). While with the use of DBSCAN, the correct number of patches was obtained (Figure 6-29 (b)). SVM_DBSCAN was again the algorithm that resulted in the lowest errors when predicting the boundaries of the patches (Figure 6-30).

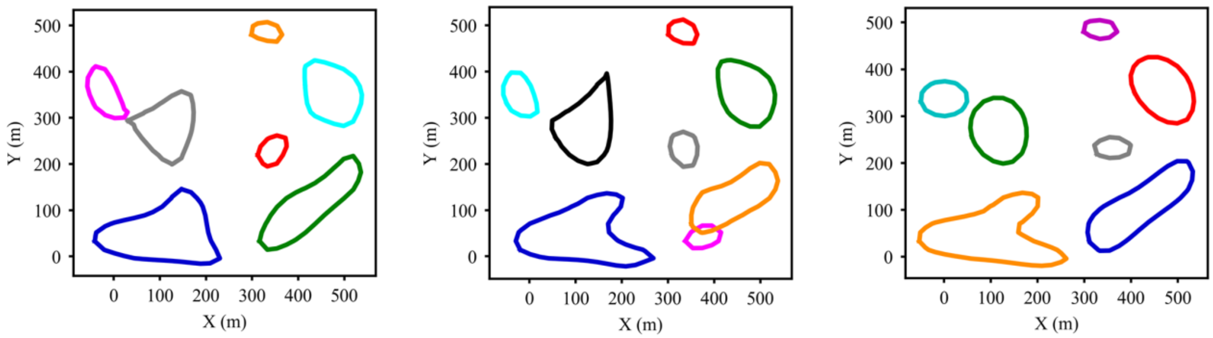

(a) (b) (c)

Figure 6-28. Performance of three classification algorithms in simulation 3: (a) with the use of only SVM (SVM_Only); (b) SVM and mean-shift clustering algorithm (SVM_MeanShift); (c) SVM and DBSCAN clustering algorithm (SVM_DBSCAN) in detecting the boundaries between areas with and without rich information.

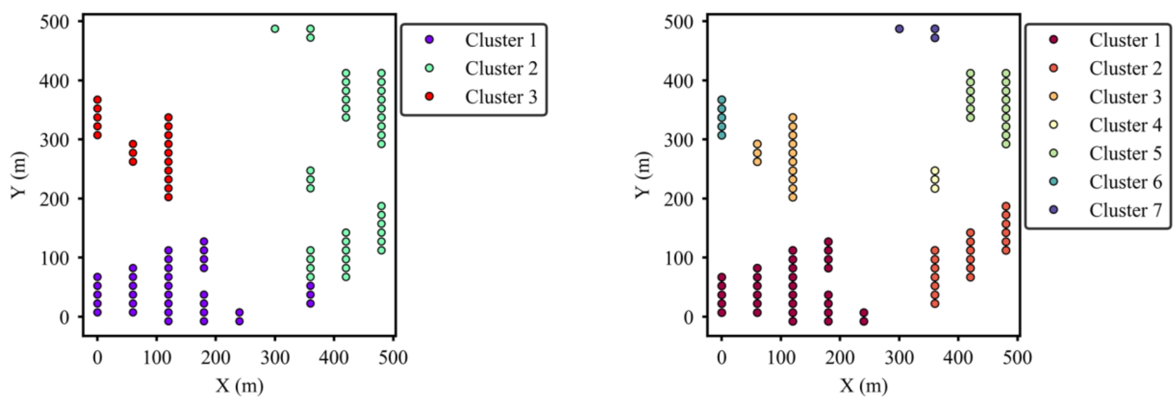

(a) (b)

Figure 6-29. Clustering result for the data with rich information shown in Figure 6-27: (a) with the use of the mean-shift clustering algorithm; (b) with the use of the DBSCAN clustering algorithm.

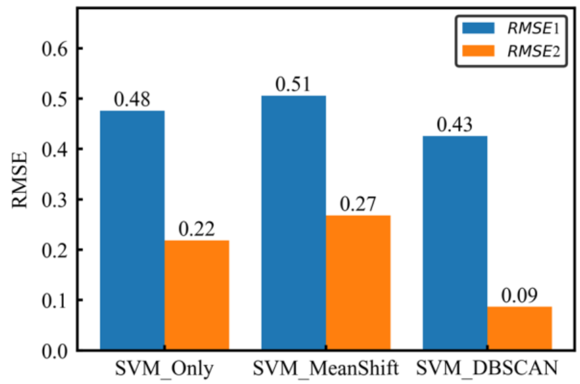

Figure 6-30. Root mean square errors (*RMSE*1 and *RMSE*2) in predicting the boundaries of patches with the use of three classification algorithms: with the use of only SVM (SVM_Only), SVM and mean-shift clustering algorithm (SVM_MeanShift), and SVM and DBSCAN clustering algorithm (SVM_DBSCAN) in simulation 3.

The area and aspect ratio of each patch were calculated after the boundary of each patch was determined through SVM_DBSCAN (Table 6-5). The mission mode, the start points for activating a mission mode, and the direction of the long axis of the patch were derived to be sent from the scout glider to followers for further delineation.

Table 6-5. Mission information (areas, mission modes, start points, and patch directions) sent to followers based on area and aspect ratio of each patch derived from the classification of SVM with DBSCAN clustering algorithm.

Patch number	Area (m^2)	Aspect ratio	Mission mode	Start point(s) (m)	Patch direction (°)
1	5695.07	1.33	1	(-1.50, 338.21)	170
2	13066.86	1.20	1	(115.61, 267.34)	105
3	2110.11	1.79	3	(329.79, 486.29)	350
4	13863.42	1.47	1	(465.65, 357.83)	310
5	2602.33	1.75	3	(360.11, 230.14)	355
6	26268.38	2.08	2	(-47.63, 61.34), (267.48, 33.77)	175
7	19142.48	3.03	2	(328.41, 44.32), (502.76, 166.40)	215

6.5 Discussion

6.5.1 Performance of the cooperation strategy and data compression method

The strategy for the scout glider to detect boundaries of potential areas with rich information and to compress data being sent to followers in the cooperation of multiple underwater gliders has the following advantages:

(1) The scout glider maps the area within a block before calling followers for further investigation. This process increases the possibility of followers collecting rich information without involving the whole team of gliders to search the entire area. Even though it seems that the followers are wasting power travelling around the block and waiting for a command, we expect this to only happen in the first block. By dividing the survey area into blocks, the scout glider can continue its work in a new block while the followers are

performing a detailed survey in a previous block, saving glider time to complete the overall mission. The efficiency of a multi-glider system improves with the number of blocks (Figure 6-31). The efficiency here was defined to be the length of time that the gliders spent in mapping regions of rich information to the total length of time used in a mission. In comparison with using only one glider and multiple gliders without cooperation, the strategy of using cooperating multiple gliders shows better efficiency in delineating oil patches underwater (Figure 6-31).

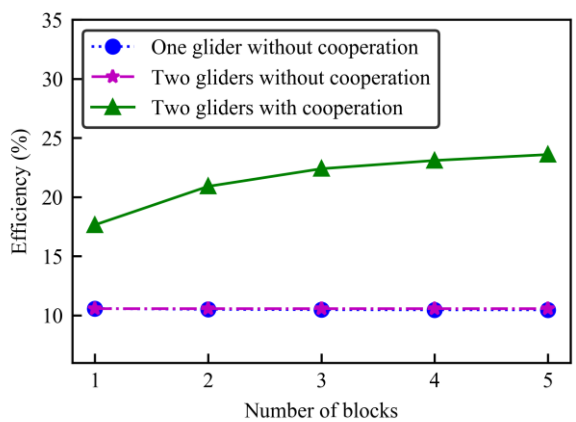

Figure 6-31. Efficiency (based on the percentage time taken by the gliders in mapping information rich areas to total mission time) of the proposed cooperation strategy compared with using one glider and multiple gliders without cooperation.

(2) As measurements from the scout glider are compressed and projected onto a grid map with only one measurement in each grid, the volume of data for boundary classification is decreased. This increases the speed of clustering and classification. The size of each grid can be changed by balancing the level of details required and the computational effort in boundary classification.

(3) The inclusion of a cluster method before the use of SVM helps simplify the characteristics of processed data. Without the use of a clustering method, the SVM alone will at times classify two patches into only one patch, as shown in the results in simulations 1 and 2, leading to the followers spending their mission time delineating areas with low information between rich-information patches.

(4) The scout glider processes boundary information before sending it to its followers leading to a decrease in the amount of data being transmitted. In addition to position information shared amongst the gliders to avoid collision, the data being sent to the followers only includes the area of a patch, the mission mode, the start point(s) for activating their mission mode, and the direction of the long axis of a patch if the aspect ratio was not smaller than 2.

In the three classification algorithms used in all simulations, the same kernel function and value of penalty factor were used in the SVM. In simulation 3, the number of boundaries for patches was successfully identified with SVM without clustering. However, the same set of kernel function and parameters used in SVM without clustering did not work in simulation 1 and simulation 2 where the SVM method used alone clustered patches 4 and 7 into one patch. The optimal parameters for SVM_Only in simulation 1 and 2 were difficult to be defined automatically by the glider. When the clustering method DBSCAN was applied, the boundary classification performed better in all simulations based on both the number of patches classified and the lower errors in predicting the boundaries with the same set of kernel function and parameters in the SVM. This shows that including the clustering method, before applying SVM, helps improve the performance of the SVM.

When identifying the boundary of the patches, the inclusion of a clustering method, especially the DBSCAN, before the application of SVM is an effective method to detect the boundaries of the patches successfully. This is because the clustering algorithm simplifies the data sets by converting a complex data set with multiple patches into a series of simpler data sets containing information of only one patch. This way, the SVM does not need to find the best hyperplane for a complex data set of multiple patches but a series of hyperplanes for single patches.

In DBSCAN, parameters that have to be determined are the size of neighborhood (*Eps*) and the minimum density (*MinPts*). The size of neighborhood is defined based on the known grid size and the minimum density is set to be 1 (each cluster has one or more data points) to group all data into clusters for all cases. In simulation 1, as the grid size was 30 m x 15 m, the size of the neighborhood was 30 m. For simulation 2 and 3, the size of the neighborhood was 60 m as the grid size was 60 m x 15 m. The size of grid was different in the simulations, but the SVM_DBSCAN algorithm had a good performance in all simulations. The performance of the mean-shift algorithm can be improved by changing the bandwidth used, but the bandwidth is an estimated value and cannot be obtained directly unlike the parameters used in the DBSCAN method. For the clustering methods, the DBSCAN algorithm performed better than the mean-shift algorithm. In Figure 6-28 (b), the SVM_MeanShift algorithm classified two potential areas of rich information for patch 7 whereas these two areas were actually overlapping. This was the result of the mean-shift method clustering patch 7 in Figure 6-26 (b) into two patches that were close to each other. If these two areas were assigned to two followers for detailed surveys, a higher risk of collision might incur. The DBSCAN approach can also cluster one patch into 2 clusters, such as clustering patch 6 in Figure 6-16 (b) into 2 groups (Figure 6-23 (c)), but this was due to the patch being a dumbbell shape and thus it was reasonable to be divided into two clusters. Besides, as the DBSCAN method clustered points that were density-connected and the parameter *MinPts* was set to be 1 in this chapter, this helped prevent clusters from being too close or overlapping to one another as a minimum distance of *Eps* between clusters was specified. Therefore, the overlapping patches can be avoided with the use of the SVM_DBSCAN algorithm.

The mission information sent to followers was based on the classification result from the SVM_DBSCAN algorithm in this chapter. Only three mission modes were defined in this chapter according to the geometric information of each patch. Although the distribution of plumes was the same for simulation 1 and 2, the paths of the scout glider in these two simulations were different, leading to a different set of missions being sent to the followers. In simulation 1, there were 7 missions waiting to be conducted by the followers, while in simulation 2, there were 8 missions for the followers, of which patch 6 was decomposed into 2 sub-patches. In addition, the area, aspect ratio and patch direction obtained from both simulations were different. However, the mission mode was the same for each patch except for patch 6 in both simulations.

The proposed strategy is not limited for use with gliders to detect fluorescence values, but can also be used for other underwater vehicles to detect other underwater features, such as plankton distributions. However, we chose to use gliders as typically the endurance of actively propelled AUVs is much shorter than gliders. The sawtooth-like motion endows gliders with inherent advantages in sampling the data through the water column. The proposed strategy can also be used for a mission with one vehicle to replan its path. As the amount of data showing an area with rich information is decreased, the data sent from the scout glider to followers can also be sent to a surface station through any vehicles on the surface for a quick response in an underwater oil spill delineation mission.

6.5.2 Future application of the proposed strategy

In this chapter, we manually simulated oil distributions which had patchy characteristics, but as they were idealized, could be to some extent different from the real situation. However, the primary objective of this chapter was to verify that the ability of the proposed algorithm to identify boundaries of oil patches could be improved with the use of a clustering method. Thus, the patchy distribution of oil plumes was what we aimed for in our verification. In a field mission with oil patches, due to dynamic changes in the ocean, the patches detected by the scout glider may not be at the detected position after the scout glider finishes the mapping of a block. However, the scout glider can detect the boundaries of patches within smaller blocks compared to the blocks used in this research to minimize the time delay in sending the position information of patches to the following gliders. Owing to the dynamics in the ocean, the currents will disperse the patches. As each glider was equipped with an adaptive ability to change its path in real-time, the followers can refer to, but not rely on the information sent from the scout glider to adaptively control their missions. For example, a follower glider can terminate its search of a patch based on both the area sent from the scout glider and the measurements from its own sensors. In this chapter, only limited shapes of oil patches were simulated which could not cover all of the shapes of patches in a real situation. However, as we only considered the aspect ratio of a patch, the shape of the patches was quantified and all of the possible aspect ratios of patches were covered. The introduction of aspect ratio is helpful for designing the behaviors of followers and improving the reliability of path planning considering the irregular and diverse shapes of oil patches. Our study was validated through simulations using manually generated patches. It could be further validated with an actual oil plume or a proxy of an oil plume both in simulations and in field studies.

6.6 Conclusion

This chapter proposed a cooperation strategy for missions involving multiple and cooperating underwater gliders. In this cooperation strategy, the mission field was discretized into a series of blocks and a team of gliders was used to delineate each block consecutively. A glider assigned as the scout glider was commanded to map the area within each block first to predefine the potential areas with rich information before calling the followers to further investigate the potential areas in detail. The measurements from the scout glider were mapped onto a grid to decrease the volume of data to be processed and communicated. The use of clustering algorithms was proposed before the application of the support vector machine (SVM) to detect the boundary of patches and to compress data before transmitting mission information to the followers in the cooperation strategy. The mean-shift and the Density-Based Spatial Clustering of Applications with Noise (DBSCAN) clustering algorithms were considered and compared through simulations.

The inclusion of a clustering method, especially the DBSCAN, before the application of SVM was found to be an effective method to define the boundaries of patches. The clustering method DBSCAN was preferred over the mean-shift method as the number of clusters found in simulations was in accordance with the number of the actual patches and overlapping boundaries were avoided.

The errors found in predicting the correct boundaries were the lowest for the classification method with the use of the DBSCAN clustering algorithm. Based on the boundaries classified, a compressed amount of information is transmitted by the scout glider to its followers, improving the efficiency of vehicle-to-vehicle communications. The proposed cooperation strategy with a boundary classification method is a potential tool to be used by a single or a group of underwater vehicles for delineating large, contaminated areas, particularly those with patchy characteristics such as oil spills. The feasibility of the proposed classification algorithm is planned to be validated further with more realistic simulated oil plumes or in the field with a proxy for an oil plume.

This chapter answered the third research question in this thesis (Q3: Is there an advantage in using a multi-glider strategy for oil spill detection?) by reviewing previous research on using multiple underwater vehicles and reached the third sub-objective (O3: To improve the performance of multiple cooperative gliders to delineate subsurface oil) by proposing a new cooperation strategy for multiple gliders to delineate underwater oil plumes.

Acknowledgement

Funding was received from Fisheries and Oceans Canada through the Multi-partner Oil Spill Research Initiative (MPRI) 1.03: Oil Spill Reconnaissance and Delineation through Robotic Autonomous Underwater Vehicle Technology in Open and Iced Waters and the School of Graduate Studies at Memorial University of Newfoundland.

References

Abt Associates, Woods Hole Oceanographic Institution, National Oceanic and Atmospheric Administration, U.S. Environmental Protection Agency, Water Mapping, L., 2020. Three-Dimensional Mapping of Dissolved Hydrocarbons and Oil Droplets Using a REMUS-600 Autonomous Underwater Vehicle.

Awad, M., Khanna, R., 2015. Support Vector Machines for Classification, in: Efficient Learning Machines. Apress, Berkeley, CA, pp. 39–66. https://doi.org/10.1007/978-1-4302-5990-9_3

Bechlioulis, C.P., Giagkas, F., Karras, G.C., Kyriakopoulos, K.J., 2019. Robust Formation Control for Multiple Underwater Vehicles. Front. Robot. AI 6. https://doi.org/10.3389/frobt.2019.00090

Berget, G.E., Fossum, T.O., Johansen, T.A., Eidsvik, J., Rajan, K., 2018. Adaptive Sampling of Ocean Processes Using an AUV with a Gaussian Proxy Model. IFAC-PapersOnLine 51, 238–243. https://doi.org/10.1016/j.ifacol.2018.09.509

Chen, B., Pompili, D., 2014. Reliable geocasting for random-access underwater acoustic sensor networks. Ad Hoc Networks 21, 134–146. https://doi.org/10.1016/j.adhoc.2014.05.013

Chen, B., Yang, D., Meneveau, C., Chamecki, M., 2018. Numerical study of the effects of chemical dispersant on oil transport from an idealized underwater blowout. Phys. Rev. Fluids 3, 083801. https://doi.org/10.1103/PhysRevFluids.3.083801

Costanzi, R., Monnini, N., Ridolfi, A., Allotta, B., Caiti, A., 2017. On field experience on underwater acoustic localization through USBL modems, in: OCEANS 2017 - Aberdeen. Institute of Electrical and Electronics Engineers Inc., Aberdeen, U.K., pp. 1–5. https://doi.org/10.1109/OCEANSE.2017.8084996

Deng, Y., Beaujean, P.P.J., An, E., Carlson, E., 2013. Task allocation and path planning for collaborative autonomous underwater vehicles operating through an underwater acoustic network. J. Robot. 2013, 1–16. https://doi.org/10.1155/2013/483095

Ester, M., Kriegel, H.-P., Sander, J., Xu, X., 1996. A Density-Based Algorithm for Discovering Clusters in Large Spatial Databases with Noise, in: Proceedings of the 2nd International Conference on Knowledge Discovery and Data Mining. pp. 226–231.

Fiorelli, E., Leonard, N.E., Bhatta, P., Paley, D.A., Bachmayer, R., Fratantoni, D.M., 2006. Multi-AUV control and adaptive sampling in Monterey Bay. IEEE J. Ocean. Eng. 31, 935–948. https://doi.org/10.1109/JOE.2006.880429

Fukunaga, K., Hostetler, L.D., 1975. The Estimation of the Gradient of a Density Function, with Applications in Pattern Recognition. IEEE Trans. Inf. Theory 21, 32–40. https://doi.org/10.1109/TIT.1975.1055330

Gholami, R., Fakhari, N., 2017. Support Vector Machine: Principles, Parameters, and Applications, in: Handbook of Neural Computation. Elsevier Inc., pp. 515–535. https://doi.org/10.1016/B978-0-12-811318-9.00027-2

Gonçalves, R.C., Iskandarani, M., Srinivasan, A., Thacker, W.C., Chassignet, E., Knio, O.M., 2016. A framework to quantify uncertainty in simulations of oil transport in the ocean. J. Geophys. Res. Ocean. 121, 2058–2077. https://doi.org/10.1002/2015JC011311

Guyeux, C., Chrétien, S., Tayeh, G.B., Demerjian, J., Bahi, J., 2019. Introducing and comparing recent clustering methods for massive data management in the internet of things. J. Sens. Actuator Networks 8. https://doi.org/10.3390/jsan8040056

Johnson, B., Hallin, N., Leidenfrost, H., O’Rourke, M., Edwards, D., 2009. Collaborative mapping with autonomous underwater vehicles in low-bandwidth conditions, in: OCEANS ’09 IEEE Bremen: Balancing Technology with Future Needs. Bremen, Germany, pp. 1–7.

https://doi.org/10.1109/OCEANSE.2009.5278277

Kinsey, J.C., Yoerger, D.R., Jakuba, M. V., Camilli, R., Fisher, C.R., German, C.R., 2011. Assessing the Deepwater Horizon oil spill with the sentry autonomous underwater vehicle, in: 2011 IEEE/RSJ International Conference on Intelligent Robots and Systems. Institute of Electrical and Electronics Engineers (IEEE), pp. 261–267. https://doi.org/10.1109/IROS.2011.6095008

Lafarge, F., Descombes, X., Zerubia, J., 2005. Textural kernel for SVM classification in remote sensing : Application to forest fire detection and Urban area extraction, in: Proceedings - International Conference on Image Processing, ICIP. Genova, Italy, Italy, pp. 1093–1096. https://doi.org/10.1109/ICIP.2005.1530587

Leigh, S., Wang, Z., Clausi, D.A., 2014. Automated ice-water classification using dual polarization SAR satellite imagery. IEEE Trans. Geosci. Remote Sens. 52, 5529–5539. https://doi.org/10.1109/TGRS.2013.2290231

Liu, S., Yu, J., Zhang, A., Zhang, F., 2014. Cooperative path planning for networked gliders under weak communication, in: Proceedings of the 9th ACM International Conference on Underwater Networks and Systems. Association for Computing Machinery, Inc, Rome, Italy, pp. 1–5. https://doi.org/10.1145/2671490.2674575

Melo, J., Matos, A.C., 2019. Tracking multiple Autonomous Underwater Vehicles. Auton. Robots 43, 1–20. https://doi.org/10.1007/s10514-018-9696-7

Paull, L., Huang, G., Seto, M., Leonard, J.J., 2015. Communication-constrained multi-AUV cooperative SLAM. Proc. - IEEE Int. Conf. Robot. Autom. 2015-June, 509–516. https://doi.org/10.1109/ICRA.2015.7139227

Qin, J., He, Z.S., 2005. A SVM face recognition method based on Gabor-featured key points. 2005

Int. Conf. Mach. Learn. Cybern. ICMLC 2005 5144–5149. https://doi.org/10.1109/icmlc.2005.1527850

Rahmati, M., Arjula, A., Pompili, D., 2019. Compressed Underwater Acoustic Communications for Dynamic Interaction with Underwater Vehicles, in: Proceedings of the International Conference on Underwater Networks & Systems. Atlanta, GA, USA, pp. 1–5. https://doi.org/10.1145/3366486.3366488

Refianti, R., Mutiara, A.B., Syamsudduha, A.A., 2016. Performance Evaluation of Affinity Propagation Approaches on Data Clustering. Int. J. Adv. Comput. Sci. Appl. 7. https://doi.org/10.14569/ijacsa.2016.070357

Rye, H., Brönner, U., Ditlevsen, M.K., Frost, T.K., Furuholt, E., Kjeilen-Eilertsen, G., Nepstad, R., Page, P., Paulsen, J.E., Ramos, R., Rønningen, P., Sørstrøm, S.E., 2014. Use of the DREAM model for control and prediction of concentrations and environmental risks associated with regular discharges to sea: Experiences and challenges, in: Proceedings - SPE Annual Technical Conference and Exhibition. pp. 2510–2521. https://doi.org/10.2118/170763-ms

Sahoo, A., Dwivedy, S.K., Robi, P.S., 2019. Advancements in the field of autonomous underwater vehicle. Ocean Eng. 181, 145–160. https://doi.org/10.1016/j.oceaneng.2019.04.011

Satapathy, S.K., Dehuri, S., Jagadev, A.K., Mishra, S., 2019. Introduction, in: EEG Brain Signal Classification for Epileptic Seizure Disorder Detection. Elsevier, pp. 1–25. https://doi.org/10.1016/b978-0-12-817426-5.00001-6

Schulz, B., Hobson, B., Kemp, M., Meyer, J., Moody, R., Pinnix, H., St. Clair, M., 2003. Field results of multi-UUV missions using ranger micro-UUVS, in: Oceans Conference Record (IEEE). pp. 956–961. https://doi.org/10.1109/oceans.2003.178457

Shmilovici, A., 2005. Support Vector Machines, in: Data Mining and Knowledge Discovery Handbook. Springer-Verlag, New York, pp. 257–276. https://doi.org/10.1007/0-387-25465-X_12

Sinaga, K.P., Yang, M.S., 2020. Unsupervised K-means clustering algorithm. IEEE Access 8, 80716–80727. https://doi.org/10.1109/ACCESS.2020.2988796

Tax, D.M.J., Duin, R.P.W., 2004. Support Vector Data Description. Mach. Learn. 54, 45–66. https://doi.org/10.1023/B:MACH.0000008084.60811.49

Tharwat, A., 2019. Parameter investigation of support vector machine classifier with kernel functions. Knowl. Inf. Syst. 61, 1269–1302. https://doi.org/10.1007/s10115-019-01335-4

Wang, H., Stoeck, C.T., Kozerke, S., Amini, A.A., 2013. Analysis of 3D cardiac deformations with 3D SinMod, in: Proceedings of the Annual International Conference of the IEEE Engineering in Medicine and Biology Society, EMBS. Annu Int Conf IEEE Eng Med Biol Soc, pp. 4386–4389. https://doi.org/10.1109/EMBC.2013.6610518

Wang, H., Xu, D., 2017. Parameter Selection Method for Support Vector Regression Based on Adaptive Fusion of the Mixed Kernel Function. J. Control Sci. Eng. 2017, 1–12. https://doi.org/10.1155/2017/3614790

Wang, L., Pedersen, P.C., Agu, E., Strong, Di.M., Tulu, B., 2017. Area Determination of Diabetic Foot Ulcer Images Using a Cascaded Two-Stage SVM-Based Classification. IEEE Trans. Biomed. Eng. 64, 2098–2109. https://doi.org/10.1109/TBME.2016.2632522

Wang, Y., Bulger, C., Thanyamanta, W., Bose, N., 2021a. A backseat control architecture for a slocum glider. J. Mar. Sci. Eng. 9. https://doi.org/10.3390/jmse9050532

Wang, Y., Thanyamanta, W., Bulger, C., Bose, N., Hwang, J., 2021b. Microbubbles as proxies for oil spill delineation in field tests. J. Mar. Sci. Eng. 9, 1–17.

https://doi.org/10.3390/jmse9020126

Zhang, F., Fratantoni, D.M., Paley, D.A., Lund, J.M., Leonard, N.E., 2007. Control of coordinated patterns for ocean sampling. Int. J. Control 80, 1186–1199. https://doi.org/10.1080/00207170701222947

Zhang, P., Ding, S.X., 2007. Fault detection of networked control systems with limited communication. Fault Detect. Superv. Saf. Tech. Process. 2006 2, 1074–1079. https://doi.org/10.1016/B978-008044485-7/50181-0

Zhang, R., Yang, S., Wang, Y., Wang, S., Gao, Z., Luo, C., 2020. Three-dimensional regional oceanic element field reconstruction with multiple underwater gliders in the Northern South China Sea. Appl. Ocean Res. 105, 102405. https://doi.org/10.1016/J.APOR.2020.102405

Zhao, Y., Shrivastava, A.K., Tsui, K.L., 2019. Regularized Gaussian Mixture Model for High-Dimensional Clustering. IEEE Trans. Cybern. 49, 3677–3688. https://doi.org/10.1109/TCYB.2018.2846404

Zhou, M., Bachmayer, R., Deyoung, B., 2017. Underwater acoustic-based navigation towards multi-vehicle operation and adaptive oceanographic sampling, in: IEEE International Conference on Intelligent Robots and Systems. Institute of Electrical and Electronics Engineers Inc., Vancouver, Canada, pp. 6091–6097. https://doi.org/10.1109/IROS.2017.8206508

7. Chapter 7

Adaptive control for follower gliders mapping underwater oil patches

Yaomei Wang[1], Neil Bose[1], Worakanok Thanyamanta[1], Craig Bulger[2], and Sarik Shaikh-Upadhye[1]

[1] Department of Ocean and Naval Architectural Engineering, Memorial University of Newfoundland, St. John's, NL A1B 3X7, Canada

[2] Centre for Applied Ocean Technology, Fisheries and Marine Institute of Memorial University of Newfoundland, NL A1C 5R3, St. John's, Canada

This chapter has been submitted as a journal manuscript.

Table 7-1 Individual Author Contribution – Article No.5

Author	Contribution
Yaomei Wang	Conceptualization, Methodology, Software, Validation, Formal analysis, Investigation, Resources, Writing—original draft preparation, Writing—review and editing, Visualization
Neil Bose	Writing—original draft preparation, Writing—review and editing, Supervision, Project administration, Funding acquisition
Worakanok Thanyamanta	Writing—original draft preparation, Writing—review and editing, Supervision
Craig Bulger	Methodology, Validation, Investigation, Resources, Writing—original draft preparation, Writing—review and editing
Sarik Shaikh-Upadhye	Methodology, Validation, Investigation, Resources, Writing—original draft preparation, Writing—review and editing

Abstract

Adaptive control was applied to follower gliders in cooperating multiple glider teams on missions to delineate underwater oil patches. The influence of water currents on the motion of the oil patches was included. The cooperation strategy with adaptive control was compared with strategies without cooperation or adaptive control through simulation experiments. In addition, the optimal number of follower gliders in a team was assessed. From the simulations, strategies with adaptive control achieved a higher score of performance, being a measure of the percentage of valuable-rich information collected to the percentage of the mission area covered by information-rich patches, only when the percentage of the area of information-rich patches was less than 60%. The cooperation strategy with adaptive control had a lower duty cycle and a longer mission duration, but had the best score of performance, especially for long-duration missions.

Keywords: multiple underwater gliders; cooperation strategy; follower glider; backseat driver; oil spill

7.1 Introduction

Underwater oil spill reconnaissance and delineation is challenging as an oil spill can extend over a large area and is, in this case, beneath the water surface. Unlike oil at the surface, a subsurface release is impractical to be monitored by conventional methods such as remote sensing. To deal with this problem, autonomous underwater vehicles (AUVs) have been increasingly employed to detect spilled oil underwater (Kinsey et al., 2011; Vasilijevic et al., 2015). AUVs expand the scope of a survey in both time and space. They can cover a wide area at a lower cost compared with ship-based surveys and can dive into deep water with relatively low risk.

A spatiotemporal aliasing problem exists in delineating oil spills underwater when using an AUV (Petillo et al., 2012). When the AUV searches a large area, the feature of the oil can change over time. On the other hand, when only a small area is surveyed, it may not cover the whole extent of the spill. In the field experiment of a project ARCTREX (Winsor et al., 2017), Rhodamine WT was injected into the water to simulate an oil plume. During the observation of dye with gliders, the dye was found to be dispersed fast. The glider could not sample it and calculate the fate and transport of the dye with the demanded accuracy both in time and space. A fleet of gliders was required and recommended for mapping the chemical plume. Petillo and Schmidt (Petillo and Schmidt, 2012) concluded that a fleet of coordinated, actively propelled AUVs with on-board autonomy would be most efficient in delineating the plume in the water.

In our previous research (Wang et al., 2022), we proposed to use multiple underwater gliders to track patchy plumes cooperatively and adaptively. Underwater gliders are characterized by their long endurance, which is a desired feature of AUVs for delineating underwater oil spills as they have been found to be able to extend over a long distance. In the Deepwater Horizon oil spill, the underwater oil was detected at a distance of over 30 km from the source (Camilli et al., 2010). The sawtooth-like motion endows gliders with inherent advantages in sampling data from different depths while moving forward. In the strategy we proposed earlier for multiple gliders, one glider was used as a scout to delineate the mission area beforehand (Wang et al., 2022). The scout glider then sent the locations and boundaries of potential information-rich oil patches to follower gliders to conduct detailed surveys of the patchy areas. However, the movement of oil plumes underwater was not considered.

A subsurface oil layer is formed by a balance of buoyancy, viscosity, surface tension, and water drag forces from a non-pressurized leaking source (Ji et al., 2020). It can also be formed from a pressurized leaking source in which the oil droplets and gas bubbles are entrained with water to form horizontal intrusions (Socolofsky et al., 2011). The lateral transport of the underwater oil layer is affected by the current and rising time, from a depth. The current speed has been found to affect the migration distance more than rising time (Sun et al., 2019). Due to the dynamics of the ocean, such as from water currents, the locations and shapes of the patches may quickly change before the scout glider can send the boundary information to the followers. Also, the gliders may not move as expected when the current speed is strong (Xue et al., 2015).

In our previous research, each glider was equipped with a backseat driver control system (Wang et al., 2022). With the backseat driver, the follower gliders could adaptively control their headings and change their missions to either move along the perimeter of a search area or conduct detailed surveys of patches with rich information. The focus of the previous study was on the ability of the scout glider to detect and determine the number of oil patches. Only the motion and data processing ability of the scout glider were tested through simulations.

In this chapter, the focus is on the follower gliders. An adaptive path planning strategy was proposed for the follower gliders by considering the motion of patches under the influence of water currents. The current speed was assumed to be less than the speed of gliders in this study. We assumed that the patches moved with the current at an average speed and the change in shape of the patches was not considered. As in our previous research (Wang et al., 2022), the survey area was divided into a number of blocks. The scout glider was commanded to follow a lawn-mower path to cover the area within the block and find potential patches with rich information. The follower gliders changed their paths based on the data of the patches collected by their onboard sensors to spend the most of their mission time inside the patches. The influence of having adaptive control was evaluated. The performance of the improved cooperative multi-glider system with adaptive control in delineating a patchy plume was calculated and compared with the performance of strategies with one glider and multiple gliders without cooperation and/or without adaptivity. The optimal number of follower gliders in the improved cooperation strategy was explored as well.

The remainder of this chapter is organized as follows. Section 2 reviews related studies on applying AUV technology to delineating underwater plumes and underwater vehicles which have been equipped with a backseat driver for realizing adaptive control. The methodology used in this chapter is introduced in Section 3, which includes the control of follower gliders in the cooperation strategy, and the evaluation metrics for assessing the improved cooperation strategy. In Section 4, we assess the influence of adaptive control and the performance of the improved cooperation strategy with adaptive control through simulation. Experimental results are discussed. Finally, a conclusion is presented in Section 5.

7.2 Related work

There are multiple types of underwater plumes, such as algal blooms, water tracer plumes, and oil spill plumes (Petillo and Schmidt, 2012). Each type of plume has its specific physical and chemical characteristics, but all plumes have common features such as being dynamic in the ocean and affected by the ocean environment. Besides, they can spread over a large area in the water.

The application of AUVs in underwater plume detection is not new. An AUV plume mapping mission may be worthless if there is nothing to be detected in the mission area. In this case, a prior investigation is essential. This prior investigation is also called exploration, as its purpose is to gain knowledge about an unknown or less-known area, prior to the accumulation of detailed information through exploitation (De Farias and Megiddo, 2004). In the work of Das et al. (Das et al., 2010), patches of algal hotspots were first detected by the measurements from remote sensing satellites. Next, the water current data from high frequency radars were implemented to have an advective effect on the detected patches. The predicted trajectory of hotspots was then used to plan the survey mission of an AUV to sample a dynamic field. Ferri et al. (Ferri et al., 2010) proposed a method called triggered spiral processing to trigger an adaptive movement of an AUV when it was localizing active hydrothermal vents. The AUV initially conducted a lawn-mower motion. When anomalous values were detected, the AUV then conducted a spiral movement to further exploit the specific position. An adaptive turbulent plume lawn-mower mapping strategy was introduced by Tian et al. (Tian et al., 2011). In the strategy, a series of behaviors were applied under the behavior-based control system. These behaviors included GoToMappingArea (steer AUV to a mission point), TracklineFollowing (steer AUV to follow a track line), PlumeMapping (steer AUV to map a plume), and PlumeExploring (steer AUV to explore the plume). With this method, the AUV responded to the sensor detection. To be specific, when the AUV detected the existence of a plume, it would follow a designed direction to exploit the plume; when the AUV did not detect a plume, it would follow a designed direction to explore the plume.

In the aforementioned approaches, only one vehicle was involved in the exploration and exploitation of an underwater plume. For plumes which are patchy and cover a large area, coordination of AUVs is required due to the spatiotemporal aliasing that arises from use of from one vehicle (Petillo et al., 2012; Petillo and Schmidt, 2012). When multiple vehicles are applied, one vehicle can be used to survey the ocean first and then the measurements are used to instruct a second AUV to further assess a specific area of interest (Abt Associates et al., 2020).

Considering the limitation of previous strategies, a cooperation strategy for multiple gliders to delineate oil patches underwater was proposed in our previous research (Wang et al., 2022). In this strategy, the mission area was discretized into a series of blocks and the underwater gliders mapped each block sequentially. Each glider was equipped with backseat control ability and oil sensors. Measurements from oil sensors which were above a certain level, such as above 10 ppb for fluorometers, were considered to have rich information. A glider called a scout was commanded to explore the unknown underwater environment. The scout glider searched a block and classified the boundaries of oil patches with rich information. Information of oil patches was then sent from the scout glider to the rest of the gliders which were followers in order to further exploit information-rich areas in detail. The scout glider explored the area within a block before calling followers for further investigation. This process separated exploration from exploitation and increased the possibility of followers collecting rich information without involving the whole team of gliders to search the entire area.

7.3 Methodology

This section mainly introduces the control of follower gliders by considering the effect of water currents. The metrics for evaluating the performance of a strategy with gliders in delineating oil patches are also introduced.

7.3.1 Cooperation control of gliders

In this chapter, we enhanced the control of follower gliders in our previous cooperation strategy by considering the influence of water currents on the motion of the oil patches. The flowchart of the control of gliders in the cooperation strategy is shown in Figure 7-1. Each glider is equipped with oil sensors to detect the existence of oil and determine whether a measurement is with rich information or not. The scout glider searches the area within a block first by using a predefined lawn-mower path. When the scout glider has finished the delineation in the current block (block i), it classifies the boundaries of rich-information patches within the block and sends the boundary information to its followers. In this process, the scout glider must wait until the followers finish their delineation in the previous block i - 1 before moving to the block i + 1 to achieve a successful underwater communication. The followers are controlled to search patches with rich information by changing their headings adaptively based on the boundary information from the scout glider and the measurements of the moving patches. The control of a follower is explained step by step as follows:

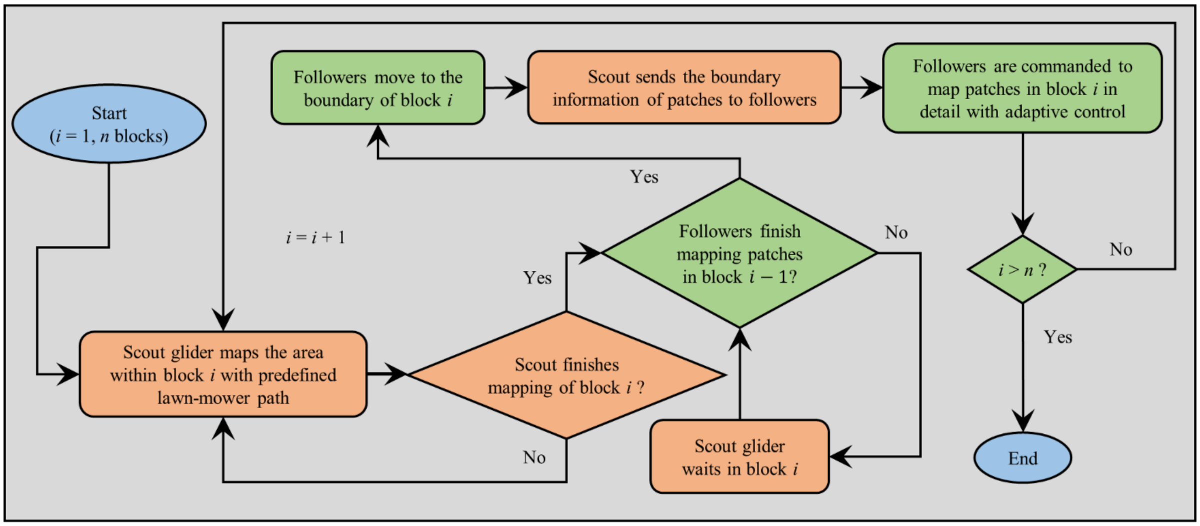

Figure 7-1. A flowchart showing the control of a scout glider and followers in the cooperative strategy.

(1) A follower is controlled to go to the center of a patch as a target waypoint to delineate the plume precisely. The patch has a dimension of W in its short axis, and a dimension of L in its long axis (Figure 7-2). The direction of long axis is perpendicular to the direction of the short axis. The direction of the long axis is found through rotating the local coordinates of the patch around its global coordinates. When the value of the aspect ratio (L/W) is the largest, the direction of the X´ in the local coordinates (Figure 7-2) is the direction of the long axis.

(2) When the distance of the follower to the target point is within a certain distance D_r, the follower is assumed to have reached the center of the patch.

(3) The follower starts a spiral motion by changing its heading to delineate the plume, during which the follower logs its location information.

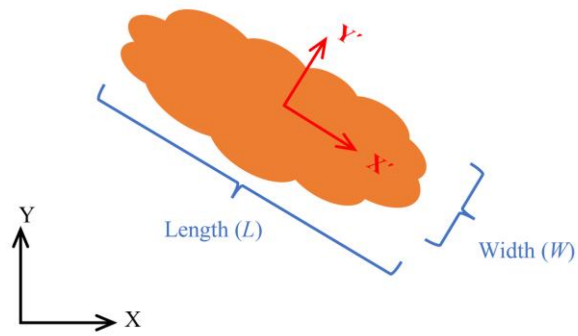

Figure 7-2. A patch with rich information in the global coordinate system (X, Y) and its local coordinate system (X´, Y´).

(4) After a certain amount of time T_s in delineating the patch with a spiral path, the backseat driver in the follower calculates the moving center of the glider (x_G, y_G) and center of the measured rich information (x_M, y_M) (Figure 7-3):

$$\begin{cases} x_G = mean\left(\sum_{i=1}^{n} x_{G,i}\right) \\ y_G = mean\left(\sum_{i=1}^{n} y_{G,i}\right) \end{cases} \tag{7-1}$$

$$\begin{cases} x_M = mean\left(\sum_{j=1}^{m} x_{M,j}\right) \\ y_M = mean\left(\sum_{j=1}^{m} y_{M,j}\right) \end{cases} \tag{7-2}$$

in which n is the number of the location logged and m is the number of information-rich measurements detected during the time period T_s from when the glider reaches the center of the patch. Then a new target waypoint (x_T, y_T) is derived which is in the direction from (x_G, y_G) to (x_M, y_M):

$$\begin{cases} x_T = x_M + L * \cos(\alpha) \\ y_T = y_M + W * \sin(\alpha) \end{cases} \tag{7-3}$$

where α is the angle between the direction from (x_G, y_G) to (x_M, y_M) and the positive direction of the X-axis in the global coordinates. The new target point for the follower glider is set in this way as the patch is driven by the current and the direction from (x_G, y_G) to (x_M, y_M) is considered to be the direction pointing to the inside of the patch.

(5) The follower glider is then commanded to go to the new target point to delineate the plume with a spiral path.

(6) Perform steps (2) - (5) until a maximum number of target points or a maximum period of time has been reached.

(7) The follower is controlled to either search a new patch or follow the boundary of the next block.

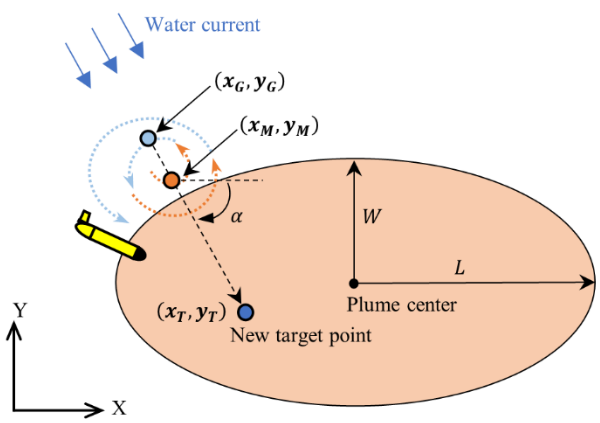

Figure 7-3 . The follower changes its path during the mission to move to a new target point (x_T, y_T) for spiral motion when delineating a patch driven by water currents; the new target point is calculated based on the moving center of the glider (x_G, y_G) and center of the measured rich information (x_M, y_M).

7.3.2 Evaluation metrics

Mission duration and duty cycle were evaluated to check the performance of the strategy of using gliders to delineate oil patches underwater. The duration of a mission or mission time is the length of time from when a glider starts mapping to the time when the glider finishes the required mission.

The duty cycle of a mission is defined to be the ratio between the length of time that the gliders are in mapping regions of rich information and the total working time of the gliders (the product of the number of gliders and the duration of the missions). Duty cycle measures the utilization rate of gliders in a mission in collecting information-rich measurements. For our cooperation strategy, assume that the number of patches in a mission is n, the number of followers is m, and the duration of the mission is T_t (see Figure 7-4), the total length of time that the scout glider and followers are taking measurements in regions of rich information is T_s and T_f respectively:

$$T_s = \sum_{i=1}^{n} T_{s,i} \tag{7-4}$$

$$T_f = \sum_{i=1}^{n} T_{f,i} \tag{7-5}$$

The duty cycle of gliders in the cooperative mission is:

$$D = \frac{T_s + T_f}{(m+1) * T_t} \tag{7-6}$$

We evaluated both the duration and duty cycle of missions here as follows: for two missions with the same duty cycle, the mission with a short duration is considered better; for two missions with the same duration, the one with a higher duty cycle is preferred.

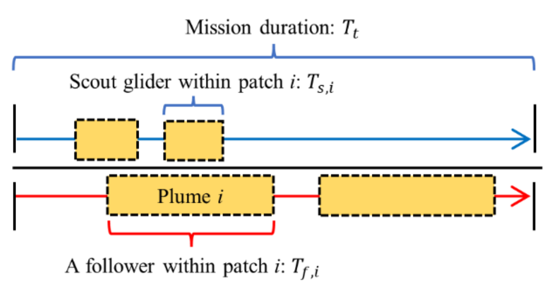

Figure 7-4. A sketch showing the duration of a mission and the length of time that a scout glider and follower gliders are in mapping information-rich patches.

In addition, we evaluated a score of performance, SoP, of a strategy. This was defined to be:

$$SoP = D * \frac{P_e}{P_a} \quad (7\text{-}7)$$

where P_e is the percentage of valuable rich information collected and P_a is the percentage of mission area which is covered by information-rich patches. We introduced SoP as the detection from one glider may be covered by another glider with the same set of sensors and the overlapping measurements are considered to be invaluable when the patches do not change significantly under the influence of the marine environment.

7.4 Experimental results

This section shows the influence of adaptive control on the performance of the glider cooperation strategy by comparisons of missions with one and multiple glider(s), with and without cooperation, and/or without adaptive control through simulations.

7.4.1 Simulation setup

The strategies for comparison are shown in Table 7-2. For a strategy with a single glider, the glider was commanded to follow a lawn-mower path defined by waypoints in a block before moving to the next block. For the strategy with multiple gliders without cooperation, all of the gliders were assigned to the same block and the gliders delineated the area within blocks simultaneously by using a lawn-mower path. For the strategies with one glider and multiple non-cooperative gliders with adaptive control, the gliders were controlled to map an information-rich patch in detail, immediately upon the detection of such a patch. For the cooperation strategy, the scout glider had the same lawn-mower path as the gliders in the other strategies. The cooperation of gliders was simulated according to the flowchart in Figure 7-1.

Table 7-2. Glider mapping strategies that were simulated in this chapter.

Strategy name	Description	Adaptive ability	Multiple gliders	Cooperation
One_Gld	One glider without adaptivity	×	×	×
One_Gld_Adp	One glider with adaptivity	✓	×	×
Multi_Glds	Multiple gliders without adaptivity and cooperation	×	✓	×
Multi_Glds_Adp	Multiple with adaptivity but without cooperation	✓	✓	×
Multi_Glds_Adp_Coop	Multiple gliders with adaptivity and cooperation	✓	✓	✓

In the simulations, the mission area was divided into 20 blocks and each block had a size of 300 m × 300 m. The width of the lawn-mower path for the scout glider was 60 m. The size of a block and the width of the lawn-mower path were set to minimize changes of patches between when the scout detected patches and when the followers reached patches. The information-rich oil patches can be in various shapes and distribution, and we only set the percentage of oil patch area in a block. In this chapter, four values were considered: 10%, 20%, 40%, and 60%. A constant current was added to the simulated environment. The current speed was the same as the measured average current speed experienced in the Deepwater Horizon oil spill disaster, which was 0.078 m/s (Camilli et al., 2010). It was assumed that oil patches were moved by the water currents in the positive X-direction in the global coordinates at the speed of 0.078 m/s (Figure 7-5). For comparison, situations with a current speed of 0.0 m/s were also simulated. Gliders were commanded to spend the same length of time in delineating patches when the average current speed was 0.0 m/s and 0.078 m/s at a given percentage of oil patch area.

The influence of the current on the shape of the patches was not considered. The shape of the patches was simplified as circular or oval, and the number of patches was in accordance with the number of followers in the strategy. These patches were in a uniform distribution. For example, if there were two followers in the cooperation strategy when the percentage of oil patch area was 10%, the number of patches in a block was 2 (Figure 7-5). These two patches were inside the block, centered at 150 m to the upper boundary of the block and 100 m and 200 m from the left boundary of the block respectively when the current speed was 0 m/s. When the current speed was 0.078 m/s, the blocks were shifted 120 m to the left compared with when the current speed was 0.0 m/s to guarantee that the gliders would not miss the patches. The setup of patches in the simulations ensured that each strategy had its best performance, such that the gliders did not spend a lot of time switching between patches and only the optimal metric values were evaluated.

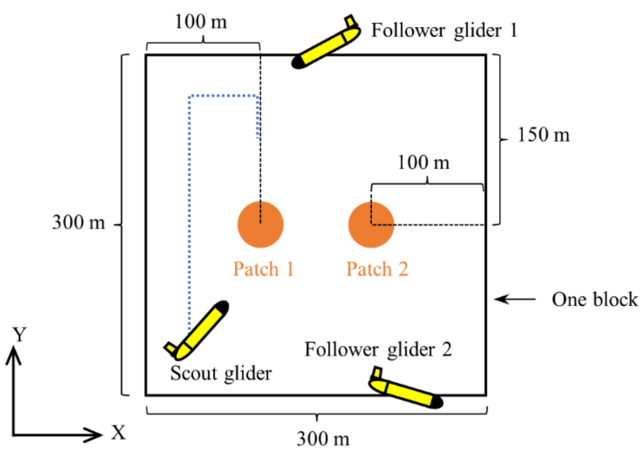

Figure 7-5. The distribution of patches when the number of followers is two and the percentage of oil patch area is 10% at a water current speed of 0.0 m/s. The predefined path of the scout glider is shown with blue dots.

7.4.2 Simulation results

To better present the simulation results, a relative mission duration was used. This was defined as the result of the mission duration of a strategy divided by the mission duration for one glider to map one block without adaptive control.

(1) Influence of adaptive control

With the use of adaptive control, the duty cycle of the gliders in a mission improved. For example, when the current speed was 0.0 m/s and oil patch area accounted for 10% of the mission area, the strategies One_Gld_Adp and Multi_Glds_Adp had a higher duty cycle than the strategies One_Gld and Multi_Glds (Figure 7-6 (a)). This is also applied to the scenarios when the oil patch areas were 20%, 40%, and 60% of the mission area (Figure 7-6). Adaptive control enabled gliders to change heading adaptively when a patch was detected. Therefore, the gliders could delineate inside a patch for longer than without adaptive ability. This also increased the length of the mission time (Figure 7-7). Figure 7-7 also shows the mission duration when current speed was 0.078 m/s as follower gliders were commanded to spend the same length of time in delineating patches at the two investigated current speeds at a given percentage of oil patch area.

The score of performance of strategies with adaptive control were higher than those without adaptive ability when the oil patch area was 10%, 20%, and 40% (Figure 7-8 (a)-(c)). This means that although adaptive control increased the mission duration, it helped to more precisely delineate the information-rich patches and increase the knowledge of information-rich areas. When the proportion of oil patch area to the total mission area increased to 60%, the score of performance of the non-adaptive strategies was superior to the adaptive strategies (Figure 7-8 (d)). This was because of the overlapping measurement from the adaptive mapping that decreased the percentage of valuable rich information collected (P_e). In addition, when the oil patch area accounted for a higher percentage of the mission area, the area with rich information could more easily be captured by a non-adaptive mapping strategy.

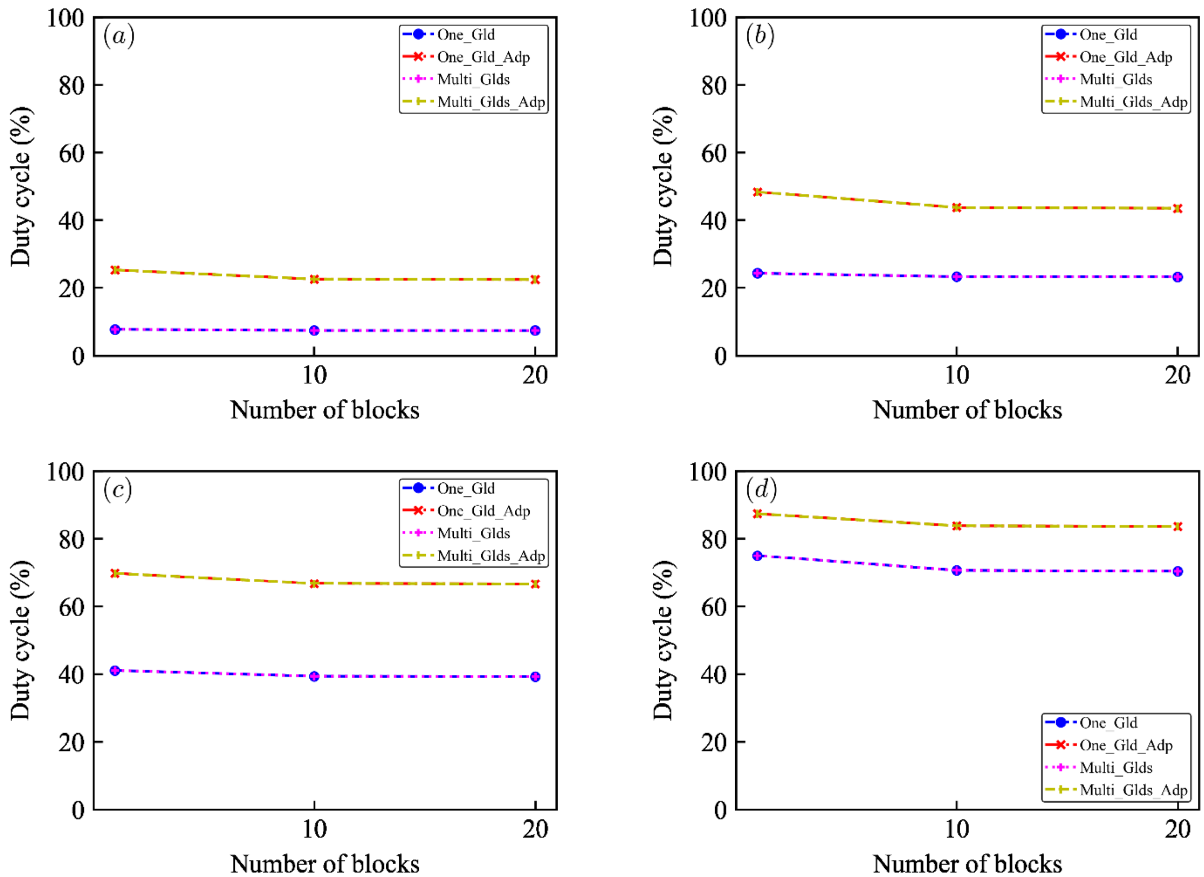

Figure 7-6. Influence of adaptive control on the duty cycle of strategies with one glider and multiple gliders without cooperation when the current speed was 0.0 m/s and the oil patch area accounted for: (a) 10%; (b) 20%; (c) 40%; and (d) 60% of the mission area.

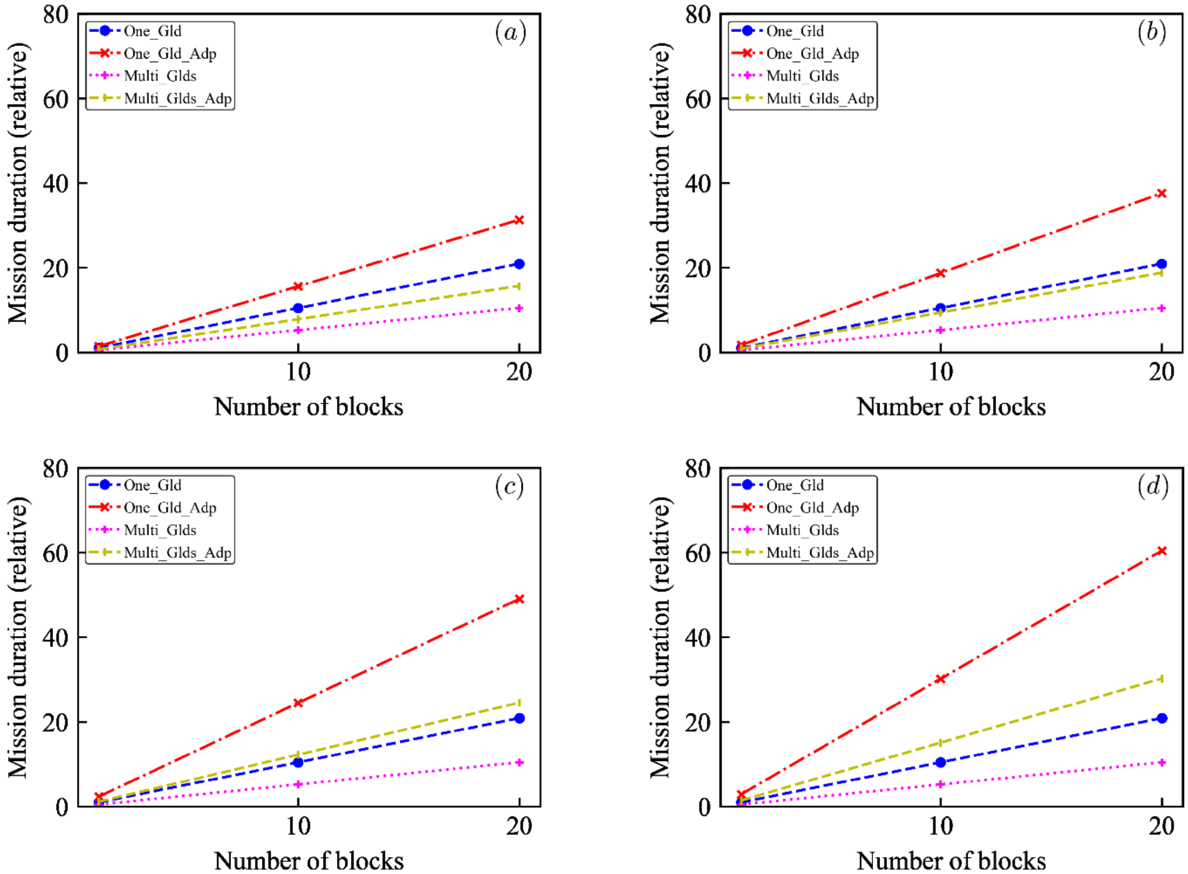

Figure 7-7. Influence of adaptive control on the relative mission duration of strategies with one glider and multiple gliders without cooperation when the current speed was 0.0 m/s or 0.078 m/s and the oil patch area accounted for: (a) 10%; (b) 20%; (c) 40%; and (d) 60% of the mission area.

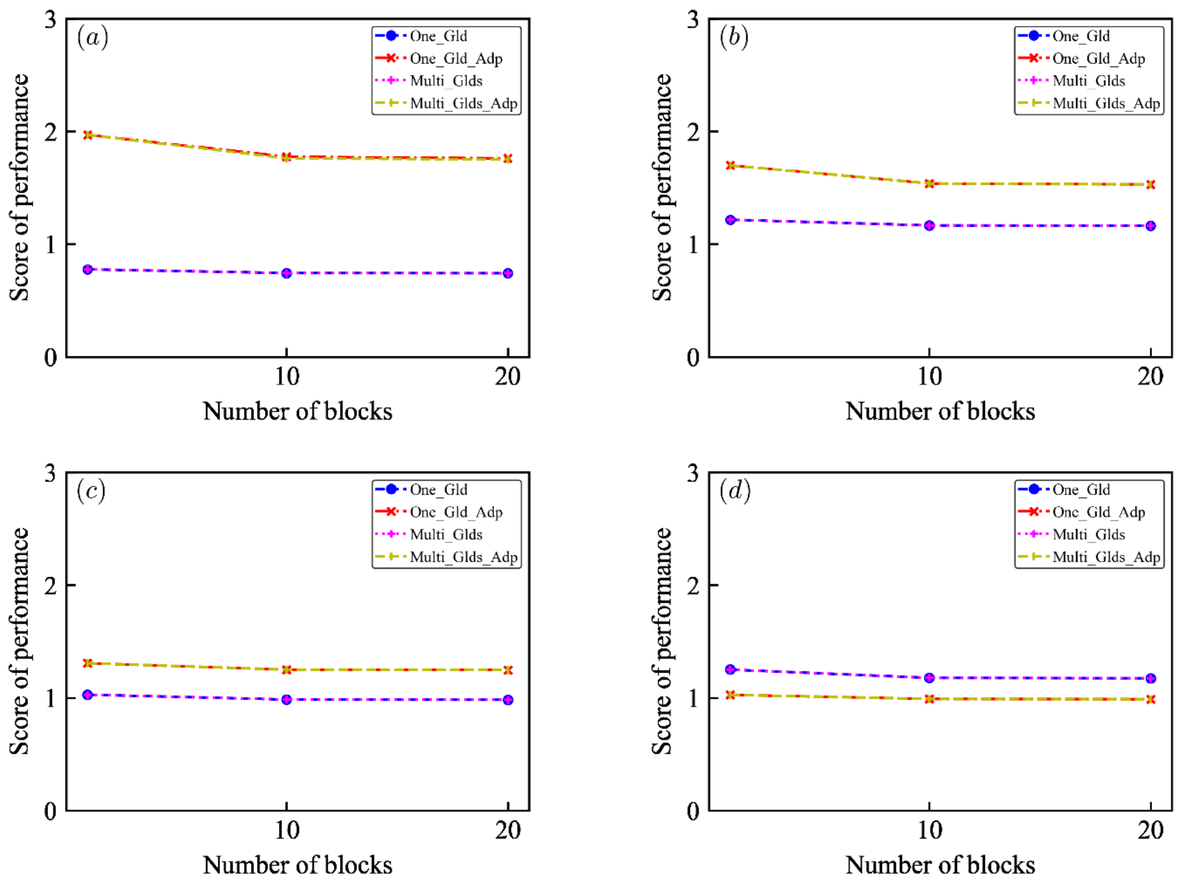

Figure 7-8. Influence of adaptive control on the score of performance of a mission when the current speed was 0.0 m/s and the oil patch area accounted for: (a) 10%; (b) 20%; (c) 40%; and (d) 60% of the mission area.

When the water current was 0.078 m/s, the relative motion between gliders and oil patches affected the outcomes. For example, the duty cycle of strategies with one glider and multiple gliders without adaptivity at a current speed of 0.078m/s (One_Gld/Multi_Glds (0.078 m/s)) was higher than those at 0.0 m/s (One_Gld/Multi_Glds (0.0 m/s)) (Figure 7-9). This means that the relative motion of gliders and patches under the influence of a water current of 0.078 m/s in our simulation increased the performance of gliders in detecting the information-rich patches when the gliders were without adaptivity. With adaptive control, the duty cycle of strategies when the current speed was 0.078

m/s (One_Gld_Adp/Multi_Glds_Adp (0.078 m/s)) was lower compared with when the current speed was 0.0 m/s (One_Gld_Adp/Multi_Glds_Adp (0.0 m/s)) (Figure 7-9). According to our simulation, a follower glider with adaptive control at a current speed of 0.078 m/s could measure 80% of the rich information collected at a current speed of 0.0 m/s.

The score of performance of strategies with adaptivity at a current speed of 0.078 m/s was higher than those without adaptivity when the oil patch area accounted for 10% and 20% of the mission area, except when the number of blocks was 1 when the proportion of oil patch area was 20% (Figure 7-10). Overall, the score of performance of missions using an adaptive strategy were lower compared with those using a non-adaptive strategy when the oil patch area was 40% and 60% at the current speed of 0.078 m/s.

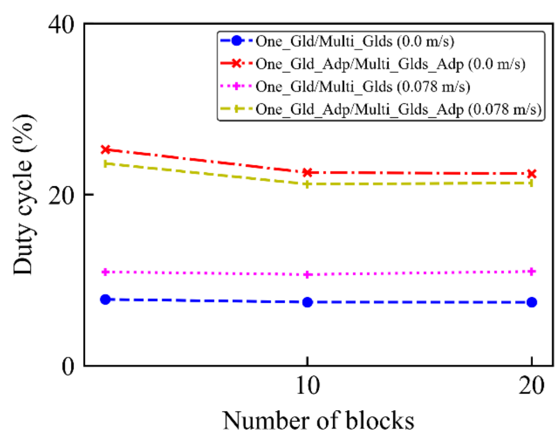

Figure 7-9. Influence of adaptive control and current speed on the duty cycle of a mission when the oil patch area accounted for 10% of the mission area.

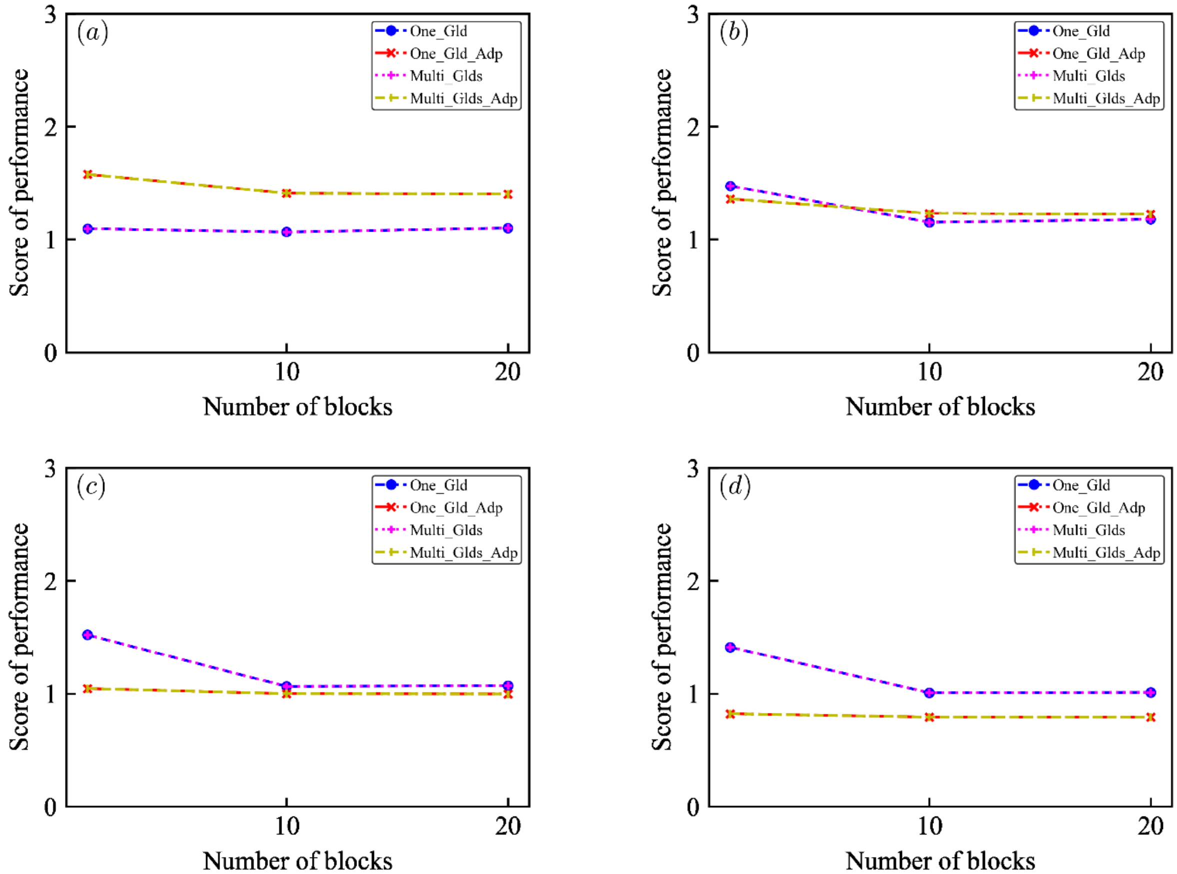

Figure 7-10. Influence of adaptive control and multiple gliders (2 gliders or more) on the score of performance of a mission when the current speed was 0.078 m/s and the oil patch area accounted for: (a) 10%; (b) 20%; (c) 40; and (d) 60% of the mission area.

(2) Performance of cooperation strategy with adaptive control

The cooperation strategy Multi_Glds_Adp_Coop had a lower duty cycle compared to the strategy Multi_Glds_Adp without cooperation (Figure 7-11 shows an example). The cooperation of gliders, such as occurs when the followers wait for the scout glider to find patches in the first block and the scout glider waits in the last block when it has finished its mission, increases the length of the mission time. For example, when the oil patch area was 10% and the current speed was 0.078 m/s, the mission time of using two gliders without cooperation was shorter than when using multiple cooperative gliders (Table 7-3). For the cooperative strategy, when the number of followers increased, the mission time decreased as the oil patch areas were mapped by multiple follower gliders simultaneously.

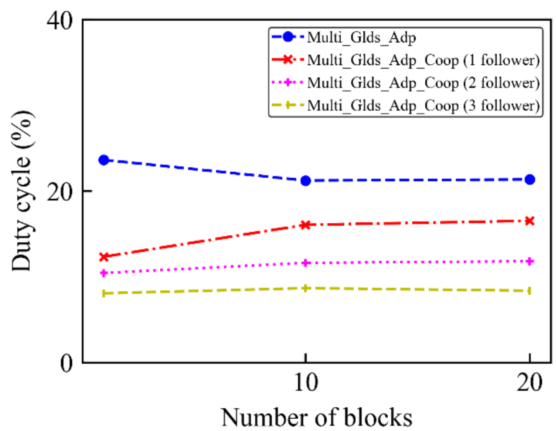

Figure 7-11. The duty cycle of strategies with multiple adaptive gliders when they were cooperative and non-cooperative at an oil patch area of 10% and a current speed of 0.078 m/s.

Using multiple gliders, but no cooperation, did not change the number of information-rich measurements but decreased the mission time in an inversely proportional manner to the number of gliders used (Figure 7-7). When multiple gliders were used, such as 2, 3, or more, the duty cycle did not change compared to using one glider (Figure 7-6). This is because the duty cycle measured the utilization rate of gliders which was the ratio of the amount of rich information collected to the total working time of the gliders. As the percentage of valuable rich information collected had not changed, having multiple gliders to map patches did not have a better score of performance compared to using one glider. Therefore, in this chapter, when duty cycle and score of performance were mentioned in a strategy with multiple gliders but no cooperation, we did not mention the number of gliders as the duty cycle and score of performance did not change with the number of gliders.

Table 7-3. Relative mission duration of strategies with multiple adaptive gliders when they were cooperative and non-cooperative at an oil patch area of 10% and a current speed of 0.078 m/s.

Number of blocks / Strategy	1	10	20
Multi_Glds_Adp (2 gliders)	0.70	7.78	15.65
Multi_Glds_Adp_Coop (1 follower)	1.47	11.20	22.05
Multi_Glds_Adp_Coop (2 follower)	1.32	11.11	21.96
Multi_Glds_Adp_Coop (3 follower)	1.25	11.04	21.87

Despite the increased mission duration lowering the duty cycle of the cooperative strategy, the cooperative strategy potentially increased the number of valuable measurements as the followers could have a different set of sensors to measure the oil patches detected by the scout. In the strategy of gliders with adaptive ability but without cooperation, a glider detected a patch in detail after an exploration. The subsequent detailed survey was able to cover the detection in the exploration as both processes were using the same set of sensors. Therefore, the score of performance of the non-cooperative strategy was lower than that of the cooperative strategy (Figure 7-12). For example, when the percentage of oil patch area was 10% and the current speed was 0.078 m/s, the *SoP* of the cooperative strategy with one follower was higher than that of the non-cooperative strategy when the number of blocks was larger than 2 (Table 7-4). The lower score of performance of the cooperative strategy when the block number was less than 3 was due to the waiting time of followers that resulted in a non-negligible ratio of the total mission time. When the oil patch area made up 60% of the mission area, the cooperation strategy could also have a higher *SoP* than one glider or multiple gliders without cooperation and/or without adaptivity, but with a minimum number of blocks of 20 required (Table 7-5). This performance revealed that the cooperation strategy performed better for long-duration missions. Besides, as the score of performance of One_Gld_Adp and Multi_Glds_Adp was lower than that of One_Gld and Multi_Glds in Figure 7-12 (d), this showed that cooperation was required to reach a higher *SoP*.

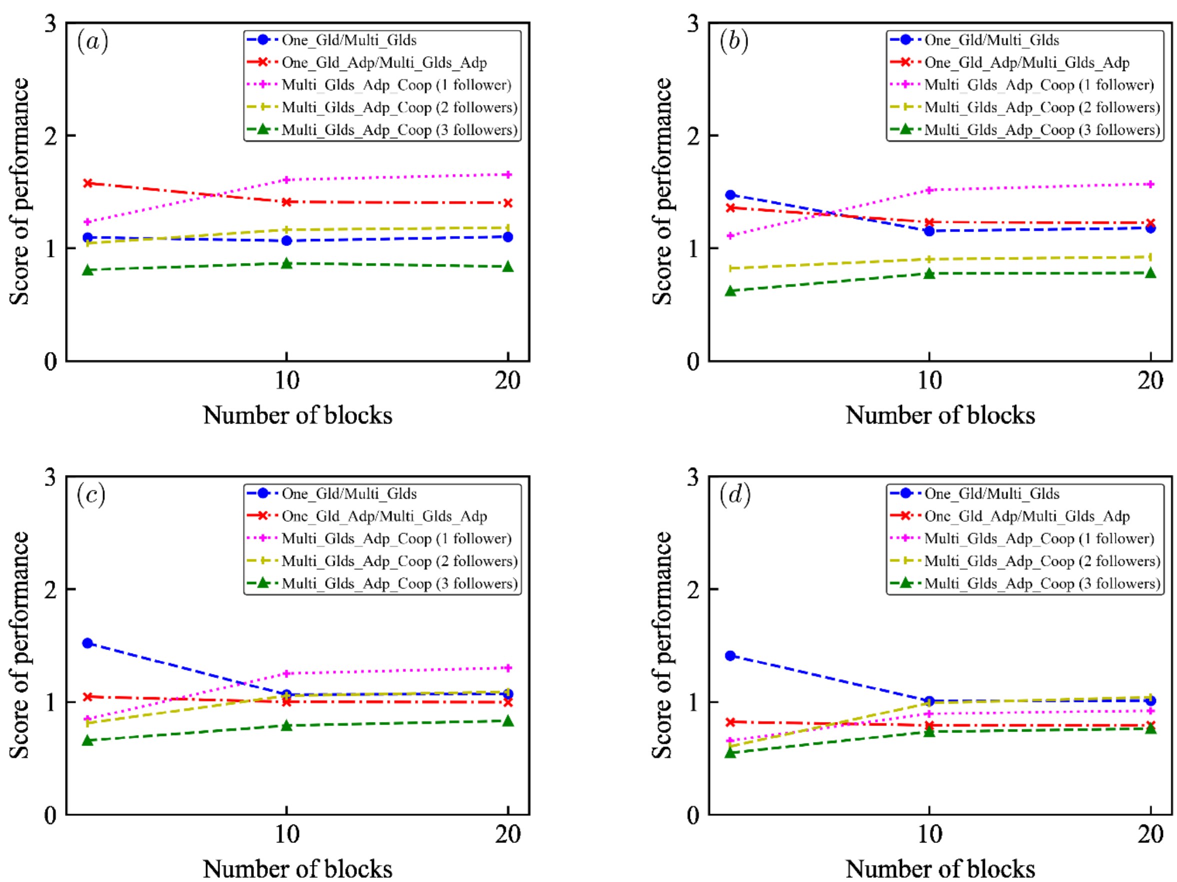

Figure 7-12. Score of performance of the investigated strategies at a current speed of 0.078 m/s when the oil patch area accounted for a certain percentage of the mission area: (a) 10%; (b) 20%; (c) 40%; and (d) 60%.

Table 7-4. Score of performance of the investigated strategies at a current speed of 0.078 m/s when the oil patch area accounted for 10% of the mission area. Values with red boundaries were the highest for the given number of blocks.

Strategy \ Number of blocks	1	2	3	4	5	6	10	20
One_Gld/ Multi_Glds	1.10	0.78	1.12	0.96	1.13	1.02	1.07	1.10
One_Gld_Adp/ Multi_Glds_Adp	1.58	1.48	1.45	1.43	1.43	1.42	1.41	1.40
Multi_Glds_Adp_Coop (1 follower)	1.23	1.29	1.51	1.48	1.58	1.55	1.61	1.65
Multi_Glds_Adp_Coop (2 follower)	1.04	1.03	1.17	1.11	1.18	1.14	1.16	1.18
Multi_Glds_Adp_Coop (3 follower)	0.81	0.71	0.84	0.81	0.89	0.87	0.87	0.84

Table 7-5. Score of performance of the investigated strategies at a current speed of 0.078 m/s when the oil patch area accounted for 60% of the mission area. Values with red boundaries were the highest for the given number of blocks.

Strategy \ Number of blocks	1	2	3	4	5	6	10	20
One_Gld/ Multi_Glds	1.41	0.98	1.14	1.00	1.09	1.00	1.01	1.01
One_Gld_Adp/ Multi_Glds_Adp	0.82	0.81	0.80	0.80	0.80	0.79	0.79	0.79
Multi_Glds_Adp_Coop (1 follower)	0.66	0.72	0.82	0.82	0.87	0.86	0.89	0.92
Multi_Glds_Adp_Coop (2 follower)	0.60	0.69	0.83	0.86	0.92	0.93	0.99	1.04
Multi_Glds_Adp_Coop (3 follower)	0.55	0.58	0.67	0.68	0.71	0.71	0.74	0.76

(3) The optimal number of followers for the cooperative control strategy

When the current speed was 0.078 m/s and the oil patch area was 10%, 20%, and 40%, the cooperative strategy with one follower had the highest *SoP* when the number of blocks mapped was less than 10 (Figure 7-12). For the scenario when the oil patch area accounted for 60% of the mission area, the cooperative strategy with two followers had the best *SoP* when the number of blocks was larger than 19. The weak performance of the cooperative strategy with one follower glider at a higher percentage area of patches was because a low number of follower gliders was used. The optimal number of followers increased with the increase of the oil patch area. The growth in the number of followers reduced the length of time that each follower delineated the patches in a block. When three followers were used, the change in the total number of valuable rich-information measurements could be neglected. The mission duration for the group of gliders was decreased. However, the total mission time that all of the gliders spent to complete a mission increased, which reduced the score of performance. The optimal number of followers in the cooperation strategy when the current speed was 0.0 m/s was similar to the situation when the current speed was 0.078 m/s (Figure 7-13), except in the number of blocks required.

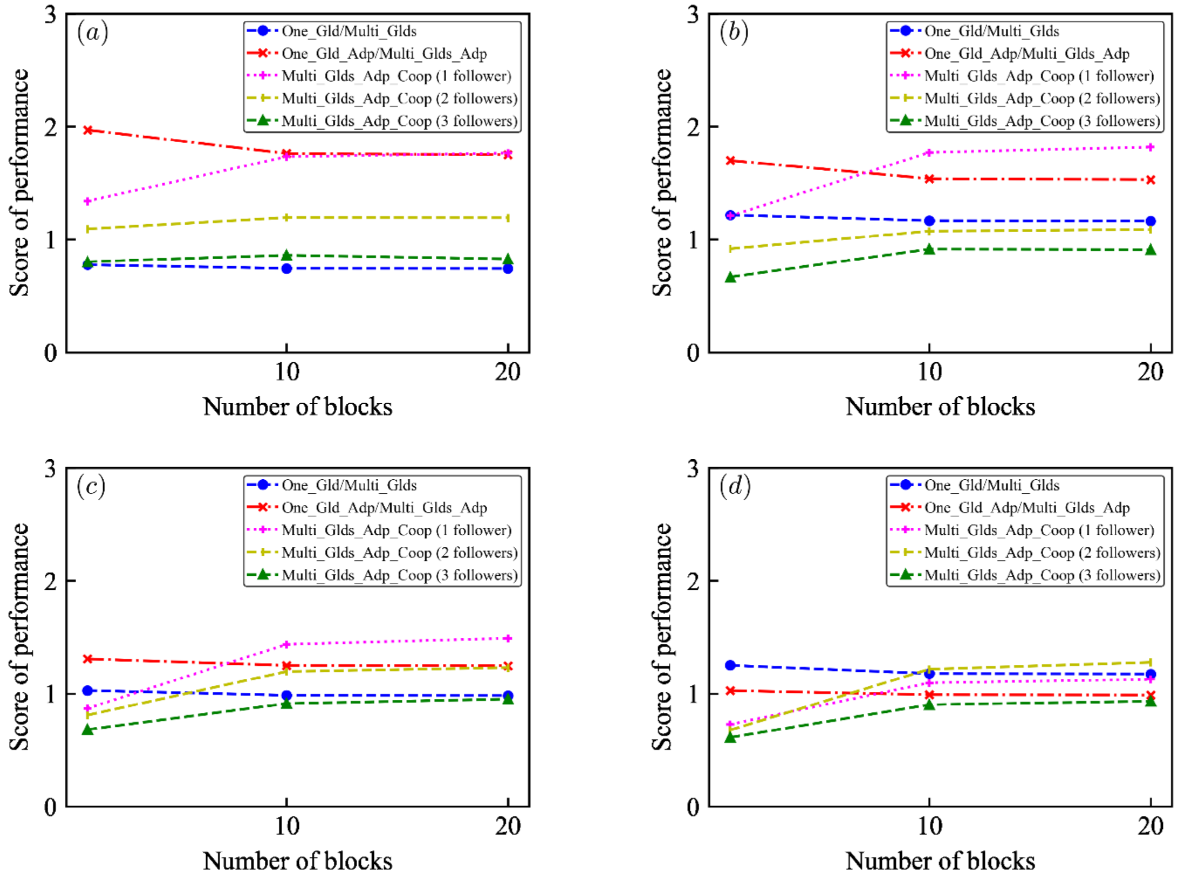

Figure 7-13. Score of performance of the investigated strategies at a current speed of 0.0 m/s when the patchy area accounted for a certain percentage of the mission area: (a) 10%; (b) 20%; (c) 40%; and (d) 60%.

7.4.3 Discussion

In the simulations, when the oil patch area accounts for a higher percentage (60% when the current speed is 0.0 m/s and 40% when the current speed is 0.078 m/s) of the mission area, the score of performance of a strategy which uses adaptive control is lower than when adaptive control is not used. The oil patch area with rich information can be easily mapped by a non-adaptive strategy and the valuable information increased by the inclusion of an adaptive strategy is not enough to balance out the increase of the mission time. The adaptive ability increases the duty cycle, but the percentage of valuable measurements may decrease at the same time if the glider is commanded to conduct adaptive mapping in detail. Therefore, adaptive control cannot guarantee a better score of performance. With the use of multiple gliders, the score of performance (*SoP*) does not change as *SoP* assesses both the duration of a mission and the number of gliders involved. Although the duty cycle of a cooperation strategy with adaptive control is lower than that without cooperation, the cooperation increases the amount of valuable information and hence the cooperative strategy has the best score of performance, especially for a higher number of blocks. The simulation results reveal the importance of adaptive control and cooperation in the improvement of the performance of a mapping strategy. It also shows why gliders are used as the proposed strategy has better *SoP* for long-endurance missions. The use of non-adaptive strategies can reach the same score of performance as the cooperative strategy when the number of blocks is less than 20 (Figure 7-12 (d)). However, as gliders do not cooperate by exchanging information and adaptively mapping a detected patch in detail, the possibility of losing collected measurements will be increased if a malfunction happens (Johnson et al., 2009). The non-cooperative strategy requires path planning of the gliders before a mission to avoid a collision, which may result in some gliders being busy with multiple tasks while some are idle.

7.5 Conclusion

In this chapter, adaptive control was applied to follower gliders in cooperating multiple glider teams on missions to delineate underwater oil patches. The influence of water currents on the motion of the oil patches was included. The influence of having adaptive control and the performance these improvements made in the cooperation strategy with adaptive control were evaluated through simulations by comparing with strategies without cooperation and/or without adaptive control. Simulation experiments were done to assess the duty cycle, the mission duration, and the score of performance of a mission, a measure of the percentage of valuable rich information collected to the percentage of the mission area covered by information-rich patches. The score of performance was an evaluation metric, which evaluated the percentage of the valuable information collected in addition to the duty cycle. The duty cycle was the utilization rate of gliders in collecting information-rich measurements considering the duration of a mission. The optimal number of follower gliders in a team was assessed.

On its own, the inclusion of adaptive control led to a higher duty cycle, but was unable to improve the score of performance of a strategy when the percentage of oil patch area in a mission area increased to 60%. The cooperation strategy with adaptive control had a lower duty cycle and longer mission duration than other strategies studied; it also was found to have the best score of performance especially for long-duration missions. The optimal number of follower gliders in the cooperation strategies depended on the percentage of oil patch area in the area of the missions; it was found to be one follower when the oil patch area was less than 60% and two followers when the oil patch area was 60%.

This chapter answered the fourth research question (Q4: What are the benefits of using multiple cooperative gliders with adaptive control in mapping oils underwater?) by comparing the strategies with and without adaptive control. The simulation results showed the performance of the proposed multi-glider cooperation strategy with adaptive control to delineate subsurface oil, which reached the fourth sub-objective (O4: To investigate the performance of a multi-glider cooperation strategy with adaptive control in delineating underwater oil plumes) of this thesis.

Acknowledgement

Funding was received from Fisheries and Oceans Canada through the Multi-partner Oil Spill Research Initiative (MPRI) 1.03: Oil Spill Reconnaissance and Delineation through Robotic Autonomous Underwater Vehicle Technology in Open and Iced Waters and the School of Graduate Studies at Memorial University of Newfoundland.

Reference

Abt Associates, Woods Hole Oceanographic Institution, National Oceanic and Atmospheric Administration, U.S. Environmental Protection Agency, Water Mapping, L., 2020. Report to BSEE: Three-Dimensional Mapping of Dissolved Hydrocarbons and Oil Droplets Using a REMUS-600 Autonomous Underwater Vehicle.

Camilli, R., Reddy, C.M., Yoerger, D.R., Van Mooy, B.A.S., Jakuba, M. V., Kinsey, J.C., McIntyre, C.P., Sylva, S.P., Maloney, J. V., 2010. Tracking hydrocarbon plume transport and biodegradation at deepwater horizon. Science (80-.). 330, 201–204. https://doi.org/10.1126/science.1195223

Das, J., Rajan, K., Frolov, S., Py, F., Ryan, J., Caron, D.A., Sukhatme, G.S., 2010. Towards marine bloom trajectory prediction for AUV mission planning. Proc. - IEEE Int. Conf. Robot. Autom. 4784–4790. https://doi.org/10.1109/ROBOT.2010.5509930

De Farias, D.P., Megiddo, N., 2004. Exploration-exploitation tradeoffs for experts algorithms in reactive environments, in: Advances in Neural Information Processing Systems. Vancouver, British Columbia, Canada, pp. 1–8.

Ferri, G., Jakuba, M. V., Yoerger, D.R., 2010. A novel trigger-based method for hydrothermal vents prospecting using an autonomous underwater robot. Auton. Robots 29, 67–83. https://doi.org/10.1007/S10514-010-9187-Y

Ji, C., Beegle-Krause, C.J., Englehardt, J.D., 2020. Formation, Detection, and Modeling of Submerged Oil: A Review. J. Mar. Sci. Eng. 2020, Vol. 8, Page 642 8, 642. https://doi.org/10.3390/JMSE8090642

Johnson, B., Hallin, N., Leidenfrost, H., O'Rourke, M., Edwards, D., 2009. Collaborative mapping with autonomous underwater vehicles in low-bandwidth conditions, in: OCEANS 2009-EUROPE. Bremen, Germany, pp. 1–7. https://doi.org/10.1109/OCEANSE.2009.5278277

Kinsey, J.C., Yoerger, D.R., Jakuba, M. V., Camilli, R., Fisher, C.R., German, C.R., 2011. Assessing the Deepwater Horizon oil spill with the sentry autonomous underwater vehicle, in: 2011 IEEE/RSJ International Conference on Intelligent Robots and Systems. Institute of Electrical and Electronics Engineers (IEEE), San Francisco, CA, USA, pp. 261–267. https://doi.org/10.1109/iros.2011.6095008

Petillo, S., Schmidt, H., Balasuriya, A., 2012. Constructing a distributed AUV network for underwater plume-tracking operations. Int. J. Distrib. Sens. Networks 2012, 1–12. https://doi.org/10.1155/2012/191235

Petillo, S.M., Schmidt, H., 2012. Autonomous and Adaptive Underwater Plume Detection and Tracking with AUVs: Concepts, Methods, and Available Technology. IFAC Proc. Vol. 45, 232–237. https://doi.org/10.3182/20120919-3-IT-2046.00040

Socolofsky, S.A., Adams, E.E., Sherwood, C.R., 2011. Formation dynamics of subsurface hydrocarbon intrusions following the Deepwater Horizon blowout. Geophys. Res. Lett. 38, 1–6. https://doi.org/10.1029/2011GL047174

Sun, Y., Cao, X., Liang, F., 2019. Investigation on underwater spreading characteristics and migration law of oil leakage from damaged submarine pipelines. Process Saf. Environ. Prot. 127, 329–347. https://doi.org/10.1016/j.psep.2019.05.030

Tian, Y., Li, W., Zhang, A., Yu, J., 2011. Behavior-based control of an autonomous underwater vehicle for adaptive plume mapping, in: Proceedings of the 2nd International Conference on Intelligent Control and Information Processing. Harbin, China, pp. 719–724. https://doi.org/10.1109/ICICIP.2011.6008343

Vasilijevic, A., Calado, P., Lopez-Castejon, F., Hayes, D., Stilinovic, N., Nad, D., Mandic, F., Dias, P., Gomes, J., Molina, J.C., Guerrero, A., Gilabert, J., Miskovic, N., Vukic, Z., Sousa, J., Georgiou, G., 2015. Heterogeneous robotic system for underwater oil spill survey, in: OCEANS 2015. Institute of Electrical and Electronics Engineers Inc., Genova, Italy, pp. 1–7. https://doi.org/10.1109/OCEANS-Genova.2015.7271492

Wang, Y., Thanyamanta, W., Bose, N., 2022. Cooperation and compressed data exchange between multiple gliders used to map oil spills in the ocean. Appl. Ocean Res. 118, 102999. https://doi.org/10.1016/J.APOR.2021.102999

Winsor, P., Simmons, H., Chant, R., 2017. Arctic Tracer Release Experiment (ARCTREX): Applications for Mapping Spilled Oil in Arctic Waters, Final Report to Bureau of Ocean Energy Management, M13AC00008, OCS Study BOEM 2017- 062. Fairbanks, AK.

Xue, D., Wu, Z., Wang, S., 2015. Dynamical analysis of autonomous underwater glider formation with environmental uncertainties. Procedia IUTAM 13, 108–117. https://doi.org/10.1016/J.PIUTAM.2015.01.007

8. Chapter 8

Experimental testing on the developed Slocum glider through field experiments

8.1 Field experiment in testing the developed backseat driver

8.1.1 Backseat driver on AUVs

A backseat driver is a unit in a vehicle which makes decisions on where to go, while a driver is the unit controlling the vehicle (Bakdash et al., 2008). The backseat driver separates the vehicle autonomy from vehicle control (Eickstedt and Sideleau, 2010). The introduction of a backseat driver equips AUVs with intelligence without changing the existing control system of the vehicle. With this added intelligence and high-level control, the AUV can explore and exploit its environment more efficiently based on measurements from sensors and the status of the vehicles. Backseat controllers have been developed and applied on the Bluefin SandShark AUV (Naglak et al., 2018), Hydroid REMUS 100 (Gallimore et al., 2018), Iver2 AUV (Eickstedt and Sideleau, 2010), Teledyne Gavia AUV (Keane et al., 2020), and so on. Table 8-1 presents some of the underwater vehicles that have been successfully implemented with backseat drivers. The main functions of a backseat driver in these AUVs were to receive data from sensors onboard the vehicle and the main vehicle control system, and control the state of the AUV after processing the data.

The previous research mentioned in Chapter 6 and 7 proposed to use multiple underwater gliders to track the patchy plume cooperatively and adaptively. Each glider was assumed to be equipped with a backseat driver. With the backseat driver, the follower gliders could change its target waypoint, change its heading to reach a target waypoint, and change its behavior from reaching a waypoint to conducting a spiral mission with adaptive control. The backseat driver we developed for a Slocum glider is described in Chapter 5. A series of simulations were conducted to test the performance of the developed backseat driver by connecting the electronics of the glider in the loop and using the vehicle's control software.

In this section, the adaptive ability is realized in a Slocum glider by adding a backseat control hardware to it. This developed Slocum glider was used as a follower glider to test the adaptive control in the cooperation strategy through a field experiment.

Table 8-1. Underwater vehicles that have been successfully implemented with backseat drivers.

Vehicle	Organization	Feature of backseat drive	Function of the backseat driver	Ref.
AutoSub	National Oceanography Center	A ROS middleware was provided.	Controlling the autonomy system of the vehicle in real time.	(Furlong et al., 2018)
Bluefin SandShark	Nonlinear and Autonomous Systems Lab at Michigan Technological University	A Raspberry Pi supported the running of ROS for implementing control algorithms.	Receiving information from sensors for a dynamic control of the vehicle or mission replanning, such as approaching a target by processing images from a camera.	(Naglak et al., 2018)
Bluefin 9	Bluefin Robotics and Laboratory of Autonomous Marine Sensing Systems at MIT	Running MOOS-IvP as a backseat driver on a Gumstix computer.	Configuring the vehicle with autonomy behaviors and managing the communication, command, and control for multiple vehicles.	(Bluefin Robotics, n.d.) (Bluefin Robotics Corporation, 2011)
Bluefin 21		Running MOOS-IvP as a backseat driver on a PC/104 computer.		
Cwolf AUV	Institute for Automation and Systems Engineering, Technische Universität Ilmena, Fraunhofer IOSB-AS et al.	Being in the payload unit.	Performing mission management, maneuver processor, and autopilot.	(Eichhorn et al., 2018)
Delphin2	University of Southampton and National Oceanography Center	As a node in ROS by using Python.	Monitoring all the critical parameters in sensors, actuator, and mission information. Publishing error flags to high-level and low-level controllers when any critical parameter exceeded a predefined limit.	(Steenson et al., 2014)
Explorer	Memorial University of Newfoundland and Labrador	A Raspberry Pi supported the running of MOOS-IvP for implementing control algorithms.	Receiving information from sensors, such as a sonar for adaptive control in oil spill delineation.	(Hwang et al., 2020)
Hydroid Remus-100	Scripps Institution of Oceanography, WHOI	Running a ROS-based system as a backseat driver.	Sending commands to and receiving telemetry from the primary CPU and operating software of the vehicle. It was able to implement high-level control with ROS. Sensors were controlled by ROS nodes.	(Gallimore et al., 2018)
Iver2	Marine Autonomy Group at the Naval Undersea Warfare Center	A payload computer with a CPU board and two General Standards 24DSI-12 8-channel A/D converter boards supported the backseat driver with MOOS-IvP.	Receiving data both from the main vehicle control system and sensors connected directly with the backseat computer. Providing decision on the state, such as speed, heading and depth, of the vehicles to a dynamic control system in the main vehicle system.	(Eickstedt and Sideleau, 2010)
Riptide Micro-UUV	BAE Systems	Supporting MOOS-IvP control engine.	Planning customized mission.	(Manley and Smith, 2017)
STARFISH	Acoustic Research Laboratory at National University of Singapore	Make decisions from a pool of backseat driver agents.	Generating a single mission or a set of missions from sensor data. Interrupting the start, coordination, oversight, and control of missions. Controlling and interacting with the optional payload module.	(Teck and Chitre, 2012)
Teledyne Gavia AUV	Royal Australian Navy, University of California, Teledyne Gavia, Mission Systems Pty Ltd.	Implementing MOOS-IvP as a backseat driver.	A homing application pHomeToBeacon, as a backseat driver, received AUV position and range report and sent dynamic waypoints to the frontseat drive to equip AUVs with adaptive maneuvering capability for homing to a single beacon.	(Keane et al., 2020)

8.1.2 Backseat driver developed on a Slocum glider

The backseat driver computer, a BeagleBone Black, was installed in the payload bay of the glider (see Figure 8-1 (a)). This computer was powered by connecting it to the glider board in the aft hull. Four connectors were connected to the backseat driver computer (Figure 8-1 (b)): one is a six-pin connector to a fluorometer, the second one is a six-pin connector to a sonar, the third one is for connecting the on-board acoustic modem to the backseat driver, and the fourth connects to the glider's science computer to realize the backseat control by communicating with the glider's main control system. With this backseat driver and the connected sensors, the glider could process measurements from the fluorometer and sonar and make a decision on states, such as heading, depth, and waypoint, for the glider (Figure 8-2). In addition, the glider could also receive information from other gliders through an acoustic modem to replan its mission (Figure 8-2).

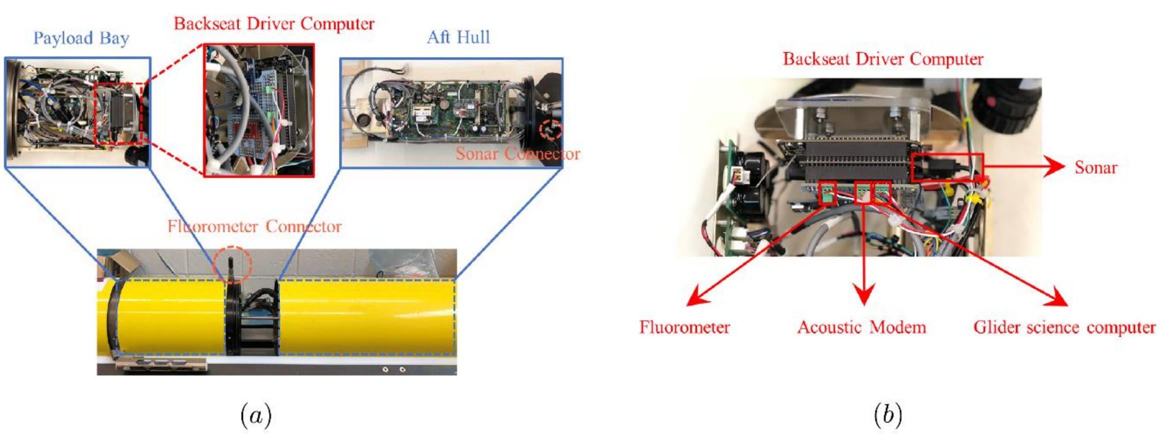

Figure 8-1. Developed backseat driver on the Slocum glider: (a) setup of the backseat driver computer inside the glider; and (b) connectors on the backseat driver for sensors.

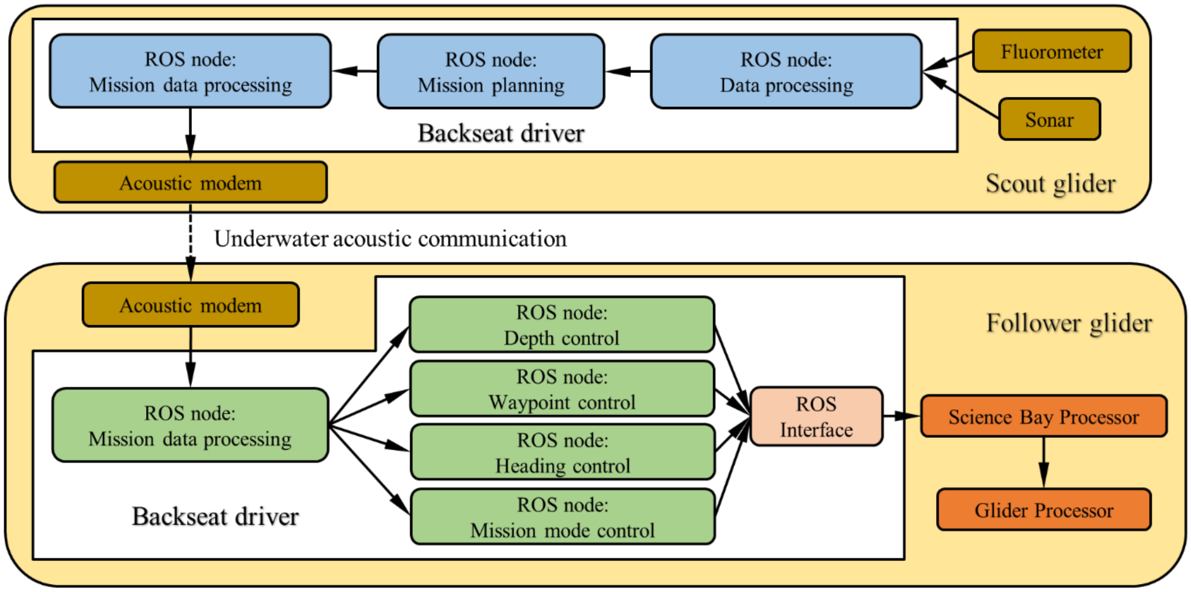

Figure 8-2. Cooperation of underwater gliders which are equipped with backseat drivers.

8.1.3 Field experimental results

8.1.3.1 Setup of the experiment

The adaptive control ability of follower gliders in a cooperation strategy was tested in Holyrood Bay, Newfoundland and Labrador, Canada. It mainly tested whether (1) the follower glider was able to receive commands from the scout glider, to go to a patch to search it, and whether (2) the backseat driver could control the follower glider adaptively, by receiving information from the scout glider. As there was only one glider available for our experiment, a Teledyne Benthos ATM-886 modem was used to emulate a scout glider and a Slocum glider as the follower. The ATM-886 modem was suspended from the side of a boat into the water (see Figure 8-3). The Slocum glider had a Teledyne Benthos ATM-900 LF1 modem in its nose. Both the ATM-886 modem and ATM-900 LF1 modem were omnidirectional and of a frequency of 9-14 kHz. As the scout glider was simulated in this research, the lawn-mower motion and the boundary classification ability of the scout glider was not tested in the field experiment.

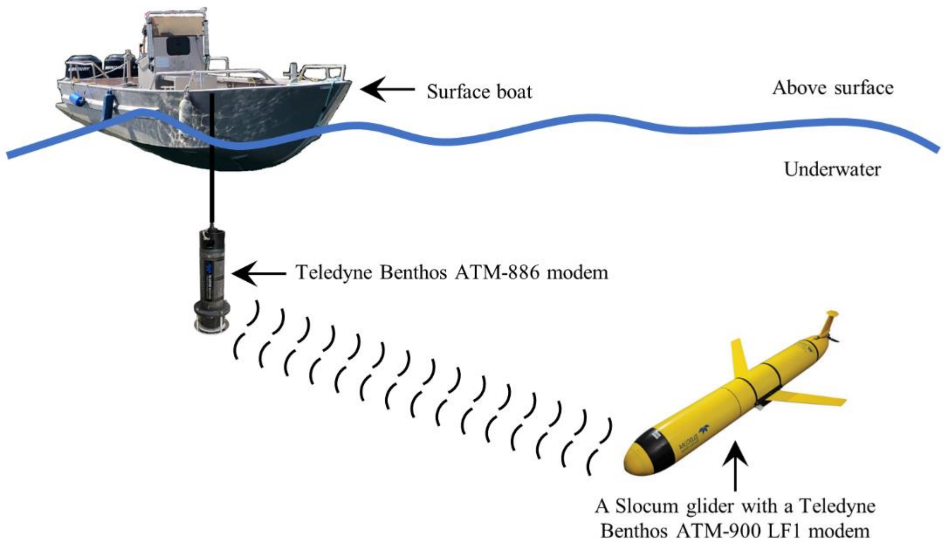

Figure 8-3. The setup of a Teledyne Benthos ATM-886 modem in a boat and a Slocum glider in the field experiment.

8.1.3.2 Results and discussion

When the follower glider started a mission from its start point, the simulated scout glider sent the localization of a patch to the follower glider for precise delineation. The follower glider received the patch information, and the backseat driver in the glider transformed the information into target waypoints. The follower glider was first commanded by the backseat driver to reach a waypoint (Target Waypoint 1 in Figure 8-4 (a)) and perform a spiral motion for four minutes ($T_s = 4\ minutes$) once the distance to the waypoint was within 20 m ($D_r = 20\ m$). Then the glider was commanded to move to another waypoint (Target Waypoint 2 in Figure 8-4 (a)), which was a second waypoint inside the patch with potential rich information. During this process, the heading of the glider was controlled by the backseat driver adaptively to reach the waypoints and to conduct the spiral motion. To reach a target waypoint, the backseat driver subscribed the location of the gliders and calculated the commanded heading by comparing the moving direction of the glider and the targeted heading to the waypoint. Then the commanded heading was published to the main vehicle controller. This commanded heading needed to be achieved by the glider before the next commanded heading was published. When the glider was conducting its spiral motion, the backseat driver published headings to the glider continuously, which steered the glider to turn in one direction. The target waypoint was in the inner side of the spiral path when the glider started its spiral motion in order to control the center position of the spiral motion. The path of the follower glider in the field experiment is shown in Figure 8-4 (a). As a comparison, the path of the glider in a simulation is presented in Figure 8-4 (b). The simulation was conducted by setting the glider in the "on_bench" mode to conduct the same mission as in the field experiment, but operated the full glider on the bench, not in the water. The glider in the simulation had the same mission duration as in the field mission. The glider in the simulation performed a spiral motion for four minutes after reaching the target waypoint 1 and performed another spiral motion after reaching target waypoint 2. These two spiral paths were very close as the distance between target waypoint 1 and target waypoint 2 were close. The glider was commanded to conduct the second spiral mission when reaching Target Waypoint 2, which was shortly after finishing the first spiral mission.

The simulation and field experiment had a difference in the initial heading of the follower glider and the time when the follower glider received the command from the scout glider. However, this difference did not affect the following control of the follower glider. In the field experiment, the glider successfully reached the patch and terminated the spiral motion after four minutes. After the spiral motion, the glider was controlled to go to Target Waypoint 2, but the path of the glider was different from the simulation result. The deviation of the path of the glider in the field experiment from the desired path in the simulation was possibly caused by the ocean environment. The backseat driver was able to adaptively control the heading of the glider in real-time based on the commanded heading and the measured heading of the glider in the field experiment (Figure 8-5). The measured heading was in accordance with the commanded heading. There was no commanded heading at the end of the mission (Figure 8-5) when the glider was on the surface waiting to be recovered. The adaptive heading behavior was supported by the control of the fin of the glider (Figure 8-6). However, the glider was not able to reach the second waypoint as smoothly as in the simulation, as the backseat driver could not change the low-speed characteristic and turning ability of the glider which made it vulnerable to influences from the ocean environment, especially currents. The accumulated error in the dead reckoning of the glider also contributed to the deviation. However, having a more accurate dead reckoning would not guarantee that the backseat driver could control the glider as in the simulation. The backseat driver was able to react to the position information in real-time and publish the command immediately, but the glider did not follow the commanded heading immediately in the field experiment.

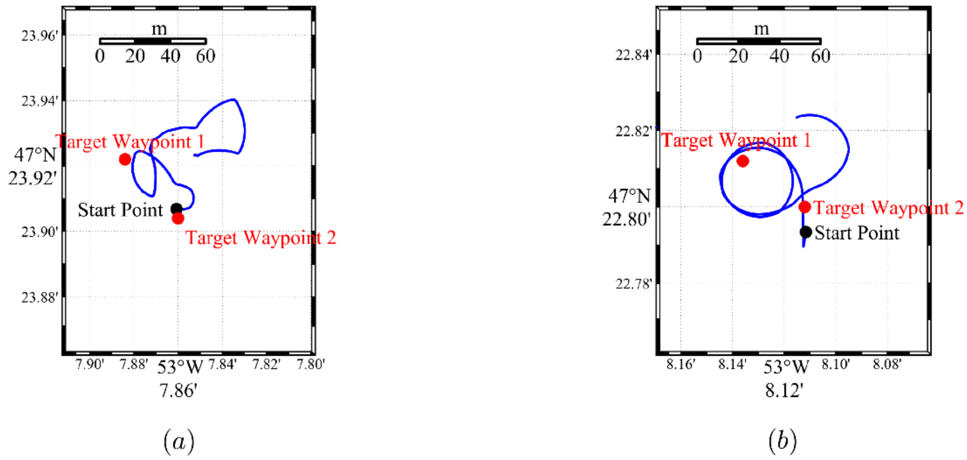

Figure 8-4. The path of the follower glider in the: (a) field experiment; (b) simulation experiment which had the same mission duration and was commanded to move to target waypoint 1 to have a spiral motion and then move to target waypoint 2 to have another spiral motion.

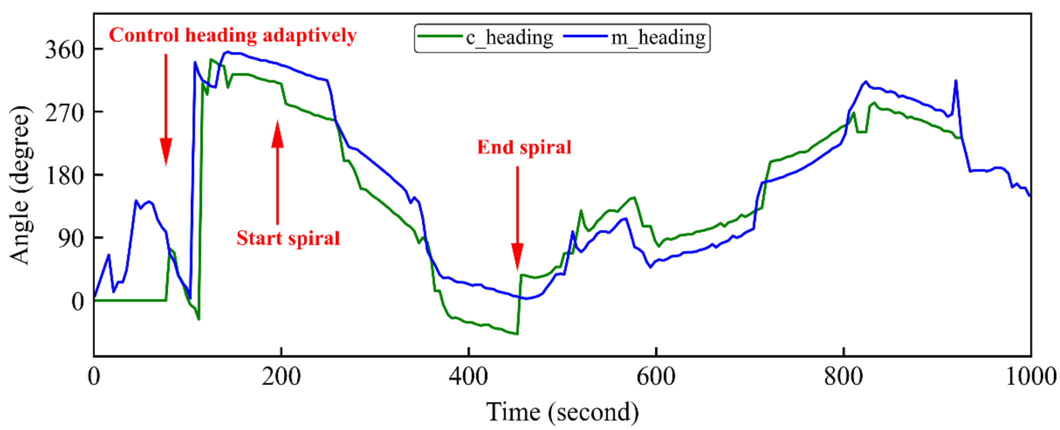

Figure 8-5. The commanded heading (c_heading) and measured heading (m_heading) from the follower glider when cooperating with a simulated scout glider in the field experiment. There was no commanded heading at the end of the mission when the glider was on the surface.

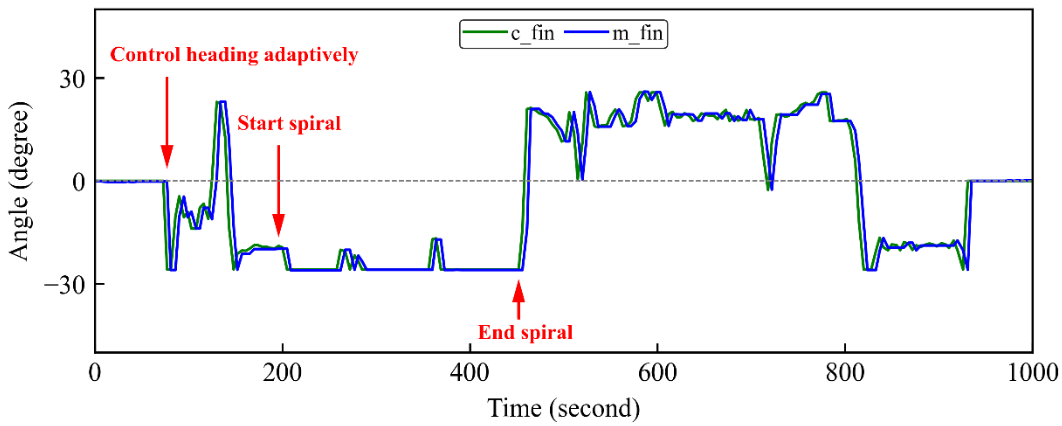

Figure 8-6. The commanded fin angle (c_fin) and measured fin angle (m_fin) from the follower glider when cooperating with a simulated scout glider in the field experiment. There was no commanded fin angle at the end of the mission when the glider was on the surface.

The field experiment mainly tested whether the follower glider had the ability to respond to the command from the scout glider and to respond to target waypoints adaptively. The follower glider was controlled to go to a waypoint to do a spiral motion; after the spiral motion, the follower was controlled to reach another waypoint. Although the glider was able to follow the control from the backseat driver (Figure 8-5), there are still concerns about whether the follower glider can respond to the moving patches in field missions under the influence of ocean dynamics on both the gliders and patches. With the use of the current glider which does not have a thruster, it is expected that the cooperation strategy with adaptive control will have lower efficiency when the current is strong, and the gliders cannot reach target waypoints in a timely manner. The follower gliders will spend a lot of time reaching the target point rather than doing their precise spiral motion. Therefore, a possible way to address this problem will be to equip the gliders with thrusters to increase their speed. The follower gliders will activate their thrusters to facilitate the control in adverse ocean environmental conditions.

8.2 Field experiment in testing sensors on a Slocum glider

In Chapter 3, the cross-validation of sensors is proposed to improve the reliability of using underwater gliders to detect the existence of underwater oil droplets. Considering the challenges in testing the developed glider for oil spill research with true oil in the ocean, environmentally friendly microbubbles are proposed in Chapter 4 to be used as potential proxies for oil droplets in field trials of underwater vehicle for underwater oil delineation. This section introduces the cooperation of sensors realized in a Slocum glider. This developed glider was tested with generated microbubbles in a field mission to check the performance of sensors and their cross-validation.

8.2.1 Experimental setup

8.2.1.1 Sensors setup on the glider

As the Cyclops 7 fluorometer used in Chapter 4 was not able to detect the micro air bubbles underwater, a Cyclops 7 turbidity sensor with a Ping360 sonar were installed in a Slocum glider. Turbidity represents "an optical property that causes light to be scattered and absorbed rather than transmitted with no change in direction or flux level through the sample" (Eaton et al., 1995). Bubbles were found to be able to cause turbidity spikes in lab experiments (Scardina et al., 2006). Different from oil droplets in the ocean which weakly scatter sound as their acoustic impedance is similar to that of the ambient seawater, gas bubbles scatter sounds much better as the acoustic impedance contrast between gas bubbles and seawater is large. The acoustic resonant characteristic of gas bubbles to a wide range of frequencies makes them scatter efficient (Brekhovskikh and Lysanov, 1982). The sonar and turbidity sensor were used as they detected the air bubbles with different signals and their measurements was expected to be able to cross-validate. Besides, these two sensors were compact and were able to be used in the glider.

These two sensors were installed in an extended nose in the front of the glider to avoid the influence of the motion of glider to the accuracy of detection (Figure 8-7). Besides, in the nose of the glider, there was an altimeter used to prevent the glider from hitting the sea floor when it was diving. The extended nose was required to be acoustically transparent underwater as both the sonar and the altimeter needed a free propagation of acoustic signals in the water. Therefore, the material acrylonitrile butadiene styrene was used for the extension as the density of this material was close to the water, which made the extension being acoustically transparent and it did not affect the performance of the sonar and altimeter to a large extent. A hole was made in front of the turbidity sensor in the nose cap, as the turbidity sensor was a point-based sensor and required a direct contact with water for its measurements.

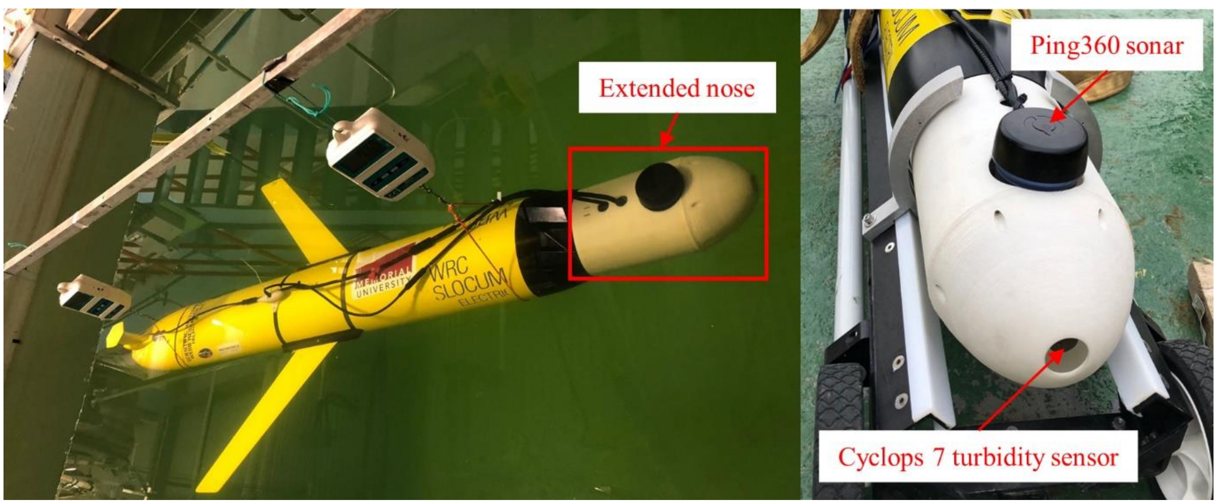

Figure 8-7. The Setup of sensors and backseat driver on the Slocum glider.

For facilitating the data logging of sensors, a BeagleBone Black computer was installed inside the science bay of the Slocum glider. This BeagleBone Black computer was powered by connecting it to the glider board in the aft hull through a power interface BeagleBone power cape. This power cape provided 3.3 Volts and 5 Volts connections for easily connecting sensors or devices to the BeagleBone Black. The power of the turbidity sensor was from the BeagleBone Power Cape which could provide the voltage the Cyclops sensor required (3-15 volts of direct current). The measurements of the turbidity sensor were logged through the BeagleBone Black computer. The sonar was powered by connecting it to the glider board in the aft hull computer through a six-pin connector in the tail of the glider as it required a minimum voltage of 11 volts. The sonar data was also logged by connecting it to the BeagleBone Black through the six-pin connector. As it was planned to cross-validate the detection from the turbidity sensor and the sonar, the sonar was set to have a maximum range of 5 m as planned in Chapter 4. This range guaranteed that the detection from the sonar was clear and of high definition for image analysis.

8.2.1.2 Mission setup

The experiment was conducted in Holyrood Bay, Newfoundland and Labrador, Canada. A KTM pump, described in Chapter 5, was placed on a nearshore vessel *Inquisitor* to generate microbubbles as proxies for oil droplets to be detected by sensors on the Slocum glider. The release depth of the bubbles was at a depth of around 4 m from the water surface. When the generator was stable in generating bubbles, the glider was deployed for a mission which involved one dive to a depth of 10 m and one climb to the surface.

8.2.2 Results and discussion

When the glider was on the water surface before its dive, the undulatory motion of the sea surface was detected by the sonar (Figure 8-8 (a)). The reading of the turbidity sensor was around 125 Nephelometric Turbidity Units (NTU), a unit used to measure the turbidity of a fluid (Figure 8-9).

When the glider was diving underwater, the sonar did not detect any bubbles or particles underwater (Figure 8-8 (b)). However, the reading of the turbidity sensor increased to over 200 NTU. When the glider was climbing, the sonar sensed objects underwater (Figure 8-10). The detection in Figure 8-10 was found to be the water surface as this detection was moving toward the sonar when the glider was climbing. The distance between glider and the detection in the sonar was in accordance with the depth of the glider under the water surface.

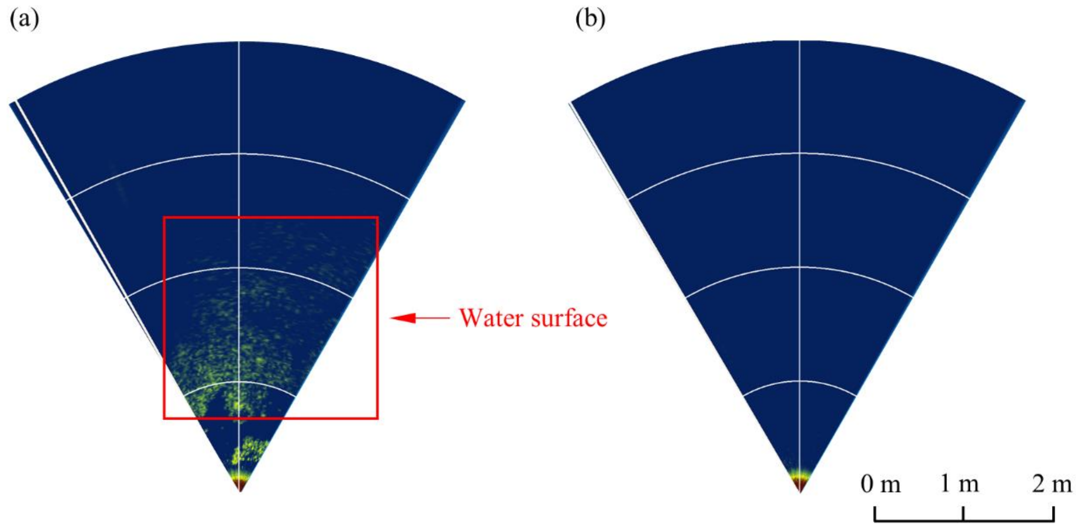

Figure 8-8. Detection from the sonar: (a) when the glider was on the water surface before its diving; (b) when the glider was underwater and the sonar did not detect the water surface.

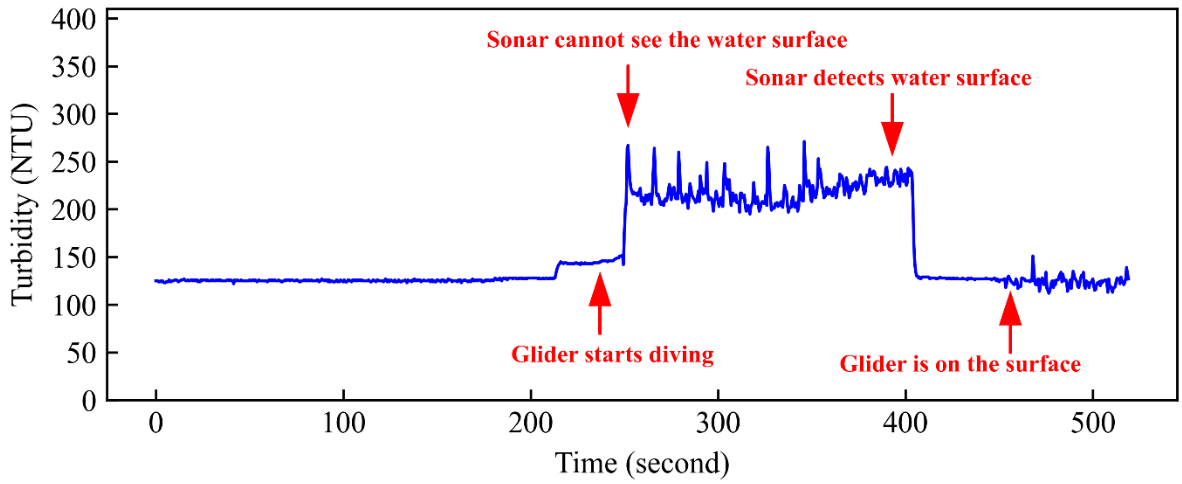

Figure 8-9. Measurements from the turbidity sensor from the start of the glider mission in which the glider dove to the depth of 10 m and then climbed to the water surface.

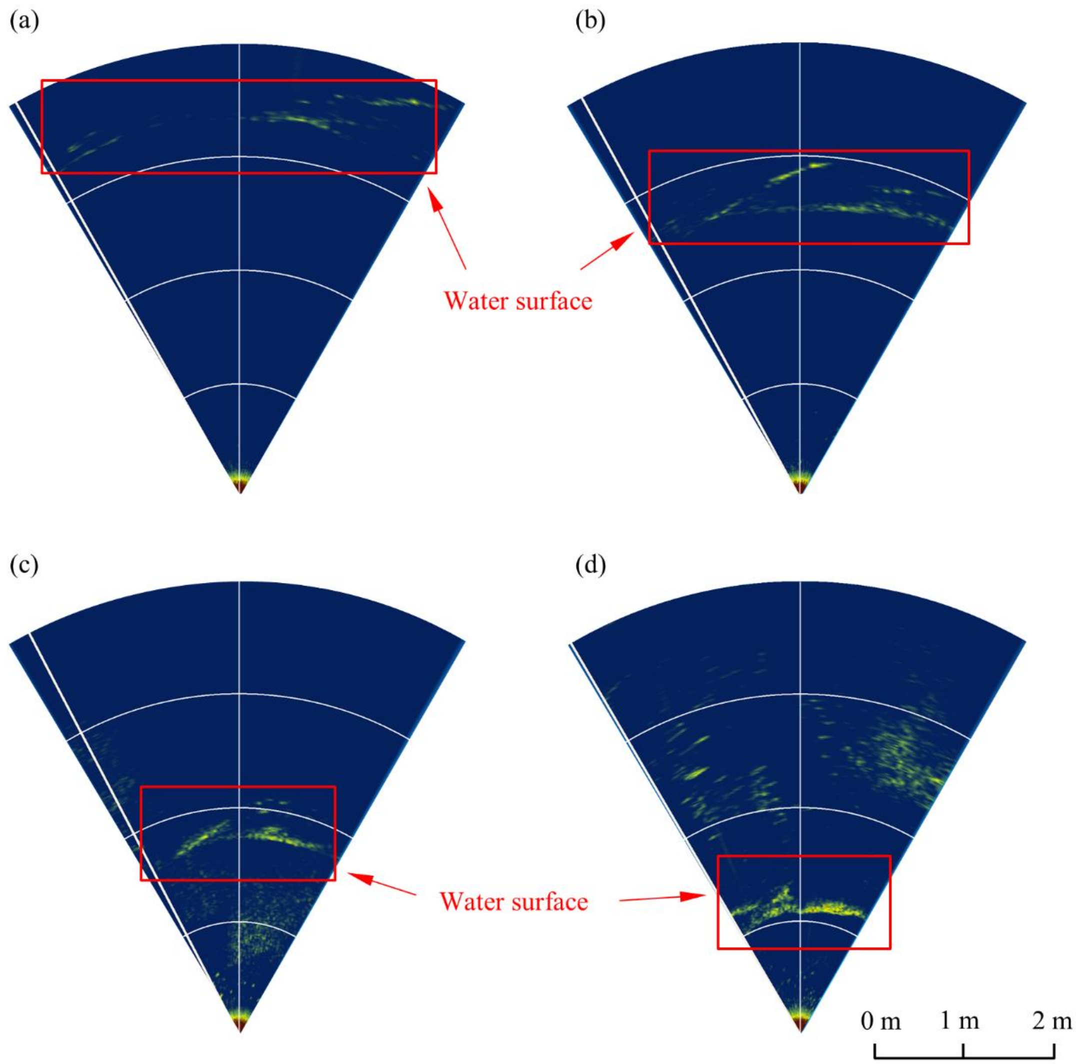

Figure 8-10. Detection from the sonar when the glider was climbing: (a) at 399 second; (b) at 411 second; (c) at 4230 second; and (d) at 435 seconds from the start of the glider mission.

When cross-validating the detection from the turbidity sensor and the sonar, their measurements of substances did not happen at the same time. The sonar was found to be able to detect the generated bubbles in Chapter 4. However, there were no substances being detected by sonar when the glider was underwater. The turbidity sensor had an increase in its reading, but this detection was not replicated in the sonar. This experiment shows the importance of having multiple different sensors to cross-validate the existence of underwater targets. The use of only one kind of sensor, such as a turbidity sensor, is not able to prove the existence of underwater microbubbles. The measurement of the sonar shows that the increase in the reading of the turbidity sensor was not from the underwater microbubbles. The cross-validation from sensors reveals that the glider missed the generated microbubbles. The generated microbubbles were released from one release nozzle and did not spread to a larger area to be detected by the sensors on glider.

The chapter addressed the first sub-objective (**O1**: To investigate the performance of a Slocum glider with cooperation between more than one sensor to delineate underwater oil) and fourth sub-objective in Section 1.3 (**O4**: To investigate the performance of a multi-glider cooperation strategy with adaptive control in delineating underwater oil plumes) through field experiments.

Reference

Bakdash, J.Z., Linkenauger, S.A., Itt, D.P., 2008. Comparing decision-making and control for learning a virtual environment: Backseat drivers learn where they are going, in: Proceedings of the Human Factors and Ergonomics Society. pp. 2117–2121. https://doi.org/10.1177/154193120805202707

Bluefin Robotics, n.d. Bluefin and MIT Demonstrate AUV Plug-n-Play Payload Autonomy [WWW Document]. URL https://defense-unmanned.com/article/1056/bluefin,-mit-demo-auv-payload-autonomy.html (accessed 11.7.21).

Bluefin Robotics Corporation, 2011. Bluefin: AUV Redefined. Mar. Technol. Mag. 64.

Brekhovskikh, L., Lysanov, Y., 1982. Scattering and Absorption of Sound by Gas Bubbles in

Water. Fundam. Ocean Acoust. 230–240. https://doi.org/10.1007/978-3-662-02342-6_11

Eaton, A.D., Clesceri, L.S., Greenberg, A.E., Franson, M.A.H., 1995. Standard Methods for the examination of water and wastewater, American Public Health Association. American Public Health Association, Washington, DC.

Eichhorn, M., Ament, C., Jacobi, M., Pfuetzenreuter, T., Karimanzira, D., Bley, K., Boer, M., Wehde, H., 2018. Modular AUV system with integrated real-time water quality analysis. Sensors (Switzerland) 18, 1–17. https://doi.org/10.3390/s18061837

Eickstedt, D.P., Sideleau, S.R., 2010. The backseat control architecture for autonomous robotic vehicles: A case study with the Iver2 AUV, in: Marine Technology Society Journal. Institute of Electrical and Electronics Engineers, pp. 42–54. https://doi.org/10.4031/MTSJ.44.4.1

Furlong, M., Marlow, R., McPhail, S., Munafo, A., Pebody, M., Phillips, A., Roper, V., Salavasidis, G., 2018. Oceanids: Building next generation maritime autonomous systems, in: Proceedings of the International Ship Control Systems Symposium. Institute of Marine Engineering Science & Technology, Glasgow, UK, pp. 1–9. https://doi.org/10.24868/issn.2631-8741.2018.003

Gallimore, E., Stokey, R., Terrill, E., 2018. Robot Operating System (ROS) on the REMUS AUV using RECON, in: 2018 IEEE/OES Autonomous Underwater Vehicle Workshop (AUV). Institute of Electrical and Electronics Engineers Inc., Porto, Portugal, pp. 1–6. https://doi.org/10.1109/AUV.2018.8729755

Hwang, J., Bose, N., Nguyen, H.D., Williams, G., 2020. Oil plume mapping: Adaptive tracking and adaptive sampling from an autonomous underwater vehicle. IEEE Access 8, 198021–198034. https://doi.org/10.1109/ACCESS.2020.3032161

Keane, J.R., Forrest, A.L., Johannsson, H., Battle, D., 2020. Autonomous Underwater Vehicle Homing with a Single Range-Only Beacon. IEEE J. Ocean. Eng. 45, 395–403. https://doi.org/10.1109/JOE.2018.2877535

Manley, J.E., Smith, J., 2017. Rapid development and evolution of a micro-UUV, in: OCEANS 2017 - Anchorage. pp. 1–4.

Naglak, J.E., Page, B.R., Mahmoudian, N., 2018. Backseat Control of SandShark AUV using ROS on RaspberryPi ∗, in: OCEANS 2018 MTS/IEEE Charleston. Institute of Electrical and Electronics Engineers Inc., Charleston, SC, USA, pp. 1–5. https://doi.org/10.1109/OCEANS.2018.8604630

Scardina, P., Letterman, R.D., Edwards, M., 2006. Particle count and on-line turbidity interference from bubble formation. J. / Am. Water Work. Assoc. 98, 97–109. https://doi.org/10.1002/j.1551-8833.2006.tb07714.x

Steenson, L. V., Turnock, S.R., Phillips, A.B., Harris, C., Furlong, M.E., Rogers, E., Wang, L., Bodles, K., Evans, D.W., 2014. Model predictive control of a hybrid autonomous underwater vehicle with experimental verification. J. Eng. Marit. Environ. 228, 166–179. https://doi.org/10.1177/1475090213506185

Teck, T.Y., Chitre, M., 2012. Hierarchical multi-agent command and control system for autonomous underwater vehicles, in: 2012 IEEE/OES Autonomous Underwater Vehicles, AUV 2012. Southampton, UK, pp. 1–6. https://doi.org/10.1109/AUV.2012.6380760

Wang, Y., Bulger, C., Thanyamanta, W., Bose, N., 2021. A backseat control architecture for a slocum glider. J. Mar. Sci. Eng. 9, 532. https://doi.org/10.3390/jmse9050532

Wang, Y., Thanyamanta, W., Bose, N., 2022. Cooperation and compressed data exchange between multiple gliders used to map oil spills in the ocean. Appl. Ocean Res. 118, 102999. https://doi.org/10.1016/J.APOR.2021.102999

9. Chapter 9

Conclusions and Recommendations

9.1 Conclusions

Underwater oil spill reconnaissance and delineation is a challenging mission, as the oil spill can cover a large area and is largely beneath the water. Autonomous underwater vehicles (AUVs), having advantages in growing intelligence, are increasingly used in oil spill tracking. By carrying various sensors, AUVs can be competent in oil spill detection. Different from screw propelled AUVs, gliders are affordable for long duration and large survey areas. With a buoyancy and weight control system, gliders bring less disturbance to the surrounding water and increase the reliability of data collected by the sensors on board the gliders. Using one glider to map the distribution of underwater spilled oil faces lots of challenges, such as spatiotemporal aliasing and lower data redundancy, and reduces the reliability in the data collected.

The main objective of this thesis is to investigates the capabilities of Slocum gliders to delineate subsurface oil plumes. The investigation is conducted from three aspects, sensors, gliders, multiple glider strategies, through a series of simulation experiments and field experiments in order to answer the research questions of this thesis. Because the advantage of using multiple sensors in other actively propelled AUVs to improve the reliability in detecting the existence of underwater oil spills, this thesis aimed to find out whether it was possible to improve the reliability of measurements by using multiple sensors in a Slocum glider (the first research question of this thesis). To find suitable sensors and increase the reliability in detecting the existence of oils with the use of gliders, two light-weight sensors were proposed to be installed in gliders to cross-validate their measurements. The cross-validation of sensors was tested in a tank experiment by using a fluorometer and sonar in an outdoor tank with the release of real oil. The cross-validation of sensors was also tested in a glider mission with the use of a Slocum glider equipped with a turbidity sensor and a sonar to detect underwater micro air bubbles proposed as proxies for underwater oil droplets. In addition, to develop a Slocum glider which was able to detect underwater oil spills, a Slocum glider was improved by having an electronic hardware for the power supply and data storage of sensors and a nose extension for the placement of sensors. A backseat driver control system was developed for the Slocum glider to equip Slocum gliders with adaptive control in oil spill investigations. This was tested by setting up the glider in simulation mode to investigate the ability of the backseat control system to control the states such as depth, heading, and waypoints of the Slocum glider. This development and test were to answer the second research question in Section 1.2 (Q2: Is it possible to equip a Slocum glider with the ability of adaptive control?). The third research question of this thesis in Section 1.2 was whether there was an advantage in using a multi-glider strategy for oil spill detection. Considering the advantages of using multiple gliders and with the aim of improving the efficiency of real-time underwater communication and cooperation of networked gliders, a cooperation strategy with adaptive control and data compression was proposed for a multi-glider system to share information between gliders in delineating oil patches underwater. In the cooperation strategy, the mission area was split up into blocks. One glider was assigned as a scout glider to conduct an overall survey within a block to find the boundaries of potential oil patches. The rest of the gliders were assigned as followers to conduct detailed surveys on each oil patch detected by the scout glider. These followers got the boundary information through underwater communication with the scout glider which identified the boundaries of the oil patches with a proposed boundary classification method. In this boundary classification method, a clustering method was proposed to be applied prior to the Support vector machine to simplify the characteristics of the data sets. The proposed cooperation strategy was further improved by considering the influence of water currents on the motion of oil patches and the adaptive control of the followers. Besides, the performance of the cooperation strategy was compared with other strategies without cooperation and/or without adaptivity. The cooperation of gliders and the adaptive control of follower gliders were tested through a field mission, with one Slocum glider equipped with a backseat control hardware as a follower and an acoustic modem as a simulated scout glider. This was to answer the fourth research question in Section 1.2 (Q4: What are the benefits of using multiple cooperative gliders with adaptive control in mapping oils underwater?).

The investigation in this thesis demonstrated that the idea of cross-validating the measurements from fluorometers and sonar can provide reliable measurements of oil when using underwater Slocum gliders. It is necessary to use multiple sensors to capture the underwater targets, such as oil droplets and the proxies of oils droplets such as underwater gas bubbles. This shows the first sub-objective of this thesis in Section 1.3 is reached (O1: To investigate the performance of a Slocum glider with cooperation between more than one sensor to delineate underwater oil). With the developed backseat driver, the Slocum glider is able to do intelligent missions and sample interesting targets by receiving measurements from sensors and publishing commands to the main vehicle control system. This reveals that the second sub-objective of this thesis is reached (O2: To develop a Slocum glider with adaptive control to investigate oil spills in the ocean intelligently). The mapping strategy with only adaptive control or multiple gliders cannot improve the score of performance of gliders when mapping oil patches. The score of performance was an evaluation metric proposed in this thesis to measure the percentage of valuable rich information collected to the percentage of the mission area covered by information-rich patches. The proposed cooperation strategy with adaptive control has a lower duty cycle and a longer mission duration compared with other strategies, but has the best score of performance, especially for a long-duration mission. The proposed boundary classification algorithm in the cooperation strategy is able to reduce the amount of information to be transmitted between gliders through underwater acoustic communication and reach the third sub-objective of this thesis in Section 1.3 (O3: To improve the performance of multiple cooperative gliders to delineate subsurface oil). The influence from the ocean environment affects the control of the follower gliders which cannot reach waypoints within a certain amount of allocated time. The performance of the follower gliders with adaptive control in the cooperation strategy is expected to be improved by having a screw type thruster in the gliders. The results of this investigation achieves the fourth sub-objective of this thesis (O4: To investigate the performance of a multi-glider cooperation strategy with adaptive control in delineating underwater oil plumes).

From the work done in this thesis, underwater gliders are found to have the ability to detect underwater oil plumes. The performance of gliders in delineating underwater oil plumes can be improved by having multiple sensors to cross validate their detection and having multiple cooperative gliders with adaptive control. The challenge in testing the developed gliders to delineate oil spills is solved by testing through a series of simulation and field experiments as well as by using micro air bubbles as proxies for oil droplets.

9.2 Recommendations

The current work studied the ability of multiple Slocum gliders to detect underwater oil spills. There are some issues that can be solved in future studies:

- In Chapter 3, the cooperation of a sonar and a fluorometer was proposed to improve the reliability in detecting the existence of oil underwater with the use of gliders. A tank experiment was conducted to test whether the measurements from these two sensors were able to be correlated. This work can be further improved by quantitatively analyzing how the multi-sensor system increases the reliability in detecting subsurface oil plumes compared to using only a single sensor through using methods such as Bayesian analysis.
- In Chapter 6, the boundary classification method for the scout glider to classify the boundary of patches and to compress the amount of data to be shared with follower gliders was tested through simulations, with simplified oil patches underwater based on previous experiments in which the oil was found to be made up of patches underwater. As underwater oil plumes were dynamic and all the possible cases could not be listed, some possible distributions of oil patches were generated in this research. The aim was to verify that the proposed algorithm with a clustering method could identify the boundaries of oil patches better than without using a clustering method. In this case, the patchy distribution of oil plumes was what really mattered to be included in the verification. It is true that the manually generated oil distribution is different from a real oil distribution. The shape of an oil plume can vary from a long and thin shape to a more compact shape depending on ocean environments and human intervention (such as the use of dispersants). The proposed algorithm can be further tested and improved with simulations by using plume models and ocean models or field experiments with true oil spills.

- In the field experiment done in this work, the Slocum glider could not reach the target waypoint in the time allocated when controlled by the backseat driver. Screw thrusters are proposed to be installed in the gliders to improve the performance of gliders in underwater oil delineation. The performance and the strengths of Slocum gliders with thrusters to delineate underwater oil spills, such as energy consumption, the change of mission duration, and the motion speed, are required to be explored in the future by comparison with the use of other actively propelled AUVs on the same missions.

Bibliography

Abt Associates, Woods Hole OceanogNational Oceanic and Atmospheric Administrationraphic Institute, U.S. Environmental Protection Agency, Water Mapping, L., 2020. Report to BSEE: Three-Dimensional Mapping of Dissolved Hydrocarbons and Oil Droplets Using a REMUS-600 Autonomous Underwater Vehicle.

Alvarez, A., Mourre, B., 2014. Cooperation or coordination of underwater glider networks? An assessment from observing system simulation experiments in the Ligurian Sea. J. Atmos. Ocean. Technol. 31, 2268–2277. https://doi.org/10.1175/JTECH-D-13-00214.1

Bakdash, J.Z., Linkenauger, S.A., Itt, D.P., 2008. Comparing decision-making and control for learning a virtual environment: Backseat drivers learn where they are going, in: Proceedings of the Human Factors and Ergonomics Society. pp. 2117–2121. https://doi.org/10.1177/154193120805202707

Baszanowska, E., Otremba, Z., 2016. Fluorometry in application to fingerprint of petroleum products present in the natural waters. J. Eur. Opt. Soc. 12, 1–9. https://doi.org/10.1186/s41476-016-0018-4

Battelle Memorial Institute, 2014. Capabilities and Uses of Sensor-Equipped Ocean Vehicles for Subsea and Surface Detection and Tracking of Oil Spills OGP-IPIECA Oil Spill Response Joint Industry Project Surveillance , Modelling & Visualization Work Package 1 : In Water Surveillance Novemb.

Bluefin Robotics, n.d. Bluefin and MIT Demonstrate AUV Plug-n-Play Payload Autonomy [WWW Document]. URL https://defense-unmanned.com/article/1056/bluefin,-mit-demo-auv-payload-autonomy.html (accessed 11.7.21).

Bluefin Robotics Corporation, 2011. Bluefin: AUV Redefined. Mar. Technol. Mag. 64.

Brekhovskikh, L., Lysanov, Y., 1982. Scattering and Absorption of Sound by Gas Bubbles in Water. Fundam. Ocean Acoust. 230–240. https://doi.org/10.1007/978-3-662-02342-6_11

Brito, M.P., Lewis, R., Bose, N., Alexander, P., Griffiths, G., Ferguson, J., 2012. The Role of adaptive mission planning and control in persistent autonomous underwater vehicles presence, in: 2012 IEEE/OES Autonomous Underwater Vehicles. Southampton, pp. 1–9. https://doi.org/10.1109/AUV.2012.6380748

Caiti, A., Calabrò, V., Munafò, A., 2012. AUV team cooperation: Emerging behaviours and networking modalities, in: IFAC Proceedings Volumes (IFAC-PapersOnline). pp. 342–347. https://doi.org/10.3182/20120919-3-IT-2046.00058

Camilli, R., Duryea, A., 2007. Characterizing marine hydrocarbons with in-situ mass spectrometry, in: Oceans Conference Record (IEEE). pp. 1–7. https://doi.org/10.1109/OCEANS.2007.4449412

Camilli, R., Reddy, C.M., Yoerger, D.R., Van Mooy, B.A.S., Jakuba, M. V., Kinsey, J.C., McIntyre, C.P., Sylva, S.P., Maloney, J. V., 2010a. Tracking hydrocarbon plume transport and biodegradation at deepwater horizon. Science. 330, 201–204. https://doi.org/10.1126/science.1195223

Camilli, R., Reddy, C.M., Yoerger, D.R., Van Mooy, B.A.S., Jakuba, M. V., Kinsey, J.C., McIntyre, C.P., Sylva, S.P., Maloney, J. V., 2010b. Tracking hydrocarbon plume transport and biodegradation at deepwater horizon. Science (80-.). 330, 201–204. https://doi.org/10.1126/science.1195223

Chappell, S.G., Komerska, R.J., 1999. An Environment for High-Level Multiple AUV Simulation. Components 1–14.

Chen, B., Pompili, D., 2012. Team formation and steering algorithms for underwater gliders using acoustic communications. Comput. Commun. 35, 1017–1028. https://doi.org/10.1016/j.comcom.2012.01.001

Chua, E.J., Savidge, W., Timothy Short, R., Cardenas-Valencia, A.M., Fulweiler, R.W., 2016. A review of the emerging field of underwater mass spectrometry. Front. Mar. Sci. 3, 209. https://doi.org/10.3389/fmars.2016.00209

Cyr, F., Tedetti, M., Besson, F., Bhairy, N., Goutx, M., 2019. A glider-compatible optical sensor for the detection of polycyclic aromatic hydrocarbons in the marine environment. Front. Mar. Sci. 6, 110. https://doi.org/10.3389/fmars.2019.00110

Deepwater Horizon Study Group, 2011. Final Report on the Investigation of the Macondo Well Blowout.

Driskell, W.B., Payne, J.R., 2018. Macondo oil in northern Gulf of Mexico waters – Part 2: Dispersant-accelerated PAH dissolution in the Deepwater Horizon plume. Mar. Pollut. Bull. 129, 412–419. https://doi.org/10.1016/j.marpolbul.2018.02.057

Eaton, A.D., Clesceri, L.S., Greenberg, A.E., Franson, M.A.H., 1995. Standard Methods for the examination of water and wastewater, American Public Health Association. American Public Health Association, Washington, DC.

Edwards, D.B., Bean, T.A., Odell, D.L., Anderson, M.J., 2004. A leader-follower algorithm for multiple AUV formations, in: 2004 IEEE/OES Autonomous Underwater Vehicles (IEEE Cat. No.04CH37578). IEEE, pp. 40–46. https://doi.org/10.1109/AUV.2004.1431191

Eichhorn, M., Ament, C., Jacobi, M., Pfuetzenreuter, T., Karimanzira, D., Bley, K., Boer, M., Wehde, H., 2018. Modular AUV system with integrated real-time water quality analysis. Sensors (Switzerland) 18, 1–17. https://doi.org/10.3390/s18061837

Eickstedt, D.P., Sideleau, S.R., 2010. The backseat control architecture for autonomous robotic vehicles: A case study with the Iver2 AUV, in: Marine Technology Society Journal. Institute of Electrical and Electronics Engineers, pp. 42–54. https://doi.org/10.4031/MTSJ.44.4.1

Eriksen, P.K., 2013a. Leakage and oil spill detection utilizing active acoustic systems, in: 2013 IEEE International Underwater Technology Symposium, UT 2013. Tokyo, Japan, pp. 1–8. https://doi.org/10.1109/UT.2013.6519891

Eriksen, P.K., 2013b. Leakage and oil spill detection utilizing active acoustic systems, in: 2013 IEEE International Underwater Technology Symposium. Tokyo, Japan, pp. 1–8. https://doi.org/10.1109/UT.2013.6519891

Fingas, M., 2017. Oil Spill Science and Technology, Gulf Professional Publishing. https://doi.org/10.1016/c2015-0-04851-1

Fiorelli, E., Leonard, N.E., Bhatta, P., Paley, D.A., Bachmayer, R., Fratantoni, D.M., 2006. Multi-AUV control and adaptive sampling in Monterey Bay, in: IEEE Journal of Oceanic Engineering. pp. 935–948. https://doi.org/10.1109/JOE.2006.880429

Fitzpatrick, M., Balsley, A., Hansen, K.A., 2014. Detection of Oil in Water Column , Final Report : Detection Prototype Tests.

Fitzpatrick, M., Tebeau, P.A., 2013. Detection of Oil in Water Column: Sensor Design, US Department of Homeland Security.

Fonti, A., Freddi, A., Longhi, S., Monteriù, A., 2011. Cooperative and decentralized navigation of Autonomous Underwater Gliders using Predictive Control, in: IFAC Proceedings Volumes (IFAC-PapersOnline). IFAC Secretariat, pp. 12813–12818. https://doi.org/10.3182/20110828-6-IT-1002.02980

Fulton-Bennett, K., 2018. Testing an undersea robot that can detect and map oil spills [WWW Document]. Monterey Bay Aquarium Res. Inst. URL https://phys.org/news/2018-10-

undersea-robot-oil.html (accessed 6.22.20).

Furlong, M., Marlow, R., McPhail, S., Munafo, A., Pebody, M., Phillips, A., Roper, V., Salavasidis, G., 2018. Oceanids: Building next generation maritime autonomous systems, in: Proceedings of the International Ship Control Systems Symposium. Institute of Marine Engineering Science & Technology, Glasgow, UK, pp. 1–9. https://doi.org/10.24868/issn.2631-8741.2018.003

Gallimore, E., Stokey, R., Terrill, E., 2018. Robot Operating System (ROS) on the REMUS AUV using RECON, in: 2018 IEEE/OES Autonomous Underwater Vehicle Workshop (AUV). Institute of Electrical and Electronics Engineers Inc., Porto, Portugal, pp. 1–6. https://doi.org/10.1109/AUV.2018.8729755

Hobson, B.W., Bellingham, J.G., Kieft, B., McEwen, R., Godin, M., Zhang, Y., 2012. Tethys-class long range AUVs-extending the endurance of propeller-driven cruising AUVs from days to weeks, in: 2012 IEEE/OES Autonomous Underwater Vehicles, AUV 2012. pp. 1–8. https://doi.org/10.1109/AUV.2012.6380735

Hwang, J., Bose, N., Nguyen, H.D., Williams, G., 2020. Oil plume mapping: Adaptive tracking and adaptive sampling from an autonomous underwater vehicle. IEEE Access 8, 198021–198034. https://doi.org/10.1109/ACCESS.2020.3032161

Kaiser, C.L., Yoerger, D.R., Kinsey, J.C., Kelley, S., Billings, A., Fujii, J., Suman, S., Jakuba, M., Berkowitz, Z., German, C.R., Bowen, A.D., 2016. The design and 200 day per year operation of the autonomous underwater vehicle sentry, in: Autonomous Underwater Vehicles 2016, AUV 2016. pp. 251–260. https://doi.org/10.1109/AUV.2016.7778680

Kalaji, H.M., Goltsev, V., Bosa, K., Allakhverdiev, S.I., Strasser, R.J., Govindjee, 2012. Experimental in vivo measurements of light emission in plants: A perspective dedicated to

David Walker. Photosynth. Res. 114, 69–96. https://doi.org/10.1007/s11120-012-9780-3

Kato, N., Choyekh, M., Dewantara, R., Senga, H., Chiba, H., Kobayashi, E., Yoshie, M., Tanaka, T., Short, T., 2017. An autonomous underwater robot for tracking and monitoring of subsea plumes after oil spills and gas leaks from seafloor. J. Loss Prev. Process Ind. 50, 386–396. https://doi.org/10.1016/j.jlp.2017.03.006

Keane, J.R., Forrest, A.L., Johannsson, H., Battle, D., 2020. Autonomous Underwater Vehicle Homing with a Single Range-Only Beacon. IEEE J. Ocean. Eng. 45, 395–403. https://doi.org/10.1109/JOE.2018.2877535

Kukulya, A.L., Bellingham, J.G., Kaeli, J.W., Reddy, C.M., Godin, M.A., Conmy, R.N., 2016. Development of a propeller driven long range autonomous underwater vehicle (LRAUV) for Under-Ice mapping of oil spills and environmental hazards an arctic domain center of awareness project (ADAC), in: Autonomous Underwater Vehicles 2016, AUV 2016. Institute of Electrical and Electronics Engineers Inc., pp. 95–100. https://doi.org/10.1109/AUV.2016.7778655

Leonard, N., Rowley, C., Marsden, J., 2003. Underwater Glider Networks for Adaptive Ocean Sampling, Department of Mechanical & Aerospace Engineering,Princeton University.

Li, Z., Lee, K., Kepkey, P.E., Mikkelsen, O., Pottsmith, C., 2011. Monitoring Dispersed Oil Droplet Size Distribution at the Gulf of Mexico Deepwater Horizon Spill Site, in: International Oil Spill Conference Proceedings. International Oil Spill Conference, pp. 1–15. https://doi.org/10.7901/2169-3358-2011-1-377

Lippsett, L., 2011. Gliders Tracked Potential for Oil to Reach the East Coast – Woods Hole Oceanographic Institution. OCEANUS.

Loranger, S.C., 2019. Acoustic Detection and Quantification of Crude Oil. University of New

Hampshire.

Lord, R., 2018. Gap in pipe the cause of Newfoundland's largest-ever oil spill, which is now impossible to clean up [WWW Document]. URL https://boom1019.com/news/4681892/oil-spill-newfoundland-2/ (accessed 6.22.20).

Maksym, T., Singh, H., Bassett, C., Lavery, A., Freitag, L., Sonnichsen, F., Wilkinson, J., 2014. Oil spill detection and mapping under Arctic sea ice using autonomous underwater vehicles.

Manley, J.E., Smith, J., 2017. Rapid development and evolution of a micro-UUV, in: OCEANS 2017 - Anchorage. pp. 1–4.

Marques, D., Kim, J., Mikols, J., O'Rourke, J.S., 2011. BP and the Gulf Oil Spill (A), BP and the Gulf Oil Spill (A). The Eugene D. Fanning Center for Business Communication, Mendoza College of Business, University of Notre Dame. https://doi.org/10.4135/9781526403957

Medagoda, L., Williams, S.B., Pizarro, O., Kinsey, J.C., Jakuba, M. V., 2016. Mid-water current aided localization for autonomous underwater vehicles. Auton. Robots 40, 1207–1227. https://doi.org/10.1007/s10514-016-9547-3

Naglak, J.E., Page, B.R., Mahmoudian, N., 2018. Backseat Control of SandShark AUV using ROS on RaspberryPi ∗, in: OCEANS 2018 MTS/IEEE Charleston. Institute of Electrical and Electronics Engineers Inc., Charleston, SC, USA, pp. 1–5. https://doi.org/10.1109/OCEANS.2018.8604630

Ögren, P., Fiorelli, E., Leonard, N.E., 2004. Cooperative control of mobile sensor networks: Adaptive gradient climbing in a distributed environment. IEEE Trans. Automat. Contr. 49, 1292–1302. https://doi.org/10.1109/TAC.2004.832203

Panetta, P.D., Argo, T., Du, H., Gong, D., Ferris, L.N., Kidwell, J., 2017. Development of acoustic methods to measure oil droplet size and slick thickness on ROV and AUV platforms.

Pärt, S., Tarmo, K., Kaimo, V., 2017. Oil detection using oil sensors on Autonomous Underwater Vehicles.

Russell-Cargill, L.M., Craddock, B.S., Dinsdale, R.B., Doran, J.G., Hunt, B.N., Hollings, B., 2018. Using autonomous underwater gliders for geochemical exploration surveys. APPEA J. 58, 367–380. https://doi.org/10.1071/aj17079

Scardina, P., Letterman, R.D., Edwards, M., 2006. Particle count and on-line turbidity interference from bubble formation. J. / Am. Water Work. Assoc. 98, 97–109. https://doi.org/10.1002/j.1551-8833.2006.tb07714.x

Steenson, L. V., Turnock, S.R., Phillips, A.B., Harris, C., Furlong, M.E., Rogers, E., Wang, L., Bodles, K., Evans, D.W., 2014. Model predictive control of a hybrid autonomous underwater vehicle with experimental verification. J. Eng. Marit. Environ. 228, 166–179. https://doi.org/10.1177/1475090213506185

Stommel, H., 1989. The Slocum Mission. Oceanography 2, 22–25. https://doi.org/10.5670/oceanog.1989.26

Teck, T.Y., Chitre, M., 2012. Hierarchical multi-agent command and control system for autonomous underwater vehicles, in: 2012 IEEE/OES Autonomous Underwater Vehicles, AUV 2012. Southampton, UK, pp. 1–6. https://doi.org/10.1109/AUV.2012.6380760

Teledyne Webb Research, 2013. Slocum G3 Glider - Autonomous Underwater Gliders - Webb Research [WWW Document]. URL http://www.teledynemarine.com/slocum-glider (accessed 12.11.20).

Thompson, D., Caress, D., Clague, D., Conlin, D., Harvey, J., Martin, E., Paduan, J., Paull, C., Ryan, J., Thomas, H., Zhang, Y., 2013. MBARI Dorado AUV's scientific results, in: OCEANS 2013 MTS/IEEE - San Diego: An Ocean in Common. pp. 1–9.

Transportation Research Board and National Research Council, 2003. Oil in the Sea III: Inputs, Fates, and Effects. National Academies Press, Washington, DC. https://doi.org/10.17226/10388

Wang, Y., Thanyamanta, W., Bose, N., 2022. Cooperation and compressed data exchange between multiple gliders used to map oil spills in the ocean. Appl. Ocean Res. 118, 102999. https://doi.org/10.1016/J.APOR.2021.102999

Wang, Y., Thanyamanta, W., Bulger, C., Bose, N., Hwang, J., 2021. Microbubbles as proxies for oil spill delineation in field tests. J. Mar. Sci. Eng. 9, 1–17. https://doi.org/10.3390/jmse9020126

Wilkinson, J., Maksym, T., Singh, H., 2013. Capabilities for detection of oil spills under sea ice from autonomous underwater vehicles.

Wynn, R.B., Huvenne, V.A.I., Le Bas, T.P., Murton, B.J., Connelly, D.P., Bett, B.J., Ruhl, H.A., Morris, K.J., Peakall, J., Parsons, D.R., Sumner, E.J., Darby, S.E., Dorrell, R.M., Hunt, J.E., 2014. Autonomous Underwater Vehicles (AUVs): Their past, present and future contributions to the advancement of marine geoscience. Mar. Geol. 352, 451–468. https://doi.org/10.1016/j.margeo.2014.03.012

Xue, D., Wu, Z., Wang, S., 2015. Dynamical analysis of autonomous underwater glider formation with environmental uncertainties, in: Procedia IUTAM. Elsevier B.V., pp. 108–117. https://doi.org/10.1016/j.piutam.2015.01.007

Zhang, Y., McEwen, R.S., Ryan, J.P., Bellingham, J.G., Thomas, H., Thompson, C.H., Rienecker, E., 2011. A peak-capture algorithm used on an autonomous underwater vehicle in the 2010 Gulf of Mexico oil spill response scientific survey. J. F. Robot. 28, 484–496. https://doi.org/10.1002/rob.20399